PB86-212404

Development and Testing of a Surrogate Species Chemical Reaction Mechanism. Volume 1

California Univ., Riverside

Prepared for

Environmental Protection Agency
Research Triangle Park, NC

Jun 86

U.S. Department of Commerce
National Technical Information Service
NTIS

TECHNICAL REPORT DATA
(Please read Instructions on the reverse before completing)

1. REPORT NO. EPA/600/3-86/031a	2.	3. RECIPIENT'S ACCESSION NO. PB86 212404/AS
4. TITLE AND SUBTITLE DEVELOPMENT AND TESTING OF A SURROGATE SPECIES CHEMICAL REACTION MECHANISM, VOLUME I		5. REPORT DATE June 1986
		6. PERFORMING ORGANIZATION CODE
7. AUTHOR(S) W. P. L. Carter, F. W. Lurmann, R. Atkinson, and A. C. Lloyd		8. PERFORMING ORGANIZATION REPORT NO.
9. PERFORMING ORGANIZATION NAME AND ADDRESS Statewide Air Pollution Research Center University of California Riverside, California 92521		10. PROGRAM ELEMENT NO. CDWA1A/01-4003 (FY-86)
		11. CONTRACT/GRANT NO. Contract 68-02-4104
12. SPONSORING AGENCY NAME AND ADDRESS Atmospheric Sciences Research Laboratory-RTP, NC Office of Research and Development U. S. Environmental Protection Agency Research Triangle Park, North Carolina 27711		13. TYPE OF REPORT AND PERIOD COVERED Interim (10/84 - 2/86)
		14. SPONSORING AGENCY CODE EPA/600/09

15. SUPPLEMENTARY NOTES

Volume II. (EPA/600/3-86/031b)

16. ABSTRACT

A photochemical reaction mechanism has been updated and extensively evaluated. The testing and refinement of the surrogate species mechanism was performed in order to create an improved chemical mechanism for the atmospheric simulation models that are used to develop ozone control strategies. The updated mechanism was tested against 400 smog chamber experiments carried out in four different chambers. Tests were performed to assess the accuracy of the chamber characterization procedures, of reactions for single organic compounds, and of the overall mechanism for complex organic mixtures, including mixtures obtained from automobile exhaust. The results indicate that the mechanism's predictions are generally consistent with the experimental data. Volume 1 contains the introduction, the documentation of the chemical mechanism, and a discussion of the chamber and light intensity characterization. Volume II contains the results of the model simulations of the environmental chamber experiments and a summary and conclusion section that includes a discussion of work to be carried out in the future to adapt this mechanism for use in atmospheric modeling.

17. KEY WORDS AND DOCUMENT ANALYSIS

a. DESCRIPTORS	b. IDENTIFIERS/OPEN ENDED TERMS	c. COSATI Field/Group

18. DISTRIBUTION STATEMENT RELEASE TO PUBLIC	19. SECURITY CLASS *(This Report)* UNCLASSIFIED	21. NO. OF PAGES 349
	20. SECURITY CLASS *(This page)* UNCLASSIFIED	22. PRICE

EPA Form 2220-1 (9-73)

PB86-212404
EPA/600/3-86/031a
June 1986

DEVELOPMENT AND TESTING OF A SURROGATE SPECIES CHEMICAL REACTION MECHANISM

VOLUME I

William P. L. Carter, Frederick W. Lurmann,
Roger Atkinson and Alan C. Lloyd

Statewide Air Pollution Research Center
University of California
Riverside, California 92521

and

Environmental Research and Technology
975 Business Center Circle
Newbury Park, CA 91320

EPA Contract No. 68-02-4104

Project Officer

Marcia C. Dodge

Atmospheric Chemistry and Physics Division
Atmospheric Sciences Research Laboratory
Research Triangle Park, NC 27711

ATMOSPHERIC SCIENCES RESEARCH LABORATORY
OFFICE OF RESEARCH AND DEVELOPMENT
U. S. ENVIRONMENTAL PROTECTION AGENCY
RESEARCH TRIANGLE PARK, NC 27711

REPRODUCED BY
NATIONAL TECHNICAL
INFORMATION SERVICE
U.S. DEPARTMENT OF COMMERCE
SPRINGFIELD, VA. 22161

NOTICE

The information in this document has been funded by the United States Environmental Protection Agency under Contract Number 68-02-4104 to the University of California at Riverside. It has been subject to the Agency's peer and administrative review, and it has been approved for publication as an EPA document. Mention of trade names or commercial products does not constitute endorsement or recommendation for use.

ABSTRACT

This interim report describes the work performed in the first year of a two-year program to develop and test a chemical mechanism using the "lumped molecule" approach for inclusion in models to assess control strategies for ozone. The specific tasks which were carried out during the period covered by this report are as follows:

- The detailed, "lumped-molecule," mechanism of Atkinson et al. (1982) was updated and expanded. A number of new species were added to the mechanism and substantial modifications were made to the aromatic photooxidation mechanism and to the approach used to represent the reactions of the higher ($\geq C_5$) alkanes. Several significant changes were also made to the mechanisms of the alkenes and the ketones, and a new approach was used for representing the reactions of peroxy radicals under conditions where radical-radical reactions become important. Explicit chemical mechanisms were developed for the following species: C_2 through C_4 alkanes; ethene, propene, 1-butene and trans-2-butene; benzene, toluene, o-xylene, m-xylene, and 1,3,5-trimethylbenzene; formaldehyde, acetaldehyde, propionaldehyde, acetone, methyl ethyl ketone, 3-pentanol, glyoxal, methylglyoxal, biacetyl, and benzaldehyde; and the representative organic nitrates 2-butyl nitrate and 4-heptyl nitrate. "Lumped reaction" schemes were also formulated for the higher alkanes n-pentane through n-nonane, 2-methylbutane, 2,3-dimethylbutane, and 2,2,4-trimethylpentane (isooctane), and for the reactions of cresols and the uncharacterized ring-opening products formed in the photooxidations of the aromatic hydrocarbons. These chemical mechanisms are fully documented in this report.

- The updated mechanism was tested against the results of experiments carried out in four different environmental chambers: The 150,000-liter dual outdoor chamber at the University of North Carolina (UNC), the 5800-liter evacuable chamber at the Statewide Air Pollution Research Center (SAPRC) at the University of California in Riverside, the 6400-liter SAPRC indoor Teflon chamber, and the 50,000-liter dual- or single-mode SAPRC outdoor Teflon chamber. Prior to conducting these computer simulations, it was necessary to review and evaluate methods to represent the major chamber effects and the intensities and spectral distributions of the light sources for each chamber. The results of this evaluation are also documented in this report.

- The data from a total of 415 environmental chamber irradiations were used for model testing. These included NO_x-air, CO-NO_x-air, and background air irradiations carried out for chamber characterization purposes, NO_x-air irradiations of single organic compounds, NO_x-air irradiations of simple and complex mixtures of organic compounds, including some carried out under multi-day conditions, irradiations of auto exhaust, and several organic-NO_x-air experiments carried out under dynamic conditions. This testing program has resulted in a detailed assessment of the strengths and weaknesses of this mechanism in simulating results of environmental chamber experiments; and its results, documented in this report, will serve as a basis against which the performance of future kinetic mechanisms can be compared.

Although there were a number of experiments which were not well simulated by the model, the model simulated reasonably well the majority of the experimental data used for model testing. Many of the discrepancies observed, particularly in the simulations of the UNC outdoor chamber experiments, were of a random nature and suggested that these were due primarily to run-to-run varying chamber-dependent parameters, rather than being due to systematic errors in the chemical mechanism. No run-to-run adjustment of uncharacterized parameters to optimize the quality of the fits of model calculations to the experimental results was carried out, since such a procedure could mask any systematic errors in the chemistry, and thus defeat the major purpose in carrying out this testing program. Indeed, certain systematic discrepancies were observed in the model simulations of some groups of experiments, indicating problem areas in either the chemical mechanism or the representation of the chamber effects. In general, however, the performance of the model in simulating the results of the 415 experiments modeled was consistent with our current state of knowledge of chamber effects and the NO_x-air photooxidation mechanisms of organic compounds.

This report is divided into two volumes. Volume I contains the introduction, the documentation of the chemical mechanism, and the discussion of the chamber and light intensity characterization. Volume II gives the results of the model simulations of the environmental chamber experiments, the references, and the summary and conclusions section of this report, which includes a discussion of the work to be carried out in adapting this mechanism for use in atmospheric modeling.

TABLE OF CONTENTS

Page

Disclaimer ii

Abstract iii

Acknowledgments xi

VOLUME I

I. INTRODUCTION I-1

II. CHEMICAL MECHANISM II-1

- A. Inorganic Reactions II-4
- B. General Peroxy and Acyl Peroxy Radical Reactions II-27
  - 1. Peroxy + NO and Peroxy + NO_2 Reactions II-28
  - 2. Peroxy + HO_2 Reactions II-30
  - 3. Peroxy + Peroxy Radical Reactions II-33
  - 4. Tests of Effects of the Approximations Employed II-39
- C. Oxygenate and Alkyl Nitrate Reaction Mechanisms II-47
  - 1. Reactions of Formaldehyde II-47
  - 2. Reactions of Acetaldehyde II-55
  - 3. Reactions of Propionaldehyde II-61
  - 4. Reactions of Acetone II-67
  - 5. Reactions of Methyl Ethyl Ketone II-70
  - 6. Reactions of Glyoxal II-75
  - 7. Reactions of Methylglyoxal II-81
  - 8. Reactions of Biacetyl II-83
  - 9. Reactions of Glycolaldehyde II-86
  - 10. Reactions of 2-Butyl Nitrate II-90
  - 11. Reactions of 4-Heptyl Nitrate II-94
  - 12. Reactions of 3-Pentanol II-99
- D. Reactions of Alkenes II-103
  - 1. Reactions of Ethene II-103
  - 2. Reactions of Propene II-109
  - 3. Reactions of 1-Butene II-120
  - 4. Reactions of _trans_-2-Butene II-131
  - 5. Reactions of Isobutene II-138
  - 6. Reactions of the Thermalized Biradicals II-147
  - 7. General $\geq C_3$ Monoalkene Model II-150

TABLE OF CONTENTS
(continued)

Page

E. Reactions of the C_2-C_4 Alkanes II-157
  1. Reactions of Ethane II-157
  2. Reactions of Propane II-157
  3. Reactions of n-Butane II-160
  4. Reactions of Isobutane II-165
F. Reactions of the Higher Alkanes II-170
  1. Summary of Alkane Photooxidation Reactions II-170
    a. Initial Reaction with OH Radicals II-171
    b. Alkyl Nitrate Formation in the Reactions of Peroxy Radicals with NO II-172
    c. Alkoxy Radical Reactions II-176
    d. Reactions of α-Hydroxy Radicals II-181
    e. Cycloalkanes II-182
  2. Representation of the Alkane Photooxidation Products II-182
    a. Compounds Represented Explicitly II-183
    b. "Lost Carbon" and "Lost Nitrogen" II-183
    c. Alkyl Nitrates II-183
    d. $\geq C_3$ Aldehydes II-184
    e. $\geq C_4$ Ketones II-184
    f. Other Products II-185
  3. Representation of Higher Alkane Reactions in the Model II-186
  4. Models for Specific Alkanes II-192
G. Reactions of Aromatic Hydrocarbons II-207
  1. Reactions of Benzene II-207
  2. Reactions of Toluene II-215
  3. Reactions of m-Xylene II-219
  4. Reactions of o-Xylene II-221
  5. Reactions of 1,3,5-Trimethylbenzene II-223
  6. Reactions of Benzaldehyde II-225
  7. Reactions of Phenols, Cresols, and Nitrophenols II-231

TABLE OF CONTENTS
(continued)

Page

8. Reactions of the Unknown Aromatic Ring-Opened Products II-241
    a. OH Radical Reactions II-245
    b. Photolysis Reactions II-252
    c. Other Reactions II-258

III. CHAMBER AND LIGHT INTENSITY CHARACTERIZATION III-1
  A. Light Characterization III-5
    1. Indoor Chambers III-5
      a. Light Intensity III-6
      b. Spectral Distribution III-9
    2. Outdoor Chambers III-10
  B. Chamber Radical Sources III-29
    1. The SAPRC Evacuable Chamber III-30
      a. Continuous Radical Source III-30
      b. Initial Nitrous Acid III-35
    2. Teflon Film Chambers III-36
      a. Continuous Radical Sources in the SAPRC Teflon Chambers III-36
      b. OH Radical Flux in the UNC Chamber III-38
      c. Formaldehyde Offgassing in the UNC Chamber III-39
      d. Dark Formation of HONO from NO_2 III-46
      e. Initial HONO in Teflon Chambers III-47
  C. NO_x Offgassing III-48
    1. The SAPRC Evacuable Chamber III-56
    2. The SAPRC Indoor Teflon Chamber III-57
    3. The SAPRC Outdoor Teflon Chamber III-57
    4. The UNC Outdoor Chamber III-58
  D. Other Heterogeneous Processes III-60
    1. N_2O_5 Hydrolysis III-60
    2. Wall Loss of Ozone III-62
    3. Wall Loss of Nitric Acid III-63
    4. Wall Loss of H_2O_2 III-64
    5. Offgassed or Background Reactive Organics III-65

TABLE OF CONTENTS
(continued)

Page

E. Other Chamber- and Run-Dependent Parameters III-67
  1. Dilution III-67
  2. Temperature III-68
  3. Humidity III-69

VOLUME II

IV. MODEL SIMULATIONS OF ENVIRONMENTAL CHAMBER EXPERIMENTS IV-1
  A. Experiments Employed for Model Testing IV-3
    1. UNC Chamber Experiments IV-3
    2. SAPRC Evacuable Chamber Experiments IV-7
    3. SAPRC Indoor Teflon Chamber Experiments IV-9
    4. SAPRC Outdoor Teflon Chamber Experiments IV-10
  B. Criteria Employed to Assess Model Performance IV-14
    1. Maximum Ozone Yields IV-14
    2. Measurements of "Timing" of Ozone Formation and NO Oxidation IV-15
    3. Other Product Yields IV-18
    4. Reactant Consumption Rates IV-18
    5. Role of Analytical Uncertanties in Assessing Model Performance IV-19
      a. Ozone IV-19
      b. NO IV-21
      c. NO_2 IV-21
      d. Hydrocarbon Reactants IV-22
      e. PAN and PPN IV-23
      f. Formaldehyde IV-24
      g. Other Photooxidation Products IV-26
      h. Characterization Data IV-27
  C. Characterization Runs IV-28
    1. NO_x-Air, Tracer-NO_x-Air, and CO-NO_x-Air Runs IV-28
    2. Acetaldehyde-Air Irradiations IV-33
    3. Background Air Irradiations IV-35

TABLE OF CONTENTS
(continued)

Page

D. Single-Component NO_x-Air Irradiations IV-38

1. Formaldehyde-Air Runs IV-38
2. Formaldehyde-NO_x-Air Runs IV-43
3. Acetaldehyde-NO_x-Air Runs IV-53
4. Propionaldehyde-NO_x-Air Runs IV-57
5. Acetone-NO_x-Air and Methyl Ethyl Ketone-NO_x-Air Runs IV-57
6. Ethene-NO_x-Air Runs IV-61
7. Propene-NO_x-Air Runs IV-69
8. 1-Butene-NO_x-Air Runs IV-87
9. _trans_-2-Butene-NO_x-Air Runs IV-97
10. Isobutene-NO_x-Air Run IV-100
11. n-Butane-NO_x-Air Runs IV-101
12. 2,3-Dimethylbutane-NO_x-Air Runs IV-120
13. Isopentane and Isooctane-NO_x-Air Runs IV-127
14. $\geq C_5$ n-Alkane-NO_x-Air Runs IV-130
15. Benzene-NO_x-Air Runs IV-137
16. Toluene-NO_x-Air Irradiations IV-144
17. o- and m-Xylene-NO_x-Air Runs IV-154
18. 1,3,5-Trimethylbenzene-NO_x-Air Runs IV-160

E. Multi-Component Irradiations and Dynamic Experiments IV-167

1. Mixed Alkene Irradiations IV-167
2. EC Mixed Alkane Runs IV-168
3. UNC Mixed Aromatic Runs IV-184
4. Mixed Alkane + Alkene Runs IV-184
5. Other Two- or Three-Component Runs IV-195
6. EC Seven-Hydrocarbon Mix Runs IV-206
7. ITC "Mini-Surrogate," Incremental Reactivity Runs IV-206
8. ITC "SAI Surrogate" Multi-Day Runs IV-225
9. OTC "SAI Surrogate" Multi-Day Runs IV-236

TABLE OF CONTENTS
(concluded)

Page

10. Runs Employing Miscellaneous UNC Mixtures IV-249
    a. Lumping Technique Employed IV-249
    b. Results of Model Simulations IV-253
11. UNC Dynamic Experiments IV-263

F. UNC Auto Exhaust Experiments IV-274
    1. Hydrocarbon Speciation and Lumping IV-275
    2. Results of Model Calculations IV-280

V. SUMMARY, CONCLUSIONS, AND FUTURE EFFORTS V-1
    A. Updated Chemical Mechanisms and Remaining Uncertainties V-4
        1. Mechanism Updates and Species Represented V-4
        2. Major Uncertainties in the Mechanisms V-7
    B. Summary of Results of Testing Program V-14
        1. Chamber Effects and Light Source Characterization and Uncertainties V-15
        2. Results of Model Testing V-20
    C. Adaptation of the Mechanism for Atmospheric Modeling V-28

VI. REFERENCES VI-1

ACKNOWLEDGMENTS

We wish to gratefully acknowledge the following people at SAPRC for their contributions to this program and their assistance in the preparation of this report: Ms. Joanne E. Lohnes and Ms. Virpi Lindfors for their major efforts in carrying out the data processing needed to carry out the model testing calculations, Ms. Minn P. Poe and Ms. Susan E. Heffron for computer programming assistance, Ms. Minn P. Poe for preparation of the plots used in this report, Ms. Christy J. LaClaire for carrying out the word processing tasks involved in preparation of this report, and the student assistants Monica L. Murata, Bret M. McMillan, Scott M. Harris, and John T. Wood. We are also extremely grateful to Dr. Harvey E. Jeffries and Dr. Kenneth G. Sexton of UNC for taking the time to explain in detail the operations of the UNC chamber and for many other helpful discussions. Finally, we wish to acknowledge the EPA Contract Officer, Dr. Marcia C. Dodge, for assistance in planning this program, and thank her for her detailed reviews and comments on drafts of this report, and for helpful discussions.

SECTION I

INTRODUCTION

In order to develop appropriate control strategies to reduce ambient levels of ozone in those urban airsheds currently not in compliance with the Federal air quality standards, the U. S. Environmental Protection Agency (EPA) requires reliable and scientifically valid means to relate the emissions of reactive organic gases and oxides of nitrogen (NO_x) to ambient ozone levels. A key component of any such approach involves the chemical mechanism employed to describe the complex chemistry occurring during the atmospheric transport of these oxides of nitrogen and reactive organic compounds from source-to-receptor. The development of such chemical mechanisms was initiated in the late '60s and early '70s as part of the overall effort for developing computer models aimed at calculating ambient ozone levels given the emission rates of organics and NO_x. Several smog chamber studies were initiated during this period to obtain data concerning the ozone forming potential of irradiated hydrocarbon-NO_x-air mixtures (Altshuller et al. 1967, Dimitriades 1970, Glasson and Tuesday 1970, Wilson and Doyle 1970, Dodge and Bufalini 1972, Laity et al. 1973). These and later experimental investigations, principally carried out using the environmental chamber facilities at the University of North Carolina (UNC) and at the Statewide Air Pollution Research Center (SAPRC) at the University of California in Riverside, have led to the progressive development of a number of detailed chemical models (Niki et al. 1972, Demerjian et al. 1974, Hecht et al. 1974, Graedel et al. 1976, Dodge 1977, Falls and Seinfeld 1978, Hendry et al. 1978, Carter et al. 1979a, Demerjian and Schere 1979, Lloyd et al. 1979, Whitten et al. 1980a,b, Atkinson et al. 1980, Hov and Derwent 1981, Killus and Whitten 1982a,b, Sakamaki et al. 1981, Atkinson et al. 1982a, Penner and Walton 1982, McRae and Seinfeld 1983, Leone et al. 1984a,b, 1985, Lurmann et al. 1984, 1986). Many of these models (e.g., Niki et al. 1972, Demerjian et al. 1974, Carter et al. 1979a, Sakamaki et al. 1981) were developed specifically to simulate results of NO_x-air irradiations of single hydrocarbon or relatively simple hydrocarbon mixtures, while others (e.g., Dodge 1977, Demerjian and Schere 1979, Atkinson et al. 1982a, Killus and Whitten

1982a, Penner and Walton 1982) were designed to represent more complex mixtures of organics representative of real atmospheres.

Because of the large number of organic species which are emitted into urban airsheds, and because of computer constraints and data limitations, chemical models designed to represent the reactions of real-world emissions must necessarily contain approximations and condensation of species and reactions. The above-referenced models incorporate several alternative approaches in this regard; these approaches are illustrated in Figure I-1, which was taken from the review of McRae et al. (1983). The "surrogate species" approach employed in the mechanism of Dodge (1977), which was incorporated in the original version of the EKMA model for predicting ozone-precursor relationships, involved representing all the emitted organics by a propene-n-butane-aldehyde mixture with a set composition designed to simulate the Bureau of Mines irradiated auto exhaust chamber data (Dodge 1977). This approach lacks the flexibility to represent the effects of changing composition of the emitted organics, and has been superseded by the alternative lumped molecule or lumped structure approaches. These approaches are much more flexible in this regard, and are incorporated into the most recently developed models.

The lumped structure approach, as implemented in the Carbon Bond models developed at Systems Applications, Inc. (SAI) [Killus and Whitten 1982a], involves representing emitted compounds by lumped species which represent different parts of the molecule, such as single-bonded carbon atoms, double bonds, carbonyl groups, aromatic rings, etc. For example, propene is represented by one "olefin" specie representing its double bond + one "alkane" specie representing its single-bonded carbon group. This approach has the advantage that there is a straightforward procedure to represent any detailed mixture of organics by the limited number of lumped species used in the model. On the other hand, this approach has the disadvantage that it is based on the implicit assumption that the various parts of the organic molecules react independently of each other, which is now known to be generally incorrect. [For example, the higher alkanes undergo significant intramolecular hydrogen shift reactions (Atkinson and Lloyd 1984, Carter and Atkinson 1986), which cannot be represented by a "Carbon Bond" type model.] However, because of the potential utility of the Carbon Bond models in simulating complex mixtures using a limited

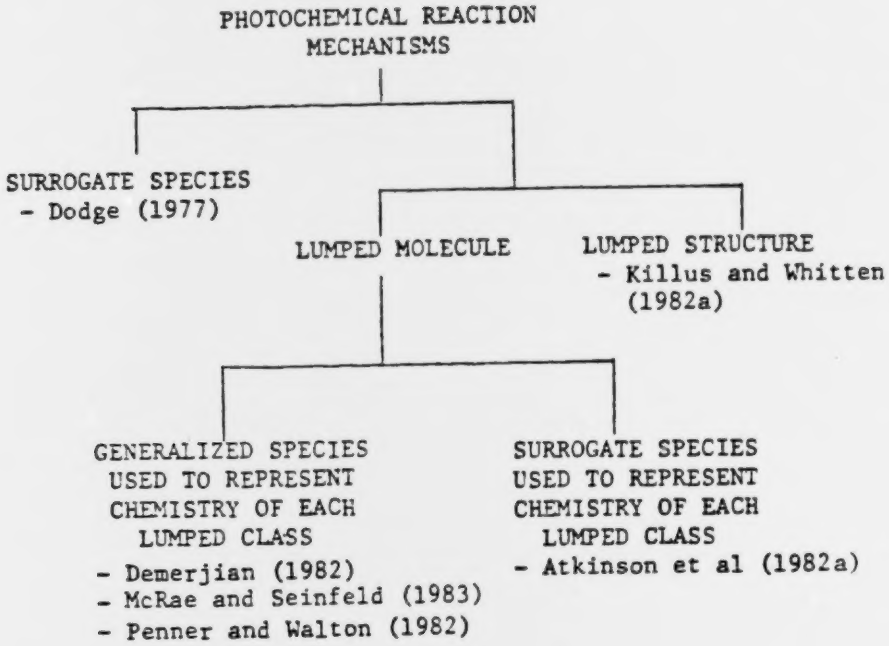
PHOTOCHEMICAL REACTION MECHANISMS
SURROGATE SPECIES
- Dodge (1977)
LUMPED MOLECULE
LUMPED STRUCTURE
- Killus and Whitten (1982a)
GENERALIZED SPECIES USED TO REPRESENT CHEMISTRY OF EACH LUMPED CLASS
- Demerjian (1982)
- McRae and Seinfeld (1983)
- Penner and Walton (1982)
SURROGATE SPECIES USED TO REPRESENT CHEMISTRY OF EACH LUMPED CLASS
- Atkinson et al (1982a)

Figure I-1. Classification of photochemical reaction mechanism (from McRae and Seinfeld 1983).

number of lumped species, the EPA has in recent years sponsored considerable research in its development and testing, and version III of the Carbon Bond model has been recommended for use in EKMA models as a replacement of the now seriously out-of-date Dodge (1977) model. Work on this model is continuing, and a fourth version (designated "Carbon Bond X") has recently been developed (Whitten et al. 1985).

The only significant alternative to the carbon bond approach which is implemented in current models is the "lumped molecule" approach, where a given specie is used to represent the reactions of all species in the same chemical class. For example, a model employing this approach may include the detailed explicit mechanism for propene, but the "propene" in the model may be used to represent the reactions of other chemically similar compounds such as 1-butene, etc. This approach has the advantage over the "lumped structure" approach such as employed in the Carbon Bond models in that it does not require the assumption that different parts of the molecule react independently. In addition, the detailed reactions of selected individual species can be represented exactly and new species can be readily added to the model without re-testing the model for all the other species, since mechanisms for the reactions of different compounds can be developed and tested independently. On the other hand, it is much more difficult to maintain a carbon balance employing this approach, and for some compounds (particularly bi- or poly-functional organics), it may not be clear which is the most appropriate specie, or set of species, to use in the model to represent its reactions.

As indicated in Figure I-1, the lumped molecule approach has been incorporated in a number of models which have been tested against selected results of environmental chamber experiments, and it is generally agreed that the model of Atkinson et al. (1982a), updated as suggested by Atkinson and Lloyd (1984) and carried out by Lurmann et al. (1984, 1986), is the most up-to-date and consistent with the most recent laboratory results. [For example, in carrying out their evaluation of different mechanisms, the "explicit mechanism" employed as the standard by Leone and Seinfeld (1984b) is essentially the same as the updated mechanism of Atkinson and co-workers (Atkinson et al. 1982a, Atkinson and Lloyd 1984).] However, despite its potential as an alternative approach to the Carbon Bond models for use in control strategy calculations, this model has not yet been as comprehensively developed and tested for this purpose as have the Carbon Bond models.

The need to examine alternative approaches for modeling complex mixtures in control strategy calculations has become apparent in recent years as a result of a number of studies in which the predictions of different models were compared (Hayes et al. 1980, Jeffries et al. 1981, Martinez and Maxwell 1981, Carter et al. 1982a, Hurt and Lurmann 1982, McRae et al. 1983). In general, different mechanisms were found to differ significantly not only in prediction of ozone levels, but also in the degree of emission controls required to reduce ozone to the desired levels. Leone and Seinfeld (1984b) were able to identify several specific aspects of the Carbon Bond model of Killus and Whitten (1982a) and the lumped molecule model of Atkinson et al. (1982a) which led to differences in their predictions, and recommended changes which could be made to each model which should lead to closer agreement. These changes primarily concerned updating the models to be consistent with the most recent laboratory results concerning photolysis rates and the aromatic photooxidation mechanisms, rather than changing the basic structure of the models. However, the most fundamental differences between the Carbon Bond model and that of Atkinson et al. (1982a) concern the general approach used to represent complex mixtures, and the effects of the differences between the two different lumping approaches that these models incorporate on the predictions of the models is still uncertain.

Because of the uncertainty concerning which species lumping approach is the most appropriate to use in control strategy calculations, it has been determined by the EPA that it is prudent to independently develop and test models based on both approaches. If the two independently developed models, based on alternative sets of approximations and assumptions, give rise to similar predictions on control strategy issues, then control officials can have much more confidence in the results. If, on the other hand, the two models give significantly different predictions, then the need for further research and development of such models before they can be used as a reliable planning tool will be evident. Thus, since as indicated above the EPA has in recent years been actively funding the development and testing of the Carbon Bond models for use in control strategy calculations, an analogous program to develop and test a model employing the "lumped molecule" approach for use in control strategy calculations was initiated.

This two-year program is being carried out by Environmental Research and Technology, Inc. (ERT) with the Statewide Air Pollution Research Center (SAPRC) at the University of California, Riverside, as a subcontractor. This program consists of two phases. The first phase, which was carried out primarily at SAPRC, is now complete and its results are discussed in this report. The specific accomplishments of this phase of this program are as follows:

- The mechanism of Atkinson et al. (1982a) has been completely updated to take into account the most recent laboratory results. The previous updates of Atkinson and Lloyd (1984) and Lurmann et al. (1984, 1986) were used as a starting point, though many aspects of the mechanism, particularly those concerning the reactions of the higher alkanes and the aromatics, were completely re-evaluated and a number of modifications were made. In addition, explicit mechanisms for a number of new species have been developed. Specifically, detailed explicit mechanisms have been derived for the C_2 through C_4 alkanes; the alkenes ethene, propene, 1-butene and trans-2-butene; the aromatics benzene, toluene, o-xylene, m-xylene, and 1,3,5-trimethylbenzene; the representative oxygenated products formaldehyde, acetaldehyde, propionaldehyde, acetone, methyl ethyl ketone, 3-pentanol, glyoxal, methylglyoxal, biacetyl, and benzaldehyde, and the representative organic nitrates 2-butyl nitrate and 4-heptyl nitrate. In addition, "lumped reaction" mechanisms for the higher alkanes n-pentane through n-nonane, 2-methyl butane, 2,3-dimethyl butane, and 2,2,4-trimethylpentane (isooctane), and parameterized, mechanisms for the reactions of cresols and the uncharacterized ring-opening products formed in the photooxidations of the aromatic hydrocarbons were developed. In some cases, parameters in the mechanisms whose appropriate values are not known a-priori were adjusted to yield acceptable fits to the environmental chamber data. The updated and expanded mechanisms are completely documented in Section II of this report.

- The updated and expanded mechanisms were tested against results of 415 environmental chamber experiments carried out using the dual 150,000-liter outdoor chamber at UNC, the SAPRC 5800-liter evacuable chamber (EC), the SAPRC 6400-liter indoor Teflon chamber (ITC), and the SAPRC 50,000-

liter single- or dual-mode outdoor Teflon chamber (OTC). In order to accomplish this testing procedure, it was first necessary to evaluate the most appropriate methods to represent the intensity and spectral distribution of the light source employed in the chamber (in order to calculate the photolysis rates), and the most appropriate methods to represent the major chamber effects and chamber-dependent parameters for each chamber. The results of this evaluation of the light and chamber-dependent parameters for these four chambers, and the specific assumptions incorporated in the model when simulating experiments carried out in these chambers, are documented in Section III of this report.

- The chemical mechanism and the chamber effects model was tested against the results of a total of 420 environmental chamber experiments carried out in the four chambers listed above. This testing of the chemical mechanism was carried out without any run-to-run adjustment of uncharacterized parameters to optimize the quality of the fits of model calculations to the experimental results. Such run-to-run adjustment is not considered appropriate to the purpose of testing the validity of the mechanism, since these adjustments could mask possible systematic errors in the chemistry. The numbers of each type of experiment carried out in each chamber used for model testing in this study are summarized in Table I-1, and the results of these model simulations are discussed in Section IV of this report.

As far as we are aware, this is the largest set of environmental chamber data ever used for the testing of a single chemical kinetic model. The second phase of this two-phase program, which is scheduled to be completed in late 1986, involves adapting the model developed and tested in the first phase for use in EKMA and other box-type airshed models, carrying out sensitivity tests on the model, and formulating and testing condensed versions of the mechanism suitable for use in multi-celled airshed models. The work to be carried out in this phase is briefly discussed in the summary and conclusions section of this report.

Table I-1. Summary of Environmental Chamber Runs Which Have Been Used for Model Testing

Types of Runs	Number of Runs[a] UNC	EC	ITC	OTC
Background air; NO_x-air; Tracer-NO_x-air; and CO-NO_x-air	25	7	5	5
HCHO-air and HCHO-NO_x-air	13	7	1	2
Acetaldehyde-air and Acetaldehyde-NO_x-air	9	3	2	5
Propionaldehyde-, MEK-, or Acetone-NO_x-air	5			
o-Cresol-NO_x-air		1		
Ethene-NO_x-air	6	6		
Propene-NO_x-air	22	15	3	5
Dynamic propene-NO_x-air	5			
1-Butene-NO_x-air	4	3		
trans-2-Butene-NO_x-air	1	3		
Isobutene-NO_x-air			1	
n-Butane-NO_x-air	7	14	3	1
$\geq C_5$ Alkane-NO_x-air	6	6	8	
Benzene-NO_x-air			6	
Toluene-NO_x-air	5	13	2	
m-Xylene-NO_x-air		4	2	
o-Xylene-NO_x-air	4			
1,3,5-Trimethylbenzene-NO_x-air		3	5	
2-, 3- and 4-Component runs, no aromatics	13	16		
2- and 3-Component runs, with aromatics	9	7		
Dynamic propene-n-butane-toluene-NO_x-air	4			
"Mini-surrogate"-NO_x-air runs (from SAPRC-ARB incremental reactivity study)[b]			18	
Surrogate-NO_x-air runs (from SAPRC-EPA study of multi-day effects)[c]			6	25
Miscellaneous multi-component runs	25	11		
Auto exhaust runs	28			
Totals (Grand Total = 415 runs)	191	119	62	43

[a] UNC = UNC outdoor chamber; EC = SAPRC evacuable indoor chamber; ITC = SAPRC indoor Teflon chamber; OTC = SAPRC outdoor Teflon chamber.

[b] Runs carried out under California ARB Contract No. A0-105-32 (Atkinson et al. 1983a).

[c] Runs carried out under EPA Cooperative Agreement No. CR810260-01 (Carter et al. 1985).

SECTION II

CHEMICAL MECHANISM

In this section, the updated chemical mechanisms for representative alkanes, alkenes, and aromatic hydrocarbons and their major atmospheric photooxidation products are discussed in detail. This discussion is organized into seven sub-sections, grouped by classes of compounds, and the reactions are numbered consecutively within each group. In Section A, the inorganic portion of the reaction mechanism, i.e., the reactions involving only NO_x, O_x, and HO_x species and those of CO and SO_2, are discussed. In Section B, the manner in which the reactions of alkyl peroxy (RO_2) and acyl peroxy (RCO_3) radicals are represented in the model is discussed. These species are involved in the atmospheric reactions of essentially all of the organics, and several approximations, which have not been previously employed in published models, are employed in the present work. These approximations allow for the representation of their reactions with each other without unduly increasing the size of the model. Section C deals with the reactions of the non-aromatic oxygenate and organic nitrate photooxidation products, Section D gives the detailed reactions of the alkenes, and Section E gives the detailed reactions of the C_2-C_4 alkanes. Because of their greater complexity, the reactions of the higher ($\geq C_5$) alkanes are represented using a "lumped reaction" scheme in this model, and this scheme, and the kinetic and mechanistic principles used to derive the parameters involved for specific alkanes, are discussed in Section F. Finally, in Section G, the photooxidation mechanisms of representative aromatic hydrocarbons are discussed, together with the reactions of the representative aromatic products benzaldehyde, nitrophenol, and o-cresol, and the empirical model used to represent the reactions of the uncharacterized aromatic ring-opened products.

The reaction mechanism used in this model, which can be considered to be an update and extension of the model of Atkinson et al. (1982a) as updated by Lurmann et al. (1984, 1986), is based to a large extent on the recent evaluations and reviews of relevant kinetic and mechanistic data carried out by Atkinson and co-workers (Atkinson and Lloyd 1984, Atkinson and Carter 1984, Carter and Atkinson 1985, Atkinson 1986). Thus, in many cases those references should be consulted for details of how specific rate constants or mechanistic assumptions were derived, and for citations to the relevant laboratory studies. However, in some cases more recent data supercede the recommendations given in one or more of these reviews; while in other cases, the model simulations of the environmental chamber experiments carried out in this study indicate that alternative assumptions concerning uncertain mechanistic details have to be made in order for the model predictions to be consistent with the experimental data. This is particularly true of the aromatic photooxidation mechanisms discussed in Section G, where recent laboratory studies showed that mechanisms previously assumed for these compounds are incorrect in several significant respects, and where, because of our lack of knowledge concerning the products formed in the ring-opening reactions, use of a semi-empirical model with parameters adjusted to fit the chamber data is required. In addition, this model incorporates a number of species and reactions which have not previously been included in the models and evaluations of Atkinson and co-workers. Those new aspects of this model are discussed in detail in the following sections.

The documentation of the reaction mechanism given in the following sections is intended to be complete in that it contains all the information necessary to implement the mechanism for computer modeling of conditions in the lower troposphere. Rate constants and (where appropriate) mechanistic parameters are given over the temperature range applicable for lower tropospheric modeling. In cases where the temperature dependences are unknown but believed to be non-negligible, they are estimated. For photolysis reactions, the absorption coefficients and quantum yields are given as a function of wavelength for the wavelength region of importance in the troposphere (and in the environmental chamber experiments used for model testing). These absorption coefficients and quantum yields are used to calculate the photolysis rates under solar lighting conditions and for environmental chamber experiments for which the spectral distribution and intensity of the light source is known or can be estimated. (The methods used to calculate the photolysis rates in the indoor and outdoor chamber experiments, given these absorption coefficients and quantum yields, are discussed in Section III of this report.) Since this model is intended to be used primarily for lower tropospheric simulations, the pressure dependences of the rate constants and reaction mechanisms have not been incorporated in this model, nor are reactions included which may be important in the stratosphere or other regions of the atmosphere, but which are believed to be of minor importance under tropospheric conditions.

The chemical mechanism discussed in the following sections has been implemented on the computer modeling software presently employed at SAPRC. The input files used by the SAPRC model preparation program to implement this model are available from the authors upon request.

II. A. INORGANIC REACTIONS

In this section, the inorganic portion of the reaction mechanism used for modeling photochemical transformations in the troposphere and in polluted urban atmospheres is discussed. The species involved include O_2, O_3, the oxides of nitrogen (NO, NO_2, NO_3, N_2O_5), HONO, HNO_3, the oxyradicals OH and HO_2, H_2O_2 and CO and CO_2. The reactions involved include both thermal and photolytic reactions. For thermal reactions, the temperature dependences of the rate constants are given for the range of temperatures appropriate for the troposphere. For photolytic reactions, the absorption coefficients and quantum yields are given as a function of wavelength for the spectral region relevant to modeling the lower troposphere. In most cases the rate constant or absorption coefficient and quantum yield assignments are based on the evaluation of Atkinson and Lloyd (1984), though some exceptions are noted, and a few minor reactions are included here which were not discussed by Atkinson and Lloyd (1984).

The discussion in this section is limited to the reactions believed to be homogeneous gas phase processes. Thus these reactions would be included in both smog chamber models and in atmospheric simulation models. However, some of the inorganic species whose reactions are discussed in this section also undergo heterogeneous, surface-dependent reactions, some of which may be appropriate only for smog chamber models. These processes are discussed in Section III, in conjunction with our discussion of the model for chamber effects.

A1. $NO_2 + h\nu \rightarrow NO + O(^3P)$

This is the key reaction in the formation of O_3 from nitrogen oxides. The NO_2 absorption cross sections and quantum yields for its photodissociation are those recommended by Atkinson and Lloyd (1984). They recommend that the quantum yield, ϕ, in the region $295 \leq \lambda \leq 375$ nm be obtained from the expression

$$\phi = 1.00 - 0.0025\ (\lambda - 295)\ \text{nm}$$

Above 375 nm, the quantum yield data of Harker et al. (1977) is recommended. The absorption cross sections used are those recommended by NASA (1985). The absorption cross sections, σ, and the quantum yields, ϕ, used are shown in Table II-1.

A2. $O(^3P) + O_2 + M \rightarrow O_3 + M$

This reaction is the primary direct cause of ozone formation in the lower troposphere. We use the NASA evaluation (1985) which gives

$$k_{A2} = 6.0 \times 10^{-34} (T/300)^{-2.3} \text{ cm}^6 \text{ molecule}^{-2} \text{ sec}^{-1} \text{ for } M = \text{air}$$

$$= 6.1 \times 10^{-34} \text{ cm}^6 \text{ molecule}^{-2} \text{ sec}^{-1} \text{ at 298 K.}$$

Table II-1. NO_2 Absorption Cross Sections, σ, (cm^2 $molecule^{-1}$, base e), and Photocomposition Quantum Yields, ϕ, at 298 K

Wavelength (nm)	$10^{19} \times \sigma$ (cm^2)	ϕ	Wavelength (nm)	$10^{19} \times \sigma$ (cm^2)	ϕ
280	0.554	1.0	350	4.10	0.86
285	0.699	1.0	355	5.13	0.85
290	0.818	1.0	360	4.51	0.84
295	0.697	1.0	365	5.78	0.83
300	1.17	0.99	370	5.42	0.81
305	1.66	0.98	375	5.35	0.73
310	1.76	0.96	380	5.99	0.81
315	2.25	0.95	385	5.94	0.70
320	2.54	0.94	390	6.00	0.74
325	2.79	0.93	395	5.89	0.81
330	2.99	0.91	400	6.76	0.65
335	3.45	0.90	405	6.32	0.32
340	3.88	0.89	410	5.77	0.14
345	4.07	0.88	415	6.30	0.07
			420	6.23	0.02

A3. $O(^3P) + NO_2 \rightarrow NO + O_2$ (a)

$\overset{M}{\rightarrow} NO_3$ (b)

These reactions can be non-negligible in polluted urban areas or in smog chamber experiments with relatively high NO_x levels. For the reaction forming O_2, NASA (1985) recommends

$$k_{A3a} = 9.3 \times 10^{-12} \text{ cm}^3 \text{ molecule}^{-1} \text{ sec}^{-1},$$

independent of temperature, with an uncertainty in the 298 K value of ±10%. For the combination reaction, NASA (1985) recommends

$$k_{A3b} = (9 \pm 1) \times 10^{-32} (T/300)^{-2\pm1} \text{ cm}^6 \text{ molecule}^{-2} \text{ sec}^{-1}$$

$$= 9.1 \times 10^{-32} \text{ cm}^6 \text{ molecule}^{-2} \text{ sec}^{-1} \text{ at 298 K},$$

which is applicable up to atmospheric pressure.

A4. $NO + O_3 \rightarrow NO_2 + O_2$

This reaction, the reverse of reactions 1a and 1b, converts NO to NO_2 and destroys O_3 in the process. These reactions essentially compose the "photostationary state" in which O_3 is formed and destroyed in the reverse and forward reaction. The rate expression recommended by NASA (1985) and Atkinson and Lloyd (1984) for this reaction is used:

$$k_{A4} = 1.8 \times 10^{-12} e^{-2720/RT} \text{ cm}^3 \text{ molecule}^{-1} \text{ sec}^{-1}$$

$$= 1.8 \times 10^{-14} \text{ cm}^3 \text{ molecule}^{-1} \text{ sec}^{-1} \text{ at 298 K},$$

(where R is in units of cal K^{-1} $mole^{-1}$) with an estimated uncertainty at 298 K of a factor of 1.2.

A5. $NO_2 + O_3 \rightarrow NO_3 + O_2$

This reaction forms the NO_3 radical, which plays an important role in nighttime chemistry and in the formation of HNO_3 (Atkinson et al. 1984). The rate constant expression chosen is that recommended by NASA (1985) and Atkinson and Lloyd (1984):

$$k_{A5} = 1.2 \times 10^{-13}\ e^{-4870/RT}\ \mathrm{cm}^3\ \mathrm{molecule}^{-1}\ \mathrm{sec}^{-1}$$

$$= 3.2 \times 10^{-17}\ \mathrm{cm}^3\ \mathrm{molecule}^{-1}\ \mathrm{sec}^{-1}\ \text{at } 298\ \mathrm{K},$$

with an uncertainty of a factor of 1.15 at 298 K.

A6. $NO + NO_3 \rightarrow 2\ NO_2$

This reaction provides a mechanism to oxidize NO, particularly during nighttime. Based upon the data of Graham and Johnston (1978), Atkinson and Lloyd (1984) recommended:

$$k_{A6} = 8 \times 10^{-12}\ e^{500/RT}\ \mathrm{cm}^3\ \mathrm{molecule}^{-1}\ \mathrm{sec}^{-1}$$

$$= 1.9 \times 10^{-11}\ \mathrm{cm}^3\ \mathrm{molecule}^{-1}\ \mathrm{sec}^{-1}\ \text{at } 298\ \mathrm{K},$$

with an uncertainty of a factor of 3 at 298 K (NASA 1983).

A7. $2\ NO + O_2 \rightarrow 2\ NO_2$

This reaction is important at higher concentrations of NO, but is generally relatively minor in the troposphere. Atkinson and Lloyd (1984) recommend the use of the NBS (1978) recommendation of

$$k_{A7} = 3.3 \times 10^{-39}\ e^{1050/RT}\ \mathrm{cm}^6\ \mathrm{molecule}^{-2}\ \mathrm{sec}^{-1}$$

$$= 2.0 \times 10^{-38}\ \mathrm{cm}^6\ \mathrm{molecule}^{-2}\ \mathrm{sec}^{-1}\ \text{at } 298\ \mathrm{K}$$

A8. $NO_2 + NO_3 \xrightarrow{M} N_2O_5$

This is an important reaction in the formation of nitric acid since N_2O_5 reacts with water vapor to produce HNO_3. There are still significant uncertainties associated with the kinetics for this reaction. Atkinson and Lloyd (1984) recommended the very recent direct experimental data of Kircher et al. (1984), of

$$k_{A8} = \left\{\frac{k_o(T)[M]}{1 + \left(\frac{k_o(T)[M]}{k_\infty(T)}\right)}\right\} F^{\left\{1 + [\frac{1}{N} \log_{10}(k_o(T)[M]/k_\infty(T))]^2\right\}^{-1}}$$

cm^3 $molecule^{-1}$ sec^{-1}, where

$N = 0.972$

$k_o(T) = 2.0 \times 10^{-30} (T/300)^{-4.3}$ cm^6 $molecule^{-2}$ sec^{-1},

$k_\infty(T) = 1.4 \times 10^{-12} (T/300)^{-0.5}$ cm^3 $molecule^{-1}$ sec^{-1}, and

$F = 0.6$ and $[M]$ = concentration of air in molecule cm^{-3}

and

$k_{A8} = 1.2 \times 10^{-12}$ cm^3 $molecule^{-1}$ sec^{-1} at 298 K and 760 torr total pressure.

These experimental data of Kircher et al. (1984) yield rate constants in good agreement with the rate expressions proposed by Malko and Troe (1982). In view of the uncertainties associated with this reaction, the rate constants derived are expected to be good to a factor of 1.5.

A9. $N_2O_5 \xrightarrow{M} NO_2 + NO_3$

We recommend the evaluation of Malko and Troe (1982). However, we will formulate this rate constant by the use of k_{A8} as given above, together with the equilibrium constant $K_{A8,A9}$ given by Kircher et al. (1984) of

$$K_{A8,A9} = 3.15 \times 10^{-30}\ T\ e^{11350/T}\ \mathrm{cm}^3\ \mathrm{molecule}^{-1}$$

Hence,

$$k_{A9} = k_{A8}/K_{A8,A9} = k_{A8} \times 1.06 \times 10^{27} (T/300)^{-1.0}\ e^{-22550/RT}\ \mathrm{sec}^{-1}$$

$$= 0.037\ \mathrm{sec}^{-1} \text{ at } 298\ \mathrm{K}$$

This equilibrium constant derived by Kircher et al. (1984) is in reasonable agreement with recent direct measurements of Tuazon et al. (1984a), Perner et al. (1985) and Burrows et al. (1985). However, there is a total spread of a factor of 1.5 between these equilibrium constant measurements at 298 K, and this uncertainty must be factored into the overall uncertainty in k_{A9}.

A10. $N_2O_5 + H_2O \rightarrow 2\ HNO_3$

This reaction is potentially important in the formation of nitric acid, particularly during nighttime and foggy conditions. Atkinson and Lloyd (1984) have summarized the experimental studies of this reaction. The most recent direct experimental data obtained by Tuazon et al. (1983) indicates that the rate constant for this reaction is:

$$k_{A10} \leq 1.3 \times 10^{-21}\ \mathrm{cm}^3\ \mathrm{molecule}^{-1}\ \mathrm{sec}^{-1} \text{ at } 298\ \mathrm{K}.$$

Analysis of ambient data (Atkinson et al. 1986a) indicate that this reaction may be important in nighttime atmospheres if k_{A10} has the upper limit value given above.

No studies have been reported on the temperature dependence of the rate constant. For modeling purposes, we recommend using a rate constant of:

$$k_{A10} = 1.0 \times 10^{-21}\ \mathrm{cm}^3\ \mathrm{molecule}^{-1}\ \mathrm{sec}^{-1}$$

This rate constant is strictly an upper limit derived from chamber experiments, but an analysis of ambient air data carried out by Atkinson et al. (1986a) indicate that this value is in the range appropriate for tropospheric modeling.

Since nothing is known about the temperature dependence of this reaction, we assume k_{A10} is independent of temperature, though this is probably not the case.

A11. $NO_3 + NO_2 \rightarrow NO + NO_2 + O_2$

The only data available for this reaction are those of Graham and Johnston (1978):

$$k_{A11} = 2.5 \times 10^{-14} e^{-2440/RT} \text{ cm}^3 \text{ molecule}^{-1} \text{ sec}^{-1}$$

$$= 4.0 \times 10^{-16} \text{ cm}^3 \text{ molecule}^{-1} \text{ sec}^{-1} \text{ at 298 K,}$$

with an estimated uncertainty of a factor of 2 at 298 K (Atkinson and Lloyd 1984).

A12. $NO_3 + h\nu \rightarrow NO + O_2$ (a)

$\xrightarrow{O_2} NO_2 + O(^3P)$ (b)

Daytime concentrations of the NO_3 radical are much lower than nighttime concentrations because the NO_3 radical undergoes photodissociation by sunlight. As discussed by Atkinson and Lloyd (1984), the absorption cross sections of Graham and Johnston (1978) have been verified by the later work of Marinelli et al. (1982). These absorption cross sections, averaged over 5 nm intervals, are given in Table II-2. The most recent and complete study of the quantum yields for the photodissociation of the NO_3 radical is that of Magnotta and Johnston (1980). This work showed that the photodissociation pathway predominates, and we recommend the quantum

Table II-2. Absorption Cross Sections, σ, (cm^2 $molecule^{-1}$, base e), for NO_3 and Quantum Yields for Formation of NO, ϕ_a, and NO_2, ϕ_b, Averaged Over 5 nm Intervals

λ (nm)	$10^{19} \times \sigma$ (cm^2)	ϕ_a	ϕ_b
400	0.00	1.0	0.0
405	0.30	1.0	0.0
410	0.40	1.0	0.0
415	0.50	1.0	0.0
420	0.80	1.0	0.0
425	1.00	1.0	0.0
430	1.30	1.0	0.0
435	1.80	1.0	0.0
440	1.90	1.0	0.0
445	2.20	1.0	0.0
450	2.80	1.0	0.0
455	3.30	1.0	0.0
460	3.70	1.0	0.0
465	4.30	1.0	0.0
470	5.10	1.0	0.0
475	6.00	1.0	0.0
480	6.40	1.0	0.0
485	6.90	1.0	0.0
490	8.80	1.0	0.0
495	9.50	1.0	0.0
500	10.10	1.0	0.0
505	11.00	1.0	0.0
510	13.20	1.0	0.0
515	14.00	1.0	0.0
520	14.50	1.0	0.0
525	14.80	1.0	0.0
530	19.40	1.0	0.0
535	20.40	1.0	0.0
540	18.10	1.0	0.0
545	18.10	1.0	0.0
550	23.60	1.0	0.0
555	26.80	1.0	0.0
560	30.70	1.0	0.0
565	25.30	1.0	0.0
570	25.40	1.0	0.0
575	27.40	1.0	0.0
580	30.50	1.0	0.0
585	27.70	1.0	0.0
590	51.40	0.75	0.25
595	40.80	0.60	0.40
600	28.30	0.55	0.25
605	34.50	0.40	0.20
610	14.50	0.30	0.20
615	19.60	0.25	0.10
620	35.80	0.20	0.10
625	92.50	0.15	0.05
630	56.60	0.05	0.05
635	14.50	0.0	0.03
640	11.10	0.0	0.0

yield data from the study of Magnotta and Johnston (1980) for pathways (a) and (b) divided by a factor of ~1.5 (to yield total photodissociation quantum yields of unity at ~580-590 nm, since the raw data of Magnotta and Johnston (1980) yielded quantum yields of ~1.5 at λ = 580-590 nm). The quantum yields used were taken from a plot given by Magnotta and Johnston (1980) [reproduced in Figure A-2 of Atkinson and Lloyd (1984)], and are tabulated in Table II-2.

A13. $O_3 + h\nu \rightarrow O_2(^1\Delta_g) + O(^3P)$ (a)

$\rightarrow O_2(^1\Delta_g) + O(^1D)$ (b)

Absorption cross sections for O_3 have been measured in numerous studies. The cross sections are all in good agreement, and have been tabulated by Moortgat and Warneck (1975) for $297.5 \leq \lambda \leq 330.0$ nm and by Arnold et al. (1977) for $295 \leq \lambda \leq 320$ nm; the maximum deviations between these two sets of data being ~7%.

The quantum yield of $O(^1D)$ production, ϕ_b, can be best considered in the two wavelength regions $\lambda \leq 300$ nm and $\lambda \geq 300$ nm. As discussed by Atkinson and Lloyd (1984), despite two absolute quantum yield determinations below 300 nm which showed that ϕ_b was unity, recent data show that ϕ_b is significantly less than unity for $248 < \lambda < 300$ nm. The two molecular beam photofragment spectroscopic studies of Fairchild et al. (1978) and Sparks et al. (1980) show that ϕ_b ~0.90 at 266 nm and 274 nm, (with ϕ_b possibly increasing somewhat over the wavelength range 274-300 nm). Brock and Watson (1980a) have determined that $\phi_b = 0.88 \pm 0.02$ at 266 nm, while Amimoto et al. (1980) have reinvestigated this system and now obtain $\phi_b = 0.85 \pm 0.02$ at 248 nm. More recently, Wine and Ravishankara (1982) and Greenblatt and Wiesenfeld (1983) have obtained $\phi_b = 0.91 \pm 0.03$ and 0.94 ± 0.01, respectively, at 248 nm.

The quantum yield determinations for $\lambda > 300$ nm have generally been relative to $\phi_b = 1.00$ at 300 nm. The value of ϕ_b decreases rapidly for $\lambda > 305$ nm, and the recent data of Moortgat and Warneck (1975), Arnold et al. (1977) and Brock and Watson (1980b) at 298 K as a function of wavelength [the quantum yields are temperature dependent, with lower quantum yields at lower temperatures (Moortgat et al. 1977)] are in good agreement.

Since it is now evident that ϕ_b is less than unity for $\lambda \lesssim 300$ nm, we recommend that for $248 \lesssim \lambda \lesssim 300$ nm,

$$\phi_b = 0.90$$

For $\lambda \geq 300$ nm, NASA (1985) has recommended the value of ϕ_b, as a function of wavelength and temperature, derived from the mathematical expression of Moortgat and Kudszus (1978), scaled by a factor of 0.9. Thus

$$\lambda \geq 300 \text{ nm}; \ \phi_b(\lambda,T) = A(\tau)\arctan\,[B(\tau)(\lambda-\lambda_o(\tau))] + C(\tau)$$

where $\tau = T-230$ K; λ is in nm, and arctan is in radians, with

$$A(\tau) = 0.332 + 2.565 \times 10^{-4}\ \tau + 1.152 \times 10^{-5}\ \tau^2 + 2.313 \times 10^{-8}\ \tau^3$$

$$B(\tau) = -0.575 + 5.59 \times 10^{-3}\ \tau - 1.439 \times 10^{-5}\ \tau^2 - 3.27 \times 10^{-8}\ \tau^3$$

$$\lambda_o(\tau) = 308.20 + 4.4871 \times 10^{-2}\ \tau + 6.9380 \times 10^{-5}\ \tau^2 - 2.5452 \times 10^{-6}\ \tau^3$$

$$C(\tau) = 0.466 + 8.883 \times 10^{-4}\ \tau - 3.546 \times 10^{-5}\ \tau^2 + 3.519 \times 10^{-7}\ \tau^3$$

and, in the limits where $\phi_b\ (\lambda,T) > 0.90$, the quantum yield is set at $\phi_b = 0.90$, and similarly, for $\phi_b\ (\lambda,T) < 0$, the quantum yield is set at $\phi_b = 0$. The uncertainties in the above recommendations are expected to be less than ± 0.05 in absolute units in ϕ_b for $266 < \lambda < 320$ nm. The quantum yield for $O(^3P)$ production, ϕ_a, is assumed to be given by $(1 - \phi_b)$ in all the wavelength regions discussed above, i.e., $(\phi_a + \phi_b)$ is unity. Reaction (A13a) is of minor importance for atmospheric modeling purposes.

Table II-3 gives the O_3 absorption coefficients and quantum yields used for modeling purposes, based on the above recommendation, with the quantum yields, ϕ_b, given for several temperatures. For temperatures between those shown on Table II-3, the quantum yields are obtained by linear interpolation.

Table II-3. Absorption Cross Sections, σ, (cm^2 $molecule^{-1}$, base e), for O_3 and Quantum Yields for $O(^3P)$ Production, ϕ_a, and for $O(^1D)$ Production, ϕ_b, at Selected Wavelengths and Temperatures

	10^{20} x σ		ϕ_b		
(nm)	(cm^2)	ϕ_a	270 K	300 K	330 K
260	1070	0.10	0.90	0.90	0.90
270	774	0.10	0.90	0.90	0.90
280	379	0.10	0.90	0.90	0.90
290	134	0.10	0.90	0.90	0.90
300	38.0	0.10	0.90	0.90	0.90
305	18.8	0.11	0.86	0.89	0.90
310	9.8	0.44	0.46	0.56	0.63
313	7.5	0.74	0.16	0.26	0.36
315	5.2	0.87	0.07	0.13	0.22
317	4.16	0.95	0.03	0.05	0.12
320	2.60	1.0	0.0	0.0	0.03
330	0.67	1.0	0.0	0.0	0.0
340	0.17	1.0	0.0	0.0	0.0
350	0.04	1.0	0.0	0.0	0.0
355	0.0				
400	0.0				
450	0.016	1.0	0.0	0.0	0.0
500	0.134	1.0	0.0	0.0	0.0
550	0.332	1.0	0.0	0.0	0.0
600	0.506	1.0	0.0	0.0	0.0
650	0.245	1.0	0.0	0.0	0.0
700	0.087	1.0	0.0	0.0	0.0
750	0.032	1.0	0.0	0.0	0.0
800	0.016	1.0	0.0	0.0	0.0
900	0.0	1.0	0.0	0.0	0.0

A14. $O(^1D) + H_2O \rightarrow 2\ OH$

This reaction can be an important source of OH radicals, especially in relatively "clean" atmospheres. We recommend the NASA (1985) rate constant of

$$k_{A14} = 2.2 \times 10^{-10}\ cm^3\ molecule^{-1}\ sec^{-1}$$

independent of temperature. This reaction leads essentially entirely to two OH radicals (Paraskevopoulos and Cvetanovic 1971, Wine and Ravishankara 1982).

A15. $O(^1D) + M \rightarrow O(^3P) + M$

We use the NASA (1985) rate constants for the reactivation of $O(^1D)$ atoms by N_2 and O_2, to yield

$$k_{A15} = 2.9 \times 10^{-11} \text{ cm}^3 \text{ molecule}^{-1} \text{ sec}^{-1},$$

approximately independent of temperature.

A16. $OH + NO \xrightarrow{M} HONO$

This reaction is the only homogeneous reaction in the chemical mechanism forming nitrous acid, which is a precursor to OH radical production during the early morning hours. We use the rate constant expression recommended by Atkinson and Lloyd (1984):

$$k_{A16} = \left\{ \frac{k_o(T)[M]}{1 + \left(\frac{k_o(T)[M]}{k_\infty(T)} \right)} \right\} F^{\left\{1 + [\log_{10}(k_o(T)[M]/k_\infty(T))]^2\right\}^{-1}}$$

$\text{cm}^3 \text{ molecule}^{-1} \text{ sec}^{-1}$, where

$$k_o(T) = 6.7 \times 10^{-31} (T/300)^{-3.3} \text{ cm}^6 \text{ molecule}^{-2} \text{ sec}^{-1}$$

$$k_\infty(T) = 3.0 \times 10^{-11} (T/300)^{-1.0} \text{ cm}^3 \text{ molecule}^{-1} \text{ sec}^{-1},$$

$F = 0.6$ and $[M]$ is the concentration of air in molecule cm^{-3},

and

$k_{16} = 6.7 \times 10^{-12} \text{ cm}^3 \text{ molecule}^{-1} \text{ sec}^{-1}$ at 298 K and 760 torr total pressure.

A17. HONO + hν → OH + NO

Concentrations of HONO, observed up to 10 ppb in urban areas at night (Harris et al. 1982), quickly drop during daylight hours because of the rapid photolysis of HONO. We use the absorption cross sections of Stockwell and Calvert (1978). Atkinson and Lloyd (1984) recommend a quantum yield of unity in the actinic region for this reaction. The absorption cross sections used in the model are given in Table II-4.

Table II-4. Absorption Cross Sections, σ, (cm^2 $molecule^{-1}$, base e), for HONO at Selected Wavelengths

λ (nm)	10^{20} x σ (cm^2)	λ (nm)	10^{20} x σ (cm^2)	λ (nm)	10^{20} x σ (cm^2)
311	0.0	338	19.1	365	13.3
312	0.2	339	16.3	366	21.3
313	0.4	340	10.5	367	35.2
314	0.5	341	8.7	368	45.0
315	0.4	342	33.5	369	29.3
316	0.3	343	20.1	370	11.9
317	0.5	344	10.2	371	9.5
318	3.6	345	8.5	372	8.9
319	6.1	346	8.3	373	7.4
320	2.1	347	8.2	374	4.8
321	4.3	348	7.5	375	2.7
322	4.0	349	7.1	376	1.9
323	3.9	350	6.8	377	1.5
324	4.0	351	17.4	378	1.9
325	4.0	352	11.4	379	5.8
326	3.1	353	37.1	380	7.78
327	4.1	354	49.6	381	11.4
328	7.6	355	24.6	382	14.0
329	6.6	356	11.9	383	17.2
330	7.3	357	9.4	384	19.9
331	8.7	358	7.8	385	19.0
332	13.8	359	7.3	386	11.9
333	5.9	360	6.8	387	5.6
334	5.9	361	6.90	388	3.2
335	6.5	362	7.3	389	1.9
336	5.9	363	9.0	390	1.2
337	4.6	364	12.1	391	0.5
				392	0.0

A18. $OH + NO_2 \xrightarrow{M} HNO_3$

This reaction is generally recognized to be the most important reaction generating HNO_3 on the regional scale. The expression used in the model is that recommended by NASA (1985):

$$k_{A18} = \left\{ \frac{k_o(T)[M]}{1 + \left(\frac{k_o(T)[M]}{k_\infty(T)} \right)} \right\} F \left\{ 1 + [\log_{10}(k_o(T)[M]/k_\infty(T))]^2 \right\}^{-1}$$

cm^3 molecule^{-1} sec^{-1}, where

$k_o(T) = 2.6 \times 10^{-30} (T/300)^{-3.2}$ cm^6 molecule^{-2} sec^{-1},

$k_\infty(T) = 2.4 \times 10^{-11} (T/300)^{-1.3}$ cm^3 molecule^{-1} sec^{-1},

$F = 0.6$, and [M] is the concentration of air in molecule cm^{-3} units

and

$k_{18} = 1.1 \times 10^{-11}$ cm^3 molecule^{-1} sec^{-1}, at 298 K and 760 torr total pressure of air.

A19. $OH + HNO_3 \rightarrow H_2O + NO_3$

This reaction converts HNO_3 to the NO_3 radical but is not likely to play a major role in the regional model chemistry. The recommended rate constant expression of Atkinson and Lloyd (1984) is

$$k_{A19} = 9.4 \times 10^{-15} e^{1546/RT} \text{ cm}^3 \text{ molecule}^{-1} \text{ sec}^{-1}$$

$$= 1.3 \times 10^{-13} \text{ cm}^3 \text{ molecule}^{-1} \text{ sec}^{-1} \text{ at 298 K,}$$

with an uncertainty of a factor of 1.3 at 298 K.

A20. $HNO_3 + h\nu \rightarrow OH + NO_2$

This photolysis reaction is of less importance for HNO_3 loss than the reactions of OH with HNO_3. The quantum yield for photodissociation is unity (Johnston et al. 1974) and the absorption cross sections are those recommended by NASA (1985) and given in Atkinson and Lloyd (1984). This reaction is of negligible importance in the lower troposphere, and thus it is ignored in the model.

A21. $OH + CO \xrightarrow{O_2} HO_2 + CO_2$

The reaction of OH with CO is an important pathway for converting OH to HO_2 under conditions of very low hydrocarbon concentration. The reaction as written is a composite of the two elementary reactions:

$$OH + CO \xrightarrow{M} H + CO_2$$

$$H + O_2 + M \rightarrow HO_2 + M$$

with the latter reaction being the sole loss process of H atoms under atmospheric conditions. Previous work (Biermann et al. 1978) suggested that the role of air was to remove the HOCO adduct via the reaction:

$$HOCO + O_2 \rightarrow HO_2 + CO_2$$

but more recent work (Paraskevopoulos and Irvin 1984) shows that the enhancement of the rate constant at higher pressures of air and other gases is a true third body (M) effect. Based upon the work of Paraskevopoulos and Irvin (1984) and of Niki et al. (1984), we recommend that the following rate constant expression be used for modeling:

$$k_{A21} = 1.50 \times 10^{-13} \left\{ \frac{1 + 9.52 \times 10^{-23} T[M]}{1 + 2.32 \times 10^{-23} T[M]} \right\} \text{ cm}^3 \text{ molecule}^{-1} \text{ sec}^{-1},$$

where [M] is the concentration of air in molecule cm^{-3}. Thus for modeling the lower troposphere (where $[M] = 7.34 \times 10^{21}\ T^{-1}$), we use $k_{A21} = 2.18 \times 10^{-13}\ cm^3\ molecule^{-1}\ sec^{-1}$, independent of temperature.

A22. $OH + O_3 \rightarrow HO_2 + O_2$

This is another pathway for converting OH to HO_2, in this case consuming O_3. NASA (1985) and Atkinson and Lloyd (1984) recommend:

$$k_{A22} = 1.6 \times 10^{-12}\ e^{-1870/RT} cm^3\ molecule^{-1}\ sec^{-1}$$

$$= 6.8 \times 10^{-14}\ cm^3\ molecule^{-1}\ sec^{-1} \text{ at 298 K,}$$

with an uncertainty of a factor of 1.3 at 298 K.

A23. $HO_2 + NO \rightarrow OH + NO_2$

This is one of the key reactions converting NO to NO_2. The most recent studies have been evaluated and the recommended rate constant expression is (Atkinson and Lloyd 1984, NASA 1985):

$$k_{A23} = 3.7 \times 10^{-12}\ e^{480/RT}\ cm^3\ molecule^{-1}\ sec^{-1}$$

$$= 8.3 \times 10^{-12}\ cm^3\ molecule^{-1}\ sec^{-1} \text{ at 298 K,}$$

with an uncertainty at 298 K of a factor of 1.2.

A24. $HO_2 + NO_2 \xrightarrow{M} HO_2NO_2$

Sander and Peterson (1984) have determined, using a flash photolysis-ultraviolet absorption technique, rate constants for reaction (A24) over the pressure and temperature ranges 50-700 torr and 229-362 K, respectively, for M = He, N_2 and O_2. The data obtained were fitted to the fall-off equation

$$k_{A24} = \left\{ \frac{k_o(T)[M]}{1 + \left(\frac{k_o(T)[M]}{k_\infty(T)}\right)} \right\} F \left\{1 + [\log_{10}(k)_o(T)[M]/k_\infty(T)]^2\right\}^{-1}$$

where F = 0.56,

$$k_o(T) = 2.3 \times 10^{-31}\ (T/300)^{-4.6}\ \text{cm}^6\ \text{molecule}^{-2}\ \text{sec}^{-1}$$

and

$$k_\infty(T) = 4.2 \times 10^{-12}\ (T/300)^{0.2}\ \text{cm}^3\ \text{molecule}^{-1}\ \text{sec}^{-1}$$

for M = N_2. Essentially identical rate constants were obtained for M = N_2 and M = O_2. These values of $k_o(T)$ and $k_\infty(T)$ are identical to those recommended by the 1983 NASA evaluation (NASA 1983), and we recommend the use of this fall-off expression. At 298 K and 760 torr total pressure of air this yields

$$k_{A24} = 1.4 \times 10^{-12}\ \text{cm}^3\ \text{molecule}^{-1}\ \text{sec}^{-1}.$$

In addition, an effect of H_2O vapor, separate from its effect as a purely third body, has been observed (Sander and Peterson 1984). However, this effect is not incorporated into the present model.

The alternative reaction pathway

$$HO_2 + NO_2 \rightarrow HONO + O_2$$

has been shown to have a rate constant of $\lesssim 3 \times 10^{-15}$ cm^3 molecule^{-1} sec^{-1} (Howard 1977), and this is ignored in the model.

A25. $HO_2NO_2 \xrightarrow{M} HO_2 + NO_2$

Peroxynitric acid readily thermally decomposes back to the reactants. At ambient temperatures encountered in the lower troposphere, this thermal decomposition keeps HO_2NO_2 concentrations low.

We use the rate constant for reaction (A24) together with the equilibrium constant for the reactions to derive k_{A25}. NASA (1985) gives $K_{A24,A25}$ as

$$K_{A24,A25} = 2.33 \times 10^{-27} e^{10870/T} \text{ cm}^3 \text{ molecule}^{-1}$$

Thus

$$k_{A25} = k_{A24} \times 4.29 \times 10^{26} \times e^{-21600/RT} \text{ sec}^{-1}$$

$$= 0.086 \text{ sec}^{-1} \text{ at 298 K and 760 torr total pressure of air.}$$

A26. $HO_2NO_2 + h\nu \rightarrow HO_2 + NO_2$

At elevated altitudes, where reaction (A25) becomes very slow, photolysis of HO_2NO_2 can become important. The quantum yield is taken as unity, and the most recent and comprehensive absorption cross-section data are those of Molina and Molina (1981). However, this reaction is unlikely to be important in the lower troposphere, and it is not included in the present model.

A27. $OH + HO_2NO_2 \rightarrow H_2O + NO_2 + O_2$

Rate constant data for this reaction have been obtained from three studies. Graham et al. (1978) obtained an upper limit of $k_{A27} \lesssim 3 \times 10^{-12}$ cm^3 molecule^{-1} sec^{-1} at T = 261-295 K; while Barnes et al. (1981) reported a rate constant of $k_{A27} = 4.1 \times 10^{-12}$ cm^3 molecule^{-1} sec^{-1} at 295 K, and Trevor et al. (1982) obtained $k_{A27} = (4.0 \pm 1.6) \times 10^{-12}$ cm^3 molecule^{-1} sec^{-1}, independent of temperature over the range 246-324 K. In view of the good agreement between these latter two studies, the following value is used in our modeling:

$$k_{A27} = 4.0 \times 10^{-12} \text{ cm}^3 \text{ molecule}^{-1} \text{ sec}^{-1},$$

independent of temperature, with an uncertainty of a factor of 2. The products are not known with any certainty, but are probably $H_2O + NO_2 + O_2$, and this is assumed in the model.

A28. $HO_2 + O_3 \rightarrow OH + 2\ O_2$

NASA (1985) and Atkinson and Lloyd (1984) recommend the following expression for this reaction:

$$k_{A28} = 1.4 \times 10^{-14}\ e^{-1150/RT}\ cm^3\ molecule^{-1}\ sec^{-1}$$

$$= 2.0 \times 10^{-15}\ cm^3\ molecule^{-1}\ sec^{-1}\ \text{at 298 K}$$

with an estimated uncertainty at 298 K of a factor of 1.5.

A29. $HO_2 + HO_2 \xrightarrow{H_2O,M} H_2O_2 + O_2$

This is the key reaction in the formation of H_2O_2 in the atmosphere and is important when NO_x concentrations are low. The reaction is dependent upon the water vapor concentration and proceeds via complex formation:

$$HO_2 + H_2O \rightleftarrows (HO_2 \cdot H_2O)$$

$$HO_2 + (HO_2 \cdot H_2O) \rightarrow (H_2O_4) + H_2O$$

$$\downarrow$$

$$H_2O_2 + O_2$$

The reaction is discussed in detail in Atkinson and Lloyd (1984). While numerous studies of this reaction have been carried out, there are still significant uncertainties concerning the rate constant for this reaction and the enhancement caused by water vapor. The recent work of Thrush and Tyndall (1982a,b), Patrick and Pilling (1982) and Kircher and Sander (1984) has considerably narrowed the uncertainties concerning the temperature dependencies of this reaction (at both the low pressure limit and at pressures near atmospheric), and the uncertainties in the involvement of water vapor on this reaction.

Based on the most recent and comprehensive study of Kircher and Sander (1984), we recommend the overall expression:

$$k_{A29} = 2.2 \times 10^{-13} e^{1230/RT} + 1.9 \times 10^{-33} [M]\ e^{1950/RT}$$

$$+ 3.1 \times 10^{34}\ [H_2O] e^{5600/RT} + 2.7 \times 10^{-54}\ [M][H_2O] e^{6230/RT}$$

$$\mathrm{cm}^3\ \mathrm{molecule}^{-1}\ \mathrm{sec}^{-1}$$

which includes the pressure (M) effect as well as the enhancement due to H_2O vapor. This expression assumes that O_2 has the same third-body effect as N_2. At 298 K and 760 torr total pressure,

$$k_{A29} = 3.02 \times 10^{-12} + 6.44 \times 10^{-30}\ [H_2O]\ \mathrm{cm}^3\ \mathrm{molecule}^{-1}\ \mathrm{sec}^{-1}$$

A30. $HO_2 + NO_3 \xrightarrow{H_2O,M} HNO_3 + O_2$

This reaction may become non-negligible under conditions of low (but not totally depleted) NO_x, and at nighttime under conditions where there may be dark sources of HO_2. However, no data are available for this reaction, nor was it discussed by Atkinson and Lloyd (1984). It is probably a complex reaction, proceeding via adducts analogous to those discussed above for HO_2 + HO_2 [reaction (A29)]. We tentatively assume that the reaction which occurs has the same rate parameters, and has the same H_2O and pressure dependences as discussed above for reaction (A29), i.e., $k_{30} = k_{A29}$. However, this reaction is more exothermic than reaction (A27), and thus it may actually have a higher rate constant. This estimate is essentially identical to that of Cantrell et al. (1985).

A31. $H_2O_2 + h\nu \rightarrow 2\ OH$

The absorption cross sections have been given by NASA (1983) and Atkinson and Lloyd (1984). This process is less important than the loss of H_2O_2 by OH radical attack under atmospheric conditions in the lower troposphere. The absorption cross section used in this model are given in Table II-5.

A32. $OH + H_2O_2 \rightarrow H_2O + HO_2$

As discusssed by Atkinson and Lloyd (1984), the rate constant for this reaction is recommended by NASA (1985) to be

$$k_{A32} = 3.1 \times 10^{-12}\ e^{-372/RT}\ \text{cm}^3\ \text{molecule}^{-1}\ \text{sec}^{-1}$$

$$= 1.7 \times 10^{-12}\ \text{cm}^3\ \text{molecule}^{-1}\ \text{sec}^{-1}\ \text{at 298 K},$$

with an estimated uncertainty at 298 K of a factor of 1.3.

Table II-5. Absorption Cross Sections, σ, ($\text{cm}^2\ \text{molecule}^{-1}$, base e), for H_2O_2 at Selected Wavelengths

λ (nm)	$10^{20} \times \sigma$ (cm^2)	λ (nm)	$10^{20} \times \sigma$ (cm^2)
250	8.3	305	0.49
255	6.7	310	0.37
260	5.2	315	0.28
265	4.2	320	0.20
270	3.2	325	0.15
275	2.5	330	0.12
280	2.0	335	0.09
285	1.5	340	0.07
290	1.13	345	0.05
295	0.87	350	0.03
300	0.66	355	0.0

A33. $OH + SO_2 \xrightarrow{O_2,} \xrightarrow{H_2O} H_2SO_4 + HO_2$

The kinetic data obtained for $M = N_2$ at pressures approaching atmospheric are those of Paraskevopoulos et al. (1983) and of Wine et al. (1984). The latter data are the most extensive, and agree within the experimental error limits with those of Paraskevopoulos et al. (1983); hence we recommend the data of Wine et al. (1984):

$$k_{A33} = \left\{ \frac{k_o(T)[M]}{1 + \left(\frac{k_o(T)[M]}{k_\infty(T)}\right)} \right\} F^{\left\{1 + [\log_{10}(k_o(T)[M]/k_\infty(T))]^2\right\}^{-1}}$$

where

$$k_o(T) = 4.5 \times 10^{-31} \ (T/300)^{-3.9} \ \mathrm{cm}^6 \ \mathrm{molecule}^{-2} \ \mathrm{sec}^{-1}$$

$$k_\infty(T) = 1.26 \times 10^{-12} \ (T/300)^{-0.7} \ \mathrm{cm}^3 \ \mathrm{molecule}^{-1} \ \mathrm{sec}^{-1}$$

and

$$F = 0.525$$

At 298 K and 760 torr total pressure of air, this yields

$$k_{A33} = 8.1 \times 10^{-13} \ \mathrm{cm}^3 \ \mathrm{molecule}^{-1} \ \mathrm{sec}^{-1}$$

Izumi et al. (1984) recently obtained a value for k_{A33} of $(1.22 \pm 0.13) \times 10^{-12}$ cm^3 $\mathrm{molecule}^{-1}$ sec^{-1} at 303 K which agrees with the expression recommended above. The rate constant was obtained using a competitive rate technique at atmospheric pressure using n-butane as the reference reactant.

The reactions as written above are complex. The initial reaction of OH with SO_2 is believed to involve formation of HSO_3 radicals

$$OH + SO_2 \xrightarrow{M} HSO_3$$

The subsequent reactions of the HSO_3 radicals are still a subject of discussion, but the recent experimental work of Stockwell and Calvert

(1983) sheds new light on the mechanisms of those reactions under atmospheric conditions. Until now, the $HOSO_2$($\equiv$ HSO_3) radical has been assumed to rapidly form H_2SO_4 without any NO to NO_2 oxidation steps, or regeneration of radicals. However, Stockwell and Calvert (1983) have shown that radical regeneration occurs, and conclude that the subsequent reaction sequence consists of:

$$HSO_3 + O_2 \rightarrow HO_2 + SO_3$$

followed by

$$SO_3 + H_2O \rightarrow H_2SO_4 \text{ (or } H_2O.SO_3\text{)}$$

(The latter complex will ultimately form H_2SO_4.)

Stockwell and Calvert (1983) also discuss the possibility that the reaction proceeds via

$$HSO_3 + H_2O \rightleftarrows HSO_3.H_2O$$

$$HSO_3.H_2O + O_2 \rightarrow H_2SO_4 + HO_2$$

in the presence of water vapor. For modeling purposes these are equivalent and we recommend that the inorganic reaction be represented as written above.

II. B. GENERAL PEROXY AND ACYL PEROXY RADICAL REACTIONS

In this section, the common features assumed in the model for the reactions of alkyl peroxy (RO_2) and acyl peroxy (RCO_3) radicals are discussed. Under conditions when ozone formation can occur, i.e., when NO_x is present, by far the most important reactions of these species is with NO and (in the case of acyl peroxy radicals) with NO_2. Although the products formed in these reactions depend on the specific radical, and are discussed in the various sections where the reactions forming these radicals are discussed, the kinetics for these reactions are assumed to be the same for all alkyl peroxy and acyl peroxy radicals, and thus are discussed in this section.

When NO or NO_x are absent or present only at very low levels, reactions of the alkyl peroxy or acyl peroxy radicals with HO_2 and with other peroxy radicals become important. In models concerned primarily with ozone formation, these reactions are of lesser importance, since NO_x is required for ozone to be formed in tropospheric systems, and these reactions are generally of negligible importance when NO_x is present. However, these reactions must be included in models concerned with multi-day pollution episodes (since such episodes are generally characterized by periods, generally at nighttime or during transport over non-emitting areas, when NO_x levels are very low), or in simulations representative of scenarios with high hydrocarbon/NO_x ratios.

In order to represent in the model in an accurate manner the reactions of peroxy radicals with HO_2 and with other peroxy radicals and the reactions of the products formed in these reactions, a significant increase in the number of reactions and reactant species is required. This is because a large number of different kinds of alkyl peroxy and acyl peroxy radicals are involved in the reactions of a realistic "urban surrogate" hydrocarbon mixture. To include the reactions of each of the corresponding hydroperoxides formed when these react with HO_2 in the model, together with all the possible combinations of peroxy + peroxy reactions, would lead to an excessive increase in the size of the model for the purpose of representing what are, under most conditions of interest, relatively minor processes. Thus in this model a number of simplifying approximations are made to represent these reactions and those of the products formed. These approximations are discussed in this section, in conjunction with the discussion of the assumptions made concerning the kinetics of these reactions.

1. Peroxy + NO and Peroxy + NO_2 Reactions

B1. $RO_2 + NO \rightarrow$ products

B2. $RCO_3 + NO \rightarrow$ products

B3. $RO_2 + NO_2 \rightarrow$ products

B4. $RCO_3 + NO_2 \rightarrow$ products

The kinetics of these reactions are discussed by Atkinson and Lloyd (1984). The only available absolute rate constant data concern the reactions of CH_3O_2, $C_2H_5O_2$ and CH_3CO_2 with NO and/or NO_2, from which Atkinson and Lloyd (1984) recommend

$$k_{B1} = 4.2 \times 10^{-12} e^{360/RT} \text{ cm}^3 \text{ molecule}^{-1} \text{ sec}^{-1}$$

$$= 7.6 \times 10^{-12} \text{ cm}^3 \text{ molecule}^{-1} \text{ sec}^{-1} \text{ at } 298K,$$

and

$$k_{B3} = 7 \times 10^{-12} \text{ cm}^3 \text{ molecule}^{-1} \text{ sec}^{-1} \text{ at } 298K,$$

with no recommendation regarding the temperature dependence for reaction B3. Since there are no absolute rate constant data for the reactions of acyl peroxy radicals with NO, Atkinson and Lloyd (1984) assume that $k_{B2} = k_{B1}$ and recommend $k_{B2}/k_{B4} = 1.5$, independent of temperature. Thus we derive

$$k_{B4} = 2.8 \times 10^{-12} e^{360/RT} \text{ cm}^3 \text{ molecule}^{-1} \text{ sec}^{-1},$$

assuming that the difference between the two reactions is mainly in the pre-exponential factor. It should be noted that the temperature dependencies of these reactions are relatively small.

The products formed in the reactions of alkyl peroxy and acyl peroxy radicals with NO depend on the specific radical, and thus they are not discussed in this section. In most cases, the primary mode of reaction is the formation of NO and the corresponding alkoxy or acyl oxy radical, generally followed by rapid reaction of the oxy radical. Some of the larger alkyl peroxy radicals are also believed to form alkyl nitrates when they react with NO, but the total RO_2 + NO rate constant is assumed to be unaffected by the relative importance of this second reaction route, and the value of k_{B1} given above is assumed to apply to all peroxy + NO reactions, regardless of the products formed.

The reactions of alkyl peroxy radicals with NO_2 are believed to result in the formation of alkyl peroxynitrates, which undergo rapid thermal back-decomposition to the reactants.

$$RO_2 + NO_2 \xrightarrow{M} ROONO_2$$

$$ROONO_2 \xrightarrow{M} RO_2 + NO_2$$

Atkinson and Lloyd (1984) summarized the available kinetic data concerning these reactions, and concluded that, since their lifetimes relative to thermal decomposition are expected to be <1 s at 298K and <1 min at 273 K, their formation can be ignored for tropospheric modeling studies. Thus their formation would be followed immediately by their rapid decomposition, resulting in no net reaction. We have carried out model calculations which indicate that including alkyl peroxynitrate chemistry results in no significant change in the model predictions at normal temperatures; this is shown in the sample calculations discussed below in Section II-B-4. Thus, in the present model we assume that reactions of RO_2 with NO_2 result in no net reaction, which means in effect that $k_{B3} = 0$.

The acyl peroxynitrates which are formed in the reactions of acyl peroxy radicals with NO_2, of which PAN ($CH_3C(O)\text{-}OONO_2$) is the simplest and most well studied example, are much more stable than the alkyl peroxynitrates, and their formation and subsequent reactions cannot be ignored. In particular, the formation of PAN can represent a significant NO_x and radical sink in many systems. The kinetics of the decomposition of the individual acyl peroxynitrates are discussed in the various sections where the formation of their specific precursors are discussed.

2. Peroxy + HO_2 Reactions

B5. $RO_2 + HO_2 \rightarrow$ products

B6. $RCO_3 + HO_2 \rightarrow$ products

These reactions can be important under conditions where NO_x or NO is low or absent, and they must be included in models for multi-day pollution episodes. The only data concerning the absolute rate constants for these reactions are for the reaction of HO_2 with methyl peroxy and ethyl peroxy radicals. For the $CH_3O_2 + HO_2$ reaction, there are significant discrepancies, since Cox and Tyndall (1979, 1980) obtained $k_{B5} = 6 \times 10^{-12}$ cm^3 molecule^{-1} sec^{-1} at 298 K, and Kan et al. (1980) obtained $k_{B5} = 1.3 \times 10^{-12}$ cm^3 molecule^{-1} sec^{-1} at the same temperature. In addition, Niki et al. (1982) estimated $k_{B5} = 1.5 \times 10^{-12}$ cm^3 molecule^{-1} sec^{-1} for $C_2H_5O_2$ at 298 K. Atkinson and Lloyd (1984) recommended using the geometric mean of those two values, and this is what we use in this model for reactions of all alkyl and acyl peroxy radicals with $HO_2\cdot$, i.e.,

$$k_{B5} = k_{B6} = 3 \times 10^{-12} \text{ cm}^3 \text{ molecule}^{-1} \text{ sec}^{-1}.$$

Any temperature dependence of this reaction is neglected in this model.

The reactions of HO_2 with alkyl and acyl peroxy radicals are expected to occur via transfer of H from HO_2 to RO_2, giving rise to O_2 and ROOH, the corresponding hydroperoxide molecule. The hydroperoxides can undergo photolysis, regenerating radicals,

$$RO_2 + HO_2 \rightarrow ROOH$$

$$ROOH + h\nu \rightarrow RO + OH$$

or they can react with OH radicals (and possibly other reactive species), depending on the exact structure of the individual hydroperoxide formed.

The subsequent reactions of the hydroperoxides formed in reactions (B5) or (B6), while probably of negligible significance in one-day simulations, may be non-negligible in multi-day simulations. Thus it is appropriate to represent them in the model. However, to represent these reactions explicitly would necessitate adding a reactive species in the model for each peroxy radical, and this would result in a significant increase in the size of the model (and the amount of computer time required to utilize it) for the purpose of representing what are, under most conditions, relatively minor processes.

Thus in the model the hydroperoxides are not represented explicitly. Instead, for any given alkyl peroxy radical R_iO_2 or acyl peroxy radical R_iCO_3, their reaction with HO_2 is represented as follows:

$$R_iO_2 + HO_2 \rightarrow \text{-OOH} + (R_iO_2 \text{ products})$$

$$R_iCO_3 + HO_2 \rightarrow \text{-OOH} + (R_iCO_3 \text{ products})$$

where "-OOH" is a lumped hydroperoxide pseudo species included in the model to represent the photolysis of the hydroperoxide group to form radicals, and "R_iO_2 products" and "R_iCO_3 products" are sets of compounds used to represent the other modes of reactions of the hydroperoxide species and the compounds formed when they react, and to maintain a carbon balance. These products are defined as being the product, or set of products, which would be formed from the corresponding alkoxy radical in the absence of NO_x. (If the alkoxy radical isomerizes or decomposes to form other peroxy radicals, these in turn are represented by their own set of "RO_2 products," defined in the same way; see the examples below.) This representation is obviously approximate, but it conserves carbon and, because the "RO_2 products" are a subset of the oxygenated species that are formed when RO_2 or RCO_3 react with NO (i.e., the products formed other than the organic nitrates), only one new reactive species, namely -OOH, has to be added to the model to represent the reaction of all of the hydroperoxides.

Examples of the representation for the hydroperoxides are shown below for the reactions of HO_2 with methyl peroxy, acetyl peroxy, and t-butyl peroxy radicals.

$$CH_3O_2\cdot + HO_2 \rightarrow HCHO + \text{-OOH}$$

$$CH_3CO_3\cdot + HO_2 \rightarrow HCHO + CO_2 + \text{-OOH}$$

$$(CH_3)_3CO_2\cdot + HO_2\cdot \rightarrow CH_3COCH_3 + HCHO + \text{-OOH}$$

In the case of methyl peroxy + HO_2, the corresponding alkoxy radical reacts with O_2 to form formaldehyde, and thus the "methyl peroxy product" is formaldehyde. In the case of acetyl peroxy + HO_2, the acetyloxy radical decomposes to form CO_2 + methyl, so the "acetyl peroxy product" is CO_2 + the "methyl peroxy product," which is formaldehyde. In the case of t-butyl peroxy, the corresponding alkoxy radical decomposes to form acetone + methyl, so the "products" for this radical are acetone + formaldehyde (the latter again representing the "methyl product"). The "RO_2" or "RCO_3" products for individual radicals are indicated in the sections where the specific reactions forming those radicals are discussed.

The photolysis of the hydroperoxide group is represented by the following reaction.

B7. $\text{-OOH} + h\nu \rightarrow OH + HO_2$

The absorption coefficients used for -OOH are those for CH_3OOH, which were reported by Molina and Arguello (1979), and are given in Table II-6. The quantum yields have not been measured, but are assumed to be unity (NASA 1985). The product HO_2 in this reaction represents the HO_2 produced from the oxidation of the alkoxy radical formed during the photolysis.

Although this representation of hydroperoxide reactions is clearly approximate, we consider it preferable to the two alternatives of either (a) ignoring their reactions altogether, which has generally been the case

Table II-6. Absorption Cross Sections, σ, (cm^2 $molecule^{-1}$, base e), for Methylhydroperoxide (From Molina and Arguello 1979)

λ (nm)	10^{20} x σ (cm^2)
270	2.50
280	1.50
290	0.90
300	0.58
310	0.34
320	0.19
330	0.11
340	0.06
350	0.04
360	0.0

for most previous models, or (b) of significantly increasing the number of species and reactions in the model in order to represent these reactions explicitly, which has only minor effects on the model predictions under most conditions (see Section II-B-4 below).

3. Peroxy + Peroxy Radical Reactions

The reactions of alkyl or acyl peroxy radicals with other alkyl or acyl peroxy radicals can also be of importance under conditions where NO_x or NO is low or absent, and must be included in the model. However, these reactions have generally been excluded from previous models because of the large number of reactions required in the model to represent all the various possible combinations. In this model, an approximate approach is taken in order to represent these processes and yet avoid including a separate reaction for each possible pair of peroxy or acyl peroxy radicals, thus increasing the size of the model to an inappropriate extent.

The approach employed involves including in the model the pseudo species "RO_2" and "RCO_3", which represent the total concentration of all peroxy or acyl peroxy radicals, respectively, in the model. This is carried out by having each reaction which forms a peroxy radical also form the pseudo species "RO_2" with the same yield, and each reaction forming an acyl peroxy radical also forming the same amount of "RCO_3", and by including in the model the following "reactions" to represent their consumption processes:

For RO_2:

B1. $RO_2 + NO \rightarrow NO$

B5. $RO_2 + HO_2 \rightarrow HO_2$

B8. $RO_2 + RO_2 \rightarrow$

B9. $RO_2 + RCO_3 \rightarrow$

For RCO_3:

B3. $RCO_3 + NO \rightarrow NO$

B4. $RCO_3 + NO_2 \rightarrow NO_2$

B6. $RCO_3 + HO_2 \rightarrow HO_2$

B9. $RCO_3 + RO_2 \rightarrow$

B10. $RCO_3 + RCO_3 \rightarrow$

Note that including these reactions in the model only affects the concentrations calculated for RO_2 and RCO_3; the changes in concentrations of other species caused by peroxy or acyl peroxy radical reactions are represented in the reactions included for the individual peroxy radicals, as indicated below.

The total alkyl peroxy and acyl peroxy radical concentrations, calculated by including the reactions listed above, are then used to calculate the total rates of the peroxy + peroxy radical reactions of the individual alkyl peroxy (R_iO_2) or acyl peroxy (R_iCO_3) radicals. These reactions are represented in the model by including the following reactions for each R_iO_2

$$R_iO_2 + RO_2 \rightarrow RO_2 + 0.5\ HO_2 + (R_iO_2\ \text{products}) \qquad (k = k_{B8})$$

$$R_iO_2 + RCO_3 \rightarrow RCO_3 + 0.5\ HO_2 + (R_iO_2\ \text{products}) \qquad (k = k_{B9})$$

and include the following for each R_iCO_3

$$R_iCO_3 + RO_2 \rightarrow RO_2 + 0.5\ HO_2 + (R_iCO_3\ \text{products}) \qquad (k = k_{B9})$$

$$R_iCO_3 + RCO_3 \rightarrow RCO_3 + HO_2 + (R_iCO_3\ \text{products}) \qquad (k = k_{B10}),$$

with the same rate constants as employed for the corresponding "lumped" peroxy radicals, as indicated above. RO_2 and RCO_3 are included as "products" as well as reactants in these reactions, because the consumption of these pseudo species is already represented in reactions (B8)-(B10), above. (The other products are discussed below.)

It should be pointed out that in the other sections of this document, where the reactions involving the individual peroxy radicals are discussed, the inclusion of the pseudo species "RO_2" as a product in any reaction forming an individual alkyl peroxy radical, and in the reactions of the individual peroxy radicals with "RO_2" (and likewise for "RCO_3"), is not shown. This is done for clarity of presentation of the mechanism being discussed, and to avoid possible confusion between pseudo species included in the model for computational convenience and true chemical species.

This representation of the radical + radical reactions tends to underestimate the overall rate of removal of radicals by this route since it does not take into account the fact that when a given radical reacts with itself, two radicals of that type are removed via this reaction route, not one. This amounts to a maximum error of a factor of 2 in the extreme cases when there is only one radical, or when one individual radical dominates in concentration over all the others (in the latter case the error being in calculations for the dominating radical, not for the minor ones). However, in more realistic cases where there are a large number of such radicals and no one radical dominates in concentration, the error caused by this representation will be much less. In view of the other approximations involved with this technique and the uncertainties in the rate constants, this source of error, which does not involve any errors in mass balance, is considered to be of minor significance. This source of error does not affect computed material balances; it only affects the relative importance of different competing reaction routes. Several test calculations showing the effects of this approximation are discussed in the following section.

Of much greater potential significance is the fact that this technique requires assuming that the rate constant for a given type of peroxy or acyl peroxy radical reaction does not depend on the nature of the individual peroxy radical. This is a reasonable assumption in the case of the reactions of these radicals with NO, NO_2 and HO_2, as discussed above, since the available data indicates that the rate constants for these reactions do not differ for different individual RO_2 or RCO_3 radicals. However, this assumption is less reasonable for the case of peroxy + peroxy reactions, since, as indicated below, the rate constants for these reactions vary over several orders of magnitude, depending on whether the radical is primary, secondary or tertiary.

The available kinetic data for peroxy + peroxy radical reactions under atmospheric conditions were reviewed by Atkinson and Lloyd (1984), and the 298 K rate constants given there are summarized in Table II-7. It can be seen that there is significant variation in the rate constants, and that data for reactions between different types of peroxy radicals are quite limited. We assume that the values given for acetyl peroxy + methyl peroxy and acetyl peroxy + acetyl peroxy radical reactions can be taken as representative of all the other $RCO_3 + RO_2$ and $RCO_3 + RCO_3$ reactions, and thus we use

$$k_{B9} = 3 \times 10^{-12} \text{ cm}^3 \text{ molecule}^{-1} \text{ sec}^{-1}$$

and

$$k_{B10} = 2.5 \times 10^{-12} \text{ cm}^3 \text{ molecule}^{-1} \text{ sec}^{-1}$$

Table II-7. Summary of Peroxy + Peroxy Radical Rate Constants[a] for for T = 298 K

k (cm^3 $molecule^{-1}$ sec^{-1})	Reaction
3.1×10^{-13}	$CH_3O_2\cdot + CH_3O_2\cdot$
1×10^{-13}	$CH_3O_2\cdot + (CH_3)_3CO_2\cdot$
5.2×10^{-14}	$C_2H_5O_2\cdot + C_2H_5O_2\cdot$
$\leq 3.8 \times 10^{-13}$	$CH_3CH_2CH_2O_2\cdot + CH_3CH_2CH_2O_2\cdot$[b]
7.6×10^{-16}	$(CH_3)_2CHO_2\cdot + (CH_3)_2CHO_2\cdot$
2.6×10^{-17}	$(CH_3)_3CO_2\cdot + (CH_3)_3CO_2\cdot$
3×10^{-12}	$CH_3O_2\cdot + CH_3CO_3\cdot$
2.5×10^{-12}	$CH_3CO_3\cdot + CH_3CO_3\cdot$

[a] From Atkinson and Lloyd (1984). Recommended values are given in cases where a recommendation was made.

[b] Erroneously given as 1-butyl peroxy by Atkinson and Lloyd (1984).

in the model. For the $RO_2 + RO_2$ reactions, where the choice of the rate constant is necessarily arbitrary because of the wide variation depending on the type of radical, we use the value for secondary + secondary peroxy radicals as representative, since it is near the geometric mean of the extremes. Furthermore, secondary peroxy radicals are commonly formed in the photooxidations of most of the organics whose reactions are included in this model. Thus we assume

$$k_{B8} = 1 \times 10^{-15} \text{ cm}^3 \text{ molecule}^{-1} \text{ sec}^{-1}.$$

Although these values are based on data for 298 K, these rate constants are assumed to be temperature independent in the model, since the uncertainties involved, and the variations of the rate constants appropriate for the individual radicals, are clearly much greater than any variation caused by temperature variation within the range appropriate for atmospheric simulations.

Peroxy + peroxy radical reactions can occur via two general types of reaction routes, both presumably involving the initial formation of an adduct of the type RO_4R. In the molecular route, the transfer of an alpha hydrogen from one of the radicals to the other via a six-member ring transition state results in one of the peroxy radicals being converted into the corresponding alcohol, and the other being converted to the corresponding carbonyl compound. This reaction route is possible as long as one of the pair is neither a tertiary radical nor an acyl peroxy radical. For example,

$$CH_3O_2\cdot + CH_3CH_2O_2 \rightarrow [CH_3OOOOCH_2CH_3] \rightarrow CH_3OH + CH_3CHO + O_2$$

$$CH_3O_2\cdot + CH_3CO_3\cdot \rightarrow [CH_3OOOOCOCH_3] \rightarrow HCHO + CH_3COOH + O_2$$

The alternative, radical reaction route, where two alkoxy radicals + O_2 are formed, i.e.,

$$RO_2\cdot + R'O_2\cdot \rightarrow [ROOOOR'] \rightarrow RO\cdot + O_2 + R'O\cdot$$

is possible in all cases. [Other reaction routes have been suggested, but they are believed to be minor (see Atkinson and Lloyd 1984).] Data concerning the relative importance of the two routes (for those systems where both routes are possible) are limited; for both methyl peroxy and the 2-propyl peroxy radical self-reactions, Atkinson and Lloyd (1984) conclude that the molecular route occurs approximately 60% of the time, and for the ethyl peroxy radical self-reaction, they conclude that the molecular route occurs approximately 40-50% of the time. Thus based on these limited data, we generalize that when the molecular route is possible, it will occur approximately 50% of the time.

In order to avoid the addition of species to the model which are formed only via the (usually unimportant) peroxy + peroxy radical reactions, the products formed in these reactions are represented in an approximate manner, as indicated for these reactions as written above. In particular, the estimated 50% regeneration of radicals in cases where the molecular route may occur, or the 100% regeneration of radicals in the RCO_3 + RCO_3 case where the molecular route is not possible, is represented in the model by the assumed formation of the corresponding amount of HO_2 in those reactions. (It is further assumed that the the molecular route is possible in all RO_2 + RO_2 and RO_2 + RCO_3 reactions, in order to avoid the necessity of adjusting the radical yield for each individual mixture, depending on the fraction of reacting alkyl peroxy radicals which are tertiary.) In all cases the organic products formed from the peroxy + peroxy reactions of a given peroxy or acyl peroxy radical are represented by the same set of compounds (designated "R_1O_2 products" or "R_1CO_3 products") as those used to represent the organic portion of the hydroperoxide formed in the RO_2 or RCO_3 + HO_2 reactions, namely the product(s) formed when the corresponding alkoxy radicals react in the absence of NO_x (see discussion in Section B-2, above). The specific products formed in these reactions for individual peroxy radicals are indicated in the sections where the reactions forming those radicals are discussed.

4. Tests of Effects of the Approximations Employed

In this section, a series of test calculations carried out in order to investigate the effects of the approximations regarding peroxy radical reactions incorporated in this model, as well as the effects of ignoring the peroxy + HO_2 and peroxy + peroxy radical reactions altogether, are discussed. In particular, four simulations were carried out employing four different models, one model using a detailed and explicit representation of the peroxy radical, hydroperoxide, and peroxynitrate chemistry, one using the approximations discussed in Sections 1-3 above, one model with the peroxy + peroxy radical reactions ignored, and one with both peroxy + peroxy and peroxy + HO_2 radical reactions ignored. Thus these four models represent increasing levels of approximation regarding the aspects of peroxy radical chemistry discussed in this section, with the first set representing very few approximations, the second representing the level of approximation used in the model discussed in this report, and the third and fourth representing those employed in most previously published models which have been used in EKMA and other airshed simulations.

The four simulations employed in these test calculations consisted of irradiations, under conditions of natural sunlight and in the absence of chamber effects, of propene-n-butane-aldehyde-NO_x-air mixtures at three different hydrocarbon/NO_x ratios and at two different temperatures. The relative composition of the organic mixture was chosen to resemble the "Dodge EKMA" surrogate (Dodge 1977) because that is one of the simplest surrogate mixtures used to represent organics in ambient air. The specific input data employed in these test calculations are given in Table II-8.

Table II-8. Input Data Employed in the Calculations Used to Test the Effects of Approximations Concerning Peroxy Radical, Peroxynitrate, and Hydroperoxide Reactions

	Calc. 1	Calc. 2	Calc. 3	Calc. 4
Initial Reactant Concentrations (ppm):				
NO	0.08	0.4	0.08	0.08
NO_2	0.02	0.1	0.02	0.02
Propene	0.833	0.25	0.25	0.25
n-Butane	1.75	0.525	0.525	0.525
Formaldehyde	0.25	0.075	0.075	0.075
Acetaldehyde	0.125	0.038	0.038	0.038
H_2O (constant)	2.0E+4	2.0E+4	2.0E+4	2.00E+4
O_2 (constant)	2.09E+5	2.09E+5	2.09E+5	2.09E+5
M (constant)	1.0E+6	1.0E+6	1.0E+6	1.0E+6
Temperature (K):	300	300	300	270
Photolysis Rates:	Theoretically calculated for diurnally-varying natural sunlight at 34 degrees latitude, 23.5 degrees solar declination. (Los Angeles in the summer.)			
Start and Stop Times:	0600 through 2100 local daylight time.			
Dilution, Emissions, etc.:	No dilution. No pollutants injected after the start of the simulation; all present initially. (The calculations were carried out with no dilution in order to make it easier to check for carbon and nitrogen balance.)			
Heterogeneous or "Chamber" Effects:	None. Only reactions believed to be homogeneous were included in the models.			

The propene/butane/aldehyde model employed in these calculations employed a somewhat shortened version of the detailed mechanism for these species as discussed in Sections II-C, II-D and II-E of this report. The model was shortened slightly in order to reduce the number of peroxy radicals, so the model which did not employ the approximations discussed in this section would be more manageable in size. This shortened model has a total of four alkyl peroxy radicals and one acyl peroxy radical, as opposed to the current standard model which has 12 alkyl peroxy radicals and two acyl peroxy radicals. The model was shortened by (1) assuming only secondary abstraction in the OH + n-butane reaction; (2) neglecting secondary reactions of methyl ethyl ketone; and (3) lumping the reactions of the peroxy radical formed in the NO_3 + propene reaction with that formed in the OH reaction. Test calculations showed this reduction in the size of the model does not have a major effect on the results of the simulations, and in any case it should not qualitatively affect the utility of these calculations in determining the effects of the approximations involving peroxy radical reactions.

The first set of model calculations employed the standard model for the reactions of peroxy radicals, peroxynitrates, and hydroperoxides, modified as follows: (1) All peroxy + peroxy radical reactions were represented explicitly, and with different rate constants depending on the types of peroxy radicals reacting. Specifically, based on the data given in Table II-7, the rate constants used (in units of cm^3 $molecule^{-1}$ sec^{-1}) were: 3×10^{-13} for primary + primary, 1.5×10^{-14} for primary + secondary, and 7.6×10^{-16} for secondary + secondary alkyl peroxy radicals. The rate constants used for the acyl peroxy + alkyl peroxy and the acyl peroxy + acyl peroxy radical reactions were the same as in the standard model. (2) The hydroperoxides formed from the reactions of HO_2 with the various peroxy radicals were represented explicitly. Their only reaction was assumed to be photolysis, with the photolysis reaction giving rise to OH and the corresponding alkoxy radical, with the photolysis rates being the same as used for -OOH in the standard model. (3) The formation and decomposition of the all the alkyl peroxynitrates are included in the model. The peroxynitrates were all assumed to decompose with a rate constant given by 2.0×10^{16} $e^{-22000/RT}$ sec^{-1}, based on the data summarized by Atkinson and Lloyd (1984). The pressure effect on the decomposition of methyl peroxynitrate was ignored. This model had the least number of approximations regarding peroxy radical chemistry, and thus the calculations employing this model, designated "D" (for "detailed") in the tabulation of the results, can serve as a standard against which the results of the more approximate model calculations can be compared.

The second set of calculations (designated "S", for "standard") employed the set of approximations regarding peroxy radical chemistry discussed in Sections 1-3 above, and represents the level of detail of the models developed in this program. The third and fourth sets of calculations both employ the standard model, except that in the third (designated "X1"), the peroxy + peroxy radical reactions are ignored, while in the fourth (designated "X2"), both the peroxy + peroxy and the peroxy + HO_2 radical reactions are ignored. Model "X2" represents the level of detail employed in the mechanism of Atkinson et al. (1982a), as well as a number of others.

The results of these test calculations are summarized in Table II-9. A comparison of the results of the calculations using the detailed model (model "D") and those using the approximations employed in the standard model developed in this program (model "S") indicate that these approximations have relatively small effects on most of the results of these simulations. Of the calculated concentrations of stable species, the greatest difference is in the total predicted hydroperoxide concentrations. In addition, as shown in Table II-9, model "S" consistently predicts higher concentrations of the oxygenated products after NO_x is consumed than does the more detailed model. On the other hand, as shown in the table, there are only very minor differences in calculated ozone, NO_2, PAN and HO_2 levels, as well as in the calculated levels of propene, n-butane, and hydroxyl radicals, and most other species which are not directly affected by these approximations.

The relatively large differences in the total hydroperoxide levels calculated by the standard model and the detailed model are expected because of the differences in the rates of the competing peroxy + peroxy radical reactions of the individual peroxy radicals, which are all lumped together in the more approximate model. The fact that the hydroperoxides

Table II-9. Selected Results of Model Calculations Testing the Effects of Approximations Concerning Peroxy Radical, Peroxynitrate and Hydroperoxide Reactions

	Calc. 1				Calc. 2				Calc. 3				Calc. 4			
Model:[a]	D	S	X1	X2	D	S	X1	X2	D	S	X1	X2	D	S	X1	X2
Ozone																
Final (ppm)	0.384	0.373	0.164	0.172	0.271	0.271	0.272	0.272	0.445	0.430	0.349	0.340	0.307	0.306	0.306	0.309
Max (ppm)	0.392[c]	0.384	0.378	0.414	0.360	0.358	0.358	0.358	0.452	0.437	0.402	0.409	0.344	0.351	0.350	0.356
(min.)[b]	720[c]	600	600	600	1080	1080	1080	1080	1140	1140	720	720	840	780	780	780
NO_2																
Final (ppb)	2.83	2.14	<0.01	<0.01	22.8	22.8	22.2	22.4	2.58	1.92	<0.01	<0.01	0.17	0.19	<0.01	<0.01
Max (ppb)	83.0	83.5	83.4	83.4	346.8	346.8	346.8	346.8	73.8	73.9	73.9	73.8	67.0	67.6	67.6	67.6
(min.)	420	420	420	420	720	720	720	720	480	480	480	480	540	540	540	540
PAN																
Final (ppb)	55.3	57.6	74.7	73.3	73.8	73.9	74.4	74.4	51.1	54.1	67.6	67.7	67.2	66.3	66.8	66.8
Max (ppb)	68.2	68.7	74.7	73.3	73.8	73.8	74.4	74.4	62.8	63.3	67.7	67.7	67.4	66.5	66.8	66.8
(min.)	660	660	1110	1110	1260	1260	1260	1260	780	780	1140	1110	960	960	1200	1230
Formaldehyde																
Final (ppm)	0.079	0.105	0.082	0.039	0.070	0.071	0.070	0.070	0.037	0.049	0.027	0.016	0.037	0.049	0.040	0.027
Max (ppm)	0.406	0.415	0.414	0.398	0.117	0.117	0.117	0.117	0.145	0.145	0.146	0.146	0.124	0.127	0.127	0.127
Acetaldehyde																
Final (ppm)	0.379	0.393	0.459	0.438	0.089	0.090	0.089	0.089	0.064	0.067	0.098	0.089	0.119	0.123	0.126	0.117
Max (ppm)	0.472	0.489	0.495	0.487	0.131	0.131	0.131	0.131	0.135	0.136	0.136	0.136	0.135	0.138	0.138	0.137
Hydroperoxides																
Final (ppb)	178	197	245	-	0.36	0.57	0.52	-	44.2	51.8	59.9	-	31.6	33.4	42.0	-
Peroxynitrates																
Max (ppb)	0.96	-	-	-	0.46	-	-	-	0.17	-	-	-	4.1	-	-	-
HO_2																
Final (ppt)	12	20	1	5	7	7	5	6	10	19	0.1	0.4	4	4	1	3
Max (ppt)	203	204	204	283	9	11	11	11	121	123	124	151	99	100	100	112

[a] Designation for models (see text for details): A = Detailed model. S = Model with standard approximations. X1 = Model with peroxy + peroxy radical reactions ignored. X2 = Model with peroxy + peroxy and peroxy + HO_2 radical reactions ignored.

[b] Minutes after midnight, solar time, given to nearest hour.

[c] Calculation also has a local maximum of 0.382 ppm at 600 min.

themselves are all lumped together in the more approximate model is believed to be a less important factor in this regard, because in both models all the reactions forming the hydroperoxides have the same rate constant, and both the lumped hydroperoxide in the more approximate model and the individual hydroperoxides in the more detailed are assumed to react only by photolysis, with the same rate constant being used for both lumped and individual hydroperoxide species.

On the other hand, the differences between the standard and the detailed models in the calculated aldehyde levels after the consumption of NO_x can be attributed largely to differences in the representation of the hydroperoxides in the two models. For example, in the more detailed model, the $HO_2 + CH_3O_2\cdot$ system is represented by:

$$HO_2 + CH_3O_2\cdot \rightarrow CH_3OOH$$

$$CH_3OOH + h\nu \rightarrow CH_3O\cdot + OH \rightarrow HCHO + HO_2 + OH$$

while in the standard, more approximate, model these reactions are represented by:

$$HO_2 + CH_3O_2\cdot \rightarrow -OOH + HCHO$$

$$-OOH + h\nu \rightarrow OH + HO_2$$

Although the net reaction is the same, in the approximate model the aldehyde is generated immediately in the HO_2 + peroxy radical reaction, while in the less approximate model it is not generated until the hydroperoxide photolyzes. However, since in the standard model the oxygenates are used as surrogates for the hydroperoxides (i.e., the reactions of the hydroperoxides, other than their photolysis at the OOH group to form radicals, are lumped with those of the oxygenates), the fact that the standard model predicts slightly higher levels of these oxygenates under conditions where hydroperoxide formation becomes non-negligible is not inappropriate.

The results of calculations using the "X1" and "X2" models, where the peroxy + peroxy radical reactions are ignored altogether, indicate that ignoring these reactions can have a significant effect on the predictions of the model. In particular, in calculations #1 and #3, the models which ignore the peroxy + peroxy reactions differ from the models including these reactions in that (1) they predict a relatively rapid consumption of ozone following the time most of the NO_2 is consumed, where the more detailed models predict it remains relatively constant; (2) they predict that PAN remains relatively constant, or increases slightly, following the consumption of NO_2, while the more detailed model predicts it declines; (3) they predict differing final levels of oxygenated products; (4) they predict significantly lower HO_2 levels, even for model "X2", where the HO_2 + peroxy radical reactions are ignored; and (5) they predict the final NO_2 concentrations are orders of magnitude lower than predicted by the models which include the peroxy + peroxy radical reactions. On the other hand, ignoring these reactions has no significant effect in calculation #2, because significant NO_x remains at the end of the simulation, and thus peroxy + NO reactions dominate at all times in the simulation; and the effects of ignoring these reactions appear to be less in the lower temperature simulation (calculation #4), though the final NO_2 and HO_2 levels are still significantly affected.

These effects of ignoring the peroxy + peroxy radical reactions on the results of the simulations after the bulk of the initially present NO_x is consumed can be attributed to a number of factors, but the most direct effect is that if these reactions are ignored, then the predicted peroxy radical concentrations are much higher. Because of the equilibrium between acyl peroxy radicals, NO_2, and PAN (see Section II-C-2, below)

$$CH_3CO_3 + NO_2 \rightleftarrows PAN$$

the higher acylperoxy radical levels result in lower NO_2 levels, and also have the effect of increasing the stability of PAN, as observed in these calculations. The much lower NO_2 levels results in a lower formation rate of ozone due to NO_2 photolysis (reaction A1 followed by reaction A2), which means in these calculations that the ozone sink processes become relatively more important, and more rapid ozone consumption occurs. The effects on peroxy radical levels and NO_2 also affect predictions of OH and HO_2 radical levels, and these can account for the other differences observed.

Thus it is clear that ignoring the peroxy + peroxy radical reactions, as is the case for most other models currently in use, is not a good approximation; and if the models are to accurately simulate processes occurring under low NO_x conditions, it is necessary for them to include some sort of representation for these reactions. The inclusion of the peroxy + HO_2 reactions clearly is not adequate to represent the fate of peroxy radicals in the absence of NO_x, since the results of calculations using model "X1", where the HO_2 reactions are included are very similar to the results using model "X2", where these are ignored. However, these test calculations also show that the approach employed in this model, which involves the addition to the model of far fewer species and reactions than would an explicit representation, is generally adequate to represent the net effects of these reactions on the chemical transformations occurring.

II. C. OXYGENATE AND ALKYL NITRATE REACTION MECHANISMS

In this section, the reactions of the simpler oxygenates and alkyl nitrates in the model are discussed. The specific compounds discussed are formaldehyde, acetaldehyde, propionaldehyde, acetone, methyl ethyl ketone, glyoxal, methylglyoxal, biacetyl, glycolaldehyde, 2-butyl nitrate, 4-heptyl nitrate and 3-pentanol.

The compounds whose reactions are discussed in this section represent the major products formed in the photooxidations of the organics emitted into the atmosphere. The major exception to this are the aromatic compounds and oxygenates and uncharacterized ring-opening products in the aromatic photooxidation mechanism; the reactions of these species are given in Section II-G, where the aromatic photooxidation mechanisms are discussed.

Several of the compounds whose reactions are discussed in this section are used in the model to represent the reactions of other, chemically similar, compounds. In particular, propionaldehyde is taken to represent the reactions of most of the higher aldehydes, methyl ethyl ketone represents most of the ketones other than acetone, and 2-butyl nitrate and 4-heptyl nitrate together represent the higher alkyl nitrates. Furthermore, as discussed in Section E, 3-pentanol and propionaldehyde or methyl ethyl ketone, are used to represent the reactions of the bifunctional products formed in the photooxidations of the long chain alkanes. This representation is used to reduce the number of species in the model, and is consistent with the "lumped molecule" approach upon which this model is based.

1. Reactions of Formaldehyde

Formaldehyde is a key organic species, being both a primary and a secondary pollutant, and is a major source of the important HO_2 radical.

C1. $HCHO + h\nu \xrightarrow{O_2} 2\ HO_2 + CO$

C2. $HCHO + h\nu \rightarrow H_2 + CO$

Photolysis is an important loss process for formaldehyde, and the first reaction is also an important source of radicals. Reaction (C1) as written consists of several steps; the initial process is

$$HCHO + h\nu \rightarrow H + HCO$$

followed by the fast reactions

$$H + O_2 + M \rightarrow HO_2 + M$$

and

$$HCO + O_2 \rightarrow CO + HO_2$$

Reaction (C2) must also be included in the model since it represents a non-negligible loss process for formaldehyde.

The quantum yields and absorption cross sections used in this model for these reactions are those recommended by Atkinson and Lloyd (1984) and NASA (1985), and are given in Table II-10.

C3. $OH + HCHO \xrightarrow{O_2} H_2O + HO_2 + CO$

This reaction also represents a major loss process for HCHO. As discussed by Atkinson (1986), the recommended rate constant for this reaction is:

$$k_{C3} = 9.0 \times 10^{-12} \text{ cm}^3 \text{ molecule}^{-1} \text{ sec}^{-1},$$

independent of temperature, with an estimated uncertainty of a factor of ~1.25 at 298 K.

C4. $HO_2 + HCHO \rightarrow O_2CH_2OH$

The existence and importance of this reaction has only been recognized in the last few years, and it explains the observations of formic

Table II-10. Absorption Cross Sections, σ, (cm^2 $molecule^{-1}$, base e), for HCHO and Quantum Yields ϕ_1, and ϕ_2 for Photodissociation of HCHO at 760 Torr Total Pressure of Air (from NASA 1985)

λ (nm)	$10^{20} \times \sigma$ (cm^2)	ϕ_1 (H + HCO)	ϕ_2 (H_2 + CO)
240	0.03	0.21	0.42
250	0.13	0.24	0.46
260	0.47	0.30	0.48
270	0.86	0.40	0.46
280	1.86	0.59	0.35
290	2.51	0.71	0.26
300	2.62	0.78	0.22
310	2.45	0.77	0.23
320	1.85	0.62	0.38
330	1.76	0.31	0.69
340	0.42	0.0	0.69[a]
350	0.42	0.0	0.40[a]
360	0.06	0.0	0.12[a]

Note: The values are averaged for 10 nm intervals centered on the indicated wavelength.

[a] Pressure dependent.

acid in both laboratory systems and the atmosphere. The reaction as written above consists of two steps; the initial reaction is believed to be

$$HO_2 + HCHO \rightarrow HO_2CH_2O$$

followed by an isomerization of the HO_2CH_2O radical to O_2CH_2OH

$$HO_2CH_2O \rightarrow O_2CH_2OH$$

As discussed by Atkinson and Lloyd (1984) the back isomerization of thermalized $HOCH_2OO$ to OCH_2OOH is estimated to have a ~23 kcal $mole^{-1}$ activation energy, and hence should be negligible under atmospheric conditions. Thus the subsequent reactions will involve O_2CH_2OH, with the initial reaction being the rate determining step.

Kinetic data at around room temperature for this reaction have been obtained by Su et al. (1979a,b), Veyret et al. (1982), and Barnes et al. (1985). At 298 K, rate constants k_{C4} of 1.0×10^{-14} cm^3 $molecule^{-1}$ sec^{-1} (Su et al. 1979a,b) and $(7.5 \pm 3.5) \times 10^{-14}$ cm^3 $molecule^{-1}$ sec^{-1} (Vegret et al. 1982) have been reported while Barnes et al. (1985) have derived $k_{C4} = (1.1 \pm 0.4) \times 10^{-13}$ cm^3 $molecule^{-1}$ sec^{-1} at 273 K. Because of the more comprehensive study of Veyret et al. (1982), Atkinson and Lloyd (1984) initially recommended $k_{C4} = 7.5 \times 10^{-14}$ cm^3 $molecule^{-1}$ sec^{-1} at room temperature, with an uncertainty of a factor of 2. However, testing against environmental chamber data indicates that the lower value of Su et al. (1979b) yields better fits to the data in modeling runs which are sensitive to this rate constant. For example, Figures II-1 and II-2 show experimental and calculated ozone, NO_2 and formaldehyde concentration-time profiles for formaldehyde-NO_x-air chamber runs carried out in the SAPRC EC and in the UNC outdoor chamber, and Figure II-3 shows selected experimental and calculated concentration-time profiles for an ethene-NO_x-air experiment which is also sensitive to this rate constant. In all three cases shown, the rate constant of Su et al. (1979b) yields better fits to the ozone and formaldehyde data, and in no case do the model calculations indicate that the higher rate constant is more appropriate. Thus, we tentatively recommend

$$k_{C4} = 1.0 \times 10^{-14} \text{ cm}^3 \text{ molecule}^{-1} \text{ sec}^{-1},$$

though clearly more direct measurements of this rate constant are required. Because of the uncertainties in this rate constant, its temperature dependence is ignored.

C5. $O_2CH_2OH + NO \xrightarrow{O_2} HCOOH + HO_2 + NO_2$

The reaction with NO is complex, being made up of the reaction:

$$HOCH_2O_2 + NO \rightarrow HOCH_2O + NO_2 \qquad (a)$$

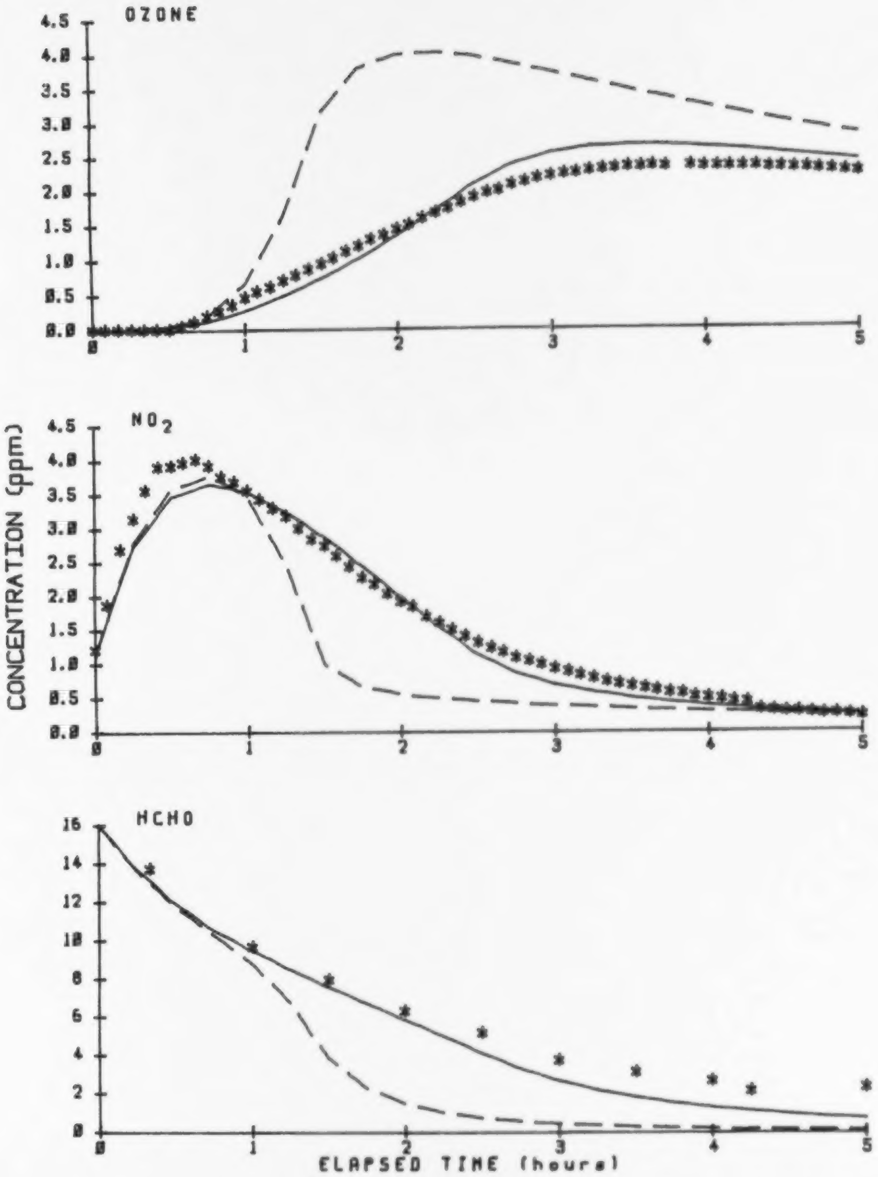

Figure II-1. Observed and calculated concentration-time profiles for ozone, NO_2, and formaldehyde for the formaldehyde-NO_x-air run EC-341.

* = Experimental data.

----- = Calculated using $k_{C4} = 1.0 \times 10^{-14}$ cm^3 $molecule^{-1}$ sec^{-1}.

-- -- = Calculated using $k_{C4} = 7.5 \times 10^{-14}$ cm^3 $molecule^{-1}$ sec^{-1}.

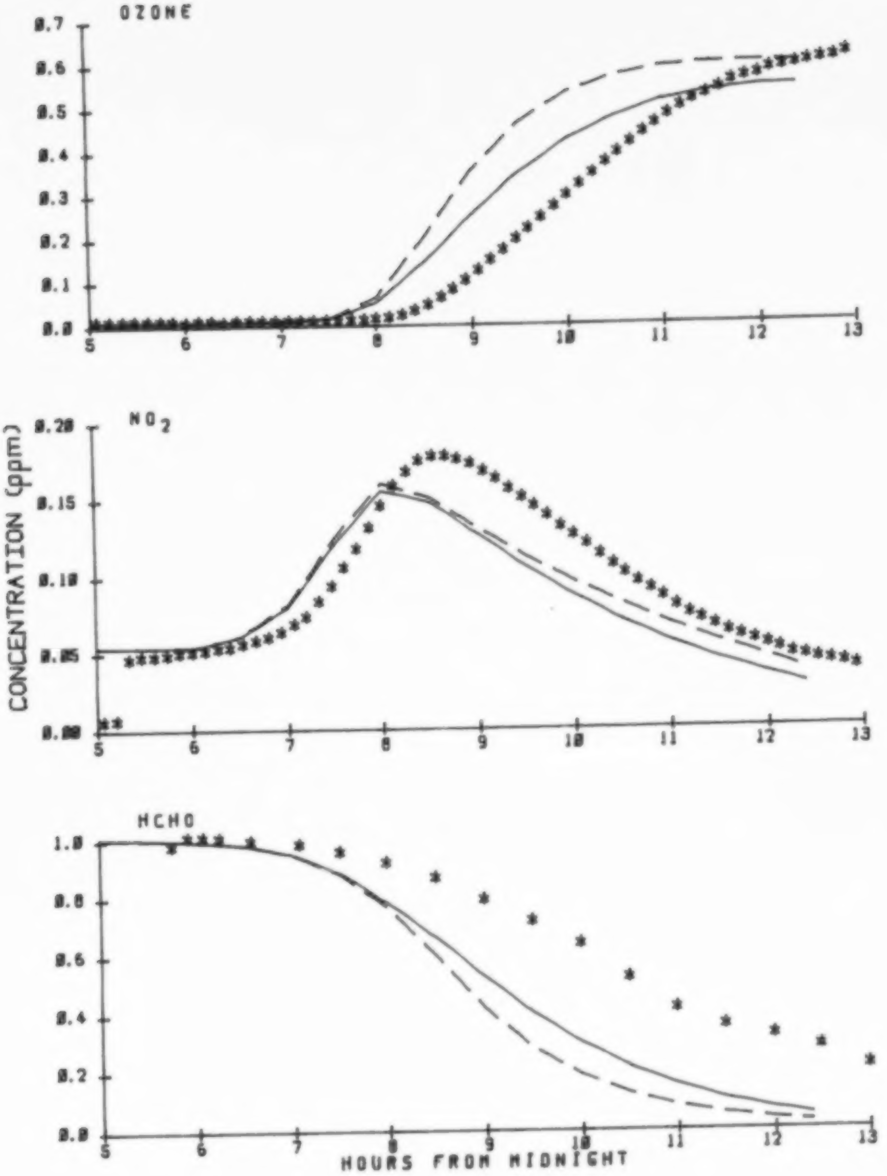

Figure II-2. Observed and calculated concentration-time profiles for ozone, NO_2, and formaldehyde for the formaldehyde-NO_x-air UNC chamber run AU0279B.

* = Experimental data.

----- = Calculated using $k_{C4} = 1.0 \times 10^{-14}$ cm^3 molecule^{-1} sec^{-1}.

-- -- = Calculated using $k_{C4} = 7.5 \times 10^{-14}$ cm^3 molecule^{-1} sec^{-1}.

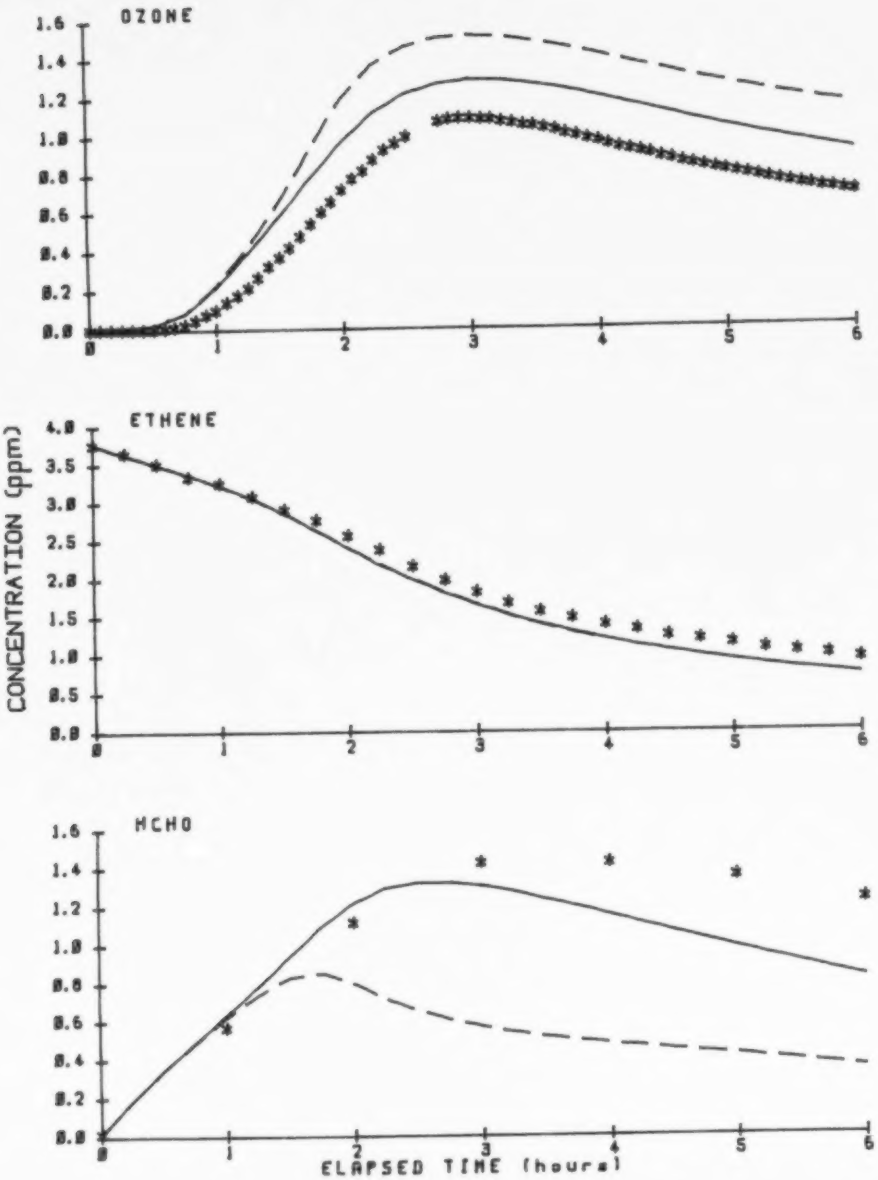

Figure II-3. Observed and calculated concentration-time profiles for ozone, ethene and formaldehyde for the ethene-NO_x-air run EC-286.

* = Experimental data.

----- = Calculated using $k_{C4} = 1.0 \times 10^{-14}$ cm^3 $molecule^{-1}$ sec^{-1}.

-- -- = Calculated using $k_{C4} = 7.5 \times 10^{-14}$ cm^3 $molecule^{-1}$ sec^{-1}.

followed by the fast reaction (Veyret et al. 1982)

$$HOCH_2O + O_2 \rightarrow HCOOH + HO_2 \qquad (b)$$

with the rate determining step being the reaction of the peroxy radical with NO. The kinetics of the reactions of peroxy radicals with NO are discussed in Section B.

Formic acid reacts with OH radicals relatively slowly, with a room temperature rate constant of $\sim 4 \times 10^{-13}$ cm^3 $molecule^{-1}$ sec^{-1} (Atkinson 1986). Because of this, and since in most instances formic acid is a relatively minor product, its reactions are ignored in the present model.

C6. $O_2CH_2OH + HO_2 \rightarrow -OOH + (O_2CH_2OH\ products)$

C7. $O_2CH_2OH + RO_2 \rightarrow HO_2 + (O_2CH_2OH\ products)$

C8. $O_2CH_2OH + RCO_3 \rightarrow HO_2 + (O_2CH_2OH\ products)$

The kinetics of these reactions and the general principles used for representing the products are discussed in Section B. As indicated there, the organic products formed in these reactions are represented by the set of products expected to be formed from the reactions of the corresponding alkoxy radical. As discussed above, the alkoxy radical is expected to react with O_2 to form acetic acid, whose subsequent reactions are ignored in the present model. Thus we use:

$$(O_2CH_2OH\ products) = \text{"lost carbon"}$$

for the above reactions.

C9. $NO_3 + HCHO \xrightarrow{O_2} HNO_3 + HO_2 + CO$

This reaction may be important under nighttime conditions. Rate constants for this reaction have been determined by Atkinson et al.

(1984a) and Cantrell et al. (1985). Significant uncertainties in the values of k_{C9} arise because of uncertainties in the equilibrium constant for the $NO_2 + NO_3 \rightleftarrows N_2O_5$ reactions. The UC Riverside group measured a rate constant k_{C9} relative to the $NO_2 + NO_3 \rightleftarrows N_2O_5$ equilibrium constant (Atkinson et al. 1984a), and subsequently (Tuazon et al. 1984a) determined this equilibrium constant directly. Although both groups recommend a rate constant at 298 K of

$$k_{C9} = 6 \times 10^{-16} \text{ cm}^3 \text{ molecule}^{-1} \text{ sec}^{-1},$$

the equilibrium constants used in these derivations are significantly different, by ~30%. However, for four of the nine experiments carried out by Cantrell et al. (1985), the values of k_{C9} derived were independent of the $NO_2 + NO_3 \rightleftarrows N_2O_5$ equilibrium constant, and these also yield $k_{C9} = 6 \times 10^{-16}$ cm^3 molecule^{-1} sec^{-1} at room temperature. Hence we use this value.

The temperature dependence for this reaction is not known, and must thus be estimated. We assume that the Arrhenius pre-exponential factor per abstractable H-atom is approximately three times that for H-atom abstraction reactions by methoxy radicals (since NO_3 has three equivalent radical atoms), which, based on the data tabulated by Kerr and Moss (1981), is ~3 x 10^{-13} cm^3 molecules^{-1} sec^{-1}. Thus we estimate,

$$k_{C9} \cong 6 \times 10^{-13} e^{-4090/RT} \text{ cm}^3 \text{ molecule}^{-1} \text{ sec}^{-1}$$

which yields the recommended value of $k_{C9} = 6 \times 10^{-16}$ cm^3 molecule^{-1} sec^{-1} at 298 K.

2. Reactions of Acetaldehyde

Reactions of acetaldehyde are important both because of their role as radical precursors, and also because of the ability of peroxyacetyl radicals to react with NO_2 to form peroxyacetyl nitrate (PAN), an important sink for NO_x. The key reactions of CH_3CHO are those of photolysis and reaction with OH and NO_3 radicals. These and subsequent reactions of the species derived from CH_3CHO are described below.

C10. $OH + CH_3CHO \xrightarrow{O_2} H_2O + CH_3CO_3\cdot$

This reaction as written is comprised of

$$OH + CH_3CHO \rightarrow H_2O + CH_3\dot{C}O$$

followed by the fast reaction

$$CH_3\dot{C}O + O_2 \rightarrow CH_3CO_3\cdot$$

The recommended rate constant for this reaction (Atkinson 1986) is that of Atkinson and Pitts (1978) of

$$k_{C10} = 6.9 \times 10^{-12}\ e^{500/RT}\ cm^3\ molecule^{-1}\ sec^{-1}$$

$$= 1.6 \times 10^{-11}\ cm^3\ molecule^{-1}\ sec^{-1}\ \text{at } 298\ K,$$

with an estimated uncertainty at 298 K of a factor of 1.25.

C11. $CH_3CHO + h\nu \xrightarrow{O_2} CH_3O_2\cdot + HO_2 + CO$ (a)

$\rightarrow CH_4 + CO$ (b)

As discussed by Atkinson and Lloyd (1984), the recent data of Horowitz and Calvert (1982) and Meyrahn et al. (1982) are in excellent agreement, and allow the quantum yields ϕ_a and ϕ_b to be derived as a function of wavelength. The absorption cross sections used are those given by Calvert and Pitts (1966), and the quantum yields ϕ_a and ϕ_b used are based on those recommended by Atkinson and Lloyd (1984). These are given in Table II-11.

It should be noted that process (a) as written consists of several steps, i.e.,

$$CH_3CHO + h\nu \rightarrow \dot{C}H_3 + HCO \qquad (a)$$

Table II-11. Absorption Cross Sections, σ, (cm^2 $molecule^{-1}$, base e), for Acetaldehyde and Quantum Yields ϕ_a and ϕ_b for its Photodissociation in Air

λ(nm)	$10^{20} \times \sigma$ (cm^2)	ϕ_a ($CH_3 + HCO$)	ϕ_b ($CH_4 + CO$)[a]
260	2.16	0.310	0.47
270	3.46	0.380	0.33
280	4.32	0.590	0.06
290	4.76	0.550	0.01
295	4.45	0.490	0.0
300	4.03	0.415	0.0
305	3.42	0.325	0.0
310	2.72	0.235	0.0
315	2.09	0.150	0.0
320	1.60	0.075	0.0
325	1.13	0.030	0.0
330	0.68	0.0	0.0

[a] This process ignored in model.

followed by the fast reactions

$$\dot{C}H_3 + O_2 \xrightarrow{M} CH_3O_2\cdot$$

and

$$HCO + O_2 \rightarrow HO_2 + CO$$

Reaction (C11b) is of negligible importance in the lower troposphere, and hence is ignored in the model.

C12. $NO_3 + CH_3CHO \xrightarrow{O_2} HNO_3 + CH_3CO_3\cdot$

This reaction as written is again comprised of two elementary reaction steps:

$$NO_3 + CH_3CHO \rightarrow HNO_3 + CH_3\dot{C}O$$

followed by the fast reaction

$$CH_3\dot{C}O + O_2 \rightarrow CH_3CO_3 \cdot$$

The recommended rate constant for this reaction (Atkinson and Lloyd 1984) is:

$$k_{C12} = 2.5 \times 10^{-15}\ cm^3\ molecule^{-1}\ sec^{-1}\ at\ 298\ K,$$

with an estimated uncertainty of a factor of 2 at this temperature. The above rate constant is based upon the $NO_2 + NO_3 \rightleftarrows N_2O_5$ equilibrium constant of Kircher et al. (1984) and Tuazon et al. (1984).

The temperature dependence for this reaction is unknown. As estimated for the NO_3 + HCHO reaction, we assume that pre-exponential factor per abstractable H atom is 3×10^{-13} cm^3 molecule $^{-1}$ sec^{-1}. Thus

$$k_{C12} = 3 \times 10^{-13} e^{-2835/RT}\ cm^3\ molecule^{-1}\ sec^{-1},$$

which gives the appropriate value for k_{C12} at 298 K.

C13. $CH_3CO_3 \cdot + NO \xrightarrow{O_2} CH_3O_2 \cdot + CO_2 + NO_2$

The kinetics of this reaction are discussed in Section B. The reaction as written consists of three elementary reactions, the first (rate determining) being

$$CH_3CO_3 \cdot + NO \rightarrow CH_3CO_2 \cdot + NO_2$$

followed by the fast reactions

$$CH_3CO_2 \cdot \rightarrow \dot{C}H_3 + CO_2$$

$$\dot{C}H_3 + O_2 \overset{M}{\rightarrow} CH_3O_2 \cdot$$

C14. $CH_3CO_3\cdot + NO_2 \rightarrow CH_3CO_3NO_2$ (PAN)

This is the important reaction producing peroxyacetyl nitrate (PAN). The kinetics of this reaction are discussed in Section B.

C15. $CH_3CO_3\cdot + HO_2 \rightarrow -OOH + (CH_3CO_3$ products)

C16. $CH_3CO_3\cdot + RO_2 \rightarrow 0.5\ HO_2 + (CH_3CO_3$ products)

C17. $CH_3CO_3\cdot + RCO_3 \rightarrow HO_2 + (CH_3CO_3$ products)

The kinetics of these reactions and the general principles used for representing the products are discussed in Section B. As indicated there, the organic products formed in these reactions are represented by the set of products expected to be formed from the reactions of the corresponding alkoxy radical; and, if the alkoxy radical decomposes to form other peroxy radicals, the products used to represent the formation of those radicals are those used to represent the products formed when those radicals react with HO_2 or other peroxy radicals. As discussed above, the acetyl oxy radical decomposes to form $CO_2 + CH_3O_2$. Since the product used to represent the reactions of CH_3O_2 with HO_2 or peroxy radicals is formaldehyde, we thus use

$$(CH_3CO_3\cdot \text{ products}) = CO_2 + HCHO$$

for the above reactions.

C18. $CH_3CO_3NO_2$ (PAN) $\rightarrow CH_3CO_3\cdot + NO_2$

PAN is thermally unstable and decomposes back to the reactants. As discussed by Atkinson and Lloyd (1984), the recommended rate constant is that determined by Hendry and Kenley (1977) of

$$k_{C18} = 2.0 \times 10^{16} e^{-26910/RT} \sec^{-1}$$

$$= 3.6 \times 10^{-4} \sec^{-1} \text{ at } 298 \text{ K},$$

with an estimated uncertainty of a factor of ~1.25 over the temperature range 280-320 K.

C19. $CH_3O_2 + NO \rightarrow CH_3O + NO_2$

The kinetics of methyl peroxy radical reactions with NO are discussed in Section B. The reactions of CH_3O_2 (and other peroxy radicals lumped as RO_2) with NO_2 is ignored, since the peroxyalkyl nitrate formed rapidly back decomposes (see Section B). Reaction (C19) as written above is now known to be the only significant process for the reaction of methyl peroxy radicals with NO.

C20. $CH_3O_2\cdot + HO_2 \rightarrow -OOH + HCHO$

C21. $CH_3O_2\cdot + RO_2 \rightarrow 0.5\ HO_2 + (CH_3O_2 \text{ products})$

C22. $CH_3O_2\cdot + RCO_3 \rightarrow 0.5\ HO_2 + (CH_3O_2 \text{ products})$

The kinetics of these reactions and the general principles used for representing the products are discussed in Section B. As indicated there, the organic products formed in these reactions are represented by the set of products expected to be formed from the reactions of the corresponding alkoxy radical in the absence of NO_x. As discussed below, in the absence of NO_x the alkoxy radical is expected to react with O_2 to form formaldehyde. Thus we use

$$(CH_3O_2\cdot \text{ products}) = HCHO$$

for the above reactions.

C23. $CH_3O^{\cdot} + O_2 \rightarrow HCHO + HO_2$

This is the major fate of alkyl radicals under tropospheric conditions. Atkinson and Lloyd (1984) recommend the rate expression given by Gutman et al. (1982), $k_{C23} = 1.05 \times 10^{-13} e^{-2600/RT}$ cm^3 molecule^{-1} sec^{-1}, i.e., 1.3×10^{-15} cm^3 molecule^{-1} sec^{-1} at 298 K. However, a more recent and extensive study of Lorenz et al. (1985) yields

$$k_{C23} = 5.5 \times 10^{-14} e^{-1990/RT} \text{ cm}^3 \text{ molecule}^{-1} \text{ sec}^{-1}$$

$$= 1.9 \times 10^{-15} \text{ cm}^3 \text{ molecule}^{-1} \text{ sec}^{-1} \text{ at 298 K.}$$

We use this more recent data (see also Carter and Atkinson 1985), with an estimated uncertainty of a factor of ~2.

C24. $CH_3O^{\cdot} + NO_2 \xrightarrow{M} CH_3ONO_2$

This is a minor process in the atmosphere, but it is included in the model since it is required to account for the formation of methyl nitrate observed in environmental chamber experiments. Comparisons of predicted versus observed methyl nitrate yields are a useful test of some aspects of the mechanism. Atkinson and Lloyd (1984) recommend

$$k_{C24} = 1.5 \times 10^{-11} \text{ cm}^3 \text{ molecule}^{-1} \text{ sec}^{-1},$$

independent of temperature, with an estimated uncertainty of a factor of ~3. This estimated uncertainty reflects the uncertainty in the magnitude of k_{C24}; in terms of affecting model predictions it is the value of the k_{C24}/k_{C23} ratio which is important, and this is probably known to within at least a factor of 2 or better.

3. Reactions of Propionaldehyde

Propionaldehyde serves as the representative of all the higher aldehydes in the chemical mechanism. Its reactions are analogous to those for acetaldehyde, with the important processes under atmospheric conditions being photolysis and reaction with OH and NO_3 radicals.

C25. $OH + CH_3CH_2CHO \xrightarrow{O_2} H_2O + CH_3CH_2CO_3.$

This reaction consists of two steps, the initial, rate determining reaction being

$$OH + CH_3CH_2CHO \rightarrow H_2O + CH_3CH_2\dot{C}O$$

followed by

$$CH_3CH_2\dot{C}O + O_2 \rightarrow CH_3CH_2CO_3.$$

As recommended by Atkinson (1986) the room temperature rate constant is

$$k_{C25} = 1.96 \times 10^{-11} \text{ cm}^3 \text{ molecule}^{-1} \text{ sec}^{-1}.$$

The temperature dependence is expected to be very similar to that for acetaldehyde, and hence

$$k_{C25} = 8.5 \times 10^{-12} e^{500/RT} \text{ cm}^3 \text{ molecule}^{-1} \text{ sec}^{-1}.$$

The initial OH radical reaction yields almost exclusively $CH_3CH_2\dot{C}O$ (Atkinson and Lloyd 1984, Atkinson 1986).

C26. $CH_3CH_2CHO + h\nu \xrightarrow{O_2} CH_3CH_2OO^{\bullet} + HO_2 + CO$ (a)

$\rightarrow$ non-radical products $(C_2H_6 + CO)$ (b)

The available data for this photolysis reaction are discussed by Atkinson and Lloyd (1984). Few data are available; Shepson and Heicklen (1982a,b) obtained a quantum yield ϕ_a at atmospheric pressure of approximately 0.20 from 254 to 334 nm. The quantum yield ϕ_b was determined to be essentially zero for $\lambda \geq 313$ nm. Further experimental work is clearly necessary.

The absorption cross sections used in the model for propionaldehyde are given in Table II-12, and were taken from Calvert and Pitts (1966). Based on the data discussed above, we use a quantum yield of $\phi_a = 0.20$, independent of wavelength over the actinic region.

Table II-12. Absorption Cross Sections for Propionaldehyde, Acetone and Methyl ethyl ketone (MEK) in the Actinic Region

λ (nm)	σ (cm^3 molecule^{-1}, base e)	
	Propionaldehyde	Acetone and MEK
280	5.3	5.9
290	5.8	5.2
300	5.1	3.4
310	3.7	1.53
320	1.66	0.46
330	0.65	0.11
340	0.14	0.0
345	0.0	0.0

C27. $NO_3 + CH_3CH_2CHO \xrightarrow{O_2} CH_3CH_2\dot{C}O_3 + HNO_3$

No data are presently available for this reaction. By analogy with OH radical reactions with aldehydes we expect that $k_{C27} \geq k_{C12}$, i.e.,

$$k_{C27} \geq 2.5 \times 10^{-15} \text{ cm}^3 \text{ molecule}^{-1} \text{ sec}^{-1} \text{ at}$$

298 K. In the absence of experimental data, we use $k_{C27} = k_{C12}$,

$$\text{i.e., } k_{C27} = 3 \times 10^{-13} e^{-2835/RT} \text{ cm}^3 \text{ molecule}^{-1} \text{ sec}^{-1}.$$

This reaction comprises the following elementary steps

$$NO_3 + CH_3CH_2CHO \rightarrow HNO_3 + CH_3CH_2\dot{C}O$$

$$CH_3CH_2\dot{C}O + O_2 \xrightarrow{M} CH_3CH_2CO_3\cdot$$

C28. $CH_3CH_2\dot{C}O_3 + NO \xrightarrow{O_2} CH_3CH_2O_2\cdot + CO_2 + NO_2$

This acyl peroxy radical $C_2H_5CO_3$ is assumed to react with the same kinetics as other acyl peroxy radicals, which are discussed in Section B. The reaction as written consists of three elementary reactions, the first (rate determining) being

$$C_2H_5CO_3\cdot + NO \rightarrow C_2H_5CO_2\cdot + NO_2$$

followed by the fast reactions

$$C_2H_5CO_2\cdot \rightarrow C_2H_5\cdot + CO_2$$

$$C_2H_5\cdot + O_2 \xrightarrow{M} C_2H_5O_2\cdot$$

C29. $C_2H_5CO_3\cdot + NO_2 \rightarrow C_2H_5CO_3NO_2$ (PPN)

This is the important reaction producing peroxypropionyl nitrate (PPN). The kinetics of this reaction, which is assumed to occur with the same rate constant for all alkyl peroxy radicals, are discussed in Section B.

C30. $C_2H_5CO_3\cdot + HO_2 \rightarrow -OOH + (C_2H_5CO_3$ products)

C31. $C_2H_5CO_3\cdot + RO_2 \rightarrow 0.5\ HO_2 + (C_2H_5CO_3$ products)

C32. $C_2H_5CO_3\cdot + RCO_3 \rightarrow HO_2 + (C_2H_5CO_3$ products)

The kinetics of these reactions and the general principles used for representing the products are discussed in Section B. As indicated there, the organic products formed in these reactions are represented by the set of products expected to be formed from the reactions of the corresponding alkoxy radical; and, if the alkoxy radical decomposes to form other peroxy radicals, the products used to represent the formation of those radicals are those used to represent the products formed when those radicals react with HO_2 or other peroxy radicals. As discussed above, the $C_2H_5CO_2$ radical decomposes to form CO_2 + $C_2H_5O_2$. Since the product used to represent the reactions of CH_3O_2 with HO_2 or peroxy radicals is acetaldehyde (see below), we thus use

$$(C_2H_5CO_3\cdot \text{ products}) = CO_2 + CH_3CHO$$

for the above reactions.

C33. $C_2H_5CO_3NO_2$ (PPN) → $C_2H_5CO_3\cdot + NO_2$

PPN is thermally unstable and decomposes back to the reactants. As discussed by Atkinson and Lloyd (1984), the recommended rate constant k_{C33} is

$$k_{C33} = 2.0 \times 10^{16}\ e^{-26910/RT}\ \text{sec}^{-1}$$

$$= 3.6 \times 10^{-4}\ \text{sec}^{-1} \text{ at } 298\ K,$$

with an estimated uncertainty of a factor of ~1.5 over the temperature range 280-320 K.

C34. $C_2H_5O_2\cdot + NO \rightarrow CH_3CHO + HO_2 + NO_2$

The kinetics of the reactions of peroxy radicals with NO are discussed in Section B. The reaction of $C_2H_5O_2$ (and of other peroxy radicals lumped as RO_2) with NO_2 is ignored, since the alkyl peroxy nitrate formed rapidly back decomposes. Reaction (C34) as written above is now known to be the only significant process for the reaction of ethyl peroxy radicals with NO.

Reaction (C34) as written consists of two steps, the first being ethoxy radical formation,

$$C_2H_5O_2\cdot + NO \rightarrow C_2H_5O^{\cdot} + NO_2$$

followed by its reaction with O_2

$$C_2H_5O^{\cdot} + O_2 \rightarrow CH_3CHO + HO_2,$$

which is the major fate of ethoxy radicals under atmospheric conditions. The most important competing process, reaction with NO_2 forming ethyl nitrate,

$$C_2H_5O^{\cdot} + NO_2 \overset{M}{\rightarrow} C_2H_5ONO_2$$

is minor under normal atmospheric conditions and is thus ignored in this model.

C35. $C_2H_5O_2\cdot + HO_2 \rightarrow -OOH + (C_2H_5O_2$ products)

C36. $C_2H_5O_2\cdot + RO_2 \rightarrow 0.5\ HO_2 + (C_2H_5O_2$ products)

C37. $C_2H_5O_2\cdot + RCO_3 \rightarrow 0.5\ HO_2 + (C_2H_5O_2$ products)

The kinetics of these reactions and the general principles used for representing the products are discussed in Section B. As indicated there, the organic products formed in these reactions are represented by the set of products expected to be formed from the reactions of the corresponding alkoxy radical in the absence of NO_x. As discussed above, the alkoxy radical is expected to react with O_2 to form acetaldehyde. Thus we use

$$(C_2H_5O_2\cdot \text{ products}) = CH_3CHO$$

for the above reactions.

4. Reactions of Acetone

The two atmospherically important reactions of acetone are photolysis and reaction with the OH radical.

C38. $OH + CH_3COCH_3 \xrightarrow{O_2} H_2O + CH_3COCH_2OO^\cdot$

This reaction is comprised of the steps

$$OH + CH_3COCH_3 \longrightarrow H_2O + CH_3CO\dot{C}H_2$$

$$CH_3CO\dot{C}H_2 + O_2 \xrightarrow{fast} CH_3COCH_2OO^\cdot$$

The recommended rate constant of Atkinson (1986) is

$$k_{C38} = 2.3 \times 10^{-13} \text{ cm}^3 \text{ molecule}^{-1} \text{ sec}^{-1} \text{ at } 298 \text{ K}.$$

Using an assumed Arrhenius pre-exponential factor of 1×10^{-11} cm^3 molecule^{-1} sec^{-1} leads to

$$k_{C38} = 1 \times 10^{-11} e^{-2235/RT} \text{ cm}^3 \text{ molecule}^{-1} \text{ sec}^{-1}.$$

C39. $CH_3COCH_3 + h\nu \xrightarrow{O_2} CH_3CO_3\cdot + CH_3O_2\cdot$

Gardner et al. (1984) have shown that the quantum yield of this photolysis reaction under atmospheric conditions is ≈0.07, independent of wavelength from 279 to 313 nm, and this is assumed in the model. The absorption cross sections used are taken from Calvert and Pitts (1966) and are summarized in Table II-12.

Previous models (e.g., Carter et al. 1979a, Atkinson et al. 1982a) have assumed unit quantum yields for the photolysis of ketones. The effects on model simulations of the acetone-NO_x-air UNC chamber run JN0480R (the only acetone-NO_x-air chamber run for which we have data -- see Section IV) are shown in Figure II-4. It can be seen that using a quantum yield of 1 significantly overpredicts the reactivity observed in that run. Indeed, the results of that run would be fit best if a quantum yield of zero were assumed. However, given the variability of the fits of the model simulations to the results of the UNC chamber experiments (see Section IV), and the uncertainties in the characterization of the light intensity in that chamber (particularly in the year 1980, where a large correction factor had to be applied to the UV data -- see Section III-A-2), adjusting the quantum yield to improve the fits to this run is not considered to be appropriate.

C40. $CH_3COCH_2OO\cdot + NO \rightarrow \rightarrow CH_3COCHO + HO_2 + NO_2$

The reaction as written is complex. The initial, rate determining, reaction is

$$CH_3COCH_2OO\cdot + NO \rightarrow CH_3COCH_2O\cdot + NO_2\cdot$$

This reaction is assumed to have the same rate constant as other peroxy radical + NO reactions, as discussed in Section B.

The alkoxy radical formed in the initial reaction can either decompose by β-scission, giving rise to acetyl peroxy radicals and formaldehyde,

$$CH_3COCH_2O\cdot \rightarrow CH_3\dot{C}O + HCHO$$

$$CH_3\dot{C}O + O_2 \rightarrow CH_3CO_3\cdot$$

or it could react with O_2 to form methylglyoxal.

$$CH_3COCH_2O\cdot + O_2 \rightarrow HO_2 + CH_3COCHO$$

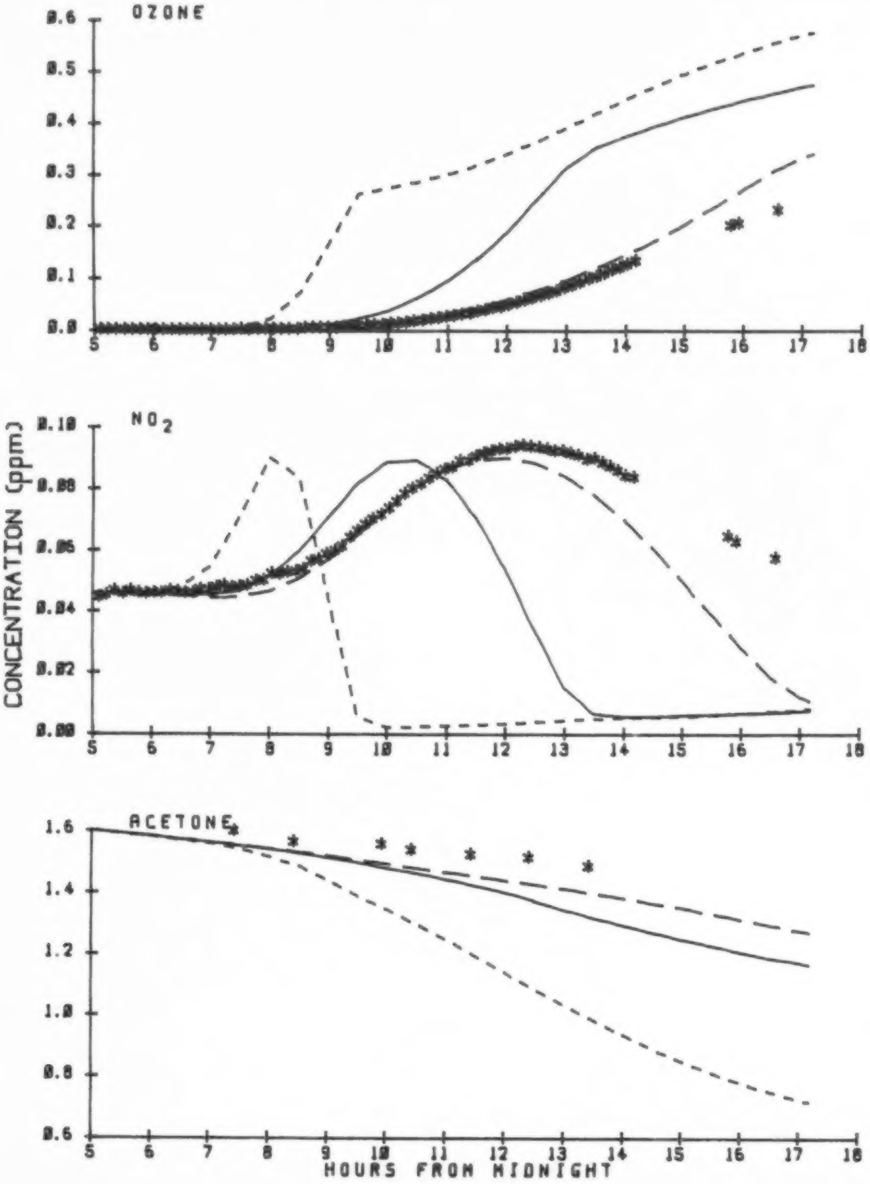

Figure II-4. Observed and calculated concentration-time profiles for ozone, NO_2 and acetone for the UNC acetone-NO_x-air run JN0480R.

* = Experimental data.

----- = Standard model (calculated using acetone photodecomposition quantum yield of 0.07.

— — = Calculated using a quantum yield of 0.

- - - = Calculated using a quantum yield of 1.

Atkinson and Lloyd (1984) estimate, based on the previous estimates of Baldwin et al. (1977), that the decomposition is relatively slow, and thus reaction with O_2 is the dominant process. This estimate is somewhat uncertain, but results of model simulations of the UNC acetone-NO_x-air irradiation are not particularly sensitive to the assumptions concerning this reaction. Therefore, in this model we assume that the estimate of Atkinson and Lloyd (1984) is correct, and that reaction with O_2, forming methylglyoxal, dominates.

C41. $CH_3COCH_2OO^{\cdot} + HO_2 \rightarrow \text{-OOH} + (CH_3COCH_2OO.\ \text{products})$

C42. $CH_3COCH_2OO^{\cdot} + RO_2 \rightarrow 0.5\ HO_2 + (CH_3COCH_2OO.\ \text{products})$

C43. $CH_3COCH_2OO^{\cdot} + RCO_3 \rightarrow 0.5\ HO_2 + (CH_3COCH_2OO.\ \text{products})$

The kinetics of these reactions and the general principles used for representing the products are discussed in Section B. As indicated there, the organic products formed in these reactions are represented by the set of products expected to be formed from the reactions of the corresponding alkoxy radical. If the alkoxy radical decomposes to form other peroxy radicals, the products used to represent the formation of those radicals are those used to represent the products formed when those radicals react with HO_2 or other peroxy radicals. As discussed above, the $CH_3COCH_2O_2$ radical is expected to react with O_2 to yield CH_3COCHO. We thus use

$$(CH_3COCH_2O_2.\ \text{products}) = CO_3COCHO$$

for the above reactions.

5. Reactions of Methyl Ethyl Ketone

This ketone is the representative higher ketone in the model, and reacts via photolysis and reaction with OH radicals.

C44. $OH + CH_3COCH_2CH_3 \xrightarrow{O_2} H_2O + 0.5\ CH_3COCH(OO.)CH_3 + 0.5\ CH_3COCH_2CH_2OO^{\cdot}$

The overall rate constant recommended by Atkinson (1986) for this reaction is

$$k_{C44} = 1.0 \times 10^{-12}\ cm^3\ molecule^{-1}\ sec^{-1} \text{ at } 300\ K.$$

If an Arrhenius pre-exponential factor of $1.2 \times 10^{-11}\ cm^3\ molecule^{-1}\ sec^{-1}$ is estimated, this yields

$$k_{C44} = 1.2 \times 10^{-11}\ e^{-1480/RT}\ cm^3\ molecule^{-1}\ sec^{-1}.$$

This reaction can occur via three possible reaction routes:

$$OH + CH_3COCH_2CH_3 \xrightarrow{O_2} H_2O + CH_3COCH(OO.)CH_3 \quad (a)$$

$$\xrightarrow{O_2} H_2O + CH_3COCH_2CH_2OO^{\cdot} \quad (b)$$

$$\xrightarrow{O_2} H_2O + {}^{\cdot}OOCH_2COCH_2CH_3 \quad (c)$$

At room temperature, pathways (a), (b) and (c) are estimated, using the group rate constant technique of Atkinson (1986), to account for 45%, 47% and 8% of the overall reaction. In view of the relatively low reactivity of methyl ethyl ketone, we neglect pathway (c) and assume that pathways (a) and (b) each account for 50% of the overall reaction.

C45. $CH_3COCH(OO.)CH_3 + NO \xrightarrow{O_2} CH_3CO_3. + CH_3CHO + NO_2$

This reaction as written consists of several steps. The initial, rate determining reaction is

$$CH_3COCH(OO.)CH_3 + NO \rightarrow CH_3COCH(O.)CH_3 + NO_2.$$

This reaction is assumed to have the same rate constant as other alkyl peroxy + NO reactions, as discussed in Section B.

The alkoxy radical could either react with O_2 or it could decompose.

$$CH_3COCH(O.)CH_3 + O_2 \rightarrow CH_3COCOCH_3 + HO_2$$

$$CH_3COCH(O.)CH_3 \rightarrow CH_3\dot{C}O + CH_3CHO$$

$$CH_3\dot{C}O + O_2 \rightarrow CH_3CO_3.$$

However, Atkinson and Lloyd (1984) estimate that decomposition is the dominant process, and Cox et al. (1981) did not observe biacetyl as a product in this methyl ethyl ketone reaction. Decomposition is hence the major process, and the overall reaction is as written above.

C46. $CH_3COCH(OO.)CH_3 + HO_2 \rightarrow \text{-OOH} + (CH_3COCH(OO.)CH_3 \text{ products})$

C47. $CH_3COCH(OO.)CH_3 + RO_2 \rightarrow 0.5\ HO_2 + (CH_3COCH(OO.)CH_3 \text{ products})$

C48. $CH_3COCH(OO.)CH_3 + RCO_3 \rightarrow 0.5\ HO_2 + (CH_3COCH(OO.)CH_3 \text{ products})$

The kinetics of these reactions and the general principles used for representing the products are discussed in Section B. As indicated there, the organic products formed in these reactions are represented by the set of products expected to be formed from the reactions of the corresponding alkoxy radical. If the alkoxy radical decomposes to form other peroxy radicals, the products used to represent the formation of those radicals are those used to represent the products formed when those radicals react with HO_2 or other peroxy radicals. As discussed above, the alkoxy radical in this case is assumed to decompose to form CH_3CHO + CH_3CO_3. Since the products used to represent the reactions of CH_3CO_3 with HO_2 or peroxy radicals are HCHO + CO_2 (see above), we thus use

$$(CH_3COCH(OO.)CH_3 \text{ products}) = CO_2 + HCHO + CH_3CHO$$

for the above reactions.

C49. $CH_3COCH_2CH_2OO^{\bullet} + NO \xrightarrow{O_2} NO_2 + {}^{\bullet}OOCH_2COCH_2CH_2OH$

This reaction as written consists of three steps. The initial, rate determining, process is the reaction of the peroxy radical with NO, whose kinetics are discussed in Section B, and which is assumed to exclusively form NO_2 together with the corresponding alkoxy radical. (Nitrate formation, by analogy with the alkanes, is estimated to be of minor importance, and is neglected.)

The alkoxy radical can undergo a number of competing processes, but, by analogy to the estimates for the corresponding reactions of 1-butoxy, isomerization is assumed to be the dominant process.

$$CH_3COCH_2CH_2O^{\bullet} \rightarrow \dot{C}H_2COCH_2CH_2OH$$

$$\dot{C}H_2COCH_2CH_2OH + O_2 \rightarrow {}^{\bullet}OOCH_2COCH_2CH_2OH$$

C50. $\cdot OOCH_2COCH_2CH_2OH + NO \xrightarrow{O_2} NO_2 + HCHO + HOCH_2CH_2CO_3\cdot\ (\equiv CH_3CH_2CO_3\cdot)$

This reaction also consists of three steps. The kinetics of the rate determining initial reaction with NO are discussed in Section B, and formation of the corresponding alkoxy radical is assumed to dominate. The alkoxy radical could react in a number of ways, the most probable being isomerization

$$\cdot OCH_2COCH_2CH_2OH \rightarrow HOCH_2COCH_2\dot{C}HOH$$

$$HOCH_2COCH_2\dot{C}HOH + O_2 \rightarrow HOCH_2COCH_2CHO + HO_2$$

or decomposition, followed by reaction of the radicals formed with O_2

$$\cdot OCH_2COCH_2CH_2OH \rightarrow HCHO + HOCH_2CH_2\dot{C}O$$

$$HOCH_2CH_2\dot{C}O + O_2 \rightarrow HOCH_2CH_2CO_3\cdot$$

We assume that the decomposition is fast, and the reaction as written above incorporates this assumption.

The radical species $HOCH_2CH_2CO_3$ is not represented explicitly in the model. It is lumped with the acyl peroxy radicals formed in the reactions of the lumped higher aldehydes, which are represented in this model as propionaldehyde. Thus this radical is represented as $CH_3CH_2CO_3$.

C51. $CH_3COCH_2CH_2OO. + HO_2 \rightarrow -OOH + (CH_3COCH_2CH_2OO.$ products)

C52. $CH_3COCH_2CH_2OO. + RO_2 \rightarrow 0.5\ HO_2 + (CH_3COCH_2CH_2OO.$ products)

C53. $CH_3COCH_2CH_2OO. + RCO_3 \rightarrow 0.5\ HO_2 + (CH_3COCH_2CH_2OO.$ products)

C54. $.OOCH_2COCH_2CH_2OH + HO_2 \rightarrow -OOH + (.OOCH_2COCH_2CH_2OH$ products)

C55. $.OOCH_2COCH_2CH_2OH + RO_2 \rightarrow 0.5\ HO_2 + (.OOCH_2COCH_2CH_2OH$ products)

C56. $.OOOH_2COCH_2CH_2OH + RCO_3 \rightarrow 0.5\ HO_2 + (.OOCH_2COCH_2CH_2OH$ products)

The kinetics of these reactions and the general principles used for representing the products are discussed in Section B. As indicated there, the organic products formed in these reactions are represented by the set of products expected to be formed from the reactions of the corresponding alkoxy radical; and, if the alkoxy radical decomposes to form other peroxy radicals, the products used to represent the formation of those radicals are those used to represent the products formed when those radicals react with HO_2 or other peroxy radicals. Since the alkoxy radical corresponding to $CH_3COCH_2CH_2OO$ isomerizes to form $OOCH_2COCH_2CH_2OH$, and its corresponding alkoxy radical is assumed to decompose to form products represented by $HCHO + CH_3CH_2CO_3.$, and the latter radical ultimately gives rise to $CH_3CHO + CO_2$, we use the following to represent the products for the above reactions:

$$\begin{aligned}(CH_3COCH_2CH_2OO\cdot \text{ products}) &= (\cdot OOCH_2COCH_2CH_2OH \text{ products}) \\ &= (CO_2 + HCHO + CH_3CHO)\end{aligned}$$

C57. $CH_3COCH_2CH_3 + h\nu \xrightarrow{O_2} CH_3CO_3\cdot + C_2H_5O_2\cdot$

The absorption cross sections for methyl ethyl ketone given by Calvert and Pitts (1977) are essentially the same in the actinic region as that for acetone, and thus we use the same absorption coefficients for both ketones. These are given in Table II-12. No data are available concerning the quantum yields of the photooxidation pathways under atmospheric conditions. Formation of $CH_3\dot{C}O + C_2H_5\cdot$ is estimated to be the dominant process, followed by the rapid reactions of these radicals with O_2 to yield the overall process shown above.

The quantum yields for this reaction may be similar to those assumed for acetone, which is 0.07 at all wavelengths in the actinic regions, but model simulations of methyl ethyl ketone-NO_x-air chamber runs carried out at UNC suggest that 0.15 may be more appropriate. This is shown in Figure II-5, which compares selected results of model simulations of one of the two such runs for which we have data. (Simulations of the other run yield similar results.) We tentatively use a quantum yield of 0.1 for this reaction, independent of wavelength in the actinic region.

6. Reactions of Glyoxal

Glyoxal is formed in the photooxidations of most aromatic hydrocarbons and is also a possible secondary product in the photooxidation of ethene (formed from glycolaldehyde). Its principal modes of reaction are photolysis and reaction with OH radicals, and its expected reaction with the NO_3 radical is also included in the model.

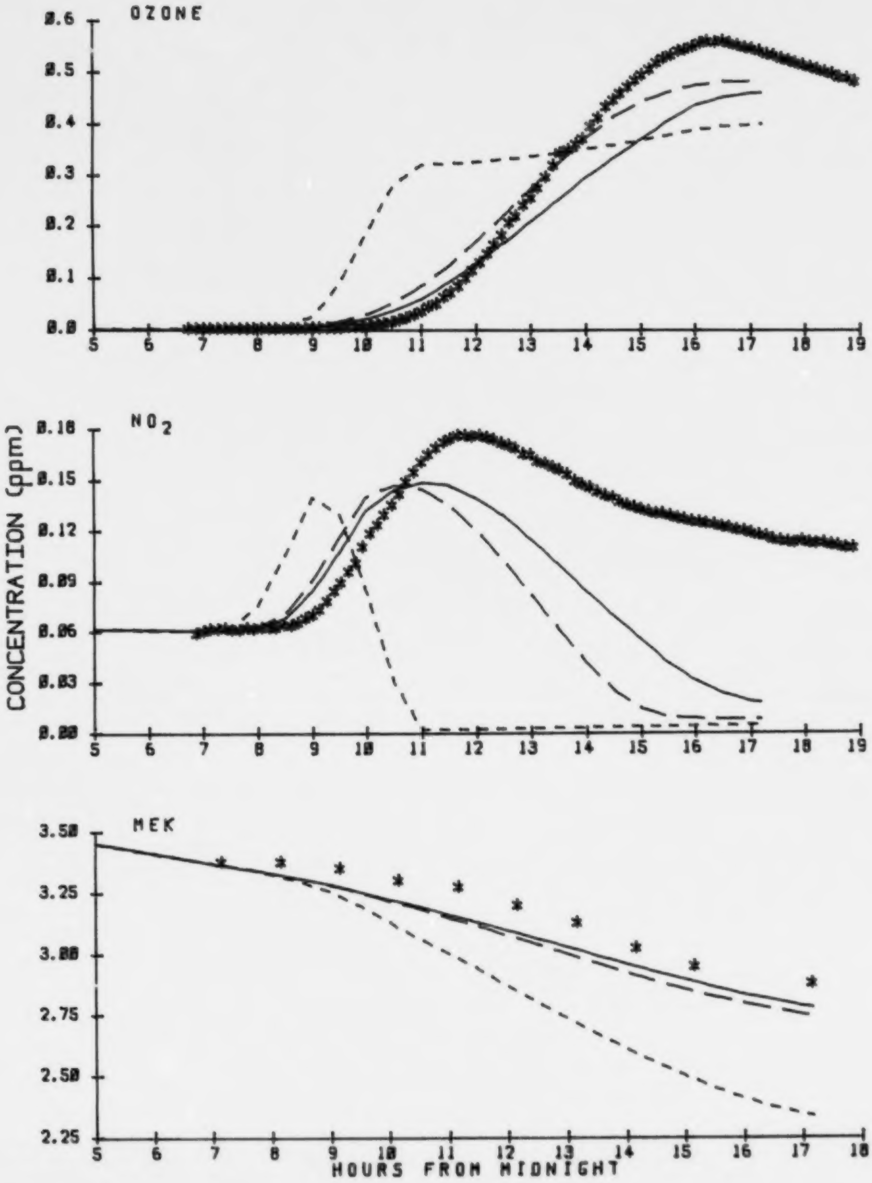

Figure II-5. Observed and calculated concentration-time profiles for ozone, NO_2, and methyl ethyl ketone observed in the UNC MEK-NO_x-air run OC2079K.

* = Experimental data.
----- = Calculated using a methyl ethyl ketone photodecomposition quantum yield of 0.10 (standard model).
-- -- = Calculated using a quantum yield of 0.15.
- - - = Calculated using a quantum yield of 1.0.

C58. $HCOCHO + h\nu \rightarrow 0.13\ HCHO + 0.87\ H_2 + 1.87\ CO$

The absorption coefficients for glyoxal have been recently measured by Plum et al. (1983), and are summarized in Table II-13. Since glyoxal absorbs radiation up to approximately 470 nm, photolysis is a potentially important loss process for glyoxal under atmospheric conditions. The quantum yields for the photolysis processes for glyoxal are not known as a function of wavelength, but Plum et al. (1983) determined that when irradiated with a Pyrex-filtered xenon-arc light source with wavelengths $\gtrsim$320 nm, it has an effective quantum yield for loss by photoreaction of 0.029. In absence of other data, we assume that this effective quantum yield is applicable, independent of wavelength, throughout the actinic region.

The photolysis products are not totally known, but its photolysis apparently does not lead to radical formation (Calvert and Pitts 1966). This suggests two possible reactions for glyoxal photolysis:

C58a. $HCOCHO + h\nu \rightarrow HCHO + CO$

C58b. $HCOCHO + h\nu \rightarrow H_2 + 2\ CO$

As discussed by Atkinson and Lloyd (1984), Plum et al. (1983) observed that formaldehyde formation [reaction (C58a)] corresponds to 13% of the photolysis pathway. We assume that reaction (C58b) accounts for the remainder of the photodecomposition of glyoxal. Thus we represent the overall process of glyoxal photolysis as indicated above, with a wavelength-independent quantum yield of 0.029.

C59. $HCOCHO + OH \rightarrow HCOCO\cdot + H_2O$

The available kinetic data concerning this reaction have been discussed by Atkinson and Lloyd (1984). They recommend using

$$k_{C59} = 1.15 \times 10^{-11}\ cm^3\ molecule^{-1}\ sec^{-1},$$

Table II-13. Absorption Cross Sections, σ, (cm^2 $molecule^{-1}$, base e), for Glyoxal

λ (nm)	10^{20} x σ (cm^2)	λ (nm)	10^{20} x σ (cm^2)	λ (nm)	10^{20} x σ (cm^2)	λ (nm)	10^{20} x σ (cm^2)	λ (nm)	10^{20} x σ (cm^2)
280	2.867	285	3.298	290	3.154	295	3.298	300	3.584
305	2.724	310	2.724	312	2.867	315	2.294	320	1.434
325	1.147	327	1.434	330	1.147	335	2.867	340	0.0
355	0.0	360	0.229	365	0.287	370	0.803	375	1.004
380	1.720	382	1.577	384	1.491	386	1.491	388	2.867
390	3.154	391	3.242	392	3.040	393	2.229	394	2.634
395	3.040	396	2.634	397	2.432	398	3.242	399	3.040
400	2.837	401	3.242	402	4.458	403	5.269	404	4.255
405	3.040	406	3.040	407	2.837	408	2.432	409	2.837
410	6.079	411	5.066	412	6.079	412	4.863	413	8.308
414	6.484	414	7.497	414	8.105	415	8.105	415	6.890
416	4.255	417	4.863	418	5.876	419	6.687	420	3.850
421	5.674	421	4.458	422	5.269	423	10.54	423	8.511
424	6.079	425	7.295	426	11.75	426	12.97	427	10.74
428	16.62	429	4.053	430	5.066	431	4.863	432	4.053
433	3.647	434	4.053	435	6.079	435	5.066	436	8.105
437	11.35	437	5.269	438	10.13	438	13.78	439	7.700
440	24.72	441	8.105	442	6.079	443	7.497	444	9.321
445	11.35	446	5.269	447	2.432	448	2.837	449	3.850
450	6.079	451	10.94	451	9.321	452	12.16	453	23.91
454	17.02	455	34.04	456	40.53	456	10.13	457	1.621
458	1.216	458	1.418	459	0.405	460	0.405	461	0.608
461	0.203	462	0.0						

independent of temperature. This is used in this model. The subsequent reactions of the radical formed are discussed below.

C60. HCOCHO + NO_3 → HCOCO. + HNO_3

The rate constant for this reaction has not been measured, but it is assumed to be the same as the rate constant for the reaction of NO_3 with formaldehyde. Thus we use

$$k_{C60} = k_{C9} = 6 \times 10^{-13}\ e^{-4090/RT}\ \mathrm{cm}^3\ \mathrm{molecule}^{-1}\ \mathrm{sec}^{-1}$$

$$= 6 \times 10^{-16}\ \mathrm{cm}^3\ \mathrm{molecule}^{-1}\ \mathrm{sec}^{-1} \text{ at 298 K.}$$

C61. $HCOCO\cdot \xrightarrow[]{\overset{O_2}{fast}} 0.63\ HO_2 + 1.26\ CO + 0.37\ HCOCO_3\cdot$

The reaction as written incorporates three competing processes,

$$HCOCO\cdot \rightarrow HCO + CO \qquad (a)$$

$$HCOCO\cdot + O_2 \rightarrow HO_2 + 2\ CO \qquad (b)$$

$$\rightarrow HCOCO_3\cdot \qquad (c)$$

where reaction (a) and (b) lead to the same set of products due to the rapid reaction of HCO with O_2 to form HO_2 + CO. In previous models, it had been assumed that either reaction (a) or (b) (or both) dominated, and thus only HO_2 and CO are formed. However, Niki et al. (1985), based on O_2-dependent CO_2 yields observed in an FT-IR study of the Cl-atom initiated reactions of glyoxal, determined that if it is assumed that k(a) = k(b), then $k(b)/k(c) = 3.6 \times 10^{18}$ molecule cm^{-3}. This corresponds to a 37% yield of $HCOCO_3\cdot$ in 1 atm air. The reaction as written above is based on these data.

C62. $HCOCO_3\cdot + NO \xrightarrow{O_2} NO_2 + HO_2 + CO + CO_2$

This reaction consists of the rate determining reaction of the peroxy radical with NO, whose kinetics are discussed in Section B, followed by the assumed rapid decomposition of the radical formed, and the reaction of HCO with O_2.

$$HCOCO_3\cdot + NO \rightarrow NO_2 + HCOCO_2\cdot$$

$$HCOCO_2\cdot \rightarrow HCO + CO_2$$

$$HCO + O_2 \rightarrow HO_2 + CO$$

The rapid decomposition of the acyloxy radical formed is analogous to reactions of other acyloxy radicals formed in the model (see, for example, Section B.)

C63. $HCOCO_3\cdot + NO_2 \rightarrow HCOCO_3NO_2$

This is analogous to the formation of PAN and PPN discussed above. This reaction is assumed to have the same kinetics as the reactions of the other acyl peroxy radicals, which are discussed in Section B.

C64. $HCOCO_3NO_2 \rightarrow HCOCO_3\cdot + NO_2$

No data are available concerning the reactions of this PAN analogue. We assume that it undergoes thermal decomposition with the same kinetics as that for PAN [reaction (C18), above]. Thus we use

$$k_{C64} = k_{C18} = 2.0 \times 10^{16}\ e^{-26910/RT}\ sec^{-1}$$

$$= 3.6 \times 10^{-4}\ sec^{-1} \text{ at } 298\ K.$$

C65. $HCOCO_3\cdot + HO_2 \rightarrow -OOH + (HCOCO_3\cdot \text{ products})$

C66. $HCOCO_3\cdot + RO_2 \rightarrow 0.5\ HO_2 + (HCOCO_3\cdot \text{ products})$

C67. $HCOCO_3\cdot + RCO_3 \rightarrow HO_2 + (HCOCO_3\cdot \text{ products})$

The kinetics of these reactions and the general principles used for representing the products are discussed in Section B. As indicated there, the organic products formed in these reactions are those expected to be formed from the reactions of the corresponding alkoxy radical. As discussed above, the alkoxy radical is expected to decompose to give rise to CO + CO_2, and thus we use

$$(HCOCO_3\cdot \text{ products}) = CO + CO_2$$

for the above reactions.

7. Reactions of Methylglyoxal

Methylglyoxal is also formed in the photooxidation of aromatic hydrocarbons, and its rapid photolysis is believed to represent a significant radical source in the aromatic photooxidation mechanism. Its reactions with OH and NO_3 radicals are also included in the model.

C68. $CH_3COCHO + h\nu \xrightarrow{O_2} CH_3CO_3\cdot + CO + HO_2$

The absorption coefficients for methylglyoxal have been recently measured by Plum et al. (1983), and are summarized in Table II-14. It can be seen that methylglyoxal absorbs radiation up to approximately 470 nm. Thus photolysis is an important loss process for this compound under atmospheric conditions. The quantum yields for the photolysis processes for methylglyoxal are not known as a function of wavelength, but Plum et al. (1983) determined that when irradiated with a Pyrex-filtered xenon-arc light source with wavelengths $\geq$320 nm, it has an effective quantum yield for loss by photoreaction of 0.107. In absence of other data, we assume that this effective quantum yield is applicable, independent of wavelength, throughout the actinic region.

The reaction as written above is based on the assumed primary process being formation of $CH_3CO\cdot$ + HCO (or possibly $CH_3CO\cdot$ + H. + CO), followed by the rapid reaction of the radicals formed with O_2 to form the species shown above. As discussed by Atkinson and Lloyd (1984), the

Table II-14. Absorption Cross Sections, σ, (cm^2 $molecule^{-1}$, base e), for Methylglyoxal

λ (nm)	$10^{20} \times \sigma$ (cm^2)	λ (nm)	$10^{20} \times \sigma$ (cm^2)	λ (nm)	$10^{20} \times \sigma$ (cm^2)	λ (nm)	$10^{20} \times \sigma$ (cm^2)	λ (nm)	$10^{20} \times \sigma$ (cm^2)
270	1.262	275	1.430	280	1.514	285	1.430	290	1.472
295	1.178	300	1.136	305	0.925	310	0.631	315	0.547
320	0.337	325	0.168	330	0.084	335	0.0	350	0.0
354	0.042	358	0.126	360	0.210	362	0.210	364	0.294
366	0.337	368	0.421	370	0.547	372	0.589	374	0.757
376	0.799	378	0.883	380	1.009	382	1.093	384	1.346
386	1.514	388	1.724	390	2.061	392	2.103	394	2.313
396	2.481	398	2.607	400	2.776	402	2.986	404	3.196
406	3.785	408	3.953	410	4.332	412	4.710	414	4.794
416	4.879	418	5.047	420	5.215	422	5.299	424	5.173
426	5.299	428	5.215	430	5.551	432	5.131	434	5.678
436	6.224	438	6.056	440	5.467	441	6.140	442	5.467
443	5.551	433	6.813	444	5.972	445	5.131	446	4.879
447	5.720	448	5.467	449	6.561	450	5.047	451	3.028
452	4.290	453	2.776	454	2.271	456	1.766	458	0.8411
460	0.420	464	0.168	468	0.0				

observation of PAN in the photolysis of methylglyoxal-NO_x-air mixtures is consistent with the fragmentation mechanism shown above. The photolysis of biacetyl is believed to occur via a totally analogous reaction route. The subsequent reactions of $CH_3CO_3\cdot$ are discussed above in conjunction with the discussion of the reactions of acetaldehyde.

C69. $CH_3COCHO + OH \xrightarrow{O_2} H_2O + CH_3CO_3\cdot + CO$

The available kinetic data concerning this reaction has been discussed by Atkinson and Lloyd (1984). They recommend using

$$k_{C69} = 1.7 \times 10^{-11}\ cm^3\ molecule^{-1}\ sec^{-1},$$

independent of temperature. This is used in this model.

This reaction is assumed to consist of the initial formation of the radical $CH_3COCO.$, which is assumed to decompose and ultimately give rise to the products shown above.

$$CH_3COCHO + OH \rightarrow H_2O + CH_3COCO.$$

$$CH_3COCO. \rightarrow CH_3CO. + CO$$

$$CH_3CO. + O_2 \rightarrow CH_3CO_3.$$

The radical $CH_3COCO.$ is expected to decompose more rapidly than HCOCO., where (as is discussed above) decomposition occurs at a rate competitive with reaction with O_2. Thus in this case, in absence of other data, we assume that decomposition dominates over reaction with O_2.

C70. $CH_3COCHO + NO_3 \xrightarrow{O_2} HNO_3 + CH_3CO_3. + CO$

The rate constant for this reaction has not been measured. It is assumed to be identical to the rate constant for the reaction of NO_3 with acetaldehyde. Thus we use

$$k_{C70} = k_{C12} = 3 \times 10^{-13}\ e^{-2835/RT}\ \text{cm}^3\ \text{molecule}^{-1}\ \text{sec}^{-1}$$

$$= 2.5 \times 10^{-15}\ \text{cm}^3\ \text{molecule}^{-1}\ \text{sec}^{-1} \text{ at } 298\text{ K}.$$

This reaction results in the initial formation of HNO_3 and $CH_3COCO.$, with the latter specie being assumed to undergo rapid decomposition to give rise to the products shown, as discussed above.

8. Reactions of Biacetyl

Biacetyl is formed in the photooxidations of certain aromatics. Because it undergoes photodecomposition even more rapidly than do glyoxal and methylglyoxal, but reacts only slowly with OH radicals and negligibly with NO_3 (since it lacks the labile -CHO group); only its photolysis is included in the model.

C71. $CH_3COCOCH_3 + h\nu \xrightarrow{O_2} 2\ CH_3CO_3\cdot$

The absorption coefficients for biacetyl have been recently measured by Plum et al. (1983), and are summarized in Table II-15. Since biacetyl absorbs radiation up to approximately 470 nm, photolysis is an important loss process under atmospheric conditions. The quantum yields are not known as a function of wavelength, but Plum et al. (1983) determined that when irradiated with a Pyrex-filtered xenon-arc light source with wavelengths $\geq$320 nm, it has an effective quantum yield for loss by photoreaction of 0.158. As with the other α-dicarbonyls discussed above, we assume that this effective quantum yield is applicable, independent of wavelength, throughout the actinic region.

Fortunately, in the case of biacetyl, there are data available to test this assumption. The applicability of this effective quantum yield for use in modeling solar irradiation can be tested using the data from the biacetyl-NO_x-air irradiation carried out in the UNC chamber (run OC0181R), and Figure II-6 shows a plot of the observed and calculated consumption of biacetyl in that run. It can be seen that the model gives reasonably good agreement to the observed biacetyl consumption rate, indicating that, since photolysis is the major mode of consumption of biacetyl under those conditions, the model is calculating the appropriate biacetyl photolysis rates.

Perhaps an even stricter test of the assumption that the effective quantum yield is not significantly dependent on wavelength in the actinic region is the measurement of the biacetyl decay rate under blacklight irradiation, which was carried out in SAPRC ITC run 676. This is of interest because at wavelengths above 380 nm, where significant absorption of light by biacetyl and other α-dicarbonyls is still occurring, the relative intensity of the blacklights are significantly lower than that of both the SAPRC solar simulator [employed in the study of Plum et al. (1983)] and of sunlight. (See Section IV-A for a discussion of the spectral distributions of these light sources.) In particular, using the

Table II-15. Absorption Cross Sections, σ, (cm^2 molecule^{-1}, base e), for Biacetyl

λ (nm)	10^{20} x σ (cm^2)	λ (nm)	10^{20} x σ (cm^2)	λ (nm)	10^{20} x σ (cm^2)	λ (nm)	10^{20} x σ (cm^2)	λ (nm)	10^{20} x σ (cm^2)
280	4.436	282	4.328	285	3.895	287	3.571	290	3.246
292	2.921	295	2.597	298	2.164	300	1.785	303	1.731
305	1.461	308	1.082	310	9.197	312	7.033	315	6.492
317	0.541	320	0.541	322	0.541	325	0.433	327	0.325
330	0.379	333	0.379	335	0.433	338	0.487	340	0.541
343	0.595	345	0.649	347	0.703	350	0.812	352	0.757
355	0.920	357	0.974	360	1.082	363	1.190	365	1.407
368	1.515	370	1.785	373	2.002	375	2.110	377	2.326
380	2.597	382	2.813	385	3.138	387	3.462	390	3.895
393	4.112	395	4.328	398	4.382	400	4.653	403	4.815
405	5.194	407	5.843	410	6.059	412	6.492	415	6.925
417	6.871	420	6.817	423	6.708	425	6.492	428	5.951
430	5.735	433	6.276	435	6.005	437	5.843	440	5.951
442	6.492	445	5.951	447	4.977	450	3.787	452	2.813
455	1.731	458	1.082	460	0.541	463	0.379	465	0.216
468	0.108	470	0.108	472	0.0				

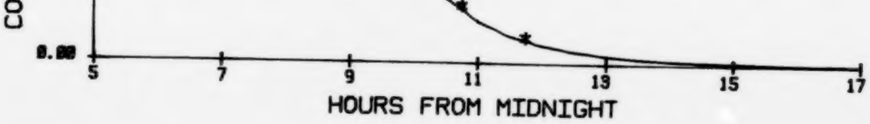

Figure II-6. Observed and calculated biacetyl concentration-time profiles for UNC biacetyl-NO$_x$-air run OC0181R.
* = Experimental data.
----- = Model calculation.

spectral distribution data discussed in Section IV-A, the ratio of the photolysis rate of biacetyl, relative to that of NO_2, is calculated to be only 0.0076 for blacklight irradiation, significantly lower than the ratio of 0.036 observed by Plum et al. (1983), and the ratio of 0.035 calculated for direct overhead sunlight. In the biacetyl-air irradiation ITC-676, biacetyl was observed to decay at a rate $(1.94 \pm 0.02) \times 10^{-3}$ min^{-1}, under conditions when NO_2 photolysis rate measurements averaged 0.296 ± 0.016 min^{-1}. This corresponds to a biacetyl/NO_2 photolysis rate ratio of 0.0066 ± 0.0004, which is only 13% lower than the value predicted using the effective quantum yield of Plum et al (1983). Considering the uncertainties involved, this is considered to be excellent agreement.

The good agreement between the observed and predicted photolysis rates of biacetyl with different light sources suggest that the use of a single effective quantum yield for the entire actinic region is probably appropriate for the other α-dicarbonyls as well as for biacetyl.

9. Reactions of Glycolaldehyde

Glycolaldehyde is formed primarily following the reaction of OH radicals with ethene. Its major modes of reaction are assumed to be similar in many respects to those for acetaldehyde, but there are enough differences, and its yield in the ethene system is sufficiently high, that it is appropriate that it be represented explicitly in the detailed model. The possibility of representing glycolaldehyde by acetaldehyde in more condensed models needs to be investigated.

C72. $HOCH_2CHO + OH \xrightarrow{O_2} HOCH_2CO_3\cdot + H_2O$

The reaction of glycolaldehyde with OH radicals, which has not been experimentally studied, can occur via three possible routes:

Abstraction from the -CHO group,

$$HOCH_2CHO + OH \rightarrow HOCH_2CO\cdot + H_2O, \qquad (a)$$

abstraction from the $-CH_2-$ group,

$$HOCH_2CHO + OH \rightarrow HOCH(.)CHO + H_2O \qquad (b)$$

or abstraction from the -OH group,

$$HOCH_2CHO + OH \rightarrow .OCH_2CHO + H_2O \qquad (c)$$

No published data are available for these reactions, but the estimation technique discussed by Atkinson (1986) can be used to estimate $k_{C72a} = 2.1 \times 10^{-11}$ cm^3 molecule^{-1} sec^{-1}, $k_{C72b} = 2.3 \times 10^{-12}$ cm^3 molecule^{-1} sec^{-1} and $k_{C72c} = 1.3 \times 10^{-13}$ cm^3 molecule^{-1} sec^{-1}. These estimates indicate that process (a) will occur almost 90% of the time, and thus in this model we neglect the other processes. Thus the reaction as written above is based on assuming process (a) dominates, followed by rapid reaction of the radical formed with O_2 to form the acyl peroxy radical indicated above.

The sum of the estimated rate constants indicate that

$$k_{C72} = 2.3 \times 10^{-11} \text{ cm}^3 \text{ molecule}^{-1} \text{ sec}^{-1}$$

at 298 K. This is used in the model. The temperature dependence for this rate constant is probably small, and is ignored.

C73. $HOCH_2CO_3. + NO \xrightarrow{O_2} NO_2 + CO_2 + HCHO + HO_2$

This reaction consists of the rate determining reaction of the peroxy radical with NO, whose kinetics are discussed in Section B, followed by the rapid reaction of the radical formed with O_2.

$$HOCH_2CO_3. + NO \rightarrow NO_2 + HOCH_2CO_2.$$

$$HOCH_2CO_2. \rightarrow HOCH_2. + CO_2$$

$$HOCH_2. + O_2 \rightarrow HCHO + HO_2.$$

The major atmospheric fate of α-hydroxy radicals, such as $HOCH_2\cdot$, have been shown to be via reaction with O_2 to form HO_2 and the corresponding carbonyl (Niki et al. 1978, Carter et al. 1979b, Ohta et al. 1982).

C74. $HOCH_2CO_3\cdot + NO_2 \rightarrow HOCH_2CO_3NO_2$

This is analogous to the formation of PAN and PPN discussed above. This reaction is assumed to have the same kinetics as the reactions of the other acyl peroxy radicals, which are discussed in Section B.

C75. $HOCH_2CO_3NO_2 \rightarrow HOCH_2CO_3\cdot + NO_2$

No data are available concerning the reactions of this PAN analogue. We assume that it undergoes thermal decomposition with the same kinetics as that for PAN [reaction (C18), above]. Thus we use

$$k_{C75} = k_{C18} = 2.0 \times 10^{16}\ e^{-26910/RT}\ \mathrm{sec}^{-1}$$

$$= 3.6 \times 10^{-4}\ \mathrm{sec}^{-1} \text{ at } 298\ \mathrm{K}.$$

C76. $HOCH_2CO_3\cdot + HO_2 \rightarrow -OOH + (HOCH_2CO_3\cdot$ products)

C77. $HOCH_2CO_3\cdot + RO_2 \rightarrow 0.5\ HO_2 + (HOCH_2CO_3\cdot$ products)

C78. $HOCH_2CO_3\cdot + RCO_3 \rightarrow HO_2 + (HOCH_2CO_3\cdot$ products)

The kinetics of these reactions and the general principles used for representing the products are discussed in Section B. As indicated there, the organic products formed in these reactions are the set of products expected to be formed from the reactions of the corresponding alkoxy radical. As discussed above, the alkoxy radical is expected to decompose to give rise to CO_2 + HCHO, and thus we use

$$(HOCH_2CO_3\cdot \text{ products}) = CO_2 + HCHO$$

for the above reactions.

C79. $HOCH_2CHO + h\nu \xrightarrow{O_2} HCHO + 2\ HO_2 + CO$

No data are available for the absorption coefficients of glycolaldehyde in the gas phase or for its quantum yields of this reaction. We assume that this photolysis occurs with the same rate constant as that for the major atmospheric photodecomposition route for acetaldehyde, i.e., $k_{C79} = k_{C11a}$. The absorption coefficients and quantum yields for this process are given in Table II-11, above.

The reaction is assumed to occur via the rate determining formation of HCO and $HOCH_2\cdot$, followed by their rapid reactions with O_2 to form the products indicated above.

$$HOCH_2CHO + h\nu \rightarrow HOCH_2\cdot + HCO$$

$$HOCH_2\cdot + O_2 \rightarrow HCHO + HO_2$$

$$HCO + O_2 \rightarrow HO_2 + CO$$

C80. $HOCH_2CHO + NO_3 \xrightarrow{O_2} HNO_3 + HOCH_2CO_3\cdot$

The rate constant for this reaction has not been measured. It is assumed to react with the same rate constant as that for the reaction of NO_3 with acetaldehyde. Thus we use

$$k_{C80} = k_{C12} = 3 \times 10^{-13}\ e^{-2835/RT}\ \text{cm}^3\ \text{molecule}^{-1}\ \text{sec}^{-1}$$

$$= 2.5 \times 10^{-15}\ \text{cm}^3\ \text{molecule}^{-1}\ \text{sec}^{-1} \text{ at } 298\ \text{K}.$$

This reaction results in the initial formation of HNO_3 and $HOCH_2CO\cdot$, with the latter species being assumed to rapidly react with O_2 to form the acyl peroxy radical. The subsequent reactions of this radical are given above.

10. Reactions of 2-Butyl Nitrate

Alkyl nitrates are formed in significant yields in the photooxidation of the $\geq C_4$ alkanes, and thus it is necessary to include their subsequent reactions in the model. As discussed in Section E below, all alkyl nitrates are represented by the surrogate species 2-butyl nitrate and of 4-heptyl nitrate. The atmospheric reactions of 2-butyl nitrate are discussed in this section.

C81. $OH + CH_3CH(ONO_2)C_2H_5 \rightarrow H_2O + 0.20\ (NO_2 + CH_3COC_2H_5)$
$+ 0.48\ CH_3CH(ONO_2)CH(OO\cdot)CH_3 + 0.32\ CH_3CH(ONO_2)CH_2CH_2OO^{\cdot}$

Reaction with the OH radical is believed to be the only significant atmospheric fate for the alkyl nitrates. The rate constant for this reaction has been measured by Atkinson et al. (1982b) to be

$$k_{C81} = 6.7 \times 10^{-13}\ cm^3\ molecule^{-1}\ sec^{-1}$$

at 299 K. This is used in the model. The temperature dependence of this reaction is unknown, but in order to obtain an approximate representation of this in the model, we assume it has a pre-exponential factor similar to that for the reaction of OH with n-butane, i.e., $1.55 \times 10^{-11}\ cm^3\ molecule^{-1}\ sec^{-1}$ (Atkinson 1986). Thus we use $k_{C81} = 2 \times 10^{-11}\ e^{-2018/RT}\ cm^3\ molecule^{-1}\ sec^{-1}$.

The reaction of OH radicals with 2-butyl nitrate can occur via H-atom abstraction at four different positions. Although there are no direct data available concerning the relative importance of the different reaction routes, these can be estimated using the group rate constant technique described by Atkinson (1986). Based on this technique, we estimate that abstraction from the 1, 2, 3 and 4 positions occur 8%, 18%, 45% and 29% of the time, respectively. Reaction at position 1 is ignored, and thus the reaction is assumed to occur 20%, 48% and 32% at the 2, 3, and 4 positions, respectively.

The alkyl radical formed following abstraction from position 2 is assumed to rapidly undergo the following decomposition, which is a highly thermodynamically favored bond-scission reaction:

$$CH_3C(.)(ONO_2)C_2H_5 \rightarrow CH_3COC_2H_5 + NO_2$$

The other alkyl radicals formed are assumed to rapidly react with O_2 to form the corresponding peroxy radical. The reaction as written above is based on these assumptions.

C82. $CH_3CH(ONO_2)CH(OO.)CH_3 + NO \rightarrow 2\ NO_2 + 2\ CH_3CHO$

This reaction consists of the rate determining reaction of the peroxy radical with NO, whose kinetics are discussed in Section B, followed by the reactions indicated below, which are assumed to be fast.

$$CH_3CH(ONO_2)CH(OO.)CH_3 + NO \rightarrow NO_2 + CH_3CH(ONO_2)CH(O.)CH_3$$

$$CH_3CH(ONO_2)CH(O.)CH_3 \rightarrow CH_3CH(ONO_2). + CH_3CHO$$

$$CH_3CH(ONO_2). \rightarrow CH_3CHO + NO_2$$

The formation of the dinitrate in the initial reaction of the peroxy radical with NO, which is estimated to occur approximately 8% of the time by analogy with the observed formation of 8% 2-butyl nitrate from the reaction of NO with 2-butoxy radicals (Atkinson et al. 1982b), is ignored.

C83. $CH_3CH(ONO_2)CH_2CH_2OO. + NO \rightarrow NO_2 + .OOCH_2CH(ONO_2)CH_2CH_2OH$

This reaction consists of the rate determining reaction of the peroxy radical with NO, whose kinetics are discussed in Section B, followed by the assumed rapid 1,5-H shift isomerization of the alkoxy radical, and then the rapid reaction of O_2 with the carbon-centered radical formed.

$$CH_3CH(ONO_2)CH_2CH_2OO\cdot + NO \rightarrow NO_2 + CH_3CH(ONO_2)CH_2CH_2O\cdot$$

$$CH_3CH(ONO_2)CH_2CH_2O\cdot \rightarrow \cdot CH_2CH(ONO_2)CH_2CH_2OH$$

$$\cdot CH_2CH(ONO_2)CH_2CH_2OH + O_2 \rightarrow \cdot OOCH_2CH(ONO_2)CH_2CH_2OH$$

The formation of the dinitrate in the initial reaction of the peroxy radical with NO, estimated to occur ~8% of the time (see above), is ignored.

C84. $\cdot OOCH_2CH(ONO_2)CH_2CH_2OH + NO \rightarrow 2\ NO_2 + HCHO + HOCH_2CH_2CHO\ (=C_2H_5CHO)$

This reaction consists of the rate determining reaction of the peroxy radical with NO, whose kinetics are discussed in Section B, followed by the reactions listed below, which are assumed to be rapid.

$$\cdot OOCH_2CH(ONO_2)CH_2CH_2OH + NO \rightarrow NO_2 + \cdot OCH_2CH(ONO_2)CH_2CH_2OH$$

$$\cdot OCH_2CH(ONO_2)CH_2CH_2OH \rightarrow HCHO + \cdot CH(ONO_2)CH_2CH_2OH$$

$$\cdot CH(ONO_2)CH_2CH_2OH \rightarrow HCOCH_2CH_2OH + NO_2$$

As is the case with the other peroxy radicals formed in the 2-butyl nitrate system, the formation of the dinitrate in the reaction of NO with the peroxy radical, estimated to occur approximately 8% of the time, is ignored. The decomposition of the β-nitrate alkoxy radical is assumed to be fast, by analogy with the known rapid decomposition of the β-hydroxy alkoxy radicals formed in the OH + alkene systems (discussed in Section D).

The 3-hydroxy propanal formed in the above reactions is represented by propionaldehyde in the model.

C85. $CH_3CH(ONO_2)CH_2(OO.)CH_3 + HO_2 \rightarrow -OOH + (CH_3CH(ONO_2)CH_2(OO.)CH_3$ products)

C86. $CH_3CH(ONO_2)CH_2CH_2OO. + HO_2 \rightarrow -OOH + (CH_3CH(ONO_2)CH_2CH_2OO.$ products)

C87. $.OOCH_2CH(ONO_2)CH_2CH_2OH + HO_2 \rightarrow -OOH + (.OOCH_2CH(ONO_2)CH_2CH_2OH$ products)

C88. $CH_3CH(ONO_2)CH_2(OO.)CH_3 + RO_2 \rightarrow 0.5\ HO_2 + (CH_3CH(ONO_2)CH_2(OO.)CH_3$ products)

C89. $CH_3CH(ONO_2)CH_2CH_2OO. + RO_2 \rightarrow 0.5\ HO_2 + (CH_3CH(ONO_2)CH_2CH_2OO.$ products)

C90. $.OOCH_2CH(ONO_2)CH_2CH_2OH + RO_2 \rightarrow 0.5\ HO_2 + (.OOCH_2CH(ONO_2)CH_2CH_2OH$ products)

C91. $CH_3CH(ONO_2)CH_2(OO.)CH_3 + RCO_3 \rightarrow 0.5\ HO_2 + (CH_3CH(ONO_2)CH_2(OO.)CH_3$ products)

C92. $CH_3CH(ONO_2)CH_2CH_2OO. + RCO_3 \rightarrow 0.5\ HO_2 + (CH_3CH(ONO_2)CH_2CH_2OO.$ products)

C93. $.OOCH_2CH(ONO_2)CH_2CH_2OH + RCO_3 \rightarrow 0.5\ HO_2 + (.OOCH_2CH(ONO_2)CH_2CH_2OH$ products)

The kinetics of these reactions and the general principles used for representing the products are discussed in Section B. As indicated there, the organic products formed in these reactions are the set of products expected to be formed from the reactions of the corresponding alkoxy radical. Thus, based on the reactions of the corresponding alkoxy radicals discussed above, we use the following in the model:

$(CH_3CH(ONO_2)CH_2(OO.)CH_3$ products) = $NO_2 + 2\ CH_3CHO$

$(CH_3CH(ONO_2)CH_2CH_2OO.$ products) = $(.OOCH_2CH(ONO_2)CH_2CH_2OH$ products)

$(.OOCH_2CH(ONO_2)CH_2CH_2OH$ products) = $NO_2 + HCHO + C_2H_5CHO$

11. Reactions of 4-Heptyl Nitrate

Alkyl nitrates are formed in significant yields in the photooxidation of the $\geq C_4$ alkanes, and thus it is necessary to include their subsequent reactions in the model. As discussed in Section E below, all alkyl nitrates are represented by the surrogate species 2-butyl nitrate and 4-heptyl nitrate. The atmospheric reactions of 4-heptyl nitrate are discussed in this section.

C94. $OH + C_3H_7CH(ONO_2)C_3H_7 \rightarrow H_2O + 0.11\ .OOC_3H_6CH(ONO_2)C_3H_7 +$
$0.66\ CH_3CH(OO.)CH_2CH(ONO_2)C_3H_7 + 0.23\ C_2H_5CH(OO.)CH(ONO_2)C_3H_7$

Reaction with the OH radical is believed to be the only significant atmospheric fate for the alkyl nitrates. The rate constant for this particular nitrate has not been measured, but is estimated using the group rate constant technique discussed by Atkinson (1986) to be

$$k_{C94} = 3.4 \times 10^{-12}\ \text{cm}^3\ \text{molecule}^{-1}\ \text{sec}^{-1}$$

at 298 K. This is used in the model. The temperature dependence of this reaction is unknown, but in order to obtain an approximate representation of this in the model, we assume it has a pre-exponential factor similar to that for the reaction of OH with n-heptane. The temperature dependence of that reaction is not known either, but from the temperature-dependent group rate constants given by Carter and Atkinson (1985), the pre-exponential factor is estimated to be 2.7×10^{-11} cm^3 molecule^{-1} sec^{-1}. Thus we use

$$k_{C94} = 3 \times 10^{-11}\ e^{-1289/RT}\ \text{cm}^3\ \text{molecule}^{-1}\ \text{sec}^{-1}.$$

The reaction of OH radicals with 4-heptyl nitrate can occur via H-atom abstraction at four different positions. There are no direct data available concerning the relative importance of the different reaction routes, but we estimate, again using the group rate constant technique described by Atkinson (1986), that abstraction from the 1, 2, 3 and 4 positions occur respectively 11%, 63%, 22% and 4% of the time. Reaction at position 4 is ignored, and thus the reaction is assumed to occur 11%, 66% and 23% at the 1, 2 and 3 positions, respectively. The reaction as written above incorporates these assumed ratios, and also incorporates the rapid reaction of the initially formed carbon-centered radicals with O_2 to form the corresponding peroxy radical.

C95. $.OOC_3H_6CH(ONO_2)C_3H_7 + NO \rightarrow 2\ NO_2 + HOC_3H_6COC_3H_7$ ($=CH_3COC_2H_5$
+ 3 "lost C")

This reaction consists of the rate determining reaction of the peroxy radical with NO, whose kinetics are discussed in Section B, followed by the assumed rapid isomerization of the alkoxy radical formed, and the assumed rapid decomposition of the α-nitrate radical formed in the 1,5-H shift isomerization.

$$.OOC_3H_6CH(ONO_2)C_3H_7 + NO \rightarrow NO_2 + .OC_3H_6CH(ONO_2)C_3H_7$$

$$.OC_3H_6CH(ONO_2)C_3H_7 \rightarrow HOC_3H_6C(.)(ONO_2)C_3H_7$$

$$HOC_3H_6C(.)(ONO_2)C_3H_7 \rightarrow HOC_3H_6COC_3H_7 + NO_2$$

This mechanism, and the mechanism assumed for the other peroxy radicals formed in the OH + 4-heptyl nitrate system, ignores the formation of the dinitrate in the initial reaction of the peroxy radical with NO. Based on the observed nitrate formation from the reactions of alkylperoxy radicals with NO, dinitrate formation is estimated, based on the formula given by Carter and Atkinson (1985) for primary alkoxy radicals, to occur approximately 12% of the time. (In the case of the secondary radicals formed in the 4-heptyl nitrate system, dinitrate formation is estimated to occur 29% of the time.) These estimates are based on the assumption that the data for unsubstituted peroxy radicals applies to radicals substituted by the nitrate group. However, as indicated in Section E, model simulations of $\geq C_7$ alkane-NO_x-air environmental chamber experiments give better fits to the data if it is assumed that nitrate formation is negligible in the reaction of hydroxy-substituted peroxy radicals with NO. Because (1) it can be argued that hydroxy-substituted peroxy radicals may be more similar to nitrate-substituted peroxy radicals than are unsubstituted alkyl peroxy radicals, and (2) representing the subsequent reactions of the dinitrates in the model requires either adding more reactive species to the model, or (if the dinitrates are represented by mononitrates), violating nitrogen balance, we assume that dinitrate formation in the reactions of NO with the radicals formed in the OH + 4-heptyl nitrate system is negligible.

C96. $CH_3CH(OO.)CH_2CH(ONO_2)C_3H_7 + NO \xrightarrow{O_2} NO_2 + CH_3CH(OH)CH_2CH(ONO_2)CH(OO.)C_2H_5$

This reaction consists of the rate determining reaction of the peroxy radical with NO, whose kinetics are discussed in Section B, followed by the assumed rapid 1,5-H shift isomerization of the alkoxy radical, and then the rapid reaction of O_2 with the carbon-centered radical formed.

$$CH_3CH(OO.)CH_2CH(ONO_2)C_3H_7 + NO \rightarrow NO_2 + CH_3CH(O.)CH_2CH(ONO_2)C_3H_7$$

$$CH_3CH(O.)CH_2CH(ONO_2)C_3H_7 \rightarrow CH_3CH(OH)CH_2CH(ONO_2)CH(.)C_2H_5$$

$$CH_3CH(OH)CH_2CH(ONO_2)CH(.)C_2H_5 + O_2 \rightarrow CH_3CH(OH)CH_2CH(ONO_2)CH(OO.)C_2H_5$$

As discussed above, the formation of the dinitrate in the initial reaction of the peroxy radical with NO is ignored.

C97. $C_2H_5CH(OO.)CH(ONO_2)C_3H_7 + NO \rightarrow 2\ NO_2 + C_2H_5CHO + C_3H_7CHO$ (=C_2H_5CHO + "lost C")

This reaction consists of the rate determining reaction of the peroxy radical with NO, whose kinetics are discussed in Section B, followed by assumed rapid reactions indicated below, which are analogous to the reactions assumed to occur following the reaction of OH radicals at the 3-position of 2-butyl nitrate, discussed above.

$$C_2H_5CH(OO.)CH(ONO_2)C_3H_7 + NO \rightarrow NO_2 + C_2H_5CH(O.)CH(ONO_2)C_3H_7$$

$$C_2H_5CH(O.)CH(ONO_2)C_3H_7 \rightarrow C_2H_5CHO + .CH(ONO_2)C_3H_7$$

$$.CH(ONO_2)C_3H_7 \rightarrow HCOC_3H_7 + NO_2$$

As discussed above, the formation of the dinitrate in the initial reaction of the peroxy radical with NO is ignored.

The butryaldehyde formed in the above reactions is represented in the model by propionaldehyde.

C98. $CH_3CH(OH)CH_2CH(ONO_2)CH(OO.)C_2H_5 + NO \rightarrow 2\ NO_2 + C_2H_5CHO$ $+ CH_3CH(OH)CH_2CHO$ (= C_2H_5CHO + "lost C")

This reaction consists of the rate determining reaction of the peroxy radical with NO, whose kinetics are discussed in Section B, followed by assumed rapid reactions indicated below.

$$CH_3CH(OH)CH_2CH(ONO_2)CH(OO.)C_2H_5 + NO \rightarrow NO_2 + CH_3CH(OH)CH_2CH(ONO_2)CH(O.)C_2H_5$$

$$CH_3CH(OH)CH_2CH(ONO_2)CH(O.)C_2H_5 \rightarrow CH_3CH(OH)CH_2CH(ONO_2). + HCOC_2H_5$$

$$CH_3CH(OH)CH_2CH(ONO_2). \rightarrow CH_3CH(OH)CH_2CHO + NO_2$$

As discussed above, the formation of the dinitrate in the initial reaction of the peroxy radical with NO is ignored.

The 3-hydroxybutanal formed in the above reactions is represented in the model by propionaldehyde.

C99. $.OOC_3H_6CH(ONO_2)C_3H_7 + HO_2 \rightarrow -OOH + (.OOC_3H_6CH(ONO_2)C_3H_7$ products)

C100. $CH_3CH(OO.)CH_2CH(ONO_2)C_3H_7 + HO_2 \rightarrow -OOH + (CH_3CH(OO.)CH_2CH(ONO_2)C_3H_7$ products)

C101. $C_2H_5CH(OO.)CH(ONO_2)C_3H_7 + HO_2 \rightarrow -OOH + (C_2H_5CH(OO.)CH(ONO_2)C_3H_7$ products)

C102. $CH_3CH(OH)CH_2CH(ONO_2)CH(OO.)C_2H_5 + HO_2 \rightarrow -OOH$ $+ (CH_3CH(OH)CH_2CH(ONO_2)CH(OO.)C_2H_5$ products)

C103. $.OOC_3H_6CH(ONO_2)C_3H_7 + RO_2 \rightarrow 0.5\ HO_2 + (.OOC_3H_6CH(ONO_2)C_3H_7$ products)

C104. $CH_3CH(OO.)CH_2CH(ONO_2)C_3H_7 + RO_2 \rightarrow 0.5\ HO_2 +$ $(CH_3CH(OO.)CH_2CH(ONO_2)C_3H_7$ products)

C105. $C_2H_5CH(OO.)CH(ONO_2)C_3H_7 + RO_2 \rightarrow 0.5\ HO_2 + (C_2H_5CH(OO.)CH(ONO_2)C_3H_7$ products)

C106. $CH_3CH(OH)CH_2CH(ONO_2)CH(OO.)C_2H_5 + RO_2 \rightarrow 0.5\ HO_2$ $+ (CH_3CH(OH)CH_2CH(ONO_2)CH(OO.)C_2H_5$ products)

C107. $.OOC_3H_6CH(ONO_2)C_3H_7 + RCO_3 \rightarrow 0.5\ HO_2 + (.OOC_3H_6CH(ONO_2)C_3H_7$ products)

C108. $CH_3CH(OO.)CH_2CH(ONO_2)C_3H_7 + RCO_3 \rightarrow 0.5\ HO_2$ $+ (CH_3CH(OO.)CH_2CH(ONO_2)C_3H_7$ products)

C109. $C_2H_5CH(OO.)CH(ONO_2)C_3H_7 + RCO_3 \rightarrow 0.5\ HO_2 + (C_2H_5CH(OO.)CH(ONO_2)C_3H_7$ products)

C110. $CH_3CH(OH)CH_2CH(ONO_2)CH(OO.)C_2H_5 + RCO_3 \rightarrow 0.5\ HO_2$
$+ (CH_3CH(OH)CH_2CH(ONO_2)CH(OO.)C_2H_5$ products)

The kinetics of these reactions and the general principles used for representing the products are discussed in Section B. As indicated there, the organic products formed in these reactions are the set of products expected to be formed from the reactions of the corresponding alkoxy radical. Thus, based on the reactions of the corresponding alkoxy radicals discussed above, we use the following in the model:

$(.OOC_3H_6CH(ONO_2)C_3H_7$ products) = $NO_2 + CH_3COC_2H_5$ + 3 "lost C"

$(CH_3CH(OO.)CH_2CH(ONO_2)C_3H_7$ products) = $(CH_3CH(OH)CH_2CH(ONO_2)CH(OO.)C_2H_5$ products)

$(C_2H_5CH(OO.)CH(ONO_2)C_3H_7$ products) = NO_2 + 2 C_2H_5CHO + "lost C"

$(CH_3CH(OH)CH_2CH(ONO_2)CH(OO.)C_2H_5$ products) = NO_2 + 2 C_2H_5CHO + "lost C"

12. Reactions of 3-Pentanol

As discussed in Section E below, 3-pentanol is used, together with methyl ethyl ketone and propionaldehyde, as a "surrogate" species to represent the reactions of the hydroxy-substituted bifunctional products formed in the photooxidations of the long chain alkanes. The representation of the products formed in the reactions of 3-pentanol is modified slightly for the purpose of this model, to avoid the addition of new species. The mechanism used is discussed in this section.

C111. $OH + C_2H_5CH(OH)C_2H_5 \xrightarrow{O_2} H_2O + 0.2\ CH_3CH(OO.)CH(OH)C_2H_5 + 0.8\ (HO_2 + C_2H_5COC_2H_5)\ (=C_2H_5COCH_3 + \text{"lost C"})$

Using the group rate constant estimation technique of Atkinson (1986), the overall 298 K rate constant for the reaction of OH radicals with 3-pentanol is estimated to be

$$k_{C111} = 1.4 \times 10^{-11}\ \text{cm}^3\ \text{molecule}^{-1}\ \text{sec}^{-1}.$$

The temperature dependence for this reaction is not known but is likely to be small. Thus this rate constant is assumed to be independent of temperature in this model.

The group rate constant estimation technique of Atkinson (1986) is also used to estimate that reaction at the 1, 2, 3, or OH positions occur respectively 3, 16, 80 and 1% of the time in the overall reaction. For simplicity, we neglect reaction at the 1 and the OH positions, and assume that reaction at the 2 and 3 positions occur 20% and 80% of the time, respectively.

The reaction as written above assumes that the α-hydroxy radical formed in the reaction at the 3 position reacts exclusively with O_2 to form HO_2 and the corresponding carbonyl compound, based on studies of the reactions of O_2 with other α-hydroxy radicals (Niki et al. 1978, Carter et al. 1979a, Ohta et al. 1982).

$$OH + C_2H_5CH(OH)C_2H_5 \rightarrow C_2H_5C(.)(OH)C_2H_5 + H_2O$$

$$C_2H_5C(.)(OH)C_2H_5 + O_2 \rightarrow C_2H_5COC_2H_5 + HO_2$$

O_2 is expected to add to the radical formed in the reaction at the 2 position to form the corresponding peroxy radical, as indicated above.

Since methyl ethyl ketone is used to represent the reactions of all the higher ketones in this model, the formation of diethyl ketone in the above reaction is represented by the formation of methyl ethyl ketone + "lost C".

C112. $CH_3CH(OO.)CH(OH)C_2H_5 + NO \xrightarrow{O_2} NO_2 + HO_2 + C_2H_5CHO + CH_3CHO$
(= 2 C_2H_5CHO - "lost C")

The kinetics of the reactions of the peroxy radicals are discussed in Section B. The reaction as written above is assumed to occur via the following steps:

$$CH_3CH(OO.)CH(OH)C_2H_5 + NO \rightarrow NO_2 + CH_3CH(O.)CH(OH)C_2H_5$$

$$CH_3CH(O.)CH(OH)C_2H_5 \rightarrow CH_3CHO + .CH(OH)C_2H_5$$

$$.CH(OH)C_2H_5 + O_2 \rightarrow C_2H_5CHO + HO_2$$

Note that the alkoxy radical formed can also undergo 1,5-H shift isomerization.

$$CH_3CH(O.)CH(OH)C_2H_5 \rightarrow CH_3CH(OH)CH(OH)CH_2CH_2$$

However, as discussed in Section D-3 below, an analogous competition between a 1,5-H shift reaction and a β-hydroxy radical decomposition occurs in the OH + 1-butene system, and available product data for that system indicate that the β-hydroxy radical decomposition reaction dominates (Atkinson et al. 1985). Thus we assume that this is the case for this system as well.

Although the organic products of this reaction are acetaldehyde + propionaldehyde, in this model we represent the products as two molecules of propionaldehyde, in order to partially compensate for the lost carbons involved by representing the diethyl ketone formed in reaction C111 by methyl ethyl ketone. This is also appropriate since 3-pentanol in this case is used to represent a general, "lumped" higher alcohol, and propionaldehyde is used to represent a general, "lumped" higher aldehyde.

C113. $CH_3CH(OO.)CH(OH)C_2H_5 + HO_2. \rightarrow$ -OOH + ($CH_3CH(OO.)CH(OH)C_2H_5$ products)

C114. $CH_3CH(OO.)CH(OH)C_2H_5 + RO_2. \rightarrow 0.5\ HO_2 + (CH_3CH(OO.)CH(OH)C_2H_5$ products)

C115. $CH_3CH(OO.)CH(OH)C_2H_5 + RCO_3. \rightarrow 0.5\ HO_2 + (CH_3CH(OO.)CH(OH)C_2H_5$ products)

The kinetics of these reactions and the general principles used for representing the products have been discussed in Section B. As indicated there, the organic products formed in these reactions are the set of products expected to be formed from the reactions of the corresponding alkoxy radical. In this model the alkyl radical is represented as forming two molecules of propionaldehyde + a regenerated "lost" carbon, and thus the we use the following in the model:

$(CH_3CH(OO.)CH(OH)C_2H_5$ products) = 2 C_2H_5CHO - "lost C"

II. D. REACTIONS OF ALKENES

In this section, the atmospheric reactions of the representative alkenes ethene, propene, 1-butene, trans-2-butene and isobutene are discussed. In addition, a general scheme for "lumping" the reactions of the C_{3+} acyclic monoalkenes, which was employed in some of the model calculations discussed in Section IV, is discussed at the end of this section. The alkenes react in the atmosphere primarily with OH radicals and with O_3, but under some conditions they can also react with NO_3 radicals and with $O(^3P)$ atoms to a non-negligible extent. Thus the reactions of the alkenes with these species are also included in the present model.

1. Reactions of Ethene

D1. $OH + CH_2{=}CH_2 \xrightarrow{O_2} HOCH_2CH_2OO^{\cdot}$

This reaction consists of the rate determining addition of OH radicals to the double bond, followed by the rapid reaction of the $HOCH_2CH_2\cdot$ radical with O_2. As reviewed and evaluated by Atkinson (1986), the rate constant for this OH radical addition reaction is given by

$$k_{D1} = 2.15 \times 10^{-12}\ e^{817/RT}\ cm^3\ molecule^{-1}\ sec^{-1}$$

$$= 8.54 \times 10^{-12}\ cm^3\ molecule^{-1}\ sec^{-1} \text{ at } 298\ K,$$

with an uncertainty factor of approximately 1.2 at 298 K.

D2. $HOCH_2CH_2OO\cdot + NO \xrightarrow{O_2} NO_2 + 0.22\ HOCH_2CHO + 1.56\ HCHO + HO_2$

The reaction as written consists of several steps. The initial, rate determining process is the reaction of NO with the peroxy radical to form the corresponding alkoxy radical.

$$HOCH_2CH_2OO\cdot + NO \rightarrow NO_2 + HOCH_2CH_2O\cdot$$

The kinetics of this reaction are discussed in Section B.

The β-hydroxy alkoxy radical can decompose or react with O_2,

$$HOCH_2CH_2O\cdot \rightarrow HOCH_2\cdot + HCHO \tag{a}$$

$$HOCH_2CH_2O\cdot + O_2 \rightarrow HOCH_2CHO + HO_2 \tag{b}$$

and both processes need to be considered in the case of ethane. Niki et al. (1981a) obtained $k_b/k_a = 5.4 \times 10^{-20}$ cm^3 molecule^{-1}, which means that under atmospheric conditions reaction with O_2 will occur 22% of the time. This is used in the model. The major atmospheric fate of α-hydroxy radicals such as $HOCH_2\cdot$ formed in the decomposition have been shown to be reactions with O_2 to form HO_2 and the corresponding carbonyl (Niki et al. 1978, Carter et al. 1979b, Ohta et al. 1982). Thus the reaction

$$HOCH_2\cdot + O_2 \rightarrow HCHO + HO_2$$

is assumed to be fast, and the net result of the decomposition process is formation of 2 HCHO + HO_2. The reaction as written above incorporates these assumptions.

The reactions of glycolaldehyde ($HOCH_2CHO$) are discussed in Section C-9.

D3. $HOCH_2CH_2OO\cdot + HO_2 \rightarrow -OOH + (HOCH_2CH_2OO\cdot \text{ products})$

D4. $HOCH_2CH_2OO\cdot + RO_2 \rightarrow 0.5\ HO_2 + (HOCH_2CH_2OO\cdot \text{ products})$

D5. $HOCH_2CH_2OO\cdot + RCO_3 \rightarrow 0.5\ HO_2 + (HOCH_2CH_2OO\cdot \text{ products})$

The kinetics of these reactions and the general principles used for representing the products are discussed in Section B. As indicated there, the organic products formed in these reactions are represented by the set of products expected to be formed from the reactions of the corresponding alkoxy radical. As discussed above, the alkoxy radical is expected to react with O_2 forming glycolaldehyde 22% of the time, and decompose to form two formaldehyde molecules the rest of the time. Thus we use

$$(HOCH_2CH_2OO.\ \text{products}) = 0.22\ HOCH_2CHO + 1.56\ HCHO$$

for the above reactions.

D6. $O_3 + CH_2{=}CH_2 \rightarrow HCHO + [.CH_2OO.^*]$

D7. $[.CH_2OO.^*] \xrightarrow[]{\overset{O_2}{\text{fast}}} 0.4\ CH_2O_2 + 0.18\ CO_2 + 0.42\ CO + 0.12\ H_2 + 0.42\ H_2O$
$+ 0.12\ HO_2$

The available data concerning the kinetics of the reaction of ozone with ethene have been summarized and evaluated by Atkinson and Carter (1984). They recommend the following expression for the rate constant,

$$k_{D6} = 1.2 \times 10^{-14}\ e^{-5232/RT}\ \text{cm}^3\ \text{molecule}^{-1}\ \text{sec}^{-1}$$

$$= 1.75 \times 10^{-18}\ \text{cm}^3\ \text{molecule}^{-1}\ \text{sec}^{-1} \text{ at } 298\ \text{K},$$

which is used in this model.

The available data concerning the mechanism of this reaction have been discussed and evaluated by Atkinson and Lloyd (1984). The major mode of this reaction is believed to be the initial formation of a primary ozonide, which rapidly fragments as shown below:

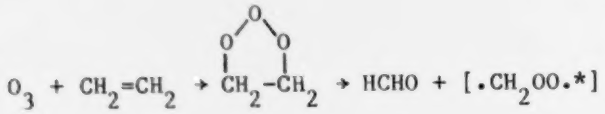

$$O_3 + CH_2{=}CH_2 \rightarrow \overset{O-O-O}{CH_2-CH_2} \rightarrow HCHO + [.CH_2OO.^*]$$

The biradical formed is believed to be energy rich, and thus it can either undergo fragmentation or be stabilized to a thermalized biradical which can undergo subsequent bimolecular reactions. Based primarily on the experimental data of Herron and Huie (1977), Su et al. (1980), Kan et al. (1981) and Niki et al. (1981b), Atkinson and Lloyd (1984) recommend the reaction sequence shown above [reaction (D7)] for the "hot" biradical formed in the ozone + ethene system under atmospheric conditions. The assumed yield of the thermalized biradical (designated CH_2O_2) is consistent with the more recent experimental determination of Hatakeyama et al. (1984). The subsequent reactions of the thermalized biradical are discussed below in Section D-6, in conjunction with the discussion of the reactions of the other thermalized biradicals formed from the reactions of ozone with the other alkenes included in this model.

D8. $O(^3P) + CH_2{=}CH_2 \xrightarrow{O_2} CH_3OO. + HO_2 + CO$

This reaction is discussed by Atkinson and Lloyd (1984). They recommend assuming ~60% fragmentation to CH_3 + HCO, 40% to $.CH_2CHO$ + H and 4-5% to $CH_2CO + H_2$. The latter pathway is ignored in this model. Under atmospheric conditions, CH_3, HCO and H react rapidly with O_2 to form CH_3O_2, CO + HO_2 and HO_2, respectively, and the vinoxy radical, $.CH_2CHO$, is assumed to react as follows (Atkinson and Lloyd 1984):

$$.CH_2CHO + O_2 \rightarrow .OOCH_2CHO$$

$$.OOCH_2CHO + NO \rightarrow NO_2 + .OCH_2CHO$$

$$.OCH_2CHO + O_2 \rightarrow HCHO + HCO$$

$$\qquad\qquad\qquad\qquad HCO \xrightarrow{O_2} CO + HO_2$$

Note that in the above scheme the same set of products are ultimately formed from $.CH_2CHO$ + H as from CH_3 + HCO, and thus the reaction as written above represents both fragmentation pathways.

The following expression for the rate constant for this reaction was recommended by Atkinson and Lloyd (1984):

$$k_{D8} = 1.04 \times 10^{-11}\ e^{-1574/RT}\ \text{cm}^3\ \text{molecule}^{-1}\ \text{sec}^{-1}$$

$$= 7.3 \times 10^{-13}\ \text{cm}^3\ \text{molecule}^{-1}\ \text{sec}^{-1} \text{ at } 298\ \text{K}.$$

This is used in the model.

This reaction is of relatively minor importance, and is included in the model primarily because it may be a non-negligible radical source under some conditions.

D9. $NO_3 + CH_2{=}CH_2 \xrightarrow{O_2} .OOCH_2CH_2ONO_2$

This reaction consists of the rate determining addition of NO_3 radicals to the double bond, followed by the rapid addition of O_2 to the radical formed. The rate constants for the reactions of NO_3 with organics are uncertain because, at the present time, all measurements of these rate constants are relative to the $NO_2 + NO_3 = N_2O_5$ equilibrium constant. Based on the recommended equilibrium constant of Malko and Troe (1982), Atkinson and Lloyd (1984) recommended $k_{D9} = 6 \times 10^{-17}$ cm^3 molecule^{-1} sec^{-1} for T = 298 K. However, the equilibrium constant we now use (see Section A) is a factor of 1.8 higher than that used by Atkinson and Lloyd (1984), and thus to be consistent, our value for k_{D9} is increased by this factor. Thus we use

$$k_{D9} = 1.1 \times 10^{-16}\ \text{cm}^3\ \text{molecule}^{-1}\ \text{sec}^{-1} \text{ at } 298\ \text{K}$$

The temperature dependence of this reaction is not known. We assume that it has a similar Arrhenius pre-exponential factor as that for OH + ethene, since both reactions involve addition to the double bond. Thus we use

$$k_{D9} = 2 \times 10^{-12}\ e^{-5808/RT}\ \text{cm}^3\ \text{molecule}^{-1}\ \text{sec}^{-1}$$

to estimate the temperature dependence of this rate constant.

D10. $.OOCH_2CH_2ONO_2 + NO \rightarrow 2\ NO_2 + 2\ HCHO$

This reaction consists of the rate determining reaction of the peroxy radical with NO, whose kinetics are discussed in Section B, followed by the following decompositions, which are assumed to be rapid.

$$^{\cdot}OOCH_2CH_2ONO_2 + NO \rightarrow NO_2 + {^{\cdot}OCH_2CH_2ONO_2}$$

$$^{\cdot}OCH_2CH_2ONO_2 \rightarrow HCHO + .CH_2ONO_2$$

$$.CH_2ONO_2 \rightarrow NO_2 + HCHO$$

Although, as discussed by Atkinson and Lloyd (1984), dinitrates are observed to be formed as products of this reaction under some conditions, such as in the dark or when high levels of NO_2 are present, under atmospheric conditions the reactions indicated above are expected to dominate.

D11. $^{\cdot}OOCH_2CH_2ONO_2 + HO_2 \rightarrow -OOH + (^{\cdot}OOCH_2CH_2ONO_2$ products)

D12. $^{\cdot}OOCH_2CH_2ONO_2 + RO_2 \rightarrow 0.5\ HO_2 + (^{\cdot}OOCH_2CH_2ONO_2$ products)

D13. $^{\cdot}OOCH_2CH_2ONO_2 + RCO_3 \rightarrow 0.5\ HO_2 + (^{\cdot}OOCH_2CH_2ONO_2$ products)

The kinetics of these reactions and the general principles used for representing the products are discussed in Section B. As indicated there, the organic products formed in these reactions are the set of products expected to be formed from the reactions of the corresponding alkoxy radical. As discussed above, the alkoxy radical is expected to decompose to give rise to 2 HCHO + NO_2, and thus we use

$$(^{\cdot}OOCH_2CH_2ONO_2 \text{ products}) = NO_2 + 2\ HCHO$$

for the above reactions.

2. Reactions of Propene

D14. $OH + CH_2{=}CHCH_3 \xrightarrow{O_2} HOCH_2C(CH_3)OO\cdot$

This reaction consists primarily of the rate determining addition of OH radicals to the double bond, followed by the rapid addition of the radical formed with O_2 to form the corresponding peroxy radical. As discussed by Atkinson and Lloyd (1984), OH radical addition is known to be the predominant reaction pathway, with the addition to the internal carbon occurring ~35% of the time (Cvetanovic 1976), i.e.,

$$OH + CH_2{=}CHCH_3 \rightarrow \underset{(35\%)}{\cdot OOCH_2CH(OH)CH_3} \text{ and } \underset{(65\%)}{HOCH_2CH(OO^{\bullet})CH_3}$$

However, as discussed below, the overall net reaction and products formed are the same regardless of the carbon atom on which the addition occurs, so no approximation is introduced by representing the reaction as occurring exclusively via terminal addition, as is shown above.

Atkinson (1986) carried out a recent evaluation of the available data concerning the kinetics of this reaction, and recommends the following expression for T $\lesssim$467 K,

$$k_{D14} = 4.85 \times 10^{-12}\ e^{1001/RT}\ \text{cm}^3\ \text{molecule}^{-1}\ \text{sec}^{-1}$$

$$= 2.63 \times 10^{-11}\ \text{cm}^3\ \text{molecule}^{-1}\ \text{sec}^{-1} \text{ at } 298\ \text{K},$$

which is used in the model.

D15. $HOCH_2C(CH_3)OO\cdot + NO \xrightarrow{O_2} NO_2 + HCHO + CH_3CHO + HO_2$

This reaction consists of the initial, rate determining reaction of NO with the peroxy radical to form the corresponding alkoxy radical,

$$HOCH_2C(CH_3)OO\cdot + NO \rightarrow NO_2 + HOCH_2C(CH_3)O\cdot$$

whose kinetics are discussed in Section B. The radical formed following the internal addition of the OH radical to propene reacts analogously.

$$.OOCH_2CH(OH)CH_3 + NO \rightarrow NO_2 + .OCH_2CH(OH)CH_3$$

Decomposition is expected to dominate for both of these alkoxy radicals, since the decomposition rates are estimated (Atkinson and Lloyd 1984) to be significantly faster than the analogous process for ethene, for which decomposition is competitive with reaction with O_2 [see discussion of Reaction (D2), above]. Both these decompositions will give rise to α-hydroxy radicals, which, as discussed above in conjunction with reaction (D2), are expected to predominantly react with O_2 to form HO_2 and the corresponding carbonyl compound.

$$HOCH_2CH(CH_3)O. \rightarrow HOCH_2. + CH_3CHO$$

$$.OCH_2CH(OH)CH_3 \rightarrow HCHO + HOCH(.)CH_3$$

$$HOCH_2. + O_2 \rightarrow HCHO + HO_2$$

$$HOCH(.)CH_3 + O_2 \rightarrow CH_3CHO + HO_2$$

In both cases, the net overall reaction yields $HCHO + CH_3CHO + HO_2$, as shown in the reaction as written above. The assumption that the major products of the OH + propene reaction in NO_x-air systems are HCHO and CH_3CHO is in agreement with the data of Niki et al. (1978).

D16. $HOCH_2CH(CH_3)OO. + HO_2 \rightarrow -OOH + (HOCH_2CH(CH_3)OO.\ \text{products})$

D17. $HOCH_2CH(CH_3)OO. + RO_2 \rightarrow 0.5\ HO_2 + (HOCH_2CH(CH_3)OO.\ \text{products})$

D18. $HOCH_2CH(CH_3)OO. + RCO_3 \rightarrow 0.5\ HO_2 + (HOCH_2CH(CH_3)OO.\ \text{products})$

The kinetics of these reactions and the general principles used for representing the products are discussed in Section B. As indicated there, the organic products formed in these reactions are represented by the set of products expected to be formed from the reactions of the corresponding alkoxy radical. As discussed above, the alkoxy radical is expected to decompose to give rise to HCHO + CH_3CHO, and thus we use

$$(HOCH_2CH(CH_3)OO.\ \text{products}) = HCHO + CH_3CHO$$

for the above reactions.

D19. $O_3 + CH_2{=}CHCH_3 \rightarrow 0.5\ (HCHO + [CH_3CH(.)OO.*]) + 0.5\ (CH_3CHO + [.CH_2OO.*])$

The available data concerning the kinetics of the reaction of ozone with propene have been evaluated by Atkinson and Carter (1984), who recommend the following expression for the rate constant for this reaction:

$$k_{D19} = 1.32 \times 10^{-14}\ e^{-4182/RT}\ \text{cm}^3\ \text{molecule}^{-1}\ \text{sec}^{-1}$$
$$= 1.13 \times 10^{-17}\ \text{cm}^3\ \text{molecule}^{-1}\ \text{sec}^{-1} \text{ at } 298\text{ K}$$

This is used in the model.

The available data concerning the mechanism of this reaction have been discussed and evaluated by Atkinson and Lloyd (1984). The major mode of reaction of ozone-alkene reactions in the gas phase is believed to be analogous to that discussed above for ethene. In the case of propene, two modes of decomposition of the ozonide are possible, one giving rise to formaldehyde and the methyl-substituted "hot" biradical designated $[CH_3CH(.)OO.*]$, and the other giving rise to acetaldehyde and $[{\cdot}CH_2OO.*]$. These two modes of decomposition are believed to occur with essentially equal probability.

With regard to the subsequent reactions of the "hot" biradicals formed, Atkinson and Lloyd (1984) assumed, based on the very limited data base available, that they are the same regardless of the alkene which formed them. This may be a questionable assumption, since one might expect that the amount of energy going into the biradical fragment would depend on the size and structure of the alkene. However, the available data are not adequate to unambiguously establish the reaction routes for propene and the higher alkenes if this assumption is not made. Thus in this model, we retain the assumption made by Atkinson and Lloyd (1984) and assume that the "hot" radical $[.CH_2OO.^*]$ reacts in exactly the same way when formed in the ozone + propene system as it does when it is formed in the ozone + ethene system, i.e., via reaction (D7). Likewise, the reactions assumed for the "hot" biradical $[CH_3CH(.)OO.^*]$ are assumed to be the same regardless of whether they are formed in the ozone + propene or the ozone + 2-butene systems. The reactions assumed for the latter biradical are discussed below.

$$\begin{aligned} \text{D20.}\quad [CH_3CH(.)OO.^*] \xrightarrow{\overset{O_2}{\text{fast}}} & \ 0.2\ CH_3CHO_2 + 0.14\ CH_4 + 0.29\ CO_2 + 0.15\ CO \\ & + 0.03\ HCHO + 0.27\ CH_3O_2 + 0.21\ HO_2 + 0.12\ OH \\ & + 0.72\ \text{"lost carbon"} \end{aligned}$$

This reaction as written represents both the stabilization and the competing fragmentation processes for this initially "hot" biradical. The stabilization process is represented by the formation of CH_3CHO_2. The recent experimental data obtained by Hatakeyama et al. (1984) concerning the stabilization ratios for the "hot" biradicals formed in the reactions of ozone with a large number of alkenes indicate that the total yield of stabilized biradicals is approximately 26% from the ozone + propene reaction and approximately 19% from ozone + trans-2-butene. Since trans-2-butene is expected to form only the methyl substituted biradical, the result for that compound suggests that it is appropriate to assume approximately 20% stabilization for $[CH_3CH(.)OO.^*]$. If this is assumed to be the case for that biradical when formed in the propene system (and if 40% stabilization is assumed for $[.CH_2OO.^*]$ based on the ethene data), then the predicted amount of stabilization in the propene system is 30%, which is in reasonable agreement with the data of Hatakeyama et al. (1984). The subsequent bimolecular reactions assumed for the thermalized biradicals formed in the ozone-alkene reaction systems are discussed below in Section D-6.

The major uncertainty concerns the decomposition pathways of the "hot" biradicals which are not stabilized and which account for 80% of those formed. The observation of an approximately 14% yield of CH_4 in the cis-2-butene-O_3-HCHO system (Niki et al. 1977) indicates that 14% of the initially formed "hot" biradical decomposes via the reaction

$$[CH_3CH(.)OO.^*] \rightarrow CH_4 + CO_2. \qquad (a)$$

However, the available data are inadequate to clearly establish the remaining reaction routes, which account for approximately 66% of the biradicals formed. Dodge and Arnts (1979) and Atkinson and Lloyd (1984) suggest the following reactions, all of which involve radical formation, account for the remaining reaction routes.

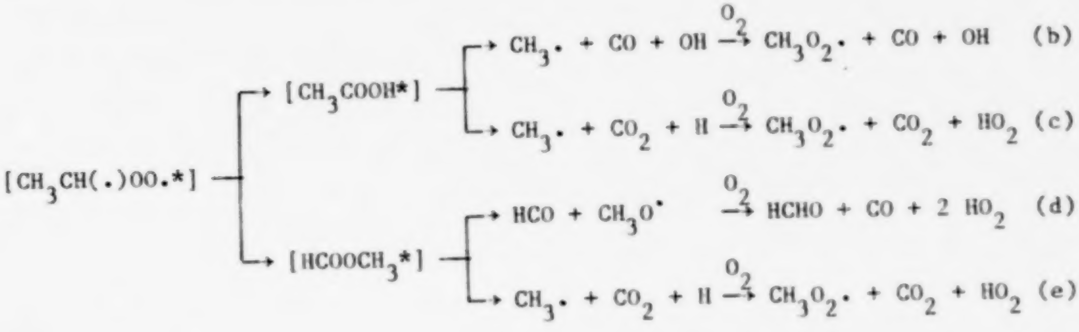

$$[CH_3CH(.)OO.^*] \rightarrow [CH_3COOH^*] \rightarrow CH_3. + CO + OH \xrightarrow{O_2} CH_3O_2. + CO + OH \qquad (b)$$

$$[CH_3CH(.)OO.^*] \rightarrow [CH_3COOH^*] \rightarrow CH_3. + CO_2 + H \xrightarrow{O_2} CH_3O_2. + CO_2 + HO_2 \qquad (c)$$

$$[CH_3CH(.)OO.^*] \rightarrow [HCOOCH_3^*] \rightarrow HCO + CH_3O^{\cdot} \xrightarrow{O_2} HCHO + CO + 2\ HO_2 \qquad (d)$$

$$[CH_3CH(.)OO.^*] \rightarrow [HCOOCH_3^*] \rightarrow CH_3. + CO_2 + H \xrightarrow{O_2} CH_3O_2. + CO_2 + HO_2 \qquad (e)$$

Based primarily on results of previous low-pressure studies and on modeling simulations of propene and ozone decay rates observed when they react at ppm levels in air, Dodge and Arnts (1979) concluded that $k_b = k_c$, $k_d = k_e$, and $(k_b + k_c)/(k_d + k_e) = 4$. Thus the four radical producing reactions can be combined to yield

$$[CH_3CH(.)OO.^*] \xrightarrow{O_2} 0.9\ CH_3O_2. + 0.7\ HO_2 + 0.4\ OH + 0.5\ CO_2 + 0.5\ CO$$
$$+\ 0.1\ HCHO.$$

Because of the lack of more definitive data obtained under atmospheric conditions, this radical producing mechanism was recommended, with minor changes, in the evaluation of Atkinson and Lloyd (1984), and is assumed in our model.

Atkinson and Lloyd (1984) and Dodge and Arnts (1979) make the additional assumption that no additional processes are occurring, and thus, if

20% stabilization and 14% methane formation is assumed, then the radical production route will occur 66% of the time. However, if this is assumed, then model simulations consistently overpredict the reactivity observed in the propene-NO_x-air irradiations carried out in the SAPRC indoor and outdoor Teflon chambers. This is shown in Figures II-7 and II-8, where observed and calculated concentration-time profiles for ozone, propene, and PAN are plotted for a representative ITC and a representative OTC run, respectively. Because of the greater variability of the fits of the model to the results of the UNC chamber experiments (discussed in Section IV), this discrepancy is less obvious in the case of the UNC runs. Plots of observed and calculated ozone profiles for three representative propene runs carried out in the UNC chamber are shown in Figure II-9.

This tendency to overpredict reactivity can be attributed to excessive radical formation in the ozone + propene mechanism, since much better fits to these data are obtained if lower radical yields in this reaction is assumed. (The model simulations of the propene experiments carried out in the SAPRC EC are less sensitive to this because the higher chamber radical source in that chamber makes radical production from homogeneous processes relatively less important in model simulations.) Specifically, the SAPRC ITC and OTC chamber data are best fit if it is assumed that the radical forming reactions occur only 30% of the time, rather than the 66% predicted based on assuming that stabilization and methane formation are the only non-radical producing processes which occur. [This adjusted model thus predicts slightly more radical formation than the original model of Atkinson et al. (1982a), where in effect radical forming reactions are assumed to occur 25% of the time.] This adjusted model also tends to be more consistent with the reactivity observed in most of the OTC chamber runs. The fits for this adjusted model are also shown in Figures II-7 through II-9.

Thus, in this model, we assume that the radical forming reactions from the "hot" [$CH_3CH(.)OO.*$] biradical occur only 30% of the time, and that the remaining 36% of the time the biradical reacts via additional, unspecified, non-radical producing processes. In view of a lack of definitive data to the contrary we can only assume that the products produced via these processes are unreactive, and thus they are represented by "lost carbon". The reaction as written above is based on these assumptions.

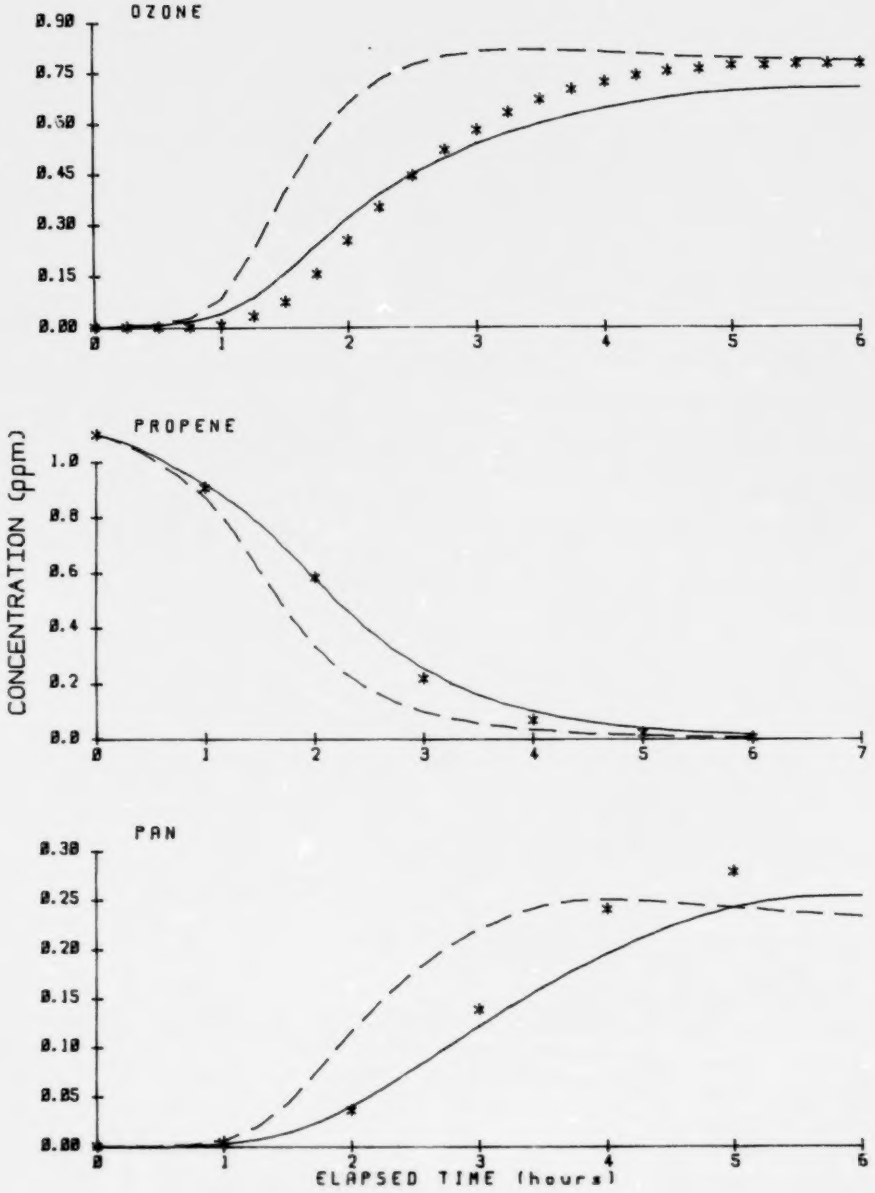

Figure II-7. Experimental and calculated concentration-time profiles of ozone, propene, and PAN for propene-NO_x-air run ITC-693.
* = Experimental data.
-- -- = Calculated assuming 66% radical production from $[CH_3CH(.)OO.^*]$ (initial estimate).
----- = Calculated assuming 30% radical production from $[CH_3CH(.)OO.^*]$ (adjusted model).

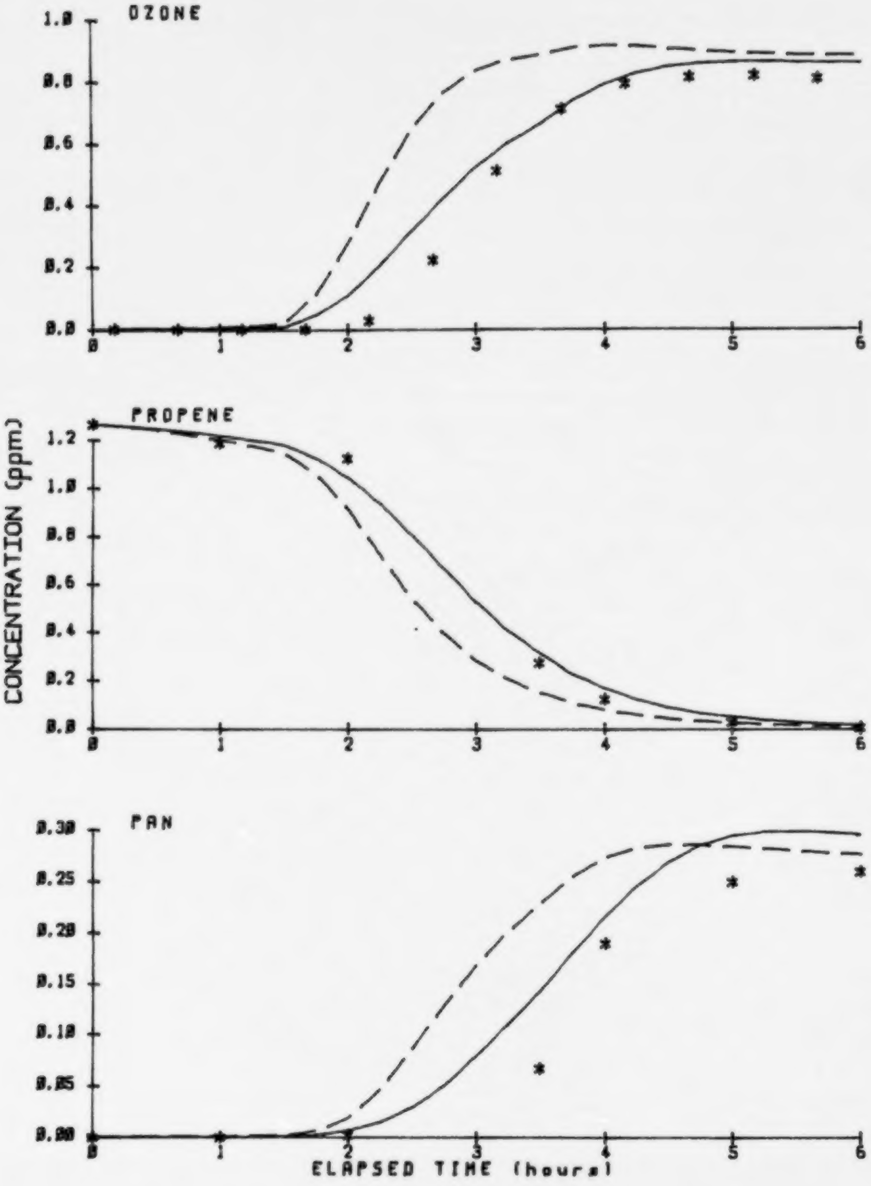

Figure II-8. Experimental and calculated concentration-time profiles of ozone, propene, and PAN for propene-NO_x-air run OTC-186.
* = Experimental data.
-- -- = Calculated assuming 66% radical production from $[CH_3CH(.)OO.^*]$ (initial estimate).
----- = Calculated assuming 30% radical production from $[CH_3CH(.)OO.^*]$ (adjusted model).

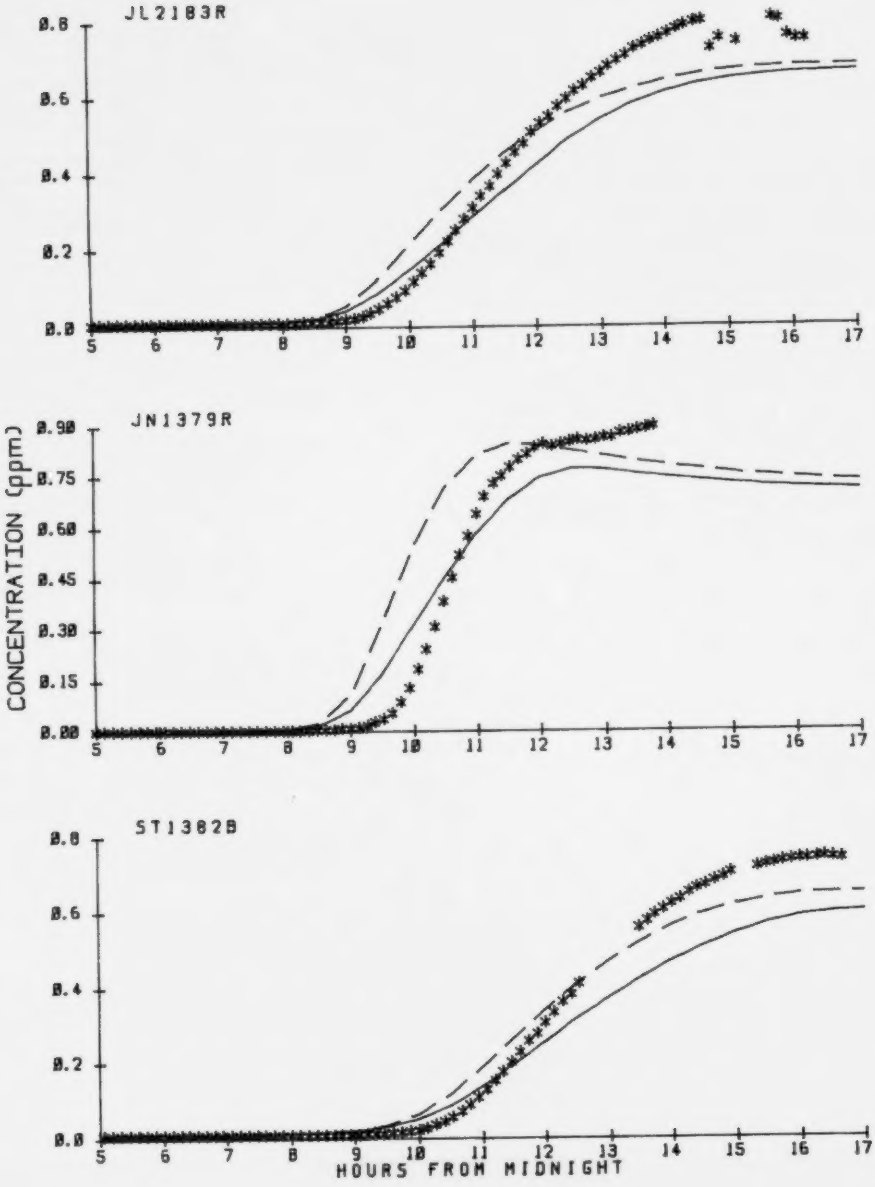

Figure II-9. Experimental and calculated concentration-time profiles of ozone for three UNC propene-NO_x-air irradiations.

* = Experimental data.

-- -- = Calculated assuming 66% radical production from $[CH_3CH(.)OO.*]$ (initial estimate).

----- = Calculated assuming 30% radical production from $[CH_3CH(.)OO.*]$ (adjusted model).

Clearly, there are significant uncertainties in this aspect of the photooxidation mechansims of propene and of the other higher alkenes. Further work is needed to define the products and radicals formed from the decomposition of these "hot" biradicals and to further confirm the stabilization yields reported by Hatakeyama et al. (1984).

D21. $O(^3P) + CH_2{=}CHCH_3 \xrightarrow{O_2} 0.6\ CH_3COCH_3 + 0.4\ CO + 0.4\ CH_3OO\cdot + 0.2\ C_2H_5OO\cdot + 0.2\ HO_2$

This reaction is discussed by Atkinson and Lloyd (1984). They recommend assuming that propionaldehyde and propene oxide are each formed 30% of the time, and that fragmentation to $\cdot CH_2CHO + CH_3$ and to $HCO + C_2H_5$ each occur 20% of the time. The reaction as written above is based on this evaluation, with acetone being taken to represent propene oxide, and the two fragmentation routes being represented respectively by $2\ CH_3OO\cdot + CO$ [see discussion of the $O(^3P)$ + ethene reaction, above] and $C_2H_5OO\cdot + CO + HO_2$. This reaction is of relatively minor importance, and is included in the model primarily because it can be a non-negligible radical source under certain conditions.

The rate constant expression recommended by Atkinson and Lloyd (1984) for this reaction is given below.

$$k_{D21} = 1.18 \times 10^{-11}\ e^{-644/RT}\ cm^3\ molecule^{-1}\ sec^{-1}$$

$$= 4.0 \times 10^{-12}\ cm^3\ molecule^{-1}\ sec^{-1} \text{ at } 298\ K$$

This is used in the model.

D22. $NO_3 + CH_2{=}CHCH_3 \xrightarrow{O_2} O_2NOCH_2CH(CH_3)OO\cdot$

This reaction consists of the rate determining addition of NO_3 radicals to the double bond, followed by the rapid addition of O_2 to the radicals formed. The reaction as shown above is based on assuming that addition occurs at the external position, but, exactly analogously to the

OH radical reaction with propene, the products ultimately formed are expected to be the same if the addition occurs at the internal position. Hence no approximation is introduced by representing the reaction as shown above.

All present determinations of the rate constant for this reaction are based on the $N_2O_5 = NO_3 + NO_2$ equilibrium constant. Based on the recommended equilibrium constant of Malko and Troe (1982), Atkinson and Lloyd (1984) recommended $k_{D22} = 4.2 \times 10^{-15}$ cm^3 molecule^{-1} sec^{-1} for T = 298 K. However, the equilibrium constant we now use (see Section A) is a factor of 1.8 higher than that used by Atkinson and Lloyd (1984), and thus to be consistent, our value for k_{D22} should be increased by this factor. Thus we use

$$k_{D22} = 7.6 \times 10^{-15} \text{ cm}^3 \text{ molecule}^{-1} \text{ sec}^{-1} \text{ at } 298 \text{ K}$$

The temperature dependence of this reaction is not known. We assume that it has a similar Arrhenius pre-exponential factor as that for OH + propene, because both reactions involve addition to the double bond. Thus we use

$$k_{D22} = 5 \times 10^{-12}\, e^{-3843/RT} \text{ cm}^3 \text{ molecule}^{-1} \text{ sec}^{-1}$$

to estimate the temperature dependence of this rate constant.

D23. $O_2NOCH_2CH(CH_3)OO\cdot + NO \rightarrow 2\ NO_2 + HCHO + CH_3CHO$

This reaction consists of the rate determining reaction of the peroxy radical with NO, whose kinetics are discussed in Section B, followed by the following decompositions, which are assumed to be rapid.

$$O_2NOCH_2CH(CH_3)OO\cdot + NO \rightarrow NO_2 + O_2NOCH_2CH(CH_3)O\cdot$$

$$O_2NOCH_2CH(CH_3)O\cdot \rightarrow CH_3CHO + \cdot CH_2ONO_2$$

$$\cdot CH_2ONO_2 \rightarrow NO_2 + HCHO$$

Although, as discussed by Atkinson and Lloyd (1984), dinitrates are observed to be formed as products of this reaction under some conditions, such as in the dark or when high levels of NO_2 are present and under atmospheric conditions in the daytime when NO_x is present, the reactions indicated above are expected to dominate. The reactions of the radical formed following internal addition of NO_3 to propene are analogous, and give rise to the same products.

D24. $O_2NOCH_2CH(CH_3)OO\cdot + HO_2 \rightarrow -OOH + (O_2NOCH_2CH(CH_3)OO\cdot \text{ products})$

D25. $O_2NOCH_2CH(CH_3)OO\cdot + RO_2 \rightarrow 0.5\ HO_2 + (O_2NOCH_2CH(CH_3)OO\cdot \text{ products})$

D26. $O_2NOCH_2CH(CH_3)OO\cdot + RCO_3 \rightarrow 0.5\ HO_2 + (O_2NOCH_2CH(CH_3)OO\cdot \text{ products})$

The kinetics of these reactions and the general principles used for representing the products are discussed in Section B. As indicated there, the organic products formed in these reactions are the set of products expected to be formed from the reactions of the corresponding alkoxy radical. As discussed above, the alkoxy radical is expected to decompose to give rise to $HCHO + CH_3CHO + NO_2$, and thus we use

$$(O_2NOCH_2CH(CH_3)OO\cdot \text{ products}) = NO_2 + HCHO + CH_3CHO$$

for the above reactions.

3. Reactions of 1-Butene

D27. $OH + CH_2{=}CHC_2H_5 \rightarrow HOCH_2CH(OO\cdot)C_2H_5$

The reaction of OH radicals with 1-butene is now believed to proceed essentially totally via OH radical addition to the double bond, based on the observation of Atkinson et al. (1985) that propionaldehyde is formed in 94 ± 12% yield in this reaction. As discussed by Atkinson et al. (1985), the abstraction route, which Atkinson and Lloyd (1984) estimated to occur ~20% of the time based on the previous experimental data of Biermann et al. (1982), is expected to give rise to products which were not observed.

Thus the reaction as written above consists of the rate determining addition of the OH radical to the double bond, followed by the rapid reaction of the adduct with O_2. As is the case with propene, only the external addition route is represented, since the internal addition route, which (by analogy with propene) is estimated to occur ~35% of the time, is believed to give rise to the same products (see discussion below).

The available data concerning the kinetics of this reaction have been reviewed and evaluated by Atkinson (1986), and the following expression for the rate constant was recommended:

$$k_{D25} = 6.53 \times 10^{-12}\ e^{930/RT}\ \mathrm{cm^3\ molecule^{-1}\ sec^{-1}}$$

$$= 3.14 \times 10^{-11}\ \mathrm{cm^3\ molecule^{-1}\ sec^{-1}}\ \text{at 298 K.}$$

This is used in the model.

D28. $HOCH_2CH(OO.)C_2H_5 + NO \rightarrow NO_2 + HCHO + C_2H_5CHO + HO_2$

The kinetics of peroxy + NO reactions are discussed in Section B. The mechanism for this reaction is analogous to that discussed above for reaction (D15), except that propionaldehyde rather than acetaldehyde is formed:

$$HOCH_2CH(OO.)C_2H_5 + NO \rightarrow HOCH_2CH(O.)C_2H_5$$

$$HOCH_2CH(O.)C_2H_5 \rightarrow HOCH_2. + C_2H_5CHO$$

$$HOCH_2. + O_2 \rightarrow HCHO + HO_2$$

The analogous reactions of the radical formed following internal addition will give rise to the same products.

$$C_2H_5CH(OH)CH_2OO. + NO \rightarrow C_2H_5CH(OH)CH_2O. + NO_2$$

$$C_2H_5CH(OH)CH_2O. \rightarrow C_2H_5CH(.)OH + HCHO$$

$$C_2H_5CH(.)OH + O_2 \rightarrow C_2H_5CHO + HO_2$$

However, in this case, the alkoxy radical can also isomerize,

$$C_2H_5CH(OH)CH_2O. \rightarrow .CH_2CH_2CH(OH)CH_2OH$$

giving rise to other products. But since, as indicated above, propionaldehyde was observed to be formed in almost 100% yield in the reaction of OH with 1-butene, we conclude that isomerization is not important, either because the OH addition at the internal position is much less than is the case for propene, or (more likely) that the decomposition of the alkoxy radical is much more rapid than the isomerization [as estimated by Atkinson and Lloyd (1984)].

It should be pointed out that Atkinson and Lloyd (1984) assume that 8% of the initial reaction of the peroxy radical results in the formation of the corresponding alkyl nitrate, by analogy with the observation of 8% 2-butyl nitrate formation in the reaction of 2-butyl peroxy radicals with NO (Atkinson et al. 1982b).

$$HOCH_2CH(OO.)C_2H_5 + NO \rightarrow HOCH_2CH(ONO_2)C_2H_5$$

However, that reaction is not included in the mechanism, because (a) assuming that an analogous reaction occurs in the trans-2-butene system (discussed in the following section) makes the fits of the model simulations to the trans-2-butene-NO_x runs worse than they would otherwise be; (b) it is also necessary to assume that alkyl nitrate formation is not important in the reactions of NO with the hydroxy-substituted peroxy radicals formed in the reactions of the higher ($\geq C_5$) alkanes in order to fit the chamber data for those species (see Section F); and (c) the model consistently underpredicts the reactivity observed in the three 1-butene-NO_x runs carried out in the SAPRC EC, and assuming that this reaction is non-negligible makes these fits even worse. Very recently Shepson et al.

(1985) have derived nitrate yields of ~1.5% from the reaction of $CH_3CHOHCH_2OO^{\cdot}$ and $CH_3CH(\overset{\bullet}{OO})CH_2OH$ radicals with NO, a factor of ~2 lower than the yields from the corresponding alkyl peroxy radicals. Thus this finding is consistent with our assumptions. Experimental and calculated concentration-time profiles for ozone in those three EC experiments are compared in Figure II-10.

On the other hand, it should also be noted that the model consistently overpredicts the reactivity observed in the four 1-butene-NO_x-air runs carried out in the UNC chamber in September 23-27 of 1983. Experimental and calculated ozone plots for two of those runs are shown in Figure II-11, where it can be seen that even assuming the 8% alkyl nitrate formation in reaction (D28) does not significantly improve the situation. Thus, in the case of model fits to the 1-butene chamber data there appears to be a discrepancy between the UNC chamber and the SAPRC EC. However, as is also shown in Figure II-11, the model also significantly overpredicts the reactivity observed in the propene-NO_x-air run carried out in the UNC chamber at the same time as one of the 1-butene runs (on September 23), despite the fact that the model is generally consistent with the results of most of the other propene runs carried out in this chamber. For this reason, we place more weight on the results of the SAPRC EC runs in terms of evaluating the 1-butene model, though those runs were also all carried out around the same time. It is thus clear that further 1-butene chamber experiments are required before the 1-butene model can be considered to be adequately validated.

D29. $HOCH_2CH(OO.)C_2H_5 + HO_2 \rightarrow -OOH + (HOCH_2CH(OO.)C_2H_5$ products)

D30. $HOCH_2CH(OO.)C_2H_5 + RO_2 \rightarrow 0.5\ HO_2 + (HOCH_2CH(OO.)C_2H_5$ products)

D31. $HOCH_2CH(OO.)C_2H_5 + RCO_3 \rightarrow 0.5\ HO_2 + (HOCH_2CH(OO.)C_2H_5$ products)

The kinetics of these reactions and the general principles used for representing the products are discussed in Section B. As indicated there, the organic products formed in these reactions are represented by the set of products expected to be formed from the reactions of the corresponding

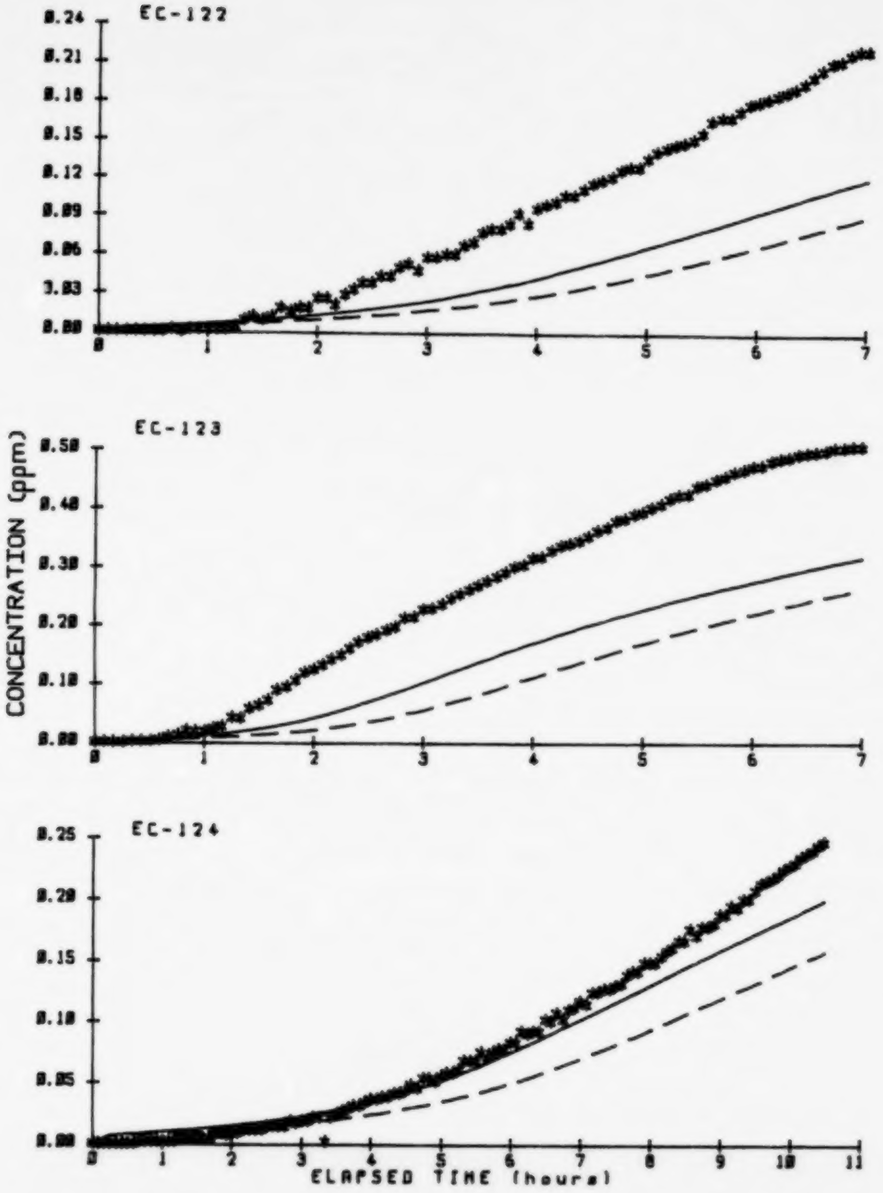

Figure II-10. Experimental and calculated concentration-time profiles of ozone for three 1-butene-NO_x-air irradiations carried out in the SAPRC EC.

* = Experimental data.

----- = Calculated assuming no nitrate formation in reaction D28 (standard model).

-- -- = Calculated assuming 8% nitrate formation in reaction D28.

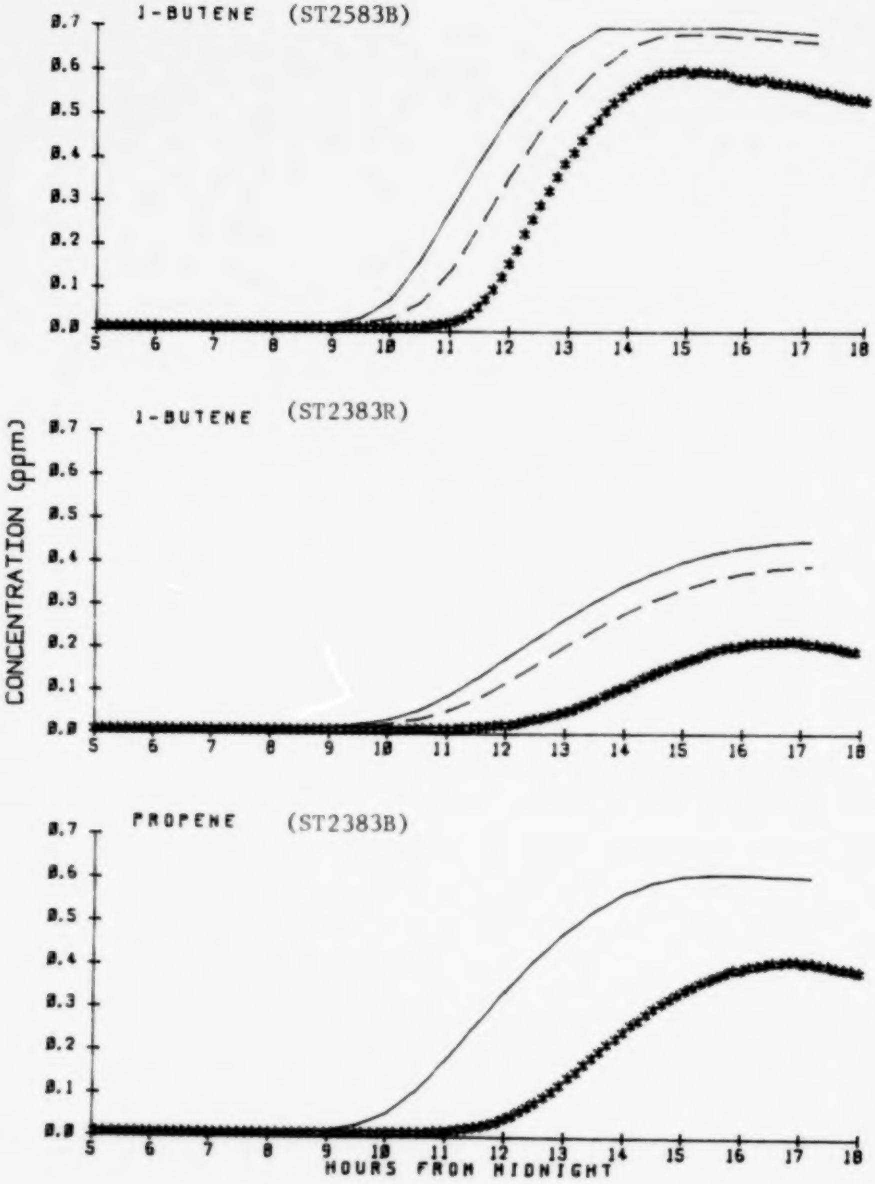

Figure II-11. Experimental and calculated concentration-time profiles of ozone for two UNC 1-butene-NO_x-air irradiations and for a propene-NO_x-air irradiation carried out at the same time.

* = Experimental data.

----- = Calculated assuming no nitrate formation in reaction D28 (standard model).

-- -- = Calculated assuming 8% nitrate formation in reaction D28.

alkoxy radical. As discussed above, the alkoxy radical is expected to decompose to form formaldehyde and propionaldehyde. Thus we use

$$(HOCH_2CH(OO.)C_2H_5 \text{ products}) = HCHO + C_2H_5CHO$$

for the above reactions.

D32. $O_3 + CH_2{=}CHC_2H_5 \rightarrow 0.5\ (HCHO + [C_2H_5CH(.)OO.*]) + 0.5\ (C_2H_5CHO + [.CH_2OO.*])$

The kinetics of this reaction have been evaluated by Atkinson and Carter (1984), who recommend the following expression for its rate constant, which is used in the model.

$$k_{D32} = 3.46 \times 10^{-15}\ e^{-3403/RT}\ cm^3\ molecule^{-1}\ sec^{-1}$$

$$= 1.10 \times 10^{-17}\ cm^3\ molecule^{-1}\ sec^{-1} \text{ at } 298\ K.$$

The available data concerning the mechanism of this reaction have been discussed and evaluated by Atkinson and Lloyd (1984). The major mode of reaction of ozone-alkene reactions in the gas phase is believed to be the formation of a primary ozonide, which rapidly fragments to form a carbonyl compound and a "hot" biradical. In the case of 1-butene, two modes of decomposition of the ozonide are possible, one giving rise to formaldehyde and the ethyl-substituted "hot" biradical designated $[C_2H_5CHO_2*]$, and the other giving rise to propionaldehyde and $[.CH_2O_2.*]$. These two decomposition pathways are assumed to occur with equal probability.

As indicated above, the subsequent reactions of the biradicals formed in the ozone-alkene systems are assumed to be the same regardless of the alkene which formed them. Thus the reaction sequence assumed for $[.CH_2OO.*]$ is reaction (D7), given above in conjunction with our discussion of the ozone + ethene system. The reaction sequence assumed for the other biradical formed in the ozone + 1-butene system is discussed below.

$$\text{D33.}\quad [C_2H_5CH(.)OO.^*] \xrightarrow[\text{fast}]{O_2} 0.2\ C_2H_5CO_2. + 0.14\ C_2H_6 + 0.29\ CO_2 + 0.15\ CO + 0.03\ CH_3CHO + 0.27\ C_2H_5O_2. + 0.21\ HO_2 + 0.12\ OH + 1.08\ \text{"lost carbon"}$$

There are no data concerning the atmospheric reactions of this "hot" ethyl substituted biradical. We estimate, as do Atkinson and Lloyd (1984), that its reactions are analogous to those assumed for the "hot" methyl substituted biradical (i.e., to reaction D20, discussed above). Thus by analogy with the reactions of the methyl substituted radical, we assume that stabilization occurs 20% of the time, ethane + CO_2 formation (analogous to decomposition pathway (a) of $[CH_3CH(.)OO.^*]$) occurs 14% of the time, radical production occurs 30% of the time, and the remainder of the reaction occurs via unspecified, non-radical producing routes, giving rise to unreactive products.

The reaction as written above is based on the further assumption that the specific radical production reactions of the ethyl substituted biradical are analogous to decomposition pathways (b-e) in the $[CH_3CH(.)OO.^*]$ system, and that each of these pathways has the same relative importance as its analogue in the methyl-substituted system. These reactions, along with their assumed percent contribution to the total of the radical production routes from $[C_2H_5CH(.)OO.^*]$ are indicated below.

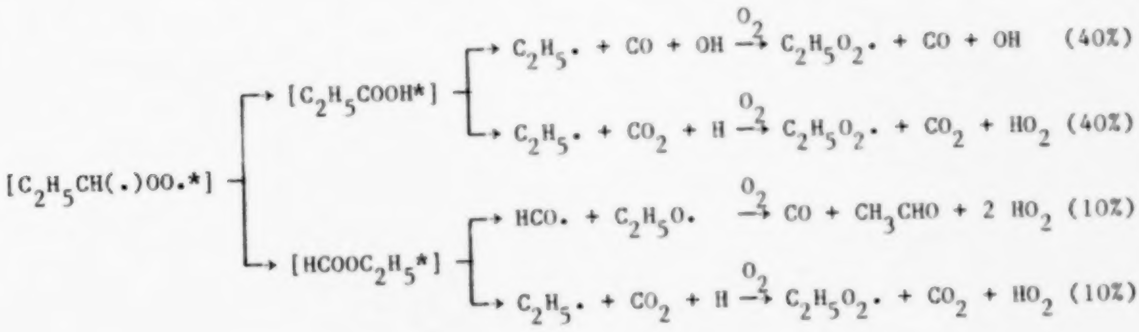
[C2H5CH(.)OO.*]
[C2H5COOH*]
C2H5. + CO + OH —O2→ C2H5O2. + CO + OH (40%)
C2H5. + CO2 + H —O2→ C2H5O2. + CO2 + HO2 (40%)
[HCOOC2H5*]
HCO. + C2H5O. —O2→ CO + CH3CHO + 2 HO2 (10%)
C2H5. + CO2 + H —O2→ C2H5O2. + CO2 + HO2 (10%)

As indicated above, these processes are assumed to account for 30% of the total reactions of the "hot" ethyl-substituted biradical.

The subsequent reactions of the thermalized biradical, $C_2H_5CHO_2$, are discussed in Section D-6.

D34. $O(^3P) + CH_2{=}CHC_2H_5 \xrightarrow{O_2} 0.44\ CH_3COC_2H_5 + 0.39\ (C_2H_5CHO + \text{"lost C"})$
$+ 0.17\ (CO + HCHO + CH_3CHO + 2\ HO_2)$

This reaction is discussed by Atkinson and Lloyd (1984). They recommended assuming formation of 44% 1-butene oxide, 39% butyraldehyde and 17% fragmentation to $.CH_2CHO + C_2H_5$ radicals in this reaction. The reaction as written is based on this recommendation, except that methyl ethyl ketone is used to represent 1-butene oxide, propionaldehyde to represent butyraldehyde and the fragmentation route is represented by $CH_3OO. + CO + C_2H_5OO.$ (As discussed above in conjunction with the discussion of the $O(^3P)$ + ethene reaction, $.CH_2CHO$ is believed to give rise to the same ultimate products under atmospheric conditions as $CH_3OO. + CO.$) The products of this reaction are treated in an approximate manner in order to avoid adding new species to the model to represent products which are formed in this relatively minor process. This reaction is included in the model primarily because it may be a non-negligible radical source under certain conditions.

Atkinson and Lloyd (1984) recommend the following expression for the rate constant for this reaction.

$$k_{D34} = 1.25 \times 10^{-11}\ e^{-648/RT}\ \text{cm}^3\ \text{molecule}^{-1}\ \text{sec}^{-1}$$

$$= 4.2 \times 10^{-12}\ \text{cm}^3\ \text{molecule}^{-1}\ \text{sec}^{-1} \text{ at } 298\ \text{K}$$

This is used in the model.

D35. $NO_3 + CH_2{=}CHC_2H_5 \xrightarrow{O_2} ONO_2CH_2CH(OO.)C_2H_5$

This reaction is represented in an analogous manner to the reaction of NO_3 radicals with propene [reaction (D22)], discussed above. In particular, although the addition of NO_3 to 1-butene can occur via both terminal and internal addition to the double bond, we assume that both processes give rise to the same ultimate products, and thus the reaction is written as if only terminal addition occurred.

Atkinson and Lloyd (1984) recommend $k_{D35} = 5.4 \times 10^{-15}$ cm^3 $molecule^{-1}$ sec^{-1} for T = 298 K. However, the rate constant determined for this reaction depends on their assumed $N_2O_5 = NO_3 + NO_2$ equilibrium constant; and, as discussed above in conjunction with the other NO_3 + alkene reactions, we now use an equilibrium constant which is a factor of 1.8 higher at 298 K than that used by Atkinson and Lloyd (1984). Thus we use

$$k_{D35} = 9.7 \times 10^{-15} \text{ cm}^3 \text{ molecule}^{-1} \text{ sec}^{-1} \text{ at } 298 \text{ K}$$

The temperature dependence of this reaction is not known. We assume that it has the same Arrhenius pre-exponential factor that we assumed for NO_3 + propene, which is similar to that for OH + 1-butene. Thus we use

$$k_{D35} = 5 \times 10^{-12} \; e^{-3698/RT} \text{ cm}^3 \text{ molecule}^{-1} \text{ sec}^{-1}$$

for the temperature dependence of this rate constant.

D36. $O_2NOCH_2CH(OO.)C_2H_5 + NO \rightarrow 2\ NO_2 + C_2H_5CHO + HCHO$

This reaction consists of the rate determining reaction of the peroxy radical with NO, whose kinetics are discussed in Section B. The reaction is assumed to result in the formation of the corresponding alkoxy radical, followed by decomposition and subsequent reaction of the α-hydroxy radical fragment with O_2:

$$O_2NOCH_2CH(OO.)C_2H_5 + NO \rightarrow O_2NOCH_2CH(O.)C_2H_5 + NO_2$$

$$O_2NOCH_2CH(O.)C_2H_5 \rightarrow O_2NOCH_2. + C_2H_5CHO$$

$$O_2NOCH_2. \rightarrow NO_2 + HCHO$$

This is totally analogous to the assumptions concerning the radicals formed in the NO_3 + propene reaction. Note in this case that the alkoxy radical formed following terminal addition has a competitive isomerization pathway,

$$C_2H_5CH(ONO_2)CH_2O. \rightarrow CH_2(.)CH_2CH(ONO_2)CH_2OH$$

which we assume is negligible compared to decomposition (analogous to the corresponding case for the OH + 1-butene reaction). This assumption is uncertain, but it should be noted that reaction with NO_3 is a relatively minor consumption route for this alkene, particularly during daytime.

The possible formation of an organic dinitrate in the reaction of the peroxy radical with NO (by analogy with the observed 8% formation of 2-butyl nitrate from the reaction of NO with 2-butyl peroxy radicals [Atkinson et al. 1982b]) is ignored in this model. This is consistent with our assumption that substituted organic peroxy radicals have less of a tendency to form organic nitrates than do unsubstituted radicals, as discussed above [in conjunction with reaction (D28)] and in Section E, and with the very recent data of Shepson et al. (1985). This would be a relatively minor reaction route in any case.

D37. $ONO_2CH_2CH(OO.)C_2H_5 + HO_2 \rightarrow -OOH + (ONO_2CH_2CH(OO.)C_2H_5 \text{ products})$

D38. $ONO_2CH_2CH(OO.)C_2H_5 + RO_2 \rightarrow 0.5\ HO_2 + (ONO_2CH_2CH(OO.)C_2H_5 \text{ products})$

D39. $ONO_2CH_2CH(OO.)C_2H_5 + RCO_3 \rightarrow 0.5\ HO_2 + (ONO_2CH_2CH(OO.)C_2H_5 \text{ products})$

The kinetics of these reactions and the general principles used for representing the products have been discussed in Section B. As indicated there, the organic products formed in these reactions are the set of products expected to be formed from the reactions of the corresponding alkoxy radical. As discussed above, the alkoxy radical is expected to decompose to give rise to HCHO + C_2H_5CHO + NO_2, and thus we use

$$(ONO_2CH_2CH(OO.)C_2H_5 \text{ products}) = HCHO + C_2H_5CHO + NO_2$$

for the above reactions.

4. Reactions of trans-2-Butene

D40. $OH + t\text{-}CH_3CH{=}CHCH_3 \xrightarrow{O_2} CH_3CH(OH)CH(OO.)CH_3$

This reaction consists primarily of the rate determining addition of OH radicals to the double bond, followed by the rapid reaction of the adduct with O_2 to form the peroxy radical indicated above. As is the case with propene and 1-butene, addition is believed to be the predominant reaction route.

Atkinson (1986) has recently evaluated the kinetic data for this reaction and recommended the following expression for its rate constant.

$$k_{D40} = 1.01 \times 10^{-11}\ e^{1091/RT}\ \text{cm}^3\ \text{molecule}^{-1}\ \text{sec}^{-1}$$

$$= 6.37 \times 10^{-11}\ \text{cm}^3\ \text{molecule}^{-1}\ \text{sec}^{-1} \text{ at } 298\text{ K.}$$

This is used in the model.

D41. $CH_3CH(OH)CH(OO.)CH_3 + NO \xrightarrow{O_2} NO_2 + (2\ CH_3CHO + HO_2)$

This reaction consists of the initial rate determining reaction of NO with the peroxy radical to form the corresponding alkoxy radical. The peroxy + NO reaction is assumed to result in the formation of the corresponding alkoxy radical followed by the rapid decomposition of the alkoxy radical and the subsequent reactions of the α-hydroxy radicals formed with O_2.

$$CH_3CH(OH)CH(OO.)CH_3 + NO \rightarrow CH_3CH(OH)CH(O.)CH_3 + NO_2$$

$$CH_3CH(OH)CH(O.)CH_3 \rightarrow CH_3\dot{C}H(OH) + CH_3CHO$$

$$CH_3\dot{C}H(OH) + O_2 \rightarrow CH_3CHO + HO_2$$

This is totally analogous to the reactions of the peroxy radicals formed in the OH + propene and OH + 1-butene systems, discussed above, except in this case, only one OH-alkene-O_2 adduct is formed because of the symmetry of the molecule.

The possible formation of a hydroxy-substituted alkyl nitrate in the reaction of this peroxy radical with NO is ignored, by analogy with the assumption for the 1-butene system, and because it adversely affects the quality of fits of the model calculation to the results of the trans-2-butene runs carried out in the SAPRC EC. Experimental and calculated concentration-time plots for selected species in a representative EC trans-2-butene run are shown in Figure II-12, where it can be seen that the model somewhat underpredicts the observed reactivity, with the fit being worse if 8% nitrate formation, as estimated by Atkinson and Lloyd (1984), is assumed. The results of the single UNC trans-2-butene-NO_x-air run for which we have data are not as sensitive to nitrate formation, as shown in Figure II-13.

D42. $CH_3CH(OH)CH(OO.)CH_3 + HO_2 \rightarrow -OOH + (CH_3CH(OH)CH(OO.)CH_3 \text{ products})$

D43. $CH_3CH(OH)CH(OO.)CH_3 + RO_2 \rightarrow 0.5\ HO_2 + (CH_3CH(OH)CH(OO.)CH_3 \text{ products})$

D44. $CH_3CH(OH)CH(OO.)CH_3 + RCO_3 \rightarrow 0.5\ HO_2 + (CH_3CH(OH)CH(OO.)CH_3 \text{ products})$

The kinetics of these reactions and the general principles used for representing the products are discussed in Section B. As indicated there, the organic products formed in these reactions are represented by the set of products expected to be formed from the reactions of the corresponding alkoxy radical. As discussed above, the alkoxy radical is expected to decompose to form 2 CH_3CHO + HO_2. Thus we use

$$(CH_3CH(OH)CH(OO.)CH_3 \text{ products}) = 2\ CH_3CHO$$

for the above reactions.

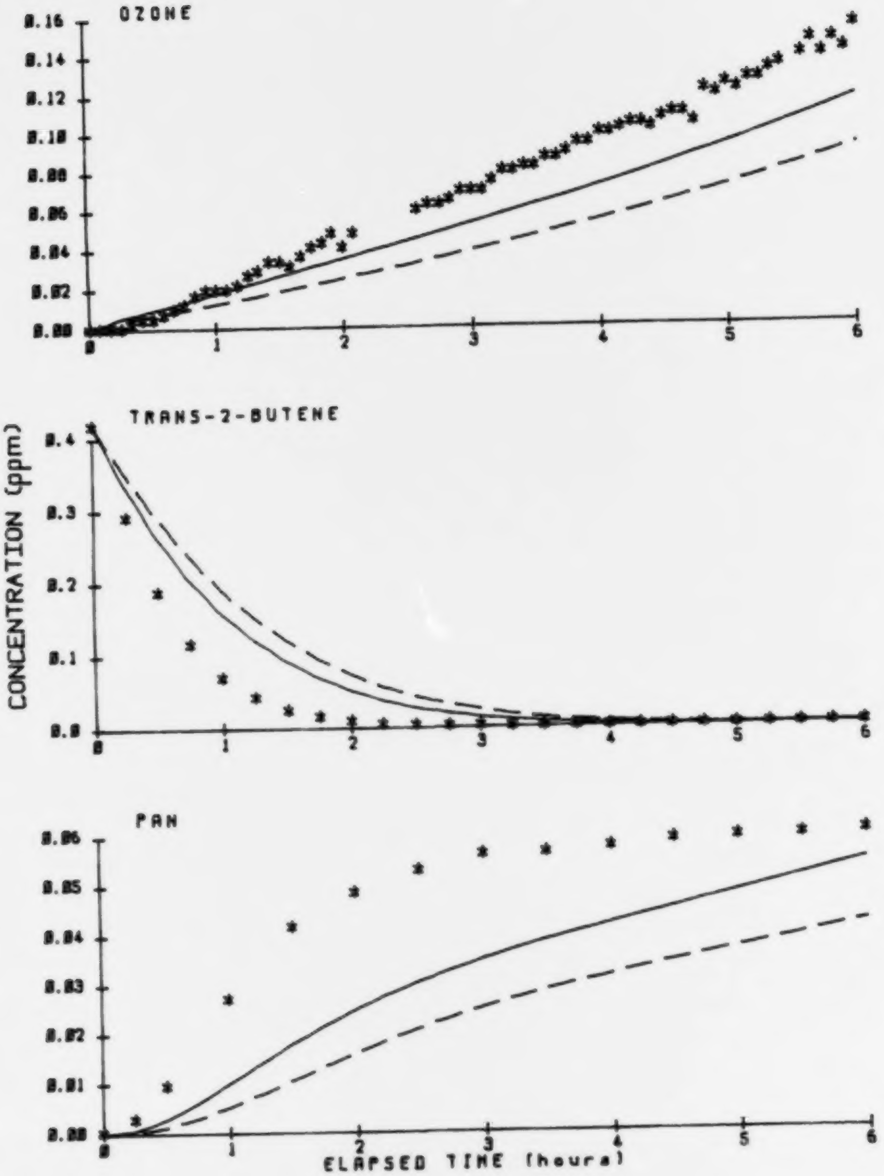

Figure II-12. Experimental and calculated concentration-time profiles of ozone, trans-2-butene and PAN for the representative trans-2-butene-NO_x-air run EC-147.

* = Experimental data.

----- = Calculated assuming no hydroxy-substituted nitrate formation in reaction D41.

-- -- = Calculated assuming 8% hydroxy-substituted nitrate formation in reaction D41.

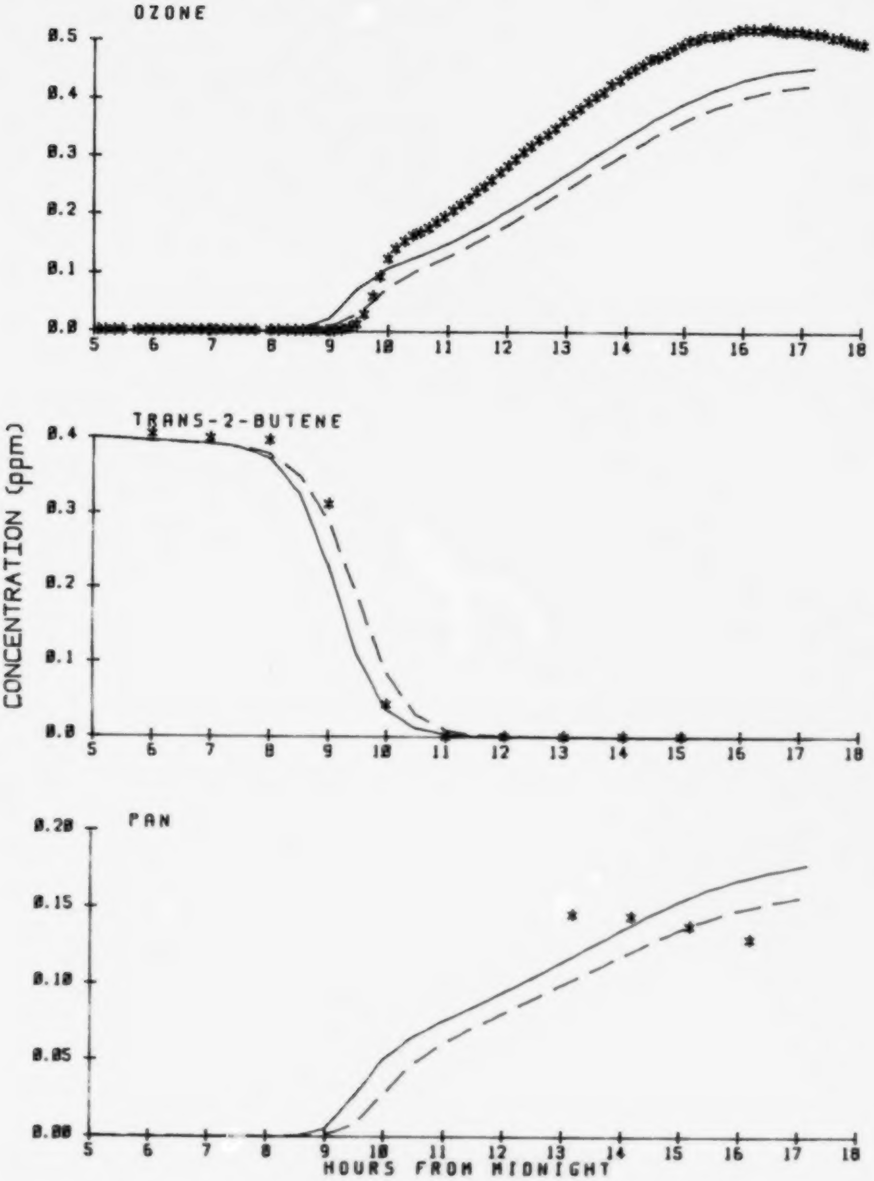

Figure II-13. Experimental and calculated concentration-time profiles of ozone, trans-2-butene and PAN for the UNC trans-2-butene-NO_x-air run ST2783B.

* = Experimental data.

----- = Calculated assuming no hydroxy-substituted nitrate formation in reaction D41.

-- -- = Calculated assuming 8% hydroxy-substituted nitrate formation in reaction D41.

D45. $O_3 + t\text{-}CH_3CH{=}CHCH_3 \rightarrow CH_3CHO + [CH_3CH(.)OO.*]$

The kinetics of the ozone + trans-2-butene reaction were recently evaluated by Atkinson and Carter (1984). They recommended the following expression for the rate constant for this reaction,

$$k_{D45} = 9.08 \times 10^{-15}\ e^{-2258/RT}\ \text{cm}^3\ \text{molecule}^{-1}\ \text{sec}^{-1}$$

$$= 2.00 \times 10^{-16}\ \text{cm}^3\ \text{molecule}^{-1}\ \text{sec}^{-1} \text{ at } 298\text{ K},$$

which is used in the model.

The available data concerning the mechanism of this reaction has been discussed and evaluated by Atkinson and Lloyd (1984). The major mode of this reaction is believed to be the formation of the primary ozonide, which subsequently decomposes to form acetaldehyde and the "hot" biradical $[CH_3CH(.)OO.*]$. As indicated above, the reaction sequence assumed for the hot biradicals are the same regardless of which ozone-alkene reaction formed them, and thus the sequence assumed for $[CH_3CH(.)OO.*]$ [reaction (D20)] is given above in conjunction with the discussion of the ozone + propene reaction.

It should be pointed out that the model simulations of the three trans-2-butene-NO_x-air irradiations which have been carried out in the SAPRC evacuable chamber, and of the one such run carried out in the UNC chamber for which we have data, fit the data better if the model assumes more radical formation in the decompositions of $[CH_3CH(.)OO.*]$ than indicated by the model simulations of the propene runs. In particular, as shown in Figures II-7 and II-8 above, the present model, in which the yield of radicals assumed to be formed from these biradicals are adjusted for optimum fits to the results of the propene runs, tends to underpredict the reactivity observed in the trans-2-butene-NO_x-air runs. Since there are many more propene runs than trans-2-butene runs, and data for propene are available for more chambers and under a greater variety of conditions, this model has not been modified to improve the fits to the trans-2-butene runs. However, this apparent discrepancy suggests that the assumption incorporated in our model that the fate of these "hot" biradicals is independent of how they are formed may not be valid. Clearly, more definitive data concerning the mechanisms of the reactions of ozone with the higher alkenes are needed to clarify this major area of uncertainty in the alkene photooxidation mechanisms.

D46. $O(^3P) + t\text{-}CH_3CH{=}CHCH_3 \xrightarrow{O_2} CH_3COC_2H_5 + 0.4\ HO_2$

There are less data available concerning this reaction than for the other $O(^3P)$ + alkene reactions discussed above. Atkinson and Lloyd (1984) recommend assuming 80% stabilization and 20% fragmentation to radicals in the overall reaction. Since the exact mechanism is unknown, and since this reaction is a relatively minor process, in this model we simply represent the radicals formed in the fragmentation route by HO_2, and all the organic products formed by methyl ethyl ketone. The reaction as written above is based on that representation.

Atkinson and Lloyd (1984) recommend use of the following expression for the rate constant of this reaction.

$$k_{D46} = 2.26 \times 10^{-11}\ e^{20/RT}\ \text{cm}^3\ \text{molecule}^{-1}\ \text{sec}^{-1}$$

$$= 2.3 \times 10^{-11}\ \text{cm}^3\ \text{molecule}^{-1}\ \text{sec}^{-1} \text{ at } 298\ \text{K}$$

This is used in the model.

D47. $NO_3 + t\text{-}CH_3CH{=}CHCH_3 \xrightarrow{O_2} CH_3CH(ONO_2)CH(OO.)CH_3$

This reaction consists of the rate determining addition of NO_3 radicals to the double bond, followed by the rapid addition of O_2 to the radicals formed. All present determinations of the rate constant for this reaction are based on the $N_2O_5 = NO_3 + NO_2$ equilibrium constant. Based on the recommended equilibrium constant of Malko and Troe (1982), Atkinson and Lloyd (1984) recommended $k_{D47} = 2.1 \times 10^{-13}$ cm^3 molecule^{-1} sec^{-1} for T = 298 K. However, the equilibrium constant we now use (see Section A) is a factor of 1.8 higher than that used by Atkinson and Lloyd (1984), and thus to be consistent with this, our value for k_{D47} is increased by this factor. Thus we use

$$k_{D47} = 3.8 \times 10^{-13} \text{ cm}^3 \text{ molecule}^{-1} \text{ sec}^{-1} \text{ at } 298 \text{ K.}$$

This is in excellent agreement with the very recent absolute measurement of k_{D47} of 3.78×10^{-13} cm^3 molecule^{-1} sec^{-1} at 298 K by Ravishankara and Mauldin (1985). The temperature dependence of this reaction is not known. We assume that it has a similar Arrhenius pre-exponential factor as that for OH + *trans*-2-butene since both reactions involve addition to the double bond. Thus we use

$$k_{D47} = 1.0 \times 10^{-11} e^{-1937/RT} \text{ cm}^3 \text{ molecule}^{-1} \text{ sec}^{-1}$$

for the temperature dependence of this rate constant.

D48. $CH_3CH(ONO_2)CH(OO.)CH_3 + NO \rightarrow 2\ NO_2 + 2\ CH_3CHO$

This reaction consists of the rate determining reaction of the peroxy radical with NO, whose kinetics are discussed in Section B. Analogous to our assumptions for the reactions following the NO_3 + 1-butene reaction, formation of the corresponding peroxy radical, which undergoes subsequent decomposition and reaction to form the products shown above, is assumed.

$$CH_3CH(ONO_2)CH(OO.)CH_3 + NO \rightarrow NO_2 + CH_3CH(ONO_2)CH(O.)CH_3$$

$$CH_3CH(ONO_2)CH(O.)CH_3 \rightarrow CH_3CH(.)ONO_2 + CH_3CHO$$

$$CH_3CH(.)ONO_2 \rightarrow CH_3CHO + NO_2$$

As is the case in the 1-butene system, the possible formation of small amounts of dinitrate from the initial peroxy + NO reaction is ignored.

D49. $CH_3CH(ONO_2)CH(OO.)CH_3 + HO_2 \rightarrow -OOH + (CH_3CH(ONO_2)CH(OO.)CH_3$ products)

D50. $CH_3CH(ONO_2)CH(OO.)CH_3 + RO_2 \rightarrow 0.5\ HO_2 + (CH_3CH(ONO_2)CH(OO.)CH_3$ products)

D51. $CH_3CH(ONO_2)CH(OO.)CH_3 + RCO_3 \rightarrow 0.5\ HO_2 + (CH_3CH(ONO_2)CH(OO.)CH_3$ products)

The kinetics of these reactions and the general principles used for representing the products are discussed in Section B. As indicated there, the organic products formed in these reactions are those expected to be formed from the reactions of the corresponding alkoxy radical. As discussed above, the alkoxy radical is expected to decompose to give rise to 2 $CH_3CHO + NO_2$, and thus we use

$$(CH_3CH(ONO_2)CH(OO.)CH_3 \text{ products}) = 2\ CH_3CHO + NO_2$$

for the above reactions.

5. Reactions of Isobutene

D52. $OH + (CH_3)_2C{=}CH_2 \xrightarrow{O_2} (CH_3)_2C(OH)CH_2OO^{\cdot}$

This reaction is believed to consist primarily of the rate determining addition of OH radicals to the double bond, followed by the rapid reaction of the adduct with O_2 to form the peroxy radical indicated above. We assume addition at the terminal carbon dominates over internal addition, but, as discussed above for the OH + propene and 1-butene reactions, addition at the internal position is expected to give rise to the same ultimate products.

Atkinson (1986) recently evaluated the kinetic data for this reaction and recommended the following expression for its rate constant:

$$k_{D52} = 9.51 \times 10^{-12}\ e^{1000/RT}\ \text{cm}^3\ \text{molecule}^{-1}\ \text{sec}^{-1}$$

$$= 5.14 \times 10^{-11}\ \text{cm}^3\ \text{molecule}^{-1}\ \text{sec}^{-1}\ \text{at 298 K.}$$

This is used in the model.

D53. $(CH_3)_2C(OH)CH_2OO\cdot + NO \xrightarrow{O_2} NO_2 + CH_3COCH_3 + HCHO + HO_2$

This reaction consists of the initial, rate determining reaction of NO with the peroxy radical, whose kinetics are discussed in Section B. The peroxy + NO reaction is assumed to result in the formation of the corresponding alkoxy radical followed by the rapid decomposition of the alkoxy radical and the subsequent reactions of the α-hydroxy radicals formed with O_2.

$$(CH_3)_2C(OH)CH_2OO\cdot + NO \rightarrow (CH_3)_2C(OH)CH_2O\cdot + NO_2$$

$$(CH_3)_2C(OH)CH_2O\cdot \rightarrow (CH_3)_2C(\cdot)OH + HCHO$$

$$(CH_3)_2C(\cdot)OH + O_2 \rightarrow CH_3COCH_3 + HO_2$$

This is totally analogous to the reactions of the peroxy radicals formed in the OH + propene, 1-butene and trans-2-butene systems, discussed above.

As is the case with the 1-butene and trans-2-butene systems, the possible formation of a hydroxy-substituted organic nitrate in this reaction is ignored.

D54. $(CH_3)_2C(OH)CH_2OO\cdot + HO_2 \rightarrow -OOH + [(CH_3)_2C(OH)CH_2OO\cdot\ \text{products}]$

D55. $(CH_3)_2C(OH)CH_2OO\cdot + RO_2 \rightarrow 0.5\ HO_2 + [(CH_3)_2C(OH)CH_2OO\cdot\ \text{products}]$

D56. $(CH_3)_2C(OH)CH_2OO\cdot + RCO_3 \rightarrow 0.5\ HO_2 + [(CH_3)_2C(OH)CH_2OO\cdot\ \text{products}]$

The kinetics of these reactions and the general principles used for representing the products are discussed in Section B. As indicated there, the organic products formed in these reactions are represented by the set of products expected to be formed from the reactions of the corresponding alkoxy radical. As discussed above, the alkoxy radical is expected to decompose to form CH_3COCH_3 + HCHO. Thus we use

$$[(CH_3)_2C(OH)CH_2OO.\ \text{products}] = CH_3COCH_3 + HCHO$$

for the above reactions.

D57. $O_3 + (CH_3)_2C{=}CH_2 \rightarrow 0.5\ (CH_3COCH_3 + [.CH_2OO.*]) + 0.5\ (HCHO + [(CH_3)_2C(.)OO.*])$

The major mode of this reaction is assumed to be the formation of the primary ozonide, which subsequently decomposes to form the fragments indicated above, which is analogous to the reaction routes assumed for the reaction of ozone with the other alkenes. The two fragmentation routes are assumed to occur with equal probability. As indicated above, the reaction sequence assumed for the hot biradicals formed in ozone-alkene systems are the same regardless of which reaction formed them, and thus the sequence assumed for $[.CH_2OO.*]$ [reaction (D7)] is given above in conjunction with the discussion of the ozone + ethene reaction. The reactions assumed for the other fragment are indicated below.

The kinetics of the ozone + isobutene reaction was recently evaluated by Atkinson and Carter (1984), who recommended the following expression for its rate constant:

$$k_{D57} = 3.55 \times 10^{-15}\ e^{-3364/RT}\ \text{cm}^3\ \text{molecule}^{-1}\ \text{sec}^{-1}$$

$$= 1.21 \times 10^{-17}\ \text{cm}^3\ \text{molecule}^{-1}\ \text{sec}^{-1}\ \text{at 298 K},$$

This is used in the model.

D58. $[(CH_3)_2C(.)OO.^*] \xrightarrow[\text{fast}]{O_2} 0.2\ (OH + CH_3COCH_2OO.) + 0.8\ (C_2H_5COCH_3$ - "lost carbon")

The most appropriate reaction route to assume for this "hot" biradical is highly uncertain. We assume that the stabilization route is not important under atmospheric conditions, based on the data of Hatakeyama et al. (1984) which indicate that the total yield of stabilized biradicals in the ozone + isobutene reaction is only 17-19%. If the "hot" biradical $[.CH_2OO.^*]$ is assumed to be formed 50% of the time and if, based on the data from the ozone + ethene system, it is stabilized 40% of the time, then this means that all of the observed stabilization is accounted for by $[.CH_2OO.^*]$ alone.

Thus we assume that the "hot" biradical must exclusively undergo unimolecular reaction under atmospheric conditions. Two reaction routes appear likely for this biradical; one involving decomposition, resulting in the formation of methyl peroxy radicals and CO_2,

$$[(CH_3)_2C(.)OO.^*] \rightarrow CH_3. + CH_3COO. \xrightarrow{O_2} 2\ CH_3OO. + CO_2$$

and the other involving H-atom abstraction by the -OO. group (via a five-member ring transition state), leading initially to an energy-rich, vibrationally excited hydroperoxide.

$$[(CH_3)_2C(.)OO.^*] \rightarrow [CH_2{=}C(CH_3)OOH^*]$$

This hydroperoxide could either be collisionally stabilized, or it could decompose.

$$[CH_2{=}C(CH_3)OOH^*] \xrightarrow{M} CH_2{=}C(CH_3)OOH$$

$$\rightarrow CH_3COCH_2. + OH$$

(The $CH_3COCH_2.$ radical, which reacts rapidly with O_2 to form $CH_3COCH_2OO.$, is also formed in the reaction of OH radicals with acetone, so its subsequent reactions are discussed in Section C-4.)

The relative importance of these possible unimolecular reaction routes are unknown, and model simulations of the SAPRC indoor Teflon chamber isobutene-NO_x-air experiment ITC-694 were used to determine which of the alternatives best fit the data. (Run ITC-694 is the only isobutene-NO_x-air chamber experiment for which we have data.) Figure II-14 shows plots of the results of calculations based on several alternative assumptions concerning these reaction routes, compared with selected results of the isobutene-NO_x-air experiment. As indicated in Figure II-14, reasonably good fits to most of the data from that run are obtained if it is assumed that isomerization to the excited hydroperoxide, followed by its collisional stabilization, dominates, except that the observed PAN yields are significantly underpredicted. Better fits to the observed PAN yield are obtained if it is assumed that the excited hydroperoxide decomposes to form $CH_3COCH_2\cdot$ (which subsequently reacts to form PAN, as discussed in Section C-4). However, in that case the overall reactivity (rates of NO to NO_2 conversion, isobutene consumption, etc.) is significantly underpredicted. Assuming that decomposition to form methylperoxy radicals and CO_2 is important is not consistent with the data, since this results both in overprediction of reactivity and an underprediction of the PAN yields. Attempts to adjust the model in a chemically reasonable manner to give appropriate predictions of PAN yields without also significantly overpredicting other aspects of reactivity were not successful.

In view of the fact that in most cases it is more important that the model perform adequately in predicting overall reactivity than adequately simulating the yield of a single product, in this model we assume that decomposition only occurrs 20% of the time, which is the largest amount of decomposition which can be assumed and yet allow adequate fits to the observed overall reactivity observed in the isobutene-NO_x-air run. The reaction as written above is based on this assumption. Thus, this model significantly underpredicts PAN yields observed in the isobutene experiment. However, there are many other, relatively more important, sources of PAN in the complex mixtures of organics which are emitted into the atmosphere, and thus in practice the contribution of isobutene to the total amount of PAN which is formed will probably usually be small. Nevertheless, it is clear that further work is needed to elucidate this

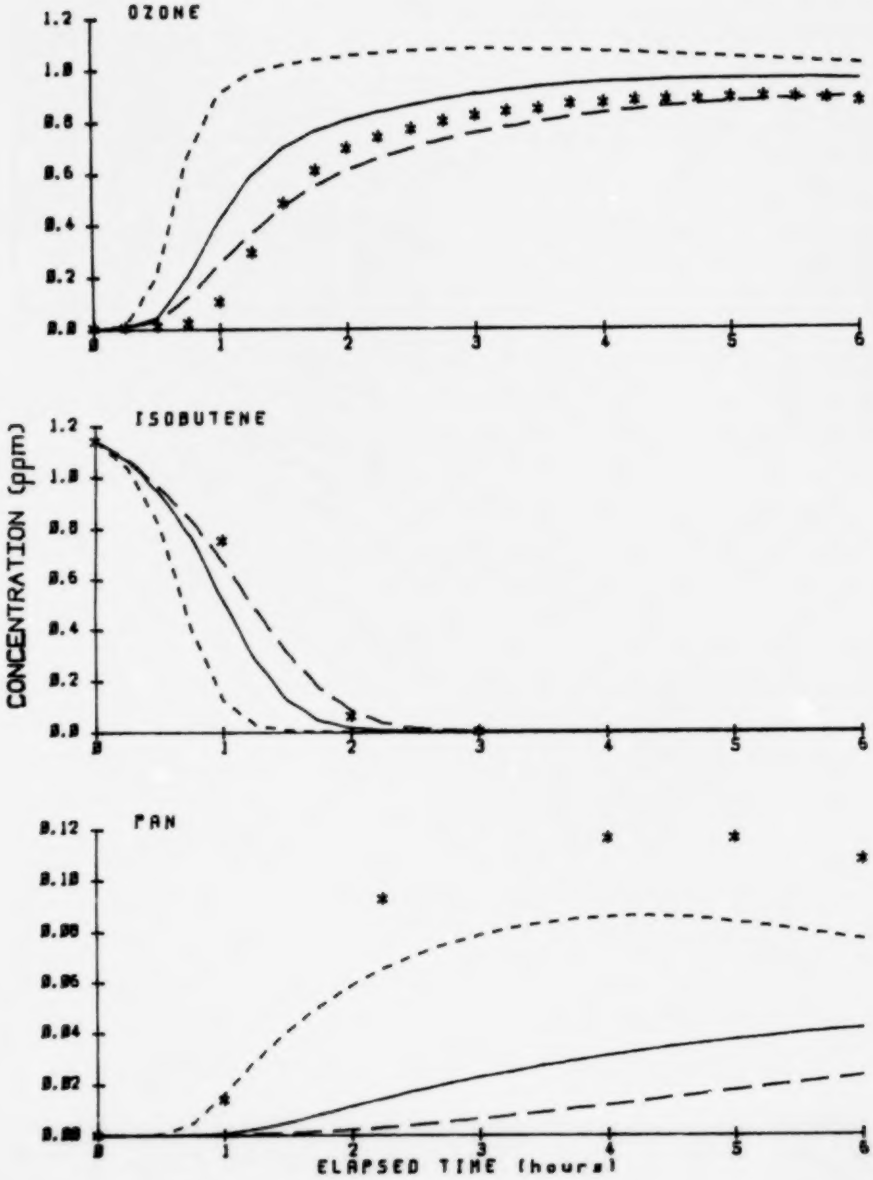

Figure II-14. Experimental and calculated concentration-time profiles of ozone, isobutene and PAN for the isobutene-NO_x-air run ITC-694.

* = Experimental data.

-- -- = Calculated assuming 100% collisional stabilization of excited hydroperoxide.

- - - - = Calculated assuming 100% decomposition of excited hydroperoxide.

―――――― = Calculated assuming 20% decomposition of excited hydroperoxide (standard model).

discrepancy between model predictions and the results of the single isobutene-NO_x-air experiment which we have used for model testing.

Since stabilization of the vibrationally excited hydroperoxide is assumed to occur 80% of the time, it is necessary to include the reactions of this hydroperoxide in the model. Its atmospheric reactions are not known, but it probably reacts primarily with the hydroxyl radical, since hydroperoxide photolysis is relatively slow under atmospheric conditions. (The hydroperoxide absorption coefficients given in Table II-6 correspond to a calculated atmospheric half-life of at least two days.) If it reacts with OH radicals, the adduct formed is expected to primarily decompose to regenerate OH radicals and to form hydroxyacetone:

$$\mathrm{OH} + \mathrm{CH_2{=}C(CH_3)OOH} \rightarrow \mathrm{HOCH_2\dot{C}CH_3OOH} \rightarrow \mathrm{HOCH_2{-}CO{-}CH_3} + \mathrm{OH}$$

Thus the net effect of this reaction is just to convert the hydroperoxide to a substituted ketone, without any other transformations occurring, which means that if this reaction is assumed to be sufficiently fast, then the hydroperoxide can be represented by the ketone in the model. This is what is assumed in this model, with methyl ethyl ketone - "lost carbon" being used to represent hydroxyacetone to avoid the addition of a new species in the model. MEK is used rather than acetone to represent hydroxyacetone since hydroxyacetone is expected to react with OH radicals with a rate constant more similar to that of MEK than to that of acetone.

It is obvious that there are major uncertainties in this aspect of our assumed mechanism for the reactions of isobutene with ozone, and the reactions of the species formed. Further work in this area is clearly needed, as is the case for all of the higher alkenes.

D59. $$\mathrm{O(^3P)} + \mathrm{(CH_3)_2C{=}CH_2} \xrightarrow{O_2} 0.5\ \mathrm{CH_3COC_2H_5} + 0.5\ (\mathrm{C_2H_5CHO} + \text{"lost C"}) + 0.4\ \mathrm{HO_2}$$

This reaction forms isobutene oxide and isobutyraldehyde, in approximately equal yields, as the major addition products (Cvetanovic 1963), and these are represented in the model by methyl ethyl ketone and propionaldehyde, respectively. The extent of fragmentation which occurs under atmospheric conditions is uncertain, and we tentatively assume that it is similar to that assumed for the other butenes, i.e., ~20%. As is the case with 1-butene, we represent the radicals formed in the fragmentation pathway by HO_2. This is clearly a highly approximate representation, but this reaction is of only minor importance under atmospheric conditions.

The rate constant expression used for this reaction is that obtained by Atkinson and Pitts (1977), which is in reasonably good agreement with previous determinations of this rate constant.

$$k_{D59} = 1.76 \times 10^{-11}\ e^{-85/RT}\ \text{cm}^3\ \text{molecule}^{-1}\ \text{sec}^{-1}$$

$$= 1.52 \times 10^{-11}\ \text{cm}^3\ \text{molecule}^{-1}\ \text{sec}^{-1}\ \text{at 298 K}$$

D60. $NO_3 + (CH_3)_2C{=}CH_2 \xrightarrow{O_2} (CH_3)_2C(OO.)CH_2ONO_2$

This reaction consists of the rate determining addition of NO_3 radicals to the double bond, followed by the rapid addition of O_2 to the radicals formed. All present determinations of the rate constant for this reaction are based on the $N_2O_5 = NO_3 + NO_2$ equilibrium constant. Based on the equilibrium constant of Malko and Troe (1982), and the rate data of Japar and Niki (1975) and Atkinson et al. (1984a), we obtain 1.3×10^{-13} and 1.7×10^{-13} cm^3 molecule^{-1} sec^{-1}, respectively, at 298 K for this rate constant k_{D60}. However, the equilibrium constant we now use (see Section A) is a factor of 1.8 higher than that used by Atkinson and Lloyd (1984), and thus to be consistent with this the value for this rate constant should be increased by this factor. Thus we use the rate constant of Atkinson et al. (1984a), increased by a factor of 1.8, or

$$k_{D60} = 3.1 \times 10^{-13}\ \text{cm}^3\ \text{molecule}^{-1}\ \text{sec}^{-1}\ \text{at 298 K.}$$

in good agreement with the value of $k_{D60} = 3.3 \times 10^{-13}$ cm^3 molecule^{-1} sec^{-1} recently determined at 298 K by Ravishankara and Mauldin (1985).

The temperature dependence of this reaction is not known. We assume that it has a similar Arrhenius pre-exponential factor to that for OH +

isobutene and trans-2-butene, since both reactions involve addition to the double bond. Thus we use

$$k_{D60} = 1.0 \times 10^{-11}\ e^{-2139/RT}\ cm^3\ molecule^{-1}\ sec^{-1}$$

to estimate the temperature dependence of this rate constant.

D61. $(CH_3)_2C(OO.)CH_2ONO_2 + NO \rightarrow 2\ NO_2 + CH_3COCH_3 + HCHO$

This reaction consists of the rate determining reaction of the peroxy radical with NO, whose kinetics are discussed in Section B. Analogous to the assumptions for the reactions following the NO_3 + 1-butene and trans-2-butene reactions, formation of the corresponding peroxy radical, which undergoes subsequent decomposition and reaction to form the products shown above, is assumed to dominate.

$$(CH_3)_2C(OO.)CH_2ONO_2 + NO \rightarrow NO_2 + (CH_3)_2C(O.)CH_2ONO_2$$

$$(CH_3)_2C(O.)CH_2ONO_2 \rightarrow CH_3COCH_3 + .CH_2ONO_2$$

$$.CH_2ONO_2 \rightarrow HCHO + NO_2$$

As is the case in the 1-butene and the trans-2 butene systems, the possible formation of small amounts of dinitrate from the initial peroxy + NO reaction is ignored.

D62. $(CH_3)_2C(OO.)CH_2ONO_2 + HO_2 \rightarrow -OOH + [(CH_3)_2C(OO.)CH_2ONO_2\ products]$

D63. $(CH_3)_2C(OO.)CH_2ONO_2 + RO_2 \rightarrow 0.5\ HO_2 + [(CH_3)_2C(OO.)CH_2ONO_2\ products]$

D64. $(CH_3)_2C(OO.)CH_2ONO_2 + RCO_3 \rightarrow 0.5\ HO_2 + [(CH_3)_2C(OO.)CH_2ONO_2\ products]$

The kinetics of these reactions and the general principles used for representing the products are discussed in Section B. As indicated there, the organic products formed in these reactions are the set of products expected to be formed from the reactions of the corresponding alkoxy radical. As discussed above, the alkoxy radical is expected to decompose to give rise to CH_3COCH_3 + HCHO + NO_2, and thus we use

$$[(CH_3)_2C(OO.)CH_2ONO_2 \text{ products}] = CH_3COCH_3 + HCHO + NO_2$$

for the above reactions.

6. Reactions of the Thermalized Biradicals

As discussed by Atkinson and Lloyd (1984), reactions of the thermalized biradicals formed in ozone-alkene systems have been observed with aldehydes, SO_2, H_2O and with other species. No absolute rate data are available for any of these reactions, but a few relative rate constant measurements have been made which can serve as a basis for estimating the atmospheric fates of these species. Relevant relative rate data for the reactions of $HCHO_2$ and CH_3CHO_2 with ethene, CO, formaldehyde, SO_2, H_2O and NO_2 are summarized in Table II-16. If it is assumed that the rate constant ratios for $HCHO_2$ are the same as those as for CH_3CHO_2, a self-consistent set of rate constant ratios can be derived from these data in Table II-16. These ratios are also summarized in Table II-16.

Also given in Table II-16 are the relative loss rates for the biradicals calculated using the water concentration corresponding to 50% RH at 300 K and, for the other reactants, the estimated maximum concentrations likely to be encountered in the atmosphere or in environmental chamber experiments which are useful for model testing. It can be seen that reaction with water and (when present) SO_2 are the most important processes. In the ambient air and in most representative environmental chamber experiments, the ratio of the water concentration to those of the other compounds is even higher than shown on the table, indicating that under those conditions it is a good approximation to assume that reaction with water is the only significant process in terms of removing the biradical. However, the reaction with SO_2 may be a non-negligible process

Table II-16. Rate Constant Ratios for the Reactions of Thermalized Biradicals Formed in Ozone-Alkene Systems

Reactant	Rate Constant Ratio $HCHO_2$[a]	 $HCHO_2$[b]	 CH_3CHO_2[c]	Combined Data	Max. Conc. (ppm)	Relative Loss Rate
C_2H_4	<1.4	(1)[d]		0.35	1	>1
CO	(1)[d]			(1)[d]	10	10
HCHO	140			140	0.5	70
SO_2	560		(1)[d]	560	0.5	280
H_2O		0.08	5×10^{-5}	0.03	2×10^4	600
NO_2		10		3.5	1	4

[a] Data of Su et al. (1980).
[b] Data of Manzanares et al. (1984).
[c] Re-analysis of the data of Cox and Penkett (1972) by Atkinson and Lloyd (1984).
[d] Reference rate set at unity.

in terms of removing SO_2 under some conditions, and thus the reaction of these biradicals with SO_2 is also included in the model.

As discussed by Atkinson and Lloyd (1984), the reaction of the biradicals with water is expected to form the corresponding organic acid. Since these acids are relatively unreactive in the atmosphere, their subsequent reactions are ignored in this model, and they are represented by the formation of "lost carbon."

The reaction of SO_2 with the stabilized biradicals is presumed to result in the formation of SO_3. This is consistent with the observations of Cox and Penkett (1972) and Hatakeyama et al. (1984) that sulfate aerosol is formed when alkenes react with ozone in the presence of SO_2.

Thus the following reactions are included in the model for the reactions of the stabilized biradicals formed in the ozone-alkene system:

D65. $CH_2O_2 + H_2O \rightarrow HCOOH$ (= 'lost C')

D66. $CH_3CHO_2 + H_2O \rightarrow CH_3COOH$ (= 2 'lost C')

D67. $C_2H_5CHO_2 + H_2O \rightarrow C_2H_5COOH$ (= 3 'lost C')

D68. $CH_2O_2 + SO_2 \rightarrow HCHO + SO_3$

D69. $CH_3CHO_2 + SO_2 \rightarrow CH_3CHO + SO_3$

D70. $C_2H_5CHO_2 + SO_2 \rightarrow C_2H_5CHO + SO_3$

These are the only reactions included in the model for these biradicals, and reaction via these processes is assumed to be sufficiently rapid that the biradicals never build up in concentration. Thus, the steady state approximation can be applied to these species, in which case it is only the ratio of the rate constants, not the absolute rate constants, which affects model predictions. With this in mind we arbitrarily set the rate constants for the reaction with SO_2 to be

$$k_{D68} = k_{D69} = k_{D70} = 1 \times 10^{-13}\ \text{cm}^3\ \text{molecule}^{-1}\ \text{sec}^{-1}$$

[the geometric mean of the range of values given by Atkinson and Lloyd (1984) for this reaction] and, based on the rate constant ratios given in Table II-16, derive

$$k_{D65} = k_{D66} = k_{D67} = 5.4 \times 10^{-18}\ \text{cm}^3\ \text{molecule}^{-1}\ \text{sec}^{-1}$$

for the rate constants for the reactions of the biradicals with water.

The approximation that these biradicals do not react significantly with aldehydes and ketones may not be strictly valid when carrying out model simulations of environmental chamber experiments under dry conditions, especially if high concentrations of aldehydes are present. However, even under those conditions, the errors introduced by using this approximation are expected to be minor, since it does not affect overall radical sources or sinks or NO to NO_2 conversions in the primary alkene photooxidation reactions. Furthermore, the reactions of the stabilized biradicals have only a relatively minor contribution to the overall yields of products formed in the NO_x-air reactions of the alkenes, and previous models have generally ignored the subsequent reactions of the secondary ozonides formed when the biradicals react with oxygenates, just as this model ignores the subsequent reactions of the acids formed when they react with water.

7. General $\geq C_3$ Monoalkene Model

The reaction mechanisms for propene and the higher alkenes discussed in the previous sections have a sufficient number of features in common that it is possible to derive a general parameterized mechanism which can be applied to other acyclic monoalkenes, and serve as a basis for "lumping" the reactions of alkenes. This general mechanism, which was employed in this study to model the "complex mixture" environmental chamber experiments, is discussed in this section, along with a summary of the parameters involved for representative $\geq C_3$ acyclic monoalkenes.

The scheme employed in this mechanism takes advantage of the fact that for all the alkenes discussed above (except for ethene) the model for the three major atmospheric consumption reactions (i.e., reaction with ozone and OH and NO_3 radicals) all have the net effect of fragmenting the molecule by breaking the double bond, and forming species from each fragment which are independent of the fragment which was on the other side of the double bond. For example, the net reactions of OH radicals, O_3, and NO_3 radicals with propene and 1-butene can be represented as follows:

$$\begin{aligned} \mathrm{OH} + \mathrm{CH_3CH{=}CH_2} \xrightarrow{\mathrm{O_2,\ NO}} \rightarrow \rightarrow\ & \mathrm{HO_2} + \mathrm{NO_2} \\ & + \mathrm{HCHO} \qquad \text{(from } \mathrm{=CH_2}\text{)} \\ & + \mathrm{CH_3CHO} \qquad \text{(from } \mathrm{=CHCH_3}\text{)} \end{aligned}$$

$$\begin{aligned} \mathrm{O_3} + \mathrm{CH_3CH{=}CH_2} \rightarrow \rightarrow \rightarrow\ & 0.5\ (\mathrm{HCHO} + [.\mathrm{CH_2OO}.^*]) \qquad \text{(from } \mathrm{=CH_2}\text{)} \\ & + 0.5\ (\mathrm{CH_3CHO} + [\mathrm{CH_3CH(.)OO}.^*]) \qquad \text{(from } \mathrm{=CHCH_3}\text{)} \end{aligned}$$

$$\begin{aligned} NO_3 + CH_3CH{=}CH_2 \xrightarrow{O_2,\ NO} \rightarrow \rightarrow\ & HO_2 + 2\ NO_2 \\ & + HCHO \qquad \text{(from } {=}CH_2\text{)} \\ & + CH_3CHO \qquad \text{(from } {=}CHCH_3\text{)} \end{aligned}$$

$$\begin{aligned} OH + C_2H_5CH{=}CH_2 \xrightarrow{O_2,\ NO} \rightarrow \rightarrow\ & HO_2 + NO_2 \\ & + HCHO \qquad \text{(from } {=}CH_2\text{)} \\ & + CH_3CH_2CHO \qquad \text{(from } {=}CHC_2H_5\text{)} \end{aligned}$$

$$\begin{aligned} O_3 + C_2H_5CH{=}CH_2 \rightarrow \rightarrow \rightarrow\ & 0.5\ (HCHO + [.CH_2OO.*]) \qquad \text{(from } {=}CH_2\text{)} \\ & + 0.5\ (CH_3CH_2CHO + [CH_3CH_2CH(.)OO.*]) \\ & \qquad \text{(from } {=}CHC_2H_5\text{)} \end{aligned}$$

$$\begin{aligned} NO_3 + C_2H_5CH{=}CH_2 \xrightarrow{O_2,\ NO} \rightarrow \rightarrow\ & HO_2 + 2\ NO_2 \\ & + HCHO \qquad \text{(from } {=}CH_2\text{)} \\ & + CH_3CH_2CHO \qquad \text{(from } {=}CHC_2H_5\text{)} \end{aligned}$$

Note that both these compounds have the $=CH_2$ group, and that group ends up either as HCHO (in the OH or NO_3 radical reactions), or as 0.5 HCHO + 0.5 $[.CH_2OO.*]$ (in the O_3 reactions), regardless of what was on the other side of the molecule. Similarly in the current model the compounds formed from the $=CHCH_3$ group are CH_3CHO or 0.5 CH_3CHO + 0.5 $[CH_3CH(.)OO.*]$ regardless of whether it is in propene or a 2-butene, and the same is assumed to be true for the other groups present in other alkenes, such as $=CHC_2H_5$ in 1-butene, and $=C(CH_3)_2$ in isobutene.

The fact that the two fragments on each side of the molecule essentially react independently in the OH radical, O_3 and NO_3 radical reactions allows the following parameterized scheme to be used to represent these reactions for any $\geq C_3$ acyclic monoalkene:

$$OH + \text{alkene} \xrightarrow{O_2} (\text{alkene-OH-}O_2\text{ adduct})$$

$$\begin{aligned}(\text{alkene-OH-}O_2\text{ adduct}) + NO \rightarrow\ & NO_2 + HO_2 + p1\ HCHO + p2\ CH_3CHO + p3\ C_2H_5CHO\\ & + p4\ CH_3COCH_3 + p5\ C_2H_5COCH_3\\ & + p6\ \text{"lost carbon"}\end{aligned}$$

$$\begin{aligned}(\text{alkene-OH-}O_2\text{ adduct}) + HO_2 \rightarrow\ & \text{-}OOH + p1\ HCHO + p2\ CH_3CHO + p3\ C_2H_5CHO\\ & + p4\ CH_3COCH_3 + p5\ C_2H_5COCH_3 +\\ & p6\ \text{"lost carbon"}\end{aligned}$$

$$\begin{aligned}(\text{alkene-OH-}O_2\text{ adduct}) + RO_2 \text{ or } RCO_3 \rightarrow\ & 0.5\ HO_2 + p1\ HCHO + p2\ CH_3CHO\\ & + p3\ C_2H_5CHO + p4\ CH_3COCH_3\\ & + p5\ C_2H_5COCH_3 + p6\ \text{"lost carbon"}\end{aligned}$$

$$\begin{aligned}O_3 + \text{alkene} \rightarrow\ & p1\ (HCHO + [.CH_2OO.^*]\\ & + p2\ (CH_3CHO + [CH_3CH(.)OO.^*])\\ & + p3\ (C_2H_5CHO + [C_2H_5CH(.)OO.^*])\\ & + p4\ (CH_3COCH_3 + [(CH_3)_2C(.)OO.^*])\\ & + p5\ (C_2H_5COCH_3 + [(CH_3)(C_2H_5)C(.)OO.^*])\\ & + p6\ \text{"lost carbon"}\end{aligned}$$

$$NO_3 + \text{alkene} \xrightarrow{O_2} (\text{alkene-}NO_3\text{-}O_2\text{ adduct})$$

$$\begin{aligned}(\text{alkene-}NO_3\text{-}O_2\text{ adduct}) + NO \rightarrow\ & 2\ NO_2 + HO_2 + p1\ HCHO + p2\ CH_3CHO\\ & + p3\ C_2H_5CHO + p4\ CH_3COCH_3 + p5\ C_2H_5COCH_3 +\\ & + p6\ \text{"lost carbon"}\end{aligned}$$

$$\begin{aligned}(\text{alkene-}NO_3\text{-}O_2\text{ adduct}) + HO_2 \rightarrow\ & \text{-}OOH + NO_2 + p1\ HCHO + p2\ CH_3CHO\\ & + p3\ C_2H_5CHO + p4\ CH_3COCH_3 + p5\ C_2H_5COCH_3\\ & + p6\ \text{"lost carbon"}\end{aligned}$$

$$\begin{aligned}(\text{alkene-}NO_3\text{-}O_2\text{ adduct}) + RO_2 \text{ or } RCO_3 \rightarrow\ & 0.5\ HO_2 + NO_2 + p1\ HCHO\\ & + p2\ CH_3CHO + p3\ C_2H_5CHO\\ & + p4\ CH_3COCH_3 + p5\ C_2H_5COCH_3\\ & + p6\ \text{"lost carbon"}\end{aligned}$$

In this representation, the "structure" parameters p1 through p5 represents the number of $=CH_2$, $=CHCH_3$, $=CHR$, $=C(CH_3)_2$, and $(=C(CH_3)R + =CR_2)$ "fragments" in the molecule, where all alkyl group other than methyl are lumped as "R", whose reactions are represented in this model by those of fragments containing the ethyl group. Obviously for a single alkene, p1 through p5 can only have the values of 0, 1, or (for symmetrical alkenes) 2, but this scheme allows mixtures of olefins to be "lumped" as a single specie whose parameters p1 through p5 are obtained by taking weighed averages of all the parameters of the species in the mixture. For example, a mixture consisting of 20% propene (with p1 = p2 = 1, and the rest 0), 50% 2-butenes (p2 = 2), and 30% isobutene (p1 = p4 = 1) can be represented by a specie with p1 = 0.5, p2 = 1.2, p4 = 0.3, and p3 = p5 = 0. It can be seen that this scheme allows different alkenes to be lumped together as a single species, and still accurately represent the types of products which are ultimately formed and, for mixtures where $R = C_2H_5$ only, still conserve carbon. This representation does involve some loss of carbon for species or mixtures containing "R" groups other than C_2H_5, and the parameter p6 is used to keep track of the carbon which is lost.

The reactions of the stable products which can be formed in these reactions have been discussed in Section II-C. The reactions of the intermediates $[.CH_2OO.*]$, $[CH_3CH(.)OO.*]$, $[C_2H_5CH(.)OO.*]$, and $[(CH_3)_2CH(.)OO.*]$ have been discussed above, and since the alkene-OH-O_2 and the alkene-NO_3-O_2 adducts are peroxy radicals, their kinetics and reactions are discussed in Section II-B. The only specie formed in the above scheme whose reactions have not been discussed is the intermediate $[(CH_3)(C_2H_5)CH(.)OO.*]$ formed from the fragment $=C(CH_3)C_2H_5$ in the ozonolysis reaction. Its subsequent reactions are unknown, and in this model its reactions are assumed to be exactly analogous to that of $[(CH_3)_2CH(.)OO.*]$, as shown above as reaction (D58), except that $CH_3COCH_2OO.$ (which is also an intermediate formed in the OH + acetone reaction) is replaced by $0.5\ CH_3COCH(OO.)CH_3 + 0.5\ CH_3COCH_2CH_2OO.$ (the intermediates formed in the OH + methyl ethyl ketone reaction):

$$[(CH_3)(C_2H_5)CH(.)OO.*] \xrightarrow{\text{fast}} 0.2\ OH + 0.1\ CH_3COCH(OO.)CH_3 + 0.1\ CH_3COCH_2CH_2OO. + 0.2\ C_2H_5COCH_3$$

The only reactions of the C_{3+} acyclic monoalkenes which are in the model and cannot be lumped using this scheme are their reactions with $O(^3P)$ atoms. This is not a serious limitation because their reactions are relatively minor under most atmospherically important situations, and indeed the model of Atkinson et al. (1982a) disregarded them completely. However, these reactions can be non-negligible under conditions of high NO_2 levels, and thus we feel they should not be ignored in detailed models. Thus for general alkanes, the following mechanism is employed:

$$O(^3P) + \text{alkene} \xrightarrow{O_2} 0.4\ HO_2 + 0.5\ (C_2H_5COCH_3 + C_2H_5CHO) + (p1 + 2\ p2 + 3\ [p3 + p4] + 4\ p5 + p6 - 3.5)\ \text{"lost carbon"}$$

This mechanism is as an approximation and generalization of the reactions of $O(^3P)$ with propene and the butenes discussed above.

The kinetic parameters for the initial reactions of the alkenes with OH radicals, O_3, NO_3 radicals, and $O(^3P)$ atoms for representative alkenes whose reactions can be modeled using this scheme are summarized in Table II-17. For the purpose of representing mixtures of alkenes as "lumped alkenes" using this scheme, the rate constants used for the reactions of the "lumped" alkene should consist of weighed averages of the corresponding rate constants for the compounds in the mixtures.

For maximum accuracy in "lumped" models, alkenes which react with significantly different rates should not be lumped together. In particular, because of its much slower reaction rates (as well as the fact that its OH radical reaction is not consistent with the above scheme, because of the formation of glycolaldehyde) ethene should probably not be lumped with the other alkenes. On the other hand, lumping all the 1-alkenes as one specie, and the internal alkenes as another, may not be a bad approximation. However, the effects on model simulations of "lumping" alkenes which react at different rates, and the extent to which they can be combined without affecting the results of the simulations to an unacceptable extent, has not yet been adequately investigated.

Table II-17. Arrhenius Parameters and 298 K Rate Constants for the Reactions of OH Radicals, Ozone, NO_3 Radicals and $O(^3P)$ Atoms with Alkenes used in the Model

Reaction	A (cm^3 $molec^{-1}$ sec^{-1})	Ea (kcal $mole^{-1}$)	k(298 K) (cm^3 $molec^{-1}$ sec^{-1})
Propene[a]			
+ OH	4.85×10^{-12}	-1.00	2.6×10^{-11}
+ O_3	1.32×10^{-14}	4.18	1.1×10^{-17}
+ NO_3	5.00×10^{-12}	3.84	7.6×10^{-15}
+ $O(^3P)$	1.18×10^{-11}	0.64	4.0×10^{-12}
1-Butene[a]			
+ OH	6.53×10^{-12}	-0.93	3.1×10^{-11}
+ O_3	3.46×10^{-15}	3.40	1.1×10^{-17}
+ NO_3	5.00×10^{-12}	3.70	9.7×10^{-15}
+ $O(^3P)$	1.25×10^{-11}	0.65	4.2×10^{-12}
trans-2-Butene[a]			
+ OH	1.01×10^{-11}	-1.09	6.4×10^{-11}
+ O_3	9.08×10^{-15}	2.26	2.0×10^{-16}
+ NO_3	1.00×10^{-11}	1.94	3.8×10^{-13}
+ $O(^3P)$	2.26×10^{-11}	-0.02	2.3×10^{-11}
cis-2-Butene			
+ OH[b]	1.09×10^{-11}	-0.97	5.6×10^{-11}
+ O_3[c]	3.52×10^{-15}	1.95	1.3×10^{-16}
+ NO_3[d]	1.00×10^{-11}	2.00	3.4×10^{-13}
+ $O(^3P)$[e]	1.21×10^{-11}	-0.24	1.8×10^{-11}
Isobutene[a]			
+ OH	9.51×10^{-12}	-1.00	5.1×10^{-11}
+ O_3	3.55×10^{-15}	3.36	1.2×10^{-17}
+ NO_3	1.00×10^{-11}	2.14	3.1×10^{-13}
+ $O(^3P)$	1.76×10^{-11}	0.09	1.5×10^{-11}

(continued)

Table II-17 (continued) - 2

Reaction	A (cm^3 $molec^{-1}$ sec^{-1})	Ea (kcal $mole^{-1}$)	k(298 K) (cm^3 $molec^{-1}$ sec^{-1})
2-Methyl-2-butene			
+ OH[b]	1.92×10^{-11}	-0.89	8.6×10^{-11}
+ O_3[c]	6.17×10^{-15}	1.59	4.2×10^{-16}
+ NO_3[d]	2.00×10^{-11}	0.46	9.2×10^{-12}
+ $O(^3P)$[f]	2.50×10^{-11}	-0.38	4.7×10^{-11}
2,3-Dimethyl-2-butene			
+ OH[b]	2.03×10^{-11}	-1.00	1.1×10^{-10}
+ O_3[c]	3.71×10^{-15}	0.69	1.2×10^{-15}
+ NO_3[d]	2.00×10^{-11}	-0.61	5.6×10^{-11}
+ $O(^3P)$[g]	5.58×10^{-12}	-1.57	7.9×10^{-11}
2-Methyl-1-butene[h]			
+ OH	9.51×10^{-12}	-1.00	5.1×10^{-11}
+ O_3	3.55×10^{-15}	3.36	$1.2 \times 10-^{17}$
+ NO_3	1.00×10^{-11}	2.14	3.1×10^{-13}
+ $O(^3P)$	1.76×10^{-11}	0.09	1.5×10^{-11}

---

[a] The sources of the rate constants for this compound are given elsewhere in this document.

[b] Recommendation of Atkinson (1986).

[c] Recommendation of Atkinson and Carter (1984).

[d] Rate constants for NO_3 + alkene reactions taken from Atkinson et al. (1984a) and references therein. All NO_3 rate constants used are relative to the $N_2O_5 = NO_3 + NO_2$ equilibrium constant used in this model. Rate constants have not been measured as a function of temperature, and the temperature dependence is estimated by assuming the NO_3 reaction has a similar Arrhenius pre-exponential factor as the OH reaction.

[e] Atkinson and Pitts (1977).

[f] Atkinson and Pitts (1978).

[g] Singleton et al. (1975).

[h] All rate constants assumed to be the same as that for the corresponding reaction of isobutene.

II. E. REACTIONS OF THE C_2-C_4 ALKANES

In this section, the atmospheric reactions of the alkanes ethane, propane, n-butane, and isobutane are discussed. The reactions of methane are ignored because of its long tropospheric lifetime. Because of the larger number of intermediates involved in the reactions of the higher alkanes, these compounds are represented using a somewhat different approach which is discussed in Section F. The alkanes are believed to be consumed in the atmosphere to a significant extent only by reaction with hydroxyl radicals. Thus this is the only mode of consumption for these compounds which is represented in this model.

1. Reactions of Ethane

E1. $OH + C_2H_6 \xrightarrow{O_2} H_2O + C_2H_5OO.$

The available data concerning the kinetics of this reaction have been summarized and evaluated by Atkinson (1986). Use of the following expression for the rate constant for this reaction is recommended:

$$k_{E1} = 1.23 \times 10^{-12}\ (T/300)^2\ e^{-882/RT}\ \text{cm}^3\ \text{molecule}^{-1}\ \text{sec}^{-1}$$

$$= 2.74 \times 10^{-13}\ \text{cm}^3\ \text{molecule}^{-1}\ \text{sec}^{-1}\ \text{at 298 K},$$

This is used in the model.

The reaction as written consists of the rate determining H-atom abstraction reaction by OH radicals, followed by the rapid reaction of the ethyl radicals with O_2. The subsequent reactions of the ethylperoxy radicals are given in Section C.

2. Reactions of Propane

E2. $OH + CH_3CH_2CH_3 \xrightarrow{O_2} H_2O + 0.31\ C_3H_7OO. + 0.69\ CH_3CH(OO.)CH_3$

The available data concerning the kinetics of this reaction have been evaluated by Atkinson (1986), and the following expression for the rate constant recommended:

$$k_{E2} = 1.14 \times 10^{-12}\ (T/300)^2\ e^{28/RT}\ \text{cm}^3\ \text{molecule}^{-1}\ \text{sec}^{-1}$$

$$= 1.18 \times 10^{-12}\ \text{cm}^3\ \text{molecule}^{-1}\ \text{sec}^{-1}\ \text{at 298 K,}$$

This is used in the model.

The reaction can occur via abstraction at the primary or the secondary position. Using the temperature-dependent group rate constant estimation technique summarized by Carter and Atkinson (1985), we estimate that abstraction from the primary position occurs 29% of the time at 270 K, 31% at 300 K, and 33% at 330 K. This small temperature variation is ignored in the model. The reaction as written above is based on the rate constant ratio for 300 K, and it incorporates the rapid reaction of O_2 with the alkyl radicals initially formed.

E3. $C_3H_7OO\cdot + NO \xrightarrow{O_2} NO_2 + C_2H_5CHO + HO_2\cdot$

The reaction as written above consists of the rate determining reaction of the peroxy radical with NO, whose kinetics are discussed in Section B, followed by the reaction of the alkoxy radical formed with O_2, which (Carter and Atkinson 1985) is believed to be its major atmospheric fate.

$$C_3H_7OO\cdot + NO \rightarrow NO_2 + C_3H_7O\cdot$$

$$C_3H_7O\cdot + O_2 \rightarrow C_2H_5CHO + HO_2$$

Decomposition of the 1-propyloxy radical is estimated to be negligible (Carter and Atkinson 1985).

The total alkyl nitrate yield observed in propane-NO_x-air systems is only 3%, (Atkinson et al. 1982c), so we ignore the formation of propyl nitrate in the reaction of propyl peroxy radicals with NO.

E4. $CH_3CH(OO.)CH_3 + NO \xrightarrow{O_2} NO_2 + CH_3COCH_3 + HO_2$

The reaction as written above consists of the rate determining reaction of the peroxy radical with NO, whose kinetics are discussed in Section B, followed by the reaction of the alkoxy radical with O_2. Decomposition of the 2-propyl alkoxy radical is estimated to be negligible compared with reaction with O_2 (Carter and Atkinson 1985). Furthermore, the reaction of the alkoxy radical with NO_2 is expected to be minor under atmospheric conditions, and is neglected.

$$CH_3CH(OO.)CH_3 + NO \rightarrow NO_2 + CH_3CH(O.)CH_3$$

$$CH_3CH(O.)CH_3 + O_2 \rightarrow CH_3COCH_3 + HO_2$$

As indicated above, the minor formation of alkyl nitrates in the reactions of NO with the peroxy radicals formed in the propane system are neglected.

E5. $C_3H_7OO. + HO_2 \rightarrow \text{-OOH} + (C_3H_7OO.\ \text{products})$

E6. $CH_3CH(OO.)CH_3 + HO_2 \rightarrow \text{-OOH} + (CH_3CH(OO.)CH_3\ \text{products})$

E7. $C_3H_7OO. + RO_2 \rightarrow 0.5\ HO_2 + (C_3H_7OO.\ \text{products})$

E8. $CH_3CH(OO.)CH_3 + RO_2 \rightarrow 0.5\ HO_2 + (CH_3CH(OO.)CH_3\ \text{products})$

E9. $C_3H_7OO. + RCO_3 \rightarrow 0.5\ HO_2 + (C_3H_7OO.\ \text{products})$

E10. $CH_3CH(OO.)CH_3 + RCO_3 \rightarrow 0.5\ HO_2 + (CH_3CH(OO.)CH_3\ \text{products})$

The kinetics of these reactions and the general principles used for representing the products are discussed in Section B. As indicated there, the organic products formed in these reactions are represented by the set of products expected to be formed from the reactions of the corresponding alkoxy radical. In the case of the two peroxy radicals formed in the reactions of propane, the primary alkoxy radical reacts to form propionaldehyde, and the secondary radical forms acetone. Thus we use

$$(C_3H_7OO\cdot \text{ products}) = C_2H_5CHO$$

$$(CH_3CH(OO\cdot)CH_3 \text{ products}) = CH_3COCH_3$$

for the above reactions.

3. Reactions of n-Butane

E11. $OH + CH_3CH_2CH_2CH_3 \rightarrow H_2O + y_{E11a}\ n\text{-}C_4H_9OO\cdot + (1-y_{E11a})\ CH_3CH(OO\cdot)C_2H_5$

The available data concerning the kinetics of this reaction have been evaluated by Atkinson (1986), and the following expression for the rate constant recommended:

$$k_{E11} = 1.55 \times 10^{-11}\ e^{-1073/RT}\ \text{cm}^3\ \text{molecule}^{-1}\ \text{sec}^{-1}$$

$$= 2.53 \times 10^{-12}\ \text{cm}^3\ \text{molecule}^{-1}\ \text{sec}^{-1} \text{ at } 298\ \text{K},$$

This is used in the model.

The reaction can occur via abstraction at the primary or the secondary position. The parameter y_{E11a} is the fraction which reacts via abstraction from the primary position, which depends on temperature. Using the temperature-dependent group rate constant estimation technique summarized by Carter and Atkinson (1985), we estimate that

$$\begin{aligned} y_{E11a} &= 0.13 \text{ at } 270\ \text{K}, \\ &= 0.15 \text{ at } 300\ \text{K}, \\ &= 0.16 \text{ at } 330\ \text{K}. \end{aligned}$$

This temperature-dependent fraction is used in the model. For temperatures between 270 and 300 K, and between 300 and 330 K, the value for this parameter is obtained by linear interpolation.

The reaction as written above incorporates the rapid reaction of O_2 with the alkyl radicals which are initially formed.

E12. $n\text{-}C_4H_9OO\cdot + NO \rightarrow y_{E12a}\ n\text{-}C_4H_9ONO_2 + (1-y_{E12a})\ (NO_2 + n\text{-}C_4H_9O\cdot)$
$(=2\text{-}C_4H_9ONO_2)$

E12b $n\text{-}C_4H_9O\cdot \xrightarrow[O_2]{fast} y_{E12b}\ HO(CH_2)_4OO\cdot + (1-y_{E12b})\ (n\text{-}C_3H_7CHO + HO_2)$

The kinetics of the initial reaction of the peroxy radical with NO are discussed in Section B. This reaction forms 1-butyl nitrate, and its yield is given by the temperature-dependent parameter y_{E13a}. The temperature dependence of the organic nitrate yields observed from the reactions of NO with the alkyl peroxy radicals formed from n-butane and other alkanes can be fit to a general expression given by Carter and Atkinson (1985) and in Section F. Based on this expression, the following values for y_{E13a}, used in the model, are derived:

$$\begin{aligned} y_{E12a} &= 0.05 \text{ at } 270 \text{ K}, \\ &= 0.03 \text{ at } 300 \text{ K}, \\ &= 0.02 \text{ at } 330 \text{ K}. \end{aligned}$$

Values of this parameter for intermediate temperatures are obtained by linear interpolation.

Because it is formed in only a relatively low yield, the 1-butyl nitrate formed in the above reaction is represented by 2-butyl nitrate in the model.

The 1-butyl alkoxy radical can react with O_2 or it can undergo 1,5-H shift isomerization.

$$n\text{-}C_4H_9O\cdot + O_2 \rightarrow n\text{-}C_3H_7CHO + HO_2$$

$$n\text{-}C_4H_9O\cdot \rightarrow HO(CH_2)_4\cdot \xrightarrow{O_2} HO(CH_2)_4OO\cdot$$

Reaction (E12b) as written above incorporates both of these competitive reactions, with the parameter y_{E12b} being the fraction of the time the alkoxy radical isomerizes. Estimates of the rate constants for the reactions of alkoxy radicals, as a function of temperature, are given by Carter and Atkinson (1985), and are also summarized in Section E-4. These estimates were specifically set to fit the experimental data for y_{E12b} (Atkinson and Lloyd 1984). Based on these estimates, we derive

$$\begin{aligned} y_{E12b} &= 0.46 \text{ at } 270 \text{ K}, \\ &= 0.78 \text{ at } 300 \text{ K}, \\ &= 0.92 \text{ at } 330 \text{ K}. \end{aligned}$$

These are used in the model. Values of this parameter for intermediate temperatures are obtained by linear interpolation.

The butyraldehyde formed in this reaction is represented in the model by propionaldehyde + "lost carbon."

E13a. $CH_3CH(OO.)C_2H_5 + NO \rightarrow y_{E13a}\ CH_3CH(ONO_2)C_2H_5$
$+ (1-y_{E13a})\ (NO_2 + CH_3CH(O.)C_2H_5)$

E13b. $CH_3CH(O.)C_2H_5 \xrightarrow[O_2]{\text{fast}} y_{E13b}\ (CH_3COC_2H_5 + HO_2)$
$+ (1-y_{E13b})\ (CH_3CHO + C_2H_5OO.)$

The kinetics of the initial reaction of the peroxy radical with NO are discussed in Section B. This reaction forms 8% 2-butyl nitrate at 299 K (Atkinson et al. 1982c) and its temperature dependence can be predicted using the general expression given by Carter and Atkinson (1985). Thus the values of y_{E13a} used in the model are derived.

$$\begin{aligned} y_{E13a} &= 0.13 \text{ at } 270 \text{ K}, \\ &= 0.08 \text{ at } 300 \text{ K}, \\ &= 0.05 \text{ at } 330 \text{ K}. \end{aligned}$$

Values for intermediate temperatures are obtained by linear interpolation.

The 2-butoxy radical will undergo the following competitive reactions under atmospheric conditions.

$$CH_3CH(O.)C_2H_5 + O_2 \rightarrow CH_3COC_2H_5 + HO_2 \tag{a}$$

$$CH_3CH(O.)C_2H_5 \rightarrow CH_3CHO + C_2H_5. \tag{b}$$

$$C_2H_5. + O_2 \rightarrow C_2H_5OO.$$

Reaction (E13b) as written above incorporates both these processes, with the parameter y_{E13b} being the fraction of the alkoxy radical which reacts with O_2 (i.e. $k_a/(k_a+k_b)$). The experimental values for k_b/k_a are 3.1 x 10^{18} molecule cm^{-3} at 303 K (Carter et al. 1979a) and 2.6 x 10^{18} molecule cm^{-3} at 296 K (Cox et al. 1981), both obtained from observed product yield ratios. The pre-exponential factors for reaction with O_2 and decomposition are estimated (Carter and Atkinson 1986; Section F) to be 1.8 x 10^{-14} cm^3 $molecule^{-1}$ sec^{-1} and 8 x 10^{14} sec^{-1}, respectively. Combining the experimentally observed room temperature ratios and the ratio of estimated pre-exponential factors, we obtain

$$k_b/k_a = 4.4 \times 10^{28}\ e^{-13960/RT}\ \text{molecule cm}^{-3}.$$

Based on this, we obtain (for 1 atm air)

$$\begin{aligned} y_{E13b} &= 0.97 \text{ at } 270 \text{ K}, \\ &= 0.63 \text{ at } 300 \text{ K}, \\ &= 0.15 \text{ at } 330 \text{ K}, \end{aligned}$$

which is used in the model. As with the other parameters, values for intermediate temperatures are obtained by linear extrapolation.

E14. $HO(CH_2)_4OO. + NO \xrightarrow{O_2} NO_2 + HO_2 + HO(CH_2)_3CHO$ $(=C_2H_5CHO$ + "lost C")

This reaction consists of the rate-determining reaction of the peroxy radical with NO, whose kinetics are discussed in Section B, followed by the assumed rapid isomerization of the alkoxy radical formed, and then reaction of O_2 with the α-hydroxy radical formed from the isomerization.

$$HO(CH_2)_4OO\cdot + NO \rightarrow NO_2 + HO(CH_2)_4O\cdot$$

$$HO(CH_2)_4O\cdot \rightarrow HOCH(\cdot)(CH_2)_3OH$$

$$HOCH(\cdot)(CH_2)_3OH + O_2 \rightarrow HCO(CH_2)_3OH + HO_2$$

The reaction shown for the α-hydroxy radical is analogous to those assumed for the α-hydroxy radicals formed in the alkene photooxidation reactions, as discussed in Section D.

The formation of alkyl nitrates in the reaction of this peroxy radical with NO is ignored in this model. If the alkyl nitrate yield in this reaction were the same as that in the reaction of 1-butyl peroxy radicals with NO, then the estimated yield would only be 5% at 270 K, and lower still at higher temperatures. In addition, as discussed in Section F, the results of model simulations of environmental chamber experiments employing the higher alkanes indicate that better fits to the data are obtained if it is assumed that nitrate formation in the reactions of NO with these hydroxy-substituted peroxy radicals is negligible.

The bifunctional aldehyde product formed in the above reaction is represented by propionaldehyde in this model.

E15. $n\text{-}C_4H_9OO\cdot + HO_2 \rightarrow \text{-OOH} + (n\text{-}C_4H_9OO\cdot \text{ products})$

E16. $CH_3CH(OO\cdot)C_2H_5 + HO_2 \rightarrow \text{-OOH} + (CH_3CH(OO\cdot)C_2H_5 \text{ products})$

E17. $HO(CH_2)_4OO\cdot + HO_2 \rightarrow \text{-OOH} + (HO(CH_2)_4OO\cdot \text{ products})$

E18. $n\text{-}C_4H_9OO\cdot + RO_2 \rightarrow 0.5\ HO_2 + (n\text{-}C_4H_9OO\cdot \text{ products})$

E19. $CH_3CH(OO\cdot)C_2H_5 + RO_2 \rightarrow 0.5\ HO_2 + (CH_3CH(OO\cdot)C_2H_5 \text{ products})$

E20. $HO(CH_2)_4OO\cdot + RO_2 \rightarrow 0.5\ HO_2 + (HO(CH_2)_4OO\cdot$ products)

E21. $n\text{-}C_4H_9OO\cdot + RCO_3 \rightarrow 0.5\ HO_2 + (n\text{-}C_4H_9OO\cdot$ products)

E22. $CH_3CH(OO\cdot)C_2H_5 + RCO_3 \rightarrow 0.5\ HO_2 + (CH_3CH(OO\cdot)C_2H_5$ products)

E23. $HO(CH_2)_4OO\cdot + RCO_3 \rightarrow 0.5\ HO_2 + (HO(CH_2)_4OO\cdot$ products)

The kinetics of these reactions and the general principles used for representing the products are discussed in Section B. As indicated there, the organic products formed in these reactions are represented by the set of products expected to be formed from the reactions of the corresponding alkoxy radical. Based on the reactions assumed for these alkoxy radicals as discussed above, we use

$$(n\text{-}C_4H_9O\cdot \text{ products}) = y_{E12b}\ (HO(CH_2)_4OO\cdot \text{ products}) + (1-y_{E12b})\ (C_2H_5CHO + \text{"lost C"})$$

$$= (C_2H_5CHO + \text{"lost C"})$$

$$(CH_3CH(OO\cdot)C_2H_5 \text{ products}) = y_{E13b}\ CH_3COC_2H_5 + (1-y_{E13b})\ (2\ CH_3CHO)$$

$$(HO(CH_2)_4OO\cdot \text{ products}) = (C_2H_5CHO + \text{"lost C"})$$

for the above reactions. The values used for the temperature-dependent parameters y_{E12b} and y_{E13b} are indicated above.

4. Reactions of Isobutane

E24. $OH + (CH_3)_3CH \xrightarrow{O_2} H_2O + y_{E24a}\ (CH_3)_2CHCH_2OO\cdot + (1-y_{E24a})\ (CH_3)_3COO\cdot$

The available data concerning the kinetics of this reaction have been evaluated by Atkinson (1986), and the following expression for the rate constant recommended:

$$k_{E24} = 8.62 \times 10^{-13}\ (T/300)^2\ e^{606/RT}\ \text{cm}^3\ \text{molecule}^{-1}\ \text{sec}^{-1}$$

$$= 2.37 \times 10^{-12}\ \text{cm}^3\ \text{molecule}^{-1}\ \text{sec}^{-1} \text{ at } 298\ \text{K},$$

This is used in the model.

The reaction can occur via abstraction at the primary or the tertiary position. The parameter y_{E11a} is the fraction which reacts via abstraction from the primary position, which depends on temperature. Using the temperature-dependent group rate constant estimation technique summarized by Carter and Atkinson (1985), we estimate that

$$\begin{aligned} y_{E24a} &= 0.18 \text{ at } 270\ \text{K}, \\ &= 0.24 \text{ at } 300\ \text{K}, \\ &= 0.29 \text{ at } 330\ \text{K}. \end{aligned}$$

This is used in the model. For temperatures between 270 and 300 K, and between 300 and 330 K, the value for this parameter is obtained by linear interpolation.

The reaction as written above incorporates the rapid reaction of O_2 with the alkyl radicals which are initially formed.

E25. $(CH_3)_2CHCH_2OO\cdot + NO \xrightarrow{O_2} y_{E25a}\ (CH_3)_2CHCH_2ONO_2 + (1-y_{E25a})\ (NO_2 + (CH_3)_2CHCHO + HO_2)$

This reaction consists of the rate-determining reaction of the peroxy radical with NO, whose kinetics are discussed in Section B, followed by the reaction of the alkoxy radical formed with O_2.

$$\begin{aligned} (CH_3)_2CHCH_2OO\cdot + NO \rightarrow\ & y_{E25a}\ (CH_3)_2CHCH_2ONO_2 \\ & + (1-y_{E25a})\ [(CH_3)_2CHCH_2O\cdot + NO_2] \end{aligned}$$

$$(CH_3)_2CHCH_2O\cdot + O_2 \rightarrow (CH_3)_2CHCHO + HO_2$$

Reaction of the this alkoxy radical with O_2 is estimated (Carter and Atkinson 1985; see also Section F) to be its only significant fate under atmospheric conditions.

The aldehyde formed in the above reactions is represented in the model by propionaldehyde + "lost carbon".

The parameter y_{E25a} is the organic nitrate yield assumed for the initial reaction of the peroxy radical with NO, whose temperature-dependent values are estimated by Carter and Atkinson (1985), and in Section F, to be as follows:

$$\begin{aligned} y_{E25a} &= 0.05 \text{ at } 270 \text{ K}, \\ &= 0.03 \text{ at } 300 \text{ K}, \\ &= 0.02 \text{ at } 330 \text{ K}, \end{aligned}$$

with values for intermediate temperatures being obtained by linear interpolation. The organic nitrate formed in this reaction is represented in the model by 2-butyl nitrate.

$$\text{E26.}\quad (CH_3)_3COO. + NO \xrightarrow{O_2} y_{E26a}\ (CH_3)_3CONO_2 + (1-y_{E26a})\ (NO_2 + CH_3COCH_3 + CH_3OO.)$$

This reaction consists of the rate-determining reaction of the peroxy radical with NO, whose kinetics are discussed in Section B, followed by the decomposition of the alkoxy radical formed, and the subsequent reaction of the methyl radical so formed with O_2.

$$(CH_3)_3COO. + NO \rightarrow y_{E26a}\ (CH_3)_3CONO_2 + (1-y_{E26a})\ [(CH_3)_3CO. + NO_2]$$

$$(CH_3)_3CO. \rightarrow CH_3COCH_3 + CH_3.$$

$$CH_3. + O_2 \rightarrow CH_3OO.$$

Since the t-butyl peroxy radical has no α-hydrogens which can react with O_2, and since it cannot undergo a 1,5-H shift isomerization, decomposition is the only significant mode of reaction for this radical under atmospheric conditions.

The parameter y_{E26a} is the organic nitrate yield assumed for the initial reaction of the peroxy radical with NO, whose temperature-dependent values are estimated by Carter and Atkinson (1985), and in Section F, to be:

$$\begin{aligned} y_{E26a} &= 0.03 \text{ at } 270\text{ K}, \\ &= 0.02 \text{ at } 300\text{ K}, \\ &= 0.01 \text{ at } 330\text{ K}, \end{aligned}$$

with values for intermediate temperatures being obtained by linear interpolation. The organic nitrate formed in this reaction is represented in the model by 2-butyl nitrate.

E27. $(CH_3)_2CHCH_2OO\cdot + HO_2 \rightarrow -OOH + ((CH_3)_2CHCH_2OO\cdot \text{ products})$

E28. $(CH_3)_3COO\cdot + HO_2 \rightarrow -OOH + ((CH_3)_3COO\cdot \text{ products})$

E29. $(CH_3)_2CHCH_2OO\cdot + RO_2 \rightarrow 0.5\ HO_2 + ((CH_3)_2CHCH_2OO\cdot \text{ products})$

E30. $(CH_3)_3COO\cdot + RO_2 \rightarrow 0.5\ HO_2 + ((CH_3)_3COO\cdot \text{ products})$

E30. $(CH_3)_2CHCH_2OO\cdot + RCO_3 \rightarrow 0.5\ HO_2 + ((CH_3)_2CHCH_2OO\cdot \text{ products})$

E31. $(CH_3)_3COO\cdot + RCO_3 \rightarrow HO_2 + ((CH_3)_3COO\cdot \text{ products})$

The kinetics of these reactions and the general principles used for representing the products are discussed in Section B. As indicated there, the organic products formed in these reactions are represented by the set of products expected to be formed from the reactions of the corresponding alkoxy radical. Based on the reactions assumed for these alkoxy radicals as discussed above, with formation of the methyl radical from t-butoxy being represented by formaldehyde, we use

$$((CH_3)_2CHCH_2OO\cdot \text{ products}) = C_2H_5CHO + \text{"lost carbon"}$$

$$((CH_3)_3COO\cdot \text{ products}) = CH_3COCH_3 + HCHO$$

for the above reactions.

II. F. REACTIONS OF THE HIGHER ALKANES

In this section, the chemical mechanisms used for the reactions of the higher ($\geq C_5$) alkanes are discussed. In general, the reactions of the higher alkanes are analogous to those for the smaller alkanes discussed in the previous section, except that alkyl nitrate formation and (in most cases) hydrogen shift isomerizations, with subsequent formation of bi- and poly-functional products, become relatively more important. In addition, for most of the higher alkanes there are many more competing reaction routes which result in large numbers of reactions and products being included in the model if represented explicitly. For this reason, in this model the number of reactions used to represent the photooxidations of the higher alkanes is minimized by using an extension of the "lumped reaction" approach used in the model of Atkinson et al. (1982a), and the total number of species used in the model to represent the reactions of the alkane photooxidation products is minimized by representing the large number of possible alkane photooxidation products by a much smaller set of compounds. In the following sections, the various types of reactions occurring in the photooxidations of the alkanes, and their estimated kinetic parameters or rate constant ratios (from Carter and Atkinson, 1985) are summarized, followed by discussions of the representation of the photooxidation products and of the reaction lumping techniques used in this model. Finally, the lumped models used to represent the atmospheric photooxidations of selected specific alkanes (for which environmental chamber data are available for model testing) are summarized.

1. Summary of Alkane Photooxidation Reactions

In this section, the reactions involved in the atmospheric photooxidations of the alkanes, and their relevant kinetic parameters or rate constant ratios are summarized. This is based on the general evaluation of the atmospheric chemistry of alkanes of Carter and Atkinson (1985), and this reference should be consulted for a more detailed discussion of these reactions and for the derivations of the results summarized here. The purpose of this section is to summarize only the relevant results of that evaluation which are required here for the purpose of deriving detailed mechanisms for the reactions of specific alkanes.

a. Initial Reaction with OH Radicals

The only significant loss process for the alkanes under atmospheric conditions is via reaction with the OH radical. This reaction involves H-atom abstraction from a C-H bond, e.g.,

$$OH + R\text{-}H \rightarrow H_2O + R\cdot$$

followed by the rapid reaction of the alkyl radical with O_2 to form an alkyl peroxy radical

$$R\cdot + O_2 \xrightarrow{M} RO_2\cdot$$

For alkanes which have more than one type of non-equivalent hydrogen atom, it is necessary to estimate the partial rate constants for abstraction of each type of hydrogen atom in order to determine the relative importance of each route. Fortunately, in the case of alkanes, techniques exist for estimating these partial OH radical rate constants (Carter and Atkinson 1985, Atkinson 1986).

The estimated expressions for the partial rate constants for the OH radical abstractions from the different positions of the alkane depend on whether the abstracted hydrogen is primary, secondary or tertiary, and are given as follows:

$$\begin{aligned} k(OH + R_1CH_2\text{-}H) &= n\ k^o{}_{prim}\ F(R_1) \\ k(OH + R_1R_2CH\text{-}H) &= n\ k^o{}_{sec}\ F(R_1)\ F(R_2) \\ k(OH + R_1R_2R_3C\text{-}H) &= n\ k^o{}_{tert}\ F(R_1)\ F(R_2)\ F(R_3) \end{aligned}$$

where n is the number of equivalent CH_3, CH_2, or CH groups (i.e., not the number of equivalent H atoms), $k^o{}_{prim}$, $k^o{}_{sec}$, and $k^o{}_{tert}$ are standard rate constants for each type of group, and the factors $F(R_1)$, etc, are substituent factors for each neighboring group. If the H atom being abstracted is bonded to a ring with an overall ring strain energy of ≥ 5

kcal mole^{-1}, these estimated rate constants are multiplied by an additional factor which corrects for the reduction in the abstraction rate constants due to ring strain. The values for all of these parameters involved in estimating the partial OH radical rate constants are given in Table II-18.

The partial rate constants estimated using the parameters given in Table II-18 can then be summed to obtain an estimate of the total OH radical rate constant for those alkanes for which experimental data are not available, or where discrepancies exist between laboratory measurements. In many cases, no data exist concerning the temperature dependences of the overall rate constants, and this technique can be used to estimate the temperature dependences of the reaction rate constants. Even for those alkanes whose total OH radical rate constants have been well characterized, estimates of partial rate constants are required to estimate the relative importance of the different reaction routes.

b. Alkyl Nitrate Formation in the Reactions of Peroxy Radicals with NO

Alkyl peroxy radicals are formed following the initial reactions of OH radicals with the alkanes, and they are also formed in some of the subsequent reactions of the alkoxy radicals, discussed below. When NO_x is present, their major fate is reaction with NO, as discussed in Section B. This reaction can occur via two different routes: that involving alkoxy radical formation

$$RO_2\cdot + NO \rightarrow RO\cdot + NO_2 \qquad \text{(a)}$$

and that involving alkyl nitrate formation.

$$RO_2\cdot + NO \xrightarrow{M} RONO_2 \qquad \text{(b)}$$

As discussed in previous sections, for most of the smaller alkyl peroxy radicals, or for the substituted peroxy radicals formed in the photooxidations of the alkenes or some of the oxygenates, pathway (a) appears to be the dominant route. However, the significant yields of alkyl nitrates

Table II-18. Parameters Used to Estimate Group Rate Constants for the Reactions of OH Radicals with Alkanes (from Carter and Atkinson 1985)

Group Rate Constants k^o	$10^{12} \times k$ (cm^3 $molecule^{-1}$ sec^{-1}) 298 K	250 K < T < 400 K
$k^o_{primary}$	0.144	$3.28 \times e^{-1850/RT}$
$k^o_{secondary}$	0.838	$5.37 \times e^{-1100/RT}$
$k^o_{tertiary}$	1.83	1.83
Substituent Factor	**Factor F(X)** 298 K	~250 K < T < 400 K
$F(-CH_3)$	1.00	1.00
$F(-CH_2)$, F(>CH-), F(>C<)	1.29	$e^{151/RT}$
Ring Strain Factor	**Factor** 298 K	~250 K < T < 400 K
Three-membered ring	0.017	$e^{-2413/RT}$
Four-membered ring	0.22	$e^{-897/RT}$
Five-membered ring	0.80	$e^{-132/RT}$
Six-membered ring	1.00	1.0
Seven-membered ring	~1.0	~1.0

observed in the photooxidations of the higher alkanes indicate that nitrate formation via pathway (b) is a non-negligible route for the radicals formed in the photooxidations of these compounds. Thus the rate constant ratio $k_b/(k_a+k_b)$ for the various peroxy radicals is an important input into the alkane photooxidation models.

The relative importance of alkyl nitrate formation has been determined for a number of alkanes, including some as a function of temperature and pressure (Atkinson et al. 1982c, 1983a, 1984b). Based on these data, a general expression for $k_b/(k_a+k_b)$ has been derived which can be used to estimate the importance of nitrate formation as a function of temperature and pressure for the reactions of NO with a given alkyl peroxy radical (Atkinson and Lloyd 1984, Carter and Atkinson 1985, Atkinson 1986). At ~760 torr total pressure, this rate constant ratio can be estimated as follows:

$$k_b/(k_a+k_b) = F_s \times \left\{ \frac{(3.65 \times 10^7\ e^{0.947N}\ T^{-3.99})}{(1 + 2.02 \times 10^{-4}\ e^{0.947N}\ T^{0.70})} \right\} \times 0.556^{[1 + (0.304 \ln T + 0.411 N \ln - 3.69)^2]^{-1}} \qquad \text{(I)}$$

where T is the temperature in K, N is the number of carbon atoms in the radical, and F_s is a structural factor which is 0.4 if the radical is primary, 1.0 if secondary, and 0.25 if tertiary. This equation is used for all unsubstituted alkyl radicals in this model.

Equation (I) was derived entirely from the measured yields of alkyl nitrates in the reactions of unsubstituted alkyl peroxy radicals formed in the initial OH + alkane reaction. Thus the applicability of this equation to reactions of NO with substituted peroxy radicals (such as, for example, the radical $HOCH_2CH_2CH_2CH_2OO\cdot$ formed after isomerization of 1-butoxy radicals, as discussed in Section E-3) is not known. This is an important consideration, since the formation of such radicals is relatively important in the photooxidations of the longer chain alkanes. In previous models (Carter et al. 1979a, Atkinson et al. 1982a), it had been assumed that substitution by -OH groups did not significantly affect nitrate yields, implying that equation (I) is applicable for such peroxy radicals.

However, if it is assumed that -OH substitution on peroxy radicals do not affect the organic nitrate yields when they react with NO, then the model consistently underpredicts the reactivities observed in a majority of the NO_x-air irradiations of n-hexane, n-heptane, n-octane and n-nonane. Consistent underprediction of reactivity by the model can be attributed to the model assuming too much alkyl nitrate formation, since pathway (b) forming the nitrate is radical-terminating, while the competing pathway is not. This discrepancy is shown in Figure II-15, where the times to achieve one-half of the experimental maximum of the quantity $([O_3]-[NO])$, calculated assuming that -OH substitution on peroxy radicals does not

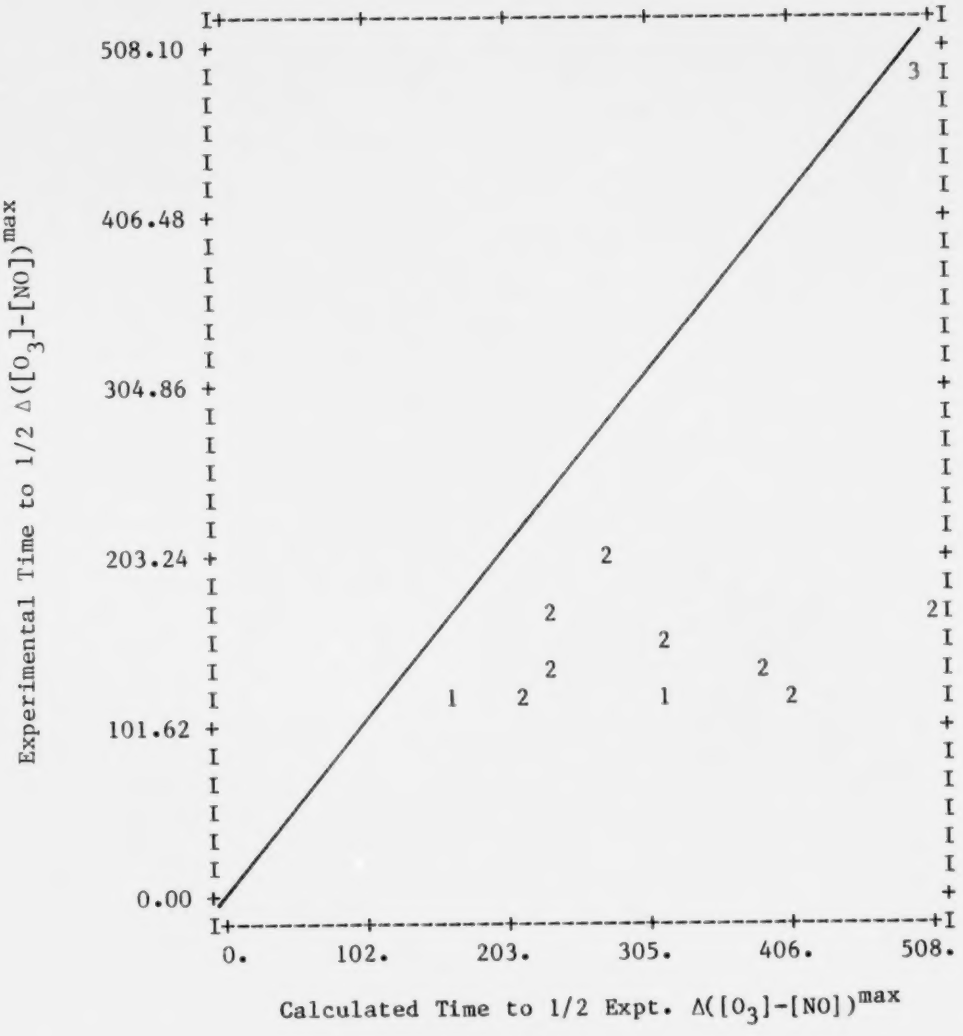

Figure II-15. Plots of predicted vs. experimental times required to achieve one-half the experimentally observed change in ($[O_3]$-[NO]) for the NO_x-air irradiations of the $\geq C_6$ n-alkane runs, where the calculations are based on the assumption that nitrates are formed in the reactions of NO with -OH substituted peroxy radicals. Chamber employed: 1 = SAPRC EC; 2 = SAPRC OTC; 3 = UNC chamber.

affect nitrate formation when they react with NO, are plotted against the experimental values. (The rate of change of the quantity ($[O_3]-[NO]$) is a useful measure of "timing" in environmental chamber experiments, since, as discussed in Section IV, it can be directly related to the total rates of NO to NO_2 conversion, and it is useful both for experiments where ozone forms rapidly and for experiments where no ozone formation occurs.) It can be seen from Figure II-15 that, except for the one n-octane-NO_x-air run carried out in the UNC outdoor chamber, the calculated times required to achieve a given amount of NO consumption and/or ozone formation are consistently greater than those experimentally observed, indicating that the model is consistently slow in predicting the rates of NO to NO_2 conversion in the $\geq C_6$ n-alkane runs.

However, if it is assumed that the reaction of NO with the OH-substituted peroxy radicals formed following isomerization of long-chain alkoxy radicals does not result in the formation of organic nitrates, then the model predictions are much more consistent with most of the experimental data. This is shown in Figure II-16, where the times to half $([O_3]-[NO])^{max}$ calculated using this assumption are plotted against the experimental results. Although (because of the extreme sensitivity of model simulations of alkane-NO_x-air irradiations to the chamber radical source, which vary from run-to-run - see Section III) there is variability in the fits of the calculated "timing" parameter to the experimentally observed values, the fits shown in Figure II-16 are clearly better than those shown in Figure II-15, since they indicate no consistent pattern of overprediction or underprediction of reactivity.

Hence in the present model we assume that alkyl nitrate formation from the reactions of NO with substituted peroxy radicals is negligible, and Equation (I) is used only for unsubstituted alkyl peroxy radicals. However, the reactions of substituted radicals represent a significant uncertainty in the photooxidation mechanisms of the higher alkanes, and direct experimental studies of these reactions are clearly necessary.

c. Alkoxy Radical Reactions

The major source of complexity in the photooxidation reaction mechanisms of the higher alkanes concerns the variety of ways in which the

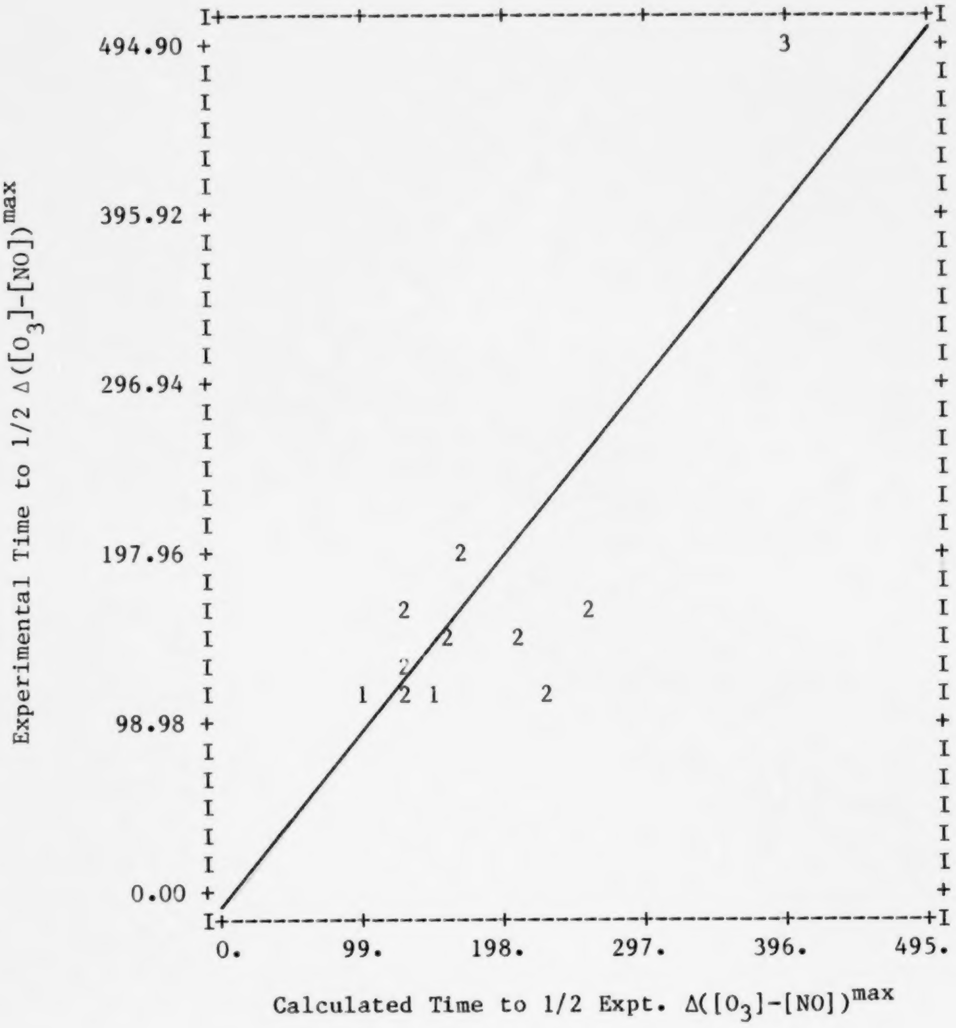

Figure II-16. Plots of predicted vs. experimental times required to achieve one-half the experimentally observed change in ($[O_3]$-[NO]) for the NO_x-air irradiations of the $\geq C_6$ n-alkane runs, where the calculations employ the standard model, which assumes that nitrates are not formed in the reactions of NO with -OH substituted peroxy radicals. Chamber employed: 1 = SAPRC EC; 2 = SAPRC OTC; 3 = UNC chamber.

alkoxy radicals formed in these photoxidations can react. In particular, under atmospheric conditions, alkoxy radicals can react with O_2,

$$RCH_2\text{-}O\cdot + O_2 \rightarrow RCHO + HO_2$$

$$R_1R_2CH\text{-}O\cdot + O_2 \rightarrow R_1\text{-}CO\text{-}R_2 + HO_2$$

decompose via β-scission,

$$RCH_2\text{-}O\cdot \rightarrow HCHO + R\cdot$$

$$R_1R_2CH\text{-}O\cdot \rightarrow R_1CHO + R_2\cdot$$

$$R_1R_2R_3C\text{-}O\cdot \rightarrow R_1\text{-}CO\text{-}R_2 + R_3\cdot$$

or undergo H-shift isomerization reactions, e.g,

$$RCH_2CH_2CH_2\text{-}O\cdot \rightarrow RCH(\cdot)CH_2CH_2OH$$

$$RCH_2CH_2CH_2CH_2\text{-}O\cdot \rightarrow RCH(\cdot)CH_2CH_2CH_2OH$$

Note that in most cases these decomposition and isomerization reactions (except as noted below) result in the eventual formation of additional alkoxy radicals.

The current data concerning the kinetics of the above reactions, and the available techniques for estimating their rate constants, are discussed by Carter and Atkinson (1985). Hence only the relevant rate constant estimates are summarized here. For the reaction of the alkoxy radicals with O_2, the estimated rate constants depend on whether the radical is primary or secondary. For 760 torr total pressure of air (i.e., where $[O_2] = 1.537 \times 10^{21}\ T^{-1}$ molecule cm^{-3}), the pseudo-unimolecular rate constant for the reaction of O_2 with primary alkoxy radicals is given by

$$k(\text{prim. RO}\cdot + O_2) = 5.69 \times 10^7\ T^{-1}\ e^{-960/RT}\ sec^{-1}$$

$$= 3.77 \times 10^4\ sec^{-1} \text{ at } 298\ K,$$

and the corresponding rate constant for secondary alkoxy radicals is given by

$$k(\text{sec. RO.} + O_2) = 2.77 \times 10^7\ T^{-1}\ e^{-390/RT}\ \text{sec}^{-1}$$

$$= 4.81 \times 10^4\ \text{sec}^{-1} \text{ at } 298\ \text{K}.$$

Tertiary alkoxy radicals do not react with O_2, since they lack the labile α-hydrogen.

The estimated Arrhenius parameters given by Carter and Atkinson (1985) for the various types of alkoxy radical decomposition and isomerization reactions are summarized in Tables II-19 and II-20, respectively. These estimated parameters are used in the model except for alkanes where direct experimental data are available. In the present model, the only

Table II-19. Estimated Arrhenius Parameters and Room Temperature Rate Constants for Decompositions of Alkoxy Radicals (from Carter and Atkinson 1985)

Reaction	$R^\bullet$	A^a (sec^{-1})	E_a (kcal mole^{-1})	$k(298\ K)^a$ (sec^{-1})
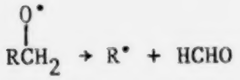 $R\overset{O^\bullet}{\overset{\vert}{CH_2}} \rightarrow R^\bullet + HCHO$	$CH_3\cdot$	8×10^{14}	21.4	1.6×10^{-1}
	$-CH_2\cdot$	8×10^{14}	18.4	2.6×10^{1}
	$>CH^\bullet$	8×10^{14}	18.0	5.0×10^{1}
	$\ngtr C^\bullet$	8×10^{14}	16.8	3.8×10^{2}
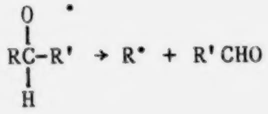 $R\underset{H}{\overset{O^\bullet}{C}}-R' \rightarrow R^\bullet + R'CHO$	$CH_3\cdot$	8×10^{14}	18.3	3.0×10^{1}
	$-CH_2\cdot$	8×10^{14}	15.3	4.8×10^{3}
	$>CH^\bullet$	8×10^{14}	14.9	9.4×10^{3}
	$\ngtr C^\bullet$	8×10^{14}	13.8	6.0×10^{4}
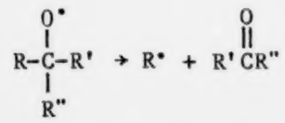 $R-\underset{R''}{\overset{O^\bullet}{C}}-R' \rightarrow R^\bullet + R'\overset{O}{\overset{\Vert}{C}}R''$	$CH_3\cdot$	8×10^{14}	16.6	5.3×10^{2}
	$-CH_2\cdot$	8×10^{14}	13.6	8.5×10^{4}
	$>CH^\bullet$	8×10^{14}	13.3	1.4×10^{5}
	$\ngtr C^\bullet$	8×10^{14}	12.1	1.1×10^{6}

[a] Applicable for a reaction path degeneracy of 1.

Table II-20. Estimated Arrhenius Parameters and Room Temperature Rate Constants for 1,4- and 1,5-H Shift Isomerizations of Alkoxy Radicals (from Carter and Atkinson 1985)

Type of H-Shift	Type of H Abstracted	A (sec^{-1})	E_a (kcal $mole^{-1}$)	k(298 K) (sec^{-1})
1,4	$-CH_3$	2.5×10^{11}	13.6	2.6×10^{1}
	$-CH_2-$	1.7×10^{11}	10.5	3.4×10^{3}
	$>CH-$	8.3×10^{11}	10.5	1.7×10^{3}
	$-CH_2OH$	1.7×10^{11}	12.4	1.4×10^{2}
	$-CH(OH)-$	8.3×10^{10}	9.3	1.3×10^{4}
1,5	$-CH_3$	1.3×10^{11}	8.2	1.3×10^{5}
	$-CH_2-$	8.4×10^{10}	5.1	1.5×10^{7}
	$>CH-$	4.2×10^{10}	5.1	7.6×10^{6}
	$-CH_2OH$	8.4×10^{10}	7.0	6.2×10^{5}
	$-CH(OH)-$	4.2×10^{10}	3.9	5.8×10^{7}

case where the estimates in these tables are not used concern the decomposition of the 2-butoxy radical (formed in the n-butane photooxidation system), for which experimental data indicate that the 298 K rate constant ratio for the decomposition relative to the competing reaction with O_2 is approximately a factor of 5 lower than estimated (Carter and Atkinson 1985). This discrepancy indicates the likely uncertainty ranges of these estimates. In the case of the isomerization reactions, the available data concerning the 1-butoxy radical isomerization were used as a basis for the estimates given in Table II-20, and the estimates in that table are applicable for all alkanes in the present model. However, as direct experimental data become available concerning these alkoxy radical rate constants or rate constant ratios, these estimates, which must be considered to be uncertain by at least a factor of 5, will be superceded.

It should be noted that OH-substituted alkoxy radicals are expected to be formed following alkoxy radical isomerizations, and estimates for the reactions of these radicals are also necessary. Estimates of Arrhenius parameters for the subsequent isomerizations of these radicals are included in Table II-20. OH substitution is not expected to affect the decomposition rates except for α- or β-hydroxyalkoxy radicals. As indicated below, α-substituted alkoxy radicals are not expected to be formed in these systems. In the case of β-substituted alkoxy radicals, β-scission decomposition to form an α-hydroxy radical is assumed to be rapid and to dominate over other possible competing reaction pathways.

For example, in the n-pentane system, the following sequence of reactions may occur,

$$\mathrm{OH + n\text{-}pentane} \xrightarrow{O_2,\ NO} \longrightarrow \mathrm{CH_3CH(O.)CH_2CH_2CH_3} \rightarrow \mathrm{CH_3CH(OH)CH_2CH(.)CH_3} \xrightarrow{O_2,\ NO} \longrightarrow$$

$$\mathrm{CH_3CH(OH)CH_2CH(O.)CH_3} \rightarrow \mathrm{.CH_2CH(OH)CH_2CH(OH)CH_3} \xrightarrow{O_2,\ NO} \longrightarrow$$

$$\mathrm{.OCH_2CH(OH)CH_2CH(OH)CH_3} \rightarrow \mathrm{HCHO} + \mathrm{.CH(OH)CH_2CH(OH)CH_3}$$

where the last reaction is an example of the rapid decomposition assumed for β-hydroxy alkoxy radicals. The assumption that this decomposition is rapid is based on data for the analogous reactions of the radicals formed following the addition of OH radicals to alkenes, which indicate that these reactions are fast (see Section D). Note, however, that reaction pathways such as that shown above are generally relatively minor, though they become increasingly important with increasing temperature. For example, the set of reactions shown above is estimated to consist of only 0.6% of the total reaction routes in the n-pentane photooxidation mechanism at 300 K, and 1.2% of the total at 330 K.

d. Reactions of α-Hydroxy Radicals

α-Hydroxy radicals can be formed in the photooxidations of the alkanes following multiple alkoxy radical isomerizations. These can be formed following decomposition of β-hydroxyalkoxy radicals, as discussed in the previous section. However, much more important examples are those expected following two 1,5-H shift isomerizations, which represent the dominant reaction pathway for the longer chain alkanes. For example, following reaction of OH radicals at the 2-position of n-pentane, the overall reaction pathway

$$OH + n\text{-pentane} \xrightarrow{O_2,\ NO} CH_3CH(O.)CH_2CH_2CH_3 \rightarrow CH_3CH(OH)CH_2CH_2CH_2. \xrightarrow{O_2,\ NO}$$

$$CH_3CH(OH)CH_2CH_2CH_2O. \rightarrow CH_3C(.)(OH)CH_2CH_2CH_2OH$$

is estimated to occur 72% of the time at 300 K. Previous studies of photooxidations of alcohols (Niki et al. 1978, Carter et al. 1979b, Ohta et al. 1982) indicate that the only significant mode of reaction of these compounds in the atmosphere is via H-atom abstraction by O_2 from the OH group, yielding HO_2 and the corresponding carbonyl compound, e.g.,

$$CH_3C(.)(OH)CH_2CH_2CH_2OH + O_2 \rightarrow CH_3COCH_2CH_2CH_2OH + HO_2$$

Thus, this is the only mode of reaction assumed for those species in this model.

e. Cycloalkanes

As discussed by Carter and Atkinson (1985), a number of other types of reactions and reaction intermediates must be considered in deriving the photooxidation mechanisms for the cycloalkanes. For example, decomposition reactions which open strained rings are expected to be relatively more favorable, and isomerizations with bicyclic ring transition states are expected to be less favorable, than the analogous reactions in acyclic systems, and formation of intermediates with carbonyl groups, as well as those with hydroxy groups, are expected. Because the reactions of cycloalkanes are not included in the current model, these considerations are not discussed further here.

2. Representation of the Alkane Photooxidation Products

Because of the variety of reactions they can undergo, the higher alkanes are expected to form a correspondingly large variety of oxygenated and organic nitrate products, particularly bi- and poly-functional species formed subsequent to alkoxy radical isomerizations. In order to maintain the number of active species in the model within manageable limits, and yet still take into account the reactions of these species, the alkane photooxidation products, including the bi- and poly-functional compounds, are represented in this model by a limited set of monofunctional products. The principles employed in this representation are discussed in this section.

a. Compounds Represented Explicitly

The reactions of the following alkane photooxidation products, or compounds to represent these products, are represented explicitly in this model. Their reaction mechanisms have been discussed in Section C above.

- Formaldehyde
- Propionaldehyde
- Methyl ethyl ketone
- 4-Heptyl nitrate
- Acetaldehyde
- Acetone
- 2-Butyl nitrate
- 3-Pentanol

b. "Lost Carbon" and "Lost Nitrogen"

These "counter species" are included in the model to take into account the amount of carbon and nitrogen which is "lost" in the process of representing one compound by another compound or group of compounds. They do not participate in any subsequent reactions in the model, though the model does calculate the reduction in their concentrations due to dilution.

c. Alkyl Nitrates

All of the alkyl nitrates are represented by 2-butyl nitrate, 4-heptyl nitrate, or by "unreactive nitrate." The representation for each organic nitrate is derived based on the number of carbons, n_C, in that nitrate, as follows:

$n_C \leq 3$. Alkyl nitrates with 3 or fewer carbons are expected to be relatively unreactive, and their reactions are ignored. These then are represented by "lost nitrogen" plus the appropriate number of "lost carbon"'s. Note that these compounds are formed in very low yields, and in this model the formation of organic nitrates from the reactions of C_1 and C_2 peroxy radicals with NO are ignored (see Section C).

$n_C = 4$. All C_4 alkyl nitrates are represented by 2-butyl nitrate, regardless of their chemical structure.

$n_C = 5$ or 6. These are represented by a combination of 2-butyl nitrate + 4-heptyl nitrate in such a way that the number of carbons is conserved. Thus if $n_C = 5$, they are represented by 0.67 2-butyl nitrate + 0.33 4-heptyl nitrate, and if $n_C = 6$, they are represented by 0.33 2-butyl nitrate + 0.67 4-heptyl nitrate.

$n_C = 7$. All C_7 nitrates are represented by 4-heptyl nitrate.

$n_C \geq 8$. The $\geq C_8$ nitrates are represented by 4-heptyl nitrate + (n_C-7) "lost carbon's".

d. $\geq C_3$ Aldehydes

All the higher monofunctional aldehydes are represented by propionaldehyde. If the aldehyde has more than 3 carbons, the extra carbon is lumped with the carbon in the bi- and poly-functional products, as discussed below.

e. $\geq C_4$ Ketones

All the higher monofunctional ketones are represented by methyl ethyl ketone. If the aldehyde has more than 4 carbons, the extra carbon is lumped with the carbon in the bi- and poly-functional products, as is the case with the extra carbon in the $\geq C_3$ aldehydes.

f. Other Products

Bi- and poly-functional oxygenated products and carbon in monofunctional $\geq C_3$ aldehydes and $\geq C_4$ ketones which are not represented by propionaldehyde and methyl ethyl ketone are represented by a combination of propionaldehyde, methyl ethyl ketone and 3-pentyl alcohol. The exact representation used is determined by the total number of carbons, n_C, to be represented, and the total number of carbonyl, n_{-CO-}, aldehyde, n_{-CHO}, and alcohol, n_{-OH}, groups present in the bifunctional products. If there are sufficient carbons such that all of the aldehyde groups can be represented by propionaldehyde, all the ketone groups can be represented by methyl ethyl ketone, and all the alcohol groups can be represented by 3-pentyl alcohol, i.e., if

$$n_{-C} = n_C - (3 \times n_{-CHO}) - (4 \times n_{-CO-}) - (5 \times n_{-OH}) \geq 0,$$

then these compounds are represented by

$$n_{-CHO} \text{ propionaldehyde} + n_{-CO-} \text{ methyl ethyl ketone}$$
$$+ \; n_{-OH} \text{ 3-pentyl alcohol} + n_{-C} \text{ "lost carbon"}.$$

If there are insufficient carbons to represent all of these groups, then the model preferentially represents the reactions at the aldehyde groups, since aldehydes in general are more reactive than ketones or alcohols. Thus, if $n_{-C} < 0$, then these compounds are represented by

$$n_{-CHO} \text{ propionaldehyde} + (f \times n_{-CO-}) \text{ methyl ethyl ketone}$$
$$+ \; (f \times n_{-OH}) \text{ 3-pentyl alcohol},$$

where f is such that all carbons are represented, i.e.,

$$f = [n_C - (3 \times n_{-CHO})] \; / \; [(4 \times n_{-CO-}) + (5 \times n_{-OH})].$$

Examples of these representations are given in the following section.

3. Representation of Higher Alkane Reactions in the Model

The reactions of the higher alkanes are represented in this model by replacing the many reactions actually involved by a much smaller number of "lumped" reactions, which represent their overall net effects in terms of products formed, molecules of NO converted to NO_2, and numbers of radicals regenerated. The technique used is analogous to that used for the reactions of the alkanes in the model of Atkinson et al. (1982a), except that in the present model additional reactions are included in order to take into account reactions of peroxy radicals with HO_2 and other peroxy and acylperoxy radicals. Under conditions where the major fate of the alkyl peroxy radicals is reaction with NO, this representation gives exactly the same predictions in computer model calculations (to within the uncertainty of the numerical integration technique, which is orders of magnitude less than the chemical uncertainties) as do calculations using models where each reaction is represented explicitly. Under conditions where the reactions of the peroxy radicals with other radicals are non-negligible, the errors caused by the additional approximations which are introduced are minor compared to those from the much more severe approximations already involved in representing these reactions in the more detailed representation (as discussed in Section B). Thus this lumping of the reactions in the models for the higher alkanes does not represent any significant compromise in the chemical validity of the overall model, other than that introduced by the lumping of the products discussed in the previous section.

The specific reactions used to represent the overall reactions of an individual higher alkane in the model (designated "ALK_n" for the purpose of this discussion) are given below. These reactions incorporate a number of mechanistic parameters, and for illustrative purposes the derivation of these parameters for n-butane, whose detailed mechanism is given is Section E-3 is given below. The values of these parameters, and the sets of individual reactions which they represent, are summarized in the following section for each of the higher alkanes which are represented in the present model.

F1n. $ALK_n + OH \xrightarrow{O_2} ALK_n\text{-}RO_2\cdot + H_2O$

This reaction represents the initial OH attack on the alkane, which is the only significant atmospheric loss process for this class of compounds. The available kinetic data for these reactions are summarized by Atkinson (1986), and the rate constants we use in the present model are summarized in the following section. For those alkanes for which Atkinson (1986) makes specific recommendations for the rate constants as a function of temperature, the recommended values are used; for the others, the rate constants were estimated for 270, 300, and 330 K using the group rate constant technique discussed above [Atkinson (1986) and Carter and Atkinson (1985)] and Arrhenius parameters were derived to fit these estimates. (For most alkanes, the estimation technique does not yield Arrhenius parameters directly, since each of the different types of reaction routes have a different set of Arrhenius parameters.)

The species designated "$ALK_n\text{-}RO_2\cdot$" represents a composite of the peroxy radicals formed in the reactions of the alkane ALK_n.

F2n. $ALK_n\text{-}RO_2\cdot + NO \xrightarrow{O_2}$ p1 $2\text{-}C_4H_9ONO_2$ + p2 $3\text{-}C_7H_{15}ONO_2$
+ p3 "lost nitrogen"
+ p4 $(HO_2 + NO_2)$ + p5 $R_2O_2\cdot$
+ p6 $HCHO$ + p7 CH_3CHO + p8 CH_3COCH_3
+ p9 C_2H_5CHO + pA $C_2H_5COCH_3$ + pB $3\text{-}C_5H_{11}OH$
+ pC "lost carbon"

F3n. $ALK_n\text{-}RO_2\cdot + HO_2\cdot \rightarrow \text{-}OOH + ALK_n\text{-}PROD$

F4n. $ALK_n\text{-}RO_2\cdot + RO_2\cdot \rightarrow 0.5\ HO_2 + ALK_n\text{-}PROD$

F5n. $ALK_n\text{-}RO_2\cdot + RCO_3\cdot \rightarrow 0.5\ HO_2 + ALK_n\text{-}PROD$

F6n. $ALK_n\text{-}PROD \xrightarrow{\text{fast}}$ p'6 $HCHO$ + p'7 CH_3CHO + p'8 CH_3COCH_3
+ p'9 C_2H_5CHO + p'A $C_2H_5COCH_3$ + p'B $3\text{-}C_5H_{11}OH$
+ p'C "lost carbon"

F7. $R_2O_2\cdot + NO \rightarrow NO_2$

F8. $R_2O_2\cdot + HO_2\cdot \rightarrow -OOH$

F9. $R_2O_2\cdot + RO_2\cdot \rightarrow$

F10. $R_2O_2\cdot + RCO_3\cdot \rightarrow$

These reactions represent the overall net effects of the reactions of all the intermediates formed in the photooxidation of the alkane. The kinetics of the reactions of peroxy radicals with NO, HO_2, and other peroxy and acyl peroxy radicals are discussed in Section B. The parameters p1 through pC and p'6 through p'C are derived for each specific alkane based on the detailed reactions estimated to be important in the photooxidation of the alkane. The parameters p1 through pC are derived for conditions when reaction with NO is the only significant reaction route for the peroxy radicals involved (which is generally the case when both NO_x and light are present), and the parameters p'6 through p'C are applicable for conditions when NO_x is absent. These parameters are discussed below, and the derivation of their values is given using n-butane as an example.

The parameters p1, p2 and p3 are used to represent all the alkyl nitrates formed in the overall reactions when NO is present. As indicated above, these are represented by 2-butyl nitrate, 4-heptyl nitrate, or inert nitrate ("lost nitrogen" + "lost carbon"), depending on the number of carbons, and the parameters p1 through p3 represent the sum of the respective yields of these model compounds. (The "lost carbon" involved in the inert nitrate is lumped into pC, which also includes the "lost carbon" involved in the oxygenate representation, if any.) In the case of n-butane (see Section E.3), only butyl nitrates are formed, and thus p2 = p3 = 0. 1-Butyl nitrate is formed in reaction E12 with a yield given by y_{E12a} and 2-butyl nitrate is formed in reaction E13a in a yield given by y_{E13a}. Since the relative importance of reactions E12 and E13a are given by y_{E11a} and $1-y_{E11a}$, respectively, then

$$p1_{n\text{-butane}} = (y_{E11a} \times y_{E12a}) + [(1-y_{E11a}) \times y_{E13a}].$$

The parameter p4 represents the total fraction of the overall reaction which results in radical regeneration (i.e., which does not result in alkyl nitrate formation) under conditions where the major fate of peroxy radicals is reaction with NO. Since the total nitrate yield is always given by p1 + p2 + p3, then

$$p4 = 1 - p1 - p2 - p3$$

for all alkanes.

Note that for alkanes where decomposition and/or isomerization reactions result in formation of additional peroxy radicals which subsequently react with NO, reaction F2 by itself does not represent all the consumption of NO, and the formation of the pseudo-species R_2O_2, is included in order to represent the additional NO to NO_2 conversions caused by these subsequently formed radicals. (Any alkyl nitrate formation occurring in these subsequent reactions is already taken into account by p1 through p3 in reaction F1.) This additional NO to NO_2 conversion is represented in the model by reaction (F7), and reactions (F8) through (F10) are used to account for the loss of NO to NO_2 conversions caused by the reactions of these subsequently formed peroxy radicals with HO_2 and other peroxy and acyl peroxy radicals. Note that no organic products or radicals are formed in these reactions, because all of the net product and radical formation processes are taken into account in the reactions of the ALK_n-RO_2 species. [On the other hand, the species -OOH, used to represent the reactions at the hydroperoxide group (see Section B), is included in reaction F8 because the additional hydroperoxide formation caused by the reactions of HO_2 with these subsequently formed peroxy radicals are not represented in reaction (F3n)]. This representation is used in order to allow the reactions of R_2O_2 to be independent of the alkane from which it is represented as being formed, which means that only a single R_2O_2 species need be included in the model, regardless of how many different alkanes are present.

It should be pointed out that this representation introduces additional approximations into the model under conditions when more than two "generations" of peroxy radicals are formed (i.e., when secondarily-formed peroxy radicals decompose or isomerize to form additional peroxy radicals), since this is based on only a two "generation" model. In particular, this formulation does not take into account the fact that if the "second generation" peroxy radicals react with HO_2, no "third generation" radicals are formed. This means that the model predicts that this reaction reduces the total peroxy radical levels to a somewhat lesser extent than would a more detailed model. However, this approximation is minor compared to some of the other approximations which have to be employed in order to represent peroxy + radical reactions in the model (Section B).

The amount of peroxy radicals formed in decomposition and isomerization reactions is reflected by the parameter p5, which gives the R_2O_2 yield, and thus the amount of additional NO to NO_2 conversion caused by these radicals. In the case of n-butane, the isomerization of 1-butoxy radicals in reaction E12b and the decomposition of 2-butoxy radicals in reaction E13b both result in the formation of additional peroxy radicals. The relative occurrence of peroxy radical formation in these reactions are given by y_{E12b} and $(1-y_{E13b})$, respectively, and the fraction of time that these reactions occur are given by, respectively, $[y_{E11a} \times (1-y_{E12a})]$ and $[(1-y_{E11a}) \times (1-y_{E13a})]$, and thus

$$\begin{aligned} p5_{n\text{-butane}} = {} & [y_{E11a} \times (1-y_{E12a}) \times y_{E12b}] \\ & + [(1-y_{E11a}) \times (1-y_{E13a}) \times (1-y_{E13b})]. \end{aligned}$$

The parameters p6, p7, and p8 refer to the overall respective yields of formaldehyde, acetaldehyde, and acetone formed when peroxy + NO reactions dominate. In the case of n-butane, formaldehyde and acetone are not formed, and acetaldehyde is formed in a yield of $2 \times (1-y_{E13b})$ in reaction E13b (both directly, and following the reaction of NO with ethyl peroxy radicals). Thus,

$$p6_{n\text{-butane}} = 0$$

$$p7_{n\text{-butane}} = (1-y_{E11a}) \times (1-y_{E13a}) \times 2 \times (1-y_{E13b})$$

$$p8_{n\text{-butane}} = 0.$$

The parameters p9, pA, and pB refer to the respective yields of the "lumped" products propionaldehyde, methyl ethyl ketone, and 3-pentyl alcohol. As discussed above in Section F-2, these are used to represent the reactions of all alkane photooxidation products except formaldehyde, acetaldehyde, and acetone. In addition, pC is used to represent the total number of "lost carbon"'s resulting in the overall representation. In the case of n-butane, propionaldehyde is used to represent the butyraldehyde formed in reaction E12b [whose yield is given by $y_{E11a} \times (1-y_{E12a}) \times (1-y_{E12b})$] and the aldehyde group in the bifunctional product formed [with a yield given by $y_{E11a} \times (1-y_{E12a}) \times y_{E12b}$] in reaction E14. Methyl ethyl ketone is formed in reaction E13b, with a yield given by $(1-y_{E11a}) \times (1-y_{E13a}) \times y_{E13b}$, and no other higher ketones are formed. The "lost carbon"'s resulting from representing butyraldehyde by propionaldehyde is used to allow 3-pentanol to represent some, though not all, of the hydroxyl groups in the bifunctional product, so that there are no net "lost carbon"'s in this n-butane model. (3-Pentanol is not used in the explicit n-butane model discussed in Section E-3.) Thus, for the "lumped reaction" n-butane model,

$$\begin{aligned} p9_{\text{n-butane}} &= [y_{E11a} \times (1-y_{E12a}) \times (1-y_{E12b})] \\ &\quad + [y_{E11a} \times (1-y_{E12a}) \times y_{E12b}] \end{aligned}$$

$$pA_{\text{n-butane}} = (1-y_{E11a}) \times (1-y_{E13a}) \times y_{E13b}$$

$$pB_{\text{n-butane}} = [y_{E11a} \times (1-y_{E12a}) \times y_{E12b}] \;/\; 5$$

$$pC_{\text{n-butane}} = 0$$

As indicated above, the parameters p'6 - p'C are used to represent the yields of products formed when the peroxy radical intermediates react with HO_2 or other peroxy or acyl peroxy radicals. The same general principles are used to represent the products for the "lumped" peroxy radicals, ALK_n-RO_2, in these reactions as are used to represent the products of these reactions in the explicit mechanisms. As discussed in Section B, the products of these reactions are represented by those expected to be formed from the corresponding alkoxy radicals. Thus in this case, the yields of these products, i.e., the parameters p'6 through p'C, are determined by the yields of products formed in the alkoxy radical reactions only. These are derived by effectively assuming that the peroxy radicals formed are immediately converted to the corresponding alkoxy radical, i.e., by assuming that alkyl nitrate formation does not occur.

Using n-butane as an example, the parameters p'6 through p'C are derived by use of the same considerations as discussed above for the derivation of p6 through pC, except that in this case the the parameters E12a and E13a, which give the alkyl nitrate yields from the two radicals which are assumed to form alkyl nitrates, are assumed to be zero. Based on this, we derive

$$p'6_{n\text{-butane}} = 0$$

$$p'7_{n\text{-butane}} = (1-y_{E11a}) \times 2 \times (1-y_{E13b})$$

$$p'8_{n\text{-butane}} = 0$$

$$p'9_{n\text{-butane}} = [y_{E11a} \times (1-y_{E12b})] + [y_{E11a} \times y_{E12b}]$$

$$p'A_{n\text{-butane}} = (1-y_{E11a}) \times y_{E13b}$$

$$p'B_{n\text{-butane}} = [y_{E11a} \times (1-y_{E12a}) \times y_{E12b}] / 5$$

$$p'C_{n\text{-butane}} = 0$$

The principles used to derive these parameters for the other alkanes are exactly analogous.

4. Models for Specific Alkanes

In this section, the OH radical rate constants and the mechanistic parameters p1 through pC and p'6 through p'C are summarized for the representitive $\geq C_5$ alkanes n-pentane through n-nonane, 2-methylbutane (isopentane), 2-methylpentane, 2,3-dimethylbutane, 2,4-dimethylpentane and 2,2,4-trimethylpentane (isooctane). Each of these alkanes were present, either singly or in mixtures, in at least some of the environmental chamber experiments used for model testing, discussed in Section IV, and thus a representation for each of these had to be derived. In all cases, these were derived using the general principles and rate constant and rate constant ratio estimates discussed above.

Table II-21 summarizes the Arrhenius parameters used in this model for the reactions of OH radicals with the alkanes listed above. The corresponding rate constants at 298 K for these reactions are also given. Footnotes to the table indicate which Arrhenius parameters and rate constants are recommended by Atkinson (1986), and which were derived from estimates (for T = 270, 300, and 330 K) using the group rate constant technique discussed in Section F-1. Note that Atkinson (1986) made

Table II-21. Arrhenius Parameters for the Reactions of OH Radicals with the $\geq C_5$ Alkanes in the Present Model

Alkane	E_a (cal $mole^{-1}$)	A (cm^3 $molecule^{-1}$ sec^{-1})	k(298 K) (cm^3 $molecule^{-1}$ sec^{-1})	Notes
n-Pentane	966	2.01×10^{-11}	3.93×10^{-12}	b
n-Hexane	922	2.53×10^{-11}	5.33×10^{-12}	b
n-Heptane	897	3.06×10^{-11}	6.73×10^{-12}	b
n-Octane	755	3.12×10^{-11}	8.72×10^{-12}	a
	880	3.59×10^{-11}	8.12×10^{-12}	b
n-Nonane	868	4.12×10^{-11}	9.51×10^{-12}	b
2-Methylbutane	402	7.92×10^{-12}	4.02×10^{-12}	b
2-Methylpentane	503	1.27×10^{-11}	5.42×10^{-12}	b
2,3-Dimethylbutane	0	6.2×10^{-12}	6.2×10^{-12}	a
	100	6.50×10^{-12}	5.49×10^{-12}	b
2,4-Dimethylpentane	241	1.04×10^{-11}	6.89×10^{-12}	b
2,2,4-Trimethyl-pentane	880	1.62×10^{-11}	3.66×10^{-12}	a
	496	1.09×10^{-11}	4.72×10^{-12}	b

[a] Arrhenius parameters recommended by Atkinson (1986).
[b] Arrhenius parameters derived from rate constants estimated using the group rate constant estimation technique, for T = 270, 300, and 330 K.

recommendations for only three of the eight alkanes listed in the table. For these three alkanes, the recommended kinetic parameters are used in the model, and for the others, the estimated parameters are employed. However, as can be seen from the table, for those alkanes for which recommended parameters are given, the differences between the recommended and estimated parameters and 298 K rate constants are relatively minor.

The mechanistic parameters p1 through pC and p'6 through p'C used to represent the overall reactions of the various alkanes were derived using a computer program written for this purpose. A detailed discussion of this computer program is beyond the scope of this document, but it is based entirely on the chemical principles and kinetic estimates summarized in this section. Briefly, this program does the following:

(1) It accepts input telling it which carbon atoms are bonded to which, which atoms are equivalent to which others, and the temperature.

(2) It then determines the partial OH radical rate constants for H-atom abstraction at each of the non-equivalent carbon atoms (by counting up the number of neighbor and next-nearest neighbor carbon atoms, and using the data in Table II-18), and then calculates the yields of each of the "first generation" radicals.

(3) For each non-OH substituted peroxy radical, it uses equation (I) to calculate the alkyl nitrate yield from its reaction with NO and thus the yield of the corresponding alkoxy radical. As discussed in Section F-2, each nitrate is represented by either an inert nitrate, 2-butyl nitrate, 4-heptyl nitrate, or a combination of the latter two, and the program keeps a running total of the yields of each type. As indicated above, -OH substituted alkoxy radicals are assumed not to form alkyl nitrates, and thus for those, as well as for C_1 and C_2 radicals, the yield of the corresponding alkoxy radical is the same as that for the peroxy radical.

(4) For each of the corresponding alkoxy radicals, it calculates the rate constants for its reaction with O_2 and for all the possible decompositions and 1,4- and 1,5-H shift isomerizations, based on its structure and the rate constant estimates summarized in Section F-1. These are then used to calculate the branching ratios, ignoring all negligible reaction routes [arbitrarily defined as being all routes whose rate is less than 1% of the total.]

(5) For each non-negligible reaction of the alkoxy radical, it determines which products and radicals are formed, and their yields. The program keeps track of the carbonyl and -OH substituents on the products and (where applicable) the radicals formed, as well as their structure and the location of the radical center on the radicals. If the radical formed is not an HO_2 radical, then it is added to the list of radicals to be processed, and the running total of the maximum amount of NO which reacts with peroxy radicals is increased to account for its reaction with the new radical formed. In addition, the yields of any stable products formed are added to cumulative totals for each type of product, and (for bi- and poly-functional products) for each type of substituent.

(6) Steps (3) through (5) are repeated until all radicals (other than HO_2) have been processed.

(7) Finally, the program calculates the appropriate "lumped product" yields to use in the model to represent the mix of $\geq C_4$ and bifunctional products, according to the principles discussed in Section F-2, and it outputs the yields of these and the other mechanistic parameters employed in this representation.

Tables II-22 through II-31 give summaries of the mechanistic and product yield parameters derived for the ten representative alkanes involved in the environmental chamber experiments used for model testing. These parameters were derived using the computer program discussed above based on the principles and the data summarized in Sections F-1 through F-3. In general these parameters are temperature dependent, and the values calculated for T = 270, 300, and 330 K are given in these tables. The mechanistic parameters for intermediate temperatures are obtained by linear interpolation.

It should be pointed out that this general representation can be used to lump the reactions of mixtures of alkanes, as well as representing individual species. In particular, if a mixture contains N different alkanes, designated ALK_i, with relative compositions in the mixture (on a molar basis) given by f_i, then all of the alkanes in the mixture can be represented by a single species which reacts with OH radicals with a rate constant, k, given by

$$k = \sum_{i=1}^{N} f_i \, k_i$$

where k_i is the OH radical rate constant for ALK_i, and whose product parameters are given by

$$pj = \sum_{i=1}^{N} f_i \, pj_i$$

where pj represents the "j'th" product parameter, e.g., p1, p2, p'1, etc., and pj_i is the corresponding parameter for ALK_i. This lumping scheme was used in this study for the model simulations of some of the complex mixture runs discussed in Section IV.

This scheme allows for accurate representation of the products formed in lumped models even if many alkanes are lumped together. Indeed, if two alkanes react with OH radicals with the same rate constant, no approximation is introduced by lumping them together in this manner. However, lumping compounds which react with significantly different rate constants is generally not appropriate, since the composition of such a mixture of alkanes will change significantly with time. The extent to which compounds with different rate constants can be lumped together without introducing unacceptable errors in the model predictions has not yet been adequately investigated.

Table II-22. Mechanistic and Product Yield Parameters Used in the Model for the Atmospheric Reactions of n-Pentane

Parameter	Product(s)	Values		
		T = 270 K	300 K	330 K
	ALK-RO_2 + NO →			
p1	2-$C_4H_9ONO_2$	0.135	0.085	0.055
p2	3-$C_7H_{15}ONO_2$	0.067	0.042	0.028
p3	"lost nitrogen"	0.0	0.0	0.001
p4	HO_2 + NO_2	0.798	0.873	0.916
p5	R_2O_2.	0.240	0.515	0.807
p6	HCHO	0.0	0.007	0.014
p7	CH_3CHO	0.0	0.074	0.281
p8	CH_3COCH_3	0.0	0.0	0.0
p9	C_2H_5CHO	0.060	0.163	0.385
pA	$C_2H_5COCH_3$	0.706	0.584	0.352
pB	3-$C_5H_{11}OH$	0.197	0.277	0.289
pC	"lost carbon"	0.0	0.001	0.002
	ALK-PROD =			
p´6	HCHO	0.0	0.008	0.015
p´7	CH_3CHO	0.0	0.085	0.308
p´8	CH_3COCH_3	0.0	0.0	0.0
p´9	C_2H_5CHO	0.065	0.181	0.417
p´A	$C_2H_5COCH_3$	0.897	0.675	0.387
p´B	3-$C_5H_{11}OH$	0.243	0.316	0.314
p´C	"lost carbon"	0.0	0.0	0.0

Table II-23. Mechanistic and Product Yield Parameters Used in the Model for the Atmospheric Reactions of n-Hexane

Parameter	Product(s)	Values		
		T = 270 K	300 K	330 K
ALK-RO$_2$ + NO →				
p1	2-$C_4H_9ONO_2$	0.106	0.066	0.043
p2	3-$C_7H_{15}ONO_2$	0.212	0.132	0.086
p3	"lost nitrogen"	0.0	0.0	0.0
p4	HO_2 + NO_2	0.682	0.801	0.870
p5	$R_2O_2\cdot$	0.459	0.711	0.857
p6	HCHO	0.0	0.0	0.001
p7	CH_3CHO	0.0	0.020	0.054
p8	CH_3COCH_3	0.0	0.0	0.0
p9	C_2H_5CHO	0.042	0.103	0.205
pA	$C_2H_5COCH_3$	0.547	0.524	0.485
pB	3-$C_5H_{11}OH$	0.356	0.473	0.512
pC	"lost carbon"	0.0	0.001	0.001
ALK-PROD =				
p´6	HCHO	0.0	0.0	0.001
p´7	CH_3CHO	0.0	0.025	0.063
p´8	CH_3COCH_3	0.0	0.0	0.0
p´9	C_2H_5CHO	0.048	0.120	0.230
p´A	$C_2H_5COCH_3$	0.815	0.661	0.561
p´B	3-$C_5H_{11}OH$	0.519	0.589	0.588
p´C	"lost carbon"	0.0	0.0	0.0

Table II-24. Mechanistic and Product Yield Parameters Used in the Model for the Atmospheric Reactions of n-Heptane

Parameter	Product(s)	Values		
		T = 270 K	300 K	330 K
	$ALK\text{-}RO_2 + NO \rightarrow$			
p1	$2\text{-}C_4H_9ONO_2$	0.0	0.0	0.0
p2	$3\text{-}C_7H_{15}ONO_2$	0.439	0.272	0.176
p3	"lost nitrogen"	0.0	0.0	0.0
p4	$HO_2 + NO_2$	0.561	0.728	0.824
p5	$R_2O_2\cdot$	0.513	0.719	0.836
p6	HCHO	0.0	0.0	0.0
p7	CH_3CHO	0.0	0.0	0.0
p8	CH_3COCH_3	0.0	0.0	0.0
p9	C_2H_5CHO	0.027	0.055	0.093
pA	$C_2H_5COCH_3$	0.442	0.538	0.586
pB	$3\text{-}C_5H_{11}OH$	0.415	0.556	0.628
pC	"lost carbon"	0.0	0.0	0.001
	ALK-PROD =			
p´6	HCHO	0.0	0.0	0.0
p´7	CH_3CHO	0.0	0.0	0.0
p´8	CH_3COCH_3	0.0	0.0	0.0
p´9	C_2H_5CHO	0.033	0.067	0.107
p´A	$C_2H_5COCH_3$	0.802	0.747	0.717
p´B	$3\text{-}C_5H_{11}OH$	0.738	0.763	0.762
p´C	"lost carbon"	0.0	0.0	0.0

Table II-25. Mechanistic and Product Yield Parameters Used in the Model for the Atmospheric Reactions of n-Octane

Parameter	Product(s)	Values T = 270 K	300 K	330 K
	ALK-RO_2 + NO →			
p1	2-$C_4H_9ONO_2$	0.0	0.0	0.0
p2	3-$C_7H_{15}ONO_2$	0.530	0.326	0.210
p3	"lost nitrogen"	0.0	0.0	0.0
p4	HO_2 + NO_2	0.470	0.674	0.790
p5	R_2O_2.	0.500	0.713	0.836
p6	HCHO	0.0	0.0	0.0
p7	CH_3CHO	0.0	0.0	0.0
p8	CH_3COCH_3	0.0	0.0	0.0
p9	C_2H_5CHO	0.001	0.002	0.003
pA	$C_2H_5COCH_3$	0.403	0.580	0.679
pB	3-$C_5H_{11}OH$	0.429	0.614	0.720
pC	"lost carbon"	0.530	0.326	0.210
	ALK-PROD =			
p´6	HCHO	0.0	0.0	0.0
p´7	CH_3CHO	0.0	0.0	0.0
p´8	CH_3COCH_3	0.0	0.0	0.0
p´9	C_2H_5CHO	0.001	0.002	0.003
p´A	$C_2H_5COCH_3$	0.869	0.866	0.863
p´B	3-$C_5H_{11}OH$	0.904	0.906	0.908
p´C	"lost carbon"	0.0	0.0	0.0

Table II-26. Mechanistic and Product Yield Parameters Used in the Model for the Atmospheric Reactions of n-Nonane

		Values		
Parameter	Product(s)	T = 270 K	300 K	330 K
	ALK-RO_2 + NO →			
p1	2-$C_4H_9ONO_2$	0.0	0.0	0.0
p2	3-$C_7H_{15}ONO_2$	0.587	0.360	0.231
p3	"lost nitrogen"	0.0	0.0	0.0
p4	HO_2 + NO_2	0.413	0.640	0.769
p5	R_2O_2.	0.445	0.688	0.830
p6	HCHO	0.0	0.0	0.0
p7	CH_3CHO	0.0	0.0	0.0
p8	CH_3COCH_3	0.0	0.0	0.0
p9	C_2H_5CHO	0.001	0.001	0.002
pA	$C_2H_5COCH_3$	0.396	0.614	0.735
pB	3-$C_5H_{11}OH$	0.427	0.661	0.795
pC	"lost carbon"	1.174	0.719	0.462
	ALK-PROD =			
p´6	HCHO	0.0	0.0	0.0
p´7	CH_3CHO	0.0	0.0	0.0
p´8	CH_3COCH_3	0.0	0.0	0.0
p´9	C_2H_5CHO	0.001	0.002	0.002
p´A	$C_2H_5COCH_3$	0.972	0.966	0.959
p´B	3-$C_5H_{11}OH$	1.022	1.027	1.031
p´C	"lost carbon"	0.0	0.0	0.0

Table II-27. Mechanistic and Product Yield Parameters Used in the Model for the Atmospheric Reactions of 2-Methylbutane

Parameter	Product(s)	Values		
		T = 270 K	300 K	330 K
	ALK-RO_2 + NO →			
p1	2-$C_4H_9ONO_2$	0.064	0.043	0.029
p2	3-$C_7H_{15}ONO_2$	0.032	0.021	0.015
p3	"lost nitrogen"	0.0	0.002	0.006
p4	$HO_2 + NO_2$	0.904	0.934	0.950
p5	$R_2O_2\cdot$	0.670	0.733	0.892
p6	HCHO	0.0	0.0	0.018
p7	CH_3CHO	0.614	0.612	0.710
p8	CH_3COCH_3	0.614	0.609	0.690
p9	C_2H_5CHO	0.101	0.132	0.161
pA	$C_2H_5COCH_3$	0.189	0.192	0.091
pB	3-$C_5H_{11}OH$	0.056	0.092	0.081
pC	"lost carbon"	0.112	0.006	0.018
	ALK-PROD =			
$p'6$	HCHO	0.0	0.0	0.019
$p'7$	CH_3CHO	0.649	0.639	0.741
$p'8$	CH_3COCH_3	0.649	0.638	0.725
$p'9$	C_2H_5CHO	0.110	0.140	0.167
$p'A$	$C_2H_5COCH_3$	0.241	0.222	0.099
$p'B$	3-$C_5H_{11}OH$	0.061	0.101	0.085
$p'C$	"lost carbon"	0.156	0.0	0.0

Table II-28. Mechanistic and Product Yield Parameters Used in the Model for the Atmospheric Reactions of 2-Methylpentane

Parameter	Product(s)	Values T = 270 K	300 K	330 K
	ALK-RO_2 + NO →			
p1	2-$C_4H_9ONO_2$	0.064	0.042	0.029
p2	3-$C_7H_{15}ONO_2$	0.128	0.084	0.057
p3	"lost nitrogen"	0.003	0.005	0.007
p4	HO_2 + NO_2	0.804	0.868	0.907
p5	$R_2O_2\cdot$	0.605	0.740	0.941
p6	HCHO	0.003	0.006	0.012
p7	CH_3CHO	0.000	0.021	0.083
p8	CH_3COCH_3	0.100	0.229	0.400
P9	C_2H_5CHO	0.499	0.541	0.660
pA	$C_2H_5COCH_3$	0.284	0.285	0.177
pB	3-$C_5H_{11}OH$	0.380	0.345	0.280
pC	"lost carbon"	0.009	0.014	0.020
	ALK-PROD =			
p'6	HCHO	0.004	0.006	0.013
p'7	CH_3CHO	0.000	0.026	0.095
p'8	CH_3COCH_3	0.110	0.251	0.432
p'9	C_2H_5CHO	0.551	0.588	0.712
p'A	$C_2H_5COCH_3$	0.424	0.361	0.205
p'B	3-$C_5H_{11}OH$	0.463	0.396	0.309
p'C	"lost carbon"	0.000	0.000	0.000

Table II-29. Mechanistic and Product Yield Parameters Used in the Model for the Atmospheric Reactions of 2,3-Dimethylbutane

Parameter	Product(s)	Values T = 270 K	300 K	330 K
	ALK-RO_2 + NO →			
p1	2-$C_4H_9ONO_2$	0.029	0.019	0.013
p2	3-$C_7H_{15}ONO_2$	0.058	0.037	0.025
p3	"lost nitrogen"	0.060	0.038	0.025
p4	HO_2 + NO_2	0.852	0.906	0.938
p5	$R_2O_2\cdot$	0.887	0.950	1.013
p6	HCHO	0.0	0.0	0.020
p7	CH_3CHO	0.0	0.0	0.020
p8	CH_3COCH_3	1.587	1.595	1.548
p9	C_2H_5CHO	0.089	0.127	0.166
pA	$C_2H_5COCH_3$	0.0	0.0	0.0
pB	3-$C_5H_{11}OH$	0.053	0.076	0.100
pC	"lost carbon"	0.180	0.114	0.074
	ALK-PROD =			
p'6	HCHO	0.0	0.0	0.021
p'7	CH_3CHO	0.0	0.0	0.021
p'8	CH_3COCH_3	1.795	1.723	1.627
p'9	C_2H_5CHO	0.102	0.139	0.176
p'A	$C_2H_5COCH_3$	0.0	0.0	0.0
p'B	3-$C_5H_{11}OH$	0.061	0.083	0.106
p'C	"lost carbon"	0.0	0.0	0.0

Table II-30. Mechanistic and Product Yield Parameters Used in the Model for the Atmospheric Reactions of 2,4-Dimethylpentane

Parameter	Product(s)	Values T = 270 K	 300 K	 330 K
	ALK-RO_2 + NO →			
p1	2-$C_4H_9ONO_2$	0.004	0.006	0.006
p2	3-$C_7H_{15}ONO_2$	0.181	0.118	0.080
p3	"lost nitrogen"	0.000	0.002	0.005
p4	HO_2 + NO_2	0.815	0.874	0.909
p5	$R_2O_2\cdot$	0.741	0.851	1.073
p6	HCHO	0.000	0.000	0.023
p7	CH_3CHO	0.000	0.000	0.005
p8	CH_3COCH_3	0.089	0.268	0.566
p9	C_2H_5CHO	0.717	0.776	0.870
pA	$C_2H_5COCH_3$	0.098	0.100	0.036
pB	3-$C_5H_{11}OH$	0.581	0.522	0.384
pC	"lost carbon"	0.001	0.007	0.014
	ALK-PROD =			
p'6	HCHO	0.000	0.000	0.025
p'7	CH_3CHO	0.000	0.000	0.006
p'8	CH_3COCH_3	0.103	0.306	0.625
p'9	C_2H_5CHO	0.822	0.860	0.948
p'A	$C_2H_5COCH_3$	0.178	0.140	0.043
p'B	3-$C_5H_{11}OH$	0.703	0.589	0.414
p'C	"lost carbon"	0.000	0.000	0.000

Table II-31. Mechanistic and Product Yield Parameters Used in the Model for the Atmospheric Reactions of 2,2,4-Trimethylpentane

Parameter	Product(s)	Values		
		T = 270 K	300 K	330 K
	$ALK\text{-}RO_2 + NO \rightarrow$			
p1	$2\text{-}C_4H_9ONO_2$	0.003	0.005	0.006
p2	$3\text{-}C_7H_{15}ONO_2$	0.264	0.171	0.114
p3	"lost nitrogen"	0.0	0.001	0.001
p4	$HO_2 + NO_2$	0.733	0.823	0.878
p5	$R_2O_2\cdot$	0.659	0.956	1.331
p6	HCHO	0.012	0.117	0.293
p7	CH_3CHO	0.0	0.0	0.001
p8	CH_3COCH_3	0.062	0.260	0.536
p9	C_2H_5CHO	0.620	0.747	0.816
pA	$C_2H_5COCH_3$	0.114	0.078	0.037
pB	$3\text{-}C_5H_{11}OH$	0.585	0.578	0.511
pC	"lost carbon"	0.704	0.446	0.116
	ALK-PROD =			
p'6	HCHO	0.027	0.175	0.357
p'7	CH_3CHO	0.0	0.0	0.001
p'8	CH_3COCH_3	0.087	0.339	0.623
p'9	C_2H_5CHO	0.750	0.884	0.925
p'A	$C_2H_5COCH_3$	0.250	0.115	0.043
p'B	$3\text{-}C_5H_{11}OH$	0.694	0.644	0.564
p'C	"lost carbon"	0.994	0.476	0.0

II. G. REACTIONS OF AROMATIC HYDROCARBONS

In this section, the atmospheric reactions of the representative aromatic hydrocarbons benzene, toluene, o- and m-xylene, and 1,3,5-trimethylbenzene are discussed. The reactions specific to each of these compounds are discussed in Sections G-1 through G-5; the reactions of the representative aromatic products benzaldehyde, phenol, o-cresol, and nitrophenol are discussed in Sections G-6 and G-7; and the representation of the reactions of the unknown ring-opening products formed from these compounds are discussed in Section G-8. There are significant uncertainties in many aspects of the photooxidation mechanisms of the aromatics, particularly concerning the nature and reactions of the ring-opening products, and a number of parameters had to be either arbitrarily assigned or adjusted to fit the results of environmental chamber experiments. These aspects of the mechanism should be re-evaluated as further data concerning the atmospheric reactions of the aromatic hydrocarbons and their photooxidation products become available.

The aromatic hydrocarbons are believed to be consumed in the atmosphere to a significant extent only by reaction with the hydroxyl radical. Thus this is the only initial mode of consumption for these compounds which is represented in this model. However, a number of their photooxidation products react via other routes, particularly photolysis (for the α-dicarbonyls and other ring-opening products) and (for the phenolic products) reaction with the nitrate (NO_3) radical. Radical initiation caused by photoreactive aromatic products and NO_x removal caused by the reactions of phenolic compounds with NO_3 and by other processes are important characteristics of the aromatic photooxidation mechanisms. Indeed, these radical initiation/removal processes significantly affect the computer model predictions for reaction mixtures which contain these compounds.

1. Reactions of Benzene

G1. OH + benzene → 0.27 (phenol + HO_2) + 0.73 (OH-benzene-O_2 adduct)

The available kinetic data for the reaction of OH radicals with benzene have been evaluated by Atkinson (1986), and the following expression for the rate constant for this reaction is recommended:

$$k_{G1} = 7.57 \times 10^{-12}\ e^{-1050/RT}\ \text{cm}^3\ \text{molecule}^{-1}\ \text{sec}^{-1}$$

$$= 1.29 \times 10^{-12}\ \text{cm}^3\ \text{molecule}^{-1}\ \text{sec}^{-1}\ \text{at 298 K.}$$

This is used in the model.

The initial reaction of OH radicals with benzene can occur via either (a) abstraction, (b) elimination, or (c) addition.

$$\text{OH} + \text{benzene} \rightarrow \text{phenyl} + H_2O \xrightarrow{O_2} \text{Ph-OO.} + H_2O \qquad \text{(a)}$$

$$\rightarrow \text{phenol} + H \xrightarrow{O_2} \text{phenol} + HO_2 \qquad \text{(b)}$$

$$\rightarrow \text{(OH-benzene adduct)} \qquad \text{(c)}$$

Atkinson (1986) reviewed the available higher temperature kinetic data, where process (c) is unimportant because the OH-benzene adduct rapidly back-decomposes, and recommends that

$$k_{a+b} = 2.93 \times 10^{-13}\ (T/300)^2\ e^{-684/RT}\ \text{cm}^3\ \text{molecule}^{-1}\ \text{sec}^{-1}$$

$$= 9.1 \times 10^{-14}\ \text{cm}^3\ \text{molecule}^{-1}\ \text{sec}^{-1}\ \text{at 298 K}$$

which implies that pathways (a) and (b) occur 7% of the time at 298 K. Thus these "high temperature" pathways occur to a non-negligible extent at room temperature.

Although the data of Madronich and Felder (1985) indicate that at high temperatures ($\geq$790 K) the major process is abstraction [pathway (a)], we found that models based on assuming formation of 7% phenyl peroxy radicals in the OH + benzene reaction could not successfully simulate the results of benzene-NO_x-air environmental chamber experiments. Thus, as shown in Section G-6, where the reactions of phenyl peroxy radicals are discussed, the formation of phenyl peroxy radicals amounts to a total radical termination path (since none of the reactions of these radicals results in radical regeneration). Assuming a 7% radical termination process in the OH + benzene mechanism then results either in significant underprediction of the reactivity observed in experiments with high benzene/NO_x ratios, or (if the photolysis rates of the uncharacterized ring-opened products, discussed in Section G-8, are adjusted upward so the high benzene-NO_x-air runs are fit) in significant overprediction of the reactivity observed in chamber experiments employing lower benzene/NO_x ratios. On the other hand, if it is assumed that the initial OH + benzene reaction involves no such radical termination route, then (with suitable adjustment of the photolysis rate of the uncharacterized products) the results of experiments carried out at both high and low benzene/NO_x ratios are much better fit. For the purpose of this model, we hence assume that for temperatures relevant for tropospheric modeling the abstraction pathway is not important. Since phenol can be formed following addition (pathway c) as well as by direct elimination (pathway b), these two pathways are not treated separately in this model.

The major process in the reaction of benzene with OH radicals is addition of OH to the aromatic ring. Under atmospheric conditions, the OH-benzene adduct can react with O_2 either by abstraction (forming the same products as the direct elimination pathway shown above) or by addition.

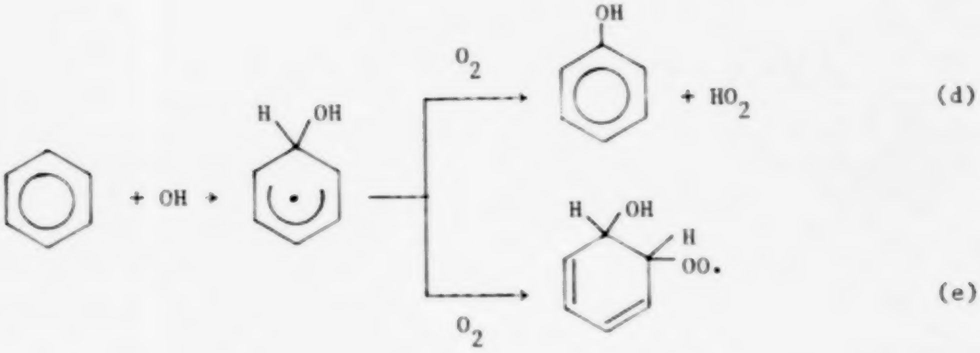

Phenol is observed to be formed in 25-30% yields in the reactions of OH radicals with benzene in the presence of O_2 at 303 K (Pitts et al. 1983), and in this model we assume that the overall phenol yield is 27%. As indicated above, phenol may also be formed by direct elimination, but its formation via O_2 abstraction from the OH-benzene adduct must clearly be also occurring, since direct elimination is estimated to occur only up to 7% of the time at 298 K. The temperature dependence of the phenol yield is not known, and is neglected in this model.

Formation of an OH-benzene-O_2 adduct is assumed to be the only significant process in the benzene photooxidation reactions other than those resulting in the formation of phenol. The expected structure for that adduct is that shown above. Addition of O_2 to the 2-position is expected (shown above) to dominate over addition to the 4-position, since the 2-adduct has resonance stabilization that the 4-adduct lacks.

G2. (OH-benzene-O_2 adduct) + NO → NO_2 + HO_2 + 0.29 HCOCHO
+ (benzene unknowns)

G3. (OH-benzene-O_2 adduct) + HO_2 → -OOH + 0.29 HCOCHO
+ (benzene unknowns)

G4. (OH-benzene-O_2 adduct) + RO_2 → 0.5 HO_2 + 0.29 HCOCHO
+ (benzene unknowns)

G5. (OH-benzene-O_2 adduct) + RCO_3 → 0.5 HO_2 + 0.29 HCOCHO
+ (benzene unknowns)

The subsequent reactions of the OH-aromatic-O_2 adducts, which are believed to result in the formation of ring-opened products, are unknown at the present time, though several speculative mechanisms are given in the literature and incorporated in current models. The most complete discussion of the possible alternative ring-opening mechanisms which account for the observed formation of α-dicarbonyls was given by Atkinson et al. (1980), and the more recently published models and evaluations of aromatic reactions incorporate one of the several possible mechanisms discussed there. While these models have generally concerned the reactions of toluene or the xylenes (since until recently environmental chamber data suitable for model testing were not available for benzene), the same general principles apply in the case of benzene, the simplest of the aromatics, and are thus discussed here.

The mechanism that Atkinson et al. (1980) found best fit the chamber data (for toluene) and which was incorporated into subsequent models of Atkinson et al. (1982a), Leone and Seinfeld (1984a), Leone et al. (1985) and Atkinson and Lloyd (1984), is based on the assumption that the OH-aromatic-O_2 adducts undergo [2.2.2] cyclization, and then undergo subsequent reactions to form α-dicarbonyls and unsaturated 1,4-dicarbonyls. In the benzene system, this mechanism is as follows:

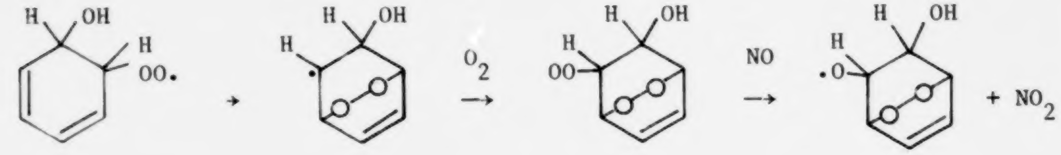

(I)

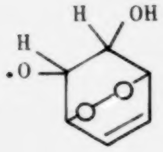

$\rightarrow HCO\dot{C}HOH + HCOCH{=}CHCHO$

$$HCO\dot{C}HOH + O_2 \rightarrow HO_2 + HCOCHO$$

This mechanism, referred to in the subsequent discussion as the "[2.2.2] cyclization" mechanism, thus predicts that one molecule of glyoxal and one molecule of 2-butene-1,4-dial are formed for each aromatic molecule of benzene which undergoes ring opening. It also predicts that one molecule of NO is converted to NO_2 in the process of forming these products and HO_2.

Another alternative mechanism discussed by Atkinson et al. (1980), and which was recently adopted by Killus and Whitten (1983) and incorporated into the most recent version of the SAI Carbon Bond model (Whitten et al. 1985) is also based on the assumption that the OH-aromatic-O_2 adduct undergoes [2.2.2] cyclization, but that the peroxy radical which is subsequently formed [species (I), above] undergoes a second [2.2.2] cyclization by the internal addition of O_2 to the double bond, and the "recyclized" specie formed then adds O_2, reacts with O_2, and then decomposes and reacts with O_2 to form three α-dicarbonyl molecules and HO_2. Thus this mechanism, referred to as the "[2.2.2] recyclization" mechanism, predicts that the ring opening reactions of benzene form three molecules of glyoxal and no other organic products. However, it is similar to the above mechanism in that it also predicts one molecule of NO is converted to NO_2 in the process of forming HO_2 and the organic products.

Atkinson et al. (1980) discuss additional possible mechanisms based on the OH-aromatic-O_2 adduct undergoing [3.2.1] cyclization or [3.2.1] recyclization, rather than the [2.2.2] cyclization and recyclization processes discussed above; but in the case of benzene the same products are ultimately predicted to be formed, and they all involve the conversion of one molecule of NO to NO_2 in the process. Thus if [3.2.1] cyclization is assumed, formation of glyoxal + 2-butene-1,4-dial is predicted, while if [3.2.1] re-cyclization is assumed to occur, complete fragmentation to glyoxal is predicted. The only real difference between these and the [2.2.2] mechanisms concerns predictions for substituted benzenes if recyclization is not assumed, where in general a different distribution of substituted products is predicted. For example, in the toluene system, the fragmentation could form either methylglyoxal + 2-butene-1,4-dial, glyoxal + 2-pentene-1-al-4-one, or glyoxal + 2-methyl-2-butene-1,4-dial, and the different models predict predict different relative yields of these alternative fragmentation routes.

Unfortunately, the recent data concerning the yields of α-dicarbonyls from benzene and the methylbenzenes obtained by Tuazon et al. (1986) and Bandow and co-workers (Bandow et al. 1985, Bandow and Washida 1985a,b), which are in good agreement with each other for the methyl-substituted benzenes, indicate yields of α-dicarbonyls which are significantly lower than predicted by any of these alternative mechanisms. In the case of benzene, the data of Tuazon et al. (1986) indicate that the glyoxal yield is approximately 21%, which corresponds to only a 29% yield relative to the formation of the OH-benzene-O_2 adduct, and accounts for only 9% of the carbon reacting via this route. [Bandow et al. (1985) also observed that glyoxal is formed from benzene, but were unable to quantify the yields.] This 29% (molar) relative yield of glyoxal is significantly lower than the 100% yield predicted by the cyclization mechanisms or the 300% yield predicted by the recyclization mechanisms discussed above.

All that is known regarding the other ring-opened products formed is that low (and unquantified) yields of formaldehyde, formic acid, and maleic anhydride are observed (Bandow et al. 1985). The observation of maleic anhydride indicates the possible formation of 2-butene-1,4-dial, since the latter may possibly heterogeneously isomerize to form the former. However, the data of Bandow et al. (1985) indicate that the yield of the anhydride is low (approximately 30% of that of glyoxal), suggesting that the yield of the dial is probably also significantly lower than predicted by the cyclization mechanism. These data suggest that while the reactions of the cyclization or recyclization mechanisms may occur, they cannot be the only, or even the most important, ring-opening reactions. Indeed, the variety of products observed in qualitative product studies on toluene, discussed in the following section, suggests that the actual aromatic ring-opening mechanism is quite complex.

In view of our obvious lack of understanding of the reactions which occur during the aromatic ring opening process, in this model no attempt is made to represent these reactions, or the subsequent reactions of the unknown ring-opened products, explicitly. Instead, the unknown ring-opening intermediates and products are lumped together and represented in an essentially parameterized manner designed to represent the net effect of their reactions, without regard to what their actual chemical structures are. However, rather than develop a totally new parameterized model which does not take advantage of previous research in developing aromatic photooxidation models, the approach we employ is to use the overall framework of "cyclization" mechanism and subsequent reactions of the ring-opening products given by Atkinson et al. (1980, 1982a), Atkinson and Lloyd (1984), Leone and Seinfeld (1984a) and Leone et al. (1985) as a starting point, and to make only the minimum number of modifications required for the model to be consistent with the observed α-dicarbonyl yields, and for its predictions to be consistent with the results of the environmental chamber experiments.

Since both the "cyclization" and the "recyclization" mechanisms assume the intermediacy of peroxy radicals which convert one molecule of NO to NO_2 in the process of forming the organic products and HO_2, reactions (G2-G5) as written above are based on this assumption. These reactions involve no assumptions concerning mechanistic details beyond this assumption, and the fact that the glyoxal yield amounts to 29% of the adduct formed (Tuazon et al. 1986). All the other products of the benzene ring opening reactions are lumped together as "(benzene unknowns)", and the subsequent reactions of this lumped species is represented in a parameterized manner discussed in section G-8.

It should be pointed out that reaction (G2) as written above does not mean that we are assuming that the OH-benzene-O_2 adduct itself is necessarily reacting with NO, since if, as assumed in both the "cyclization" and the "recyclization" mechanisms, the OH-aromatic-O_2 adducts undergo rapid unimolecular reactions and O_2 additions prior to forming species which react with NO, then the net effect is the same as shown in reaction (G2). Reaction (G2) [as well as reactions (G3-G5)] should be interpreted as representing the net effects of a set of reactions (possibly very complex) whose specifics are unknown.

Although the models of Atkinson et al. (1980, 1982a) assume 25% formation of an organic nitrate in the reactions of NO with the peroxy radicals involved in aromatic ring opening, the subsequent modeling work of Leone and Seinfeld (1984a) and Leone et al. (1985), which employed updated α-dicarbonyl photolysis rates, indicated that use of this assumption was not necessary to fit the available environmental chamber data. Since there is no experimental evidence for the formation of organic nitrates in these aromatic ring opening reactions, and since we assume that nitrate formation is negligible in the reactions of NO with OH-substituted peroxy radicals formed from other organics (e.g., alkenes), we assume that organic nitrate formation in these aromatic reactions is also negligible.

The kinetics of these and other peroxy radical reactions are discussed in Section B. In addition, the representation used for the products of the reactions of the peroxy intermediate(s) with HO_2 and other peroxy and acyl peroxy radicals is inconsistent with what is assumed for the analogous reactions of the other peroxy radicals in this model, which is also discussed in Section B.

2. Reactions of Toluene

$$\text{G6.}\quad OH + \text{toluene} \xrightarrow{O_2} 0.08\ PhCH_2\text{-}OO. + 0.16\ (\text{cresol} + HO_2)$$
$$+ 0.76\ (\text{OH-toluene-}O_2\ \text{adduct})$$

The kinetic data for the reaction of toluene with OH radicals, which is believed to be its only significant atmospheric removal process, has been evaluated by Atkinson (1986). For temperatures less than 325 K, the recommended rate constant for this reaction is given by

$$k_{G6} = 2.10 \times 10^{-12}\ e^{640/RT}\ cm^3\ molecule^{-1}\ sec^{-1}$$

$$= 6.19 \times 10^{-12}\ cm^3\ molecule^{-1}\ sec^{-1}\ \text{at 298 K.}$$

This is used in the model.

The reaction as written above represents the following competing processes:

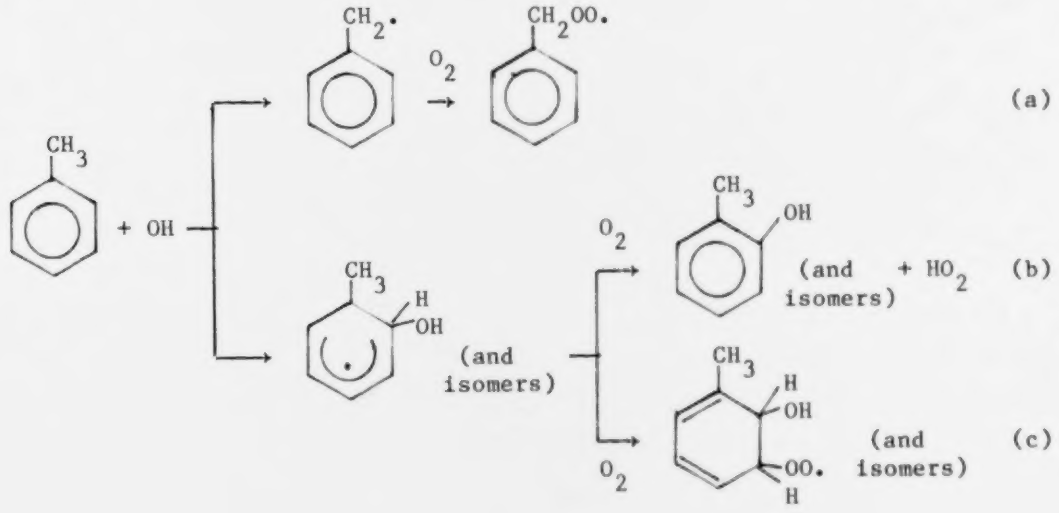

The available data concerning the relative importance of these processes have been evaluated by Atkinson and Lloyd (1984). Based on the observed yields of benzaldehyde (which is formed from $PhCH_2OO.$ as shown below) and the cresols in NO_x-air photooxidations of toluene, they conclude that pathway (a), yielding benzaldehyde, occurs 8% of the time, and that k(b)/k(c) = 0.21. The reaction as written above is based on these recommendations. Based on the data of Kenley et al. (1981), the relative o-, m-, and p-cresol isomer yields are 1.0 : 0.06 : 0.18, respectively, and thus o-cresol (shown above) is the major cresol isomer formed. The three cresol isomers are represented by a single specie in this model. Atkinson et al. (1983b) observed that the yields of benzaldehyde and o-cresol from toluene were independent of both temperature and pressure, and thus no temperature dependence of these yields is included in this model.

G7. $PhCH_2\text{-}OO. + NO \rightarrow NO_2 + PhCHO + HO_2$

G8. $PhCH_2\text{-}OO. + HO_2 \rightarrow \text{-}OOH + PhCHO$

G9. $PhCH_2\text{-}OO. + RO_2 \rightarrow 0.5\ HO_2 + PhCHO$

G10. $PhCH_2\text{-}OO. + RCO_3 \rightarrow 0.5\ HO_2 + PhCHO$

The kinetics of peroxy radical reactions are discussed in Section B. Reaction (G7) as written represents the following two reactions,

$$PhCH_2\text{-}OO. + NO \rightarrow PhCH_2\text{-}O. + NO_2$$

$$PhCH_2\text{-}O. + O_2 \rightarrow PhCHO + HO_2$$

with the reaction of the peroxy radical with NO being rate determining, and the reaction of the alkoxy radical with O_2 being assumed to be its only significant fate under atmospheric conditions. As discussed in Section B, the organic products formed in the reactions of peroxy radicals with HO_2 and other peroxy and acyl peroxy radicals are represented by those formed from the corresponding alkoxy radical(s), and reactions (G8)-(G10) as written above are based on that representation.

The toluene models of Atkinson et al. (1980, 1982a) assumed 25% organic nitrate (i.e., $PhCH_2ONO_2$) formation from the reaction of $PhCH_2OO\cdot$ and other peroxy radicals formed in the toluene system with NO, based on the observed formation of nitrates in the alkane photooxidations. However, the more recent toluene model of Leone and Seinfeld (1984a) does not assume organic nitrate formation in these reactions. Hoshino et al. (1978) observed approximately 10% yield of benzyl nitrate in this reaction, suggesting that some nitrate formation may indeed be occurring from this reaction, though not at the yields assumed by Atkinson et al. (1980, 1982a). Since a 10% nitrate yield in the reaction of benzyl peroxy radicals with NO corresponds to only 1% of the overall toluene photooxidation products, it is a minor process in the toluene system, and is thus ignored in this model.

G11. $(\text{OH-toluene-}O_2\text{ adduct}) + NO \rightarrow NO_2 + HO_2 + 0.15\ HCOCHO + 0.19\ CH_3COCHO + (\text{toluene unknowns})$

G12. $(\text{OH-toluene-}O_2\text{ adduct}) + HO_2 \rightarrow -OOH + 0.15\ HCOCHO + 0.19\ CH_3COCHO + (\text{toluene unknowns})$

G13. $(\text{OH-toluene-}O_2\text{ adduct}) + RO_2 \rightarrow 0.5\ HO_2 + 0.15\ HCOCHO + 0.19\ CH_3COCHO + (\text{toluene unknowns})$

G14. $(\text{OH-toluene-}O_2\text{ adduct}) + RCO_3 \rightarrow 0.5\ HO_2 + 0.15\ HCOCHO + 0.19\ CH_3COCHO + (\text{toluene unknowns})$

The reaction routes which do not result in the formation of benzaldehyde or the cresols are assumed to consist of ring opening reactions following the initial formation of the OH-toluene-O_2 adduct. The toluene system has probably been the most extensively studied of the aromatics, but the yields of only a small fraction of the ring-opened products have been determined quantitatively. The most definitive data concern the yields of glyoxal and methylglyoxal, where weighed least squares averages of the data of Tuazon et al. (1984b), Tuazon et al. (1986), and Bandow et al. (1985) indicate that glyoxal and methylglyoxal are formed in yields of 0.112 ± 0.015 and 0.146 ± 0.005, respectively, in the photooxidation of toluene. In addition, Shepson et al. (1984) observed low yields of $CH_3COCOCH{=}CH_2$ (1.5%), HCOCH=CHCHO (1%), $CH_3COCH{=}CHCHO$ (yield not given), 2-methylfuran (possibly formed from $CH_3COCH{=}CHCHO$) (0.4%), and lesser amounts of several other C_4 and C_5 unsaturated oxygenates and cyclic compounds which might be formed from unsaturated oxygenates. Dumdei and O'Brien (1984) in a qualitative product study observed an even wider variety of unsaturated oxygenates, including C_6 and C_7 unsaturated oxygenates such as $CH_3COCH{=}C(OH){=}CHCH{=}CH_2$, $CH_3COCH{=}CHCH{=}CHCHO$, and $CH_3COC(OH){=}CHCH{=}CHCHO$, as well as the C_4 and C_5 unsaturated oxygenates observed by Shepson et al. (1984).

These experimental observations are not consistent with any of the aromatic ring opening mechanisms which have been proposed to date. As discussed above, these mechanisms predict either the formation of three molecules of α-dicarbonyls for each molecule of toluene which undergoes ring opening [as predicted by the "recyclization" mechanism assumed by Killus and Whitten (1983), and incorporated into the latest Carbon Bond model (Whitten et al. 1985)] or that one α-dicarbonyl molecule and one homologue to 2-butene-1,4-dial is formed [as predicted by the "cyclization" mechanism assumed in the models of Atkinson et al. (1980, 1982a), Atkinson and Lloyd (1984), Leone and Seinfeld (1984a) and Leone et al. (1985)]. Both of these are totally inconsistent with the α-dicarbonyl product yield data which indicate that these products (glyoxal and methylglyoxal) account for only 35% of the ring-opening reaction route if the cyclization mechanism is assumed, and only 12% of the reaction if recyclization is assumed. In addition, the qualitative product studies of Shepson et al. (1984) and Dumdei and O'Brien (1984) do indicate that 2-butene-1,4-dial, or its methyl-substituted analogues 2-pentene-1,4-dial and 2-methyl-2-butene-1,4-dial, predicted to be formed from toluene by the cyclization mechanism, are not the only unsaturated ring-opening products. Indeed, these studies show that the actual toluene ring-opening reaction mechanism is much more complex than previously assumed.

No attempt is thus made in this model to explicitly represent the ring-opening reactions of toluene, and the same approach is employed for toluene (and the other aromatics) as discussed above for benzene. As is the case with the analogous reactions in the benzene system, reactions (G11)-(G14) above are based on the aromatic models formulated by Atkinson et al. (1980, 1982a), Atkinson and Lloyd (1984), Leone and Seinfeld (1984a) and Leone et al. (1985), modified to be consistent with the recently observed α-dicarbonyl yields, and with no organic nitrate formation assumed to occur from the reactions of NO with the intermediates involved. The yields of glyoxal and methylglyoxal in reaction (G11) are based on the observed yields reported by Tuazon et al. (1986) and Bandow et al. (1985a), and all of the ring-opened products are lumped together and represented by "(toluene unknowns)", whose subsequent reactions are discussed in Section G-8. Based on the previous models (see above) it is assumed that one molecule of NO is converted to NO_2 in the process of forming HO_2 and the products, and that the intermediates involved can be represented as peroxy radicals. Thus the kinetics of reactions (G11-G14), and the methods used to represent the products in the reactions with HO_2 and other peroxy and acyl peroxy radicals are the same as assumed for other peroxy radicals in this model, as discussed in Section B.

3. Reactions of m-Xylene

G15. $\text{OH} + \text{m-Xylene} \xrightarrow{O_2} 0.04\ \text{PhCH}_2\text{OO}\cdot + 0.17\ (\text{cresol} + \text{HO}_2)$
$+ 0.79\ (\text{OH-m-xylene-O}_2\ \text{adduct}) + 0.21\ \text{"lost carbon"}$

The kinetic data for the reaction of m-xylene with OH radicals has been evaluated by Atkinson (1986). For temperatures less than 325 K, the recommended rate constant for this reaction is given by

$$k_{G15} = 1.66 \times 10^{-11}\ e^{231/RT}\ \text{cm}^3\ \text{molecule}^{-1}\ \text{sec}^{-1}$$

$$= 2.45 \times 10^{-11}\ \text{cm}^3\ \text{molecule}^{-1}\ \text{sec}^{-1}\ \text{at 298 K.}$$

This is used in the model.

The reaction as written above are based on the three competing processes which are analogous to those shown above for the initial reactions of OH radicals with toluene. In the case of m-xylene, tolualdehyde formation, resulting from the initial H-atom abstraction by OH radicals from one of the methyl groups, was observed to occur 4% of the time (Bandow and Washida 1985a), and the reaction as written above is based on this. In this model, the reactions of all the aromatic aldehydes formed in this way are represented by those of benzaldehyde, so the tolualdehyde precursor, m-CH_3-Ph-CH_2OO., is represented by the benzaldehyde precursor PhCH_2OO. + "lost carbon".

No quantitative data have been published concerning the yield of phenolic compounds from the reactions of OH radicals with the xylenes, so in this model we assume that the ratio of O_2 abstraction from the OH-xylene adduct to form phenolic products, relative to addition to form OH-xylene-O_2 adducts, is the same as in the toluene system. (Thus the overall yield of phenolics is slightly higher since relatively more OH-aromatic adduct is formed.) In addition, "cresol" is used to represent all the substituted phenols formed in the reactions of the methyl-substituted benzenes, so the formation of these compounds in the m-xylene system is represented by cresol + "lost carbon". The reaction as written above incorporates these assumptions.

G16. (OH-m-xylene-O_2 adduct) + NO → NO_2 + HO_2 + 0.12 HCOCHO
+ 0.40 CH_3COCHO + (m-xylene unknowns)

G17. (OH-m-xylene-O_2 adduct) + HO_2 → -OOH + 0.12 HCOCHO
+ 0.40 CH_3COCHO + (m-xylene unknowns)

G18. (OH-m-xylene-O_2 adduct) + RO_2 → 0.5 HO_2 + 0.12 HCOCHO
+ 0.40 CH_3COCHO + (m-xylene unknowns)

G19. (OH-m-xylene-O_2 adduct) + RCO_3 → 0.5 HO_2 + 0.12 HCOCHO
+ 0.40 CH_3COCHO + (m-xylene unknowns)

These reactions are included to represent the formation of ring-opened products which are believed to result following the initial formation of the OH-aromatic-O_2 adducts. As discussed above, the mechanism of the aromatic ring-opening reactions are unknown, and thus a simplified and "lumped" representation of these processes is used in this model. Except for the products formed, the same representation is used for benzene and for all the alkylbenzenes in this model, as discussed above for benzene and toluene.

As for the other aromatic hydrocarbons, the only quantitative data available concerning the ring-opened products in the m-xylene system are the yields of the α-dicarbonyls. In the case of m-xylene, the weighed averages of the data of Tuazon et al. (1984b, 1986) and Bandow and Washida (1985a) indicate overall glyoxal and methylglyoxal yields of 0.094 ± 0.016 and 0.319 ± 0.023, respectively. These yields, which correspond to a total α-dicarbonyl yield from ring opening of 52% (molar) and are thus inconsistent with the predictions of any previous aromatic photooxidation models, are incorporated into the reactions as written above. All the other ring-opened products formed in the m-xylene system are lumped together as "m-xylene unknowns," and the representation of their subsequent reactions in this model is discussed in Section G-8.

4. Reactions of o-Xylene

G20. $\text{OH} + \text{o-Xylene} \xrightarrow{O_2} 0.05\ \text{PhCH}_2\text{OO}\cdot + 0.17\ (\text{cresol} + \text{HO}_2)$
$+ 0.78\ (\text{OH-o-xylene-O}_2\ \text{adduct}) + 0.22\ \text{"lost carbon"}$

The kinetic data for the reaction of o-xylene with OH radicals has been evaluated by Atkinson (1986). For temperatures less than 325 K, the recommended rate constant for this reaction is given by

$$k_{G20} = 1.47 \times 10^{-11}\ \text{cm}^3\ \text{molecule}^{-1}\ \text{sec}^{-1},$$

independent of temperature for the temperature range $298 \leq T \leq 320$ K. This is used in the model. No data are available for the rate constant for this reaction for temperatures below 298 K, and we assume that the above rate constant is applicable to the lower temperatures used for modeling the lower troposphere.

The reaction as written above are based on the three competing processes which are analogous to those shown above for the initial reactions of OH radicals with the other aromatic hydrocarbons. In the case of o-xylene, tolualdehyde formation, resulting from the initial H-atom abstraction by OH radicals from one of the methyl groups, was observed to occur 5% of the time (Bandow and Washida 1985a), and the reaction as written above is based on this. No data are available concerning the yield of phenolic compounds from o-xylene, and we make the same assumption regarding the yield of these products in the o-xylene system, represented by "cresol" + "lost carbon", as we do for m-xylene, discussed above. As with m-xylene, the precursors of the tolualdehydes formed in the o-xylene system are represented in this model by the precursor of benzaldehyde, and the phenolic products are represented by "cresol".

G21. (OH-o-xylene-O_2 adduct) + NO → NO_2 + HO_2 + 0.11 HCOCHO + 0.31 CH_3COCHO + 0.17 $CH_3COCOCH_3$ + (o-xylene unknowns)

G22. (OH-o-xylene-O_2 adduct) + HO_2 → -OOH + 0.11 HCOCHO + 0.31 CH_3COCHO + 0.17 $CH_3COCOCH_3$ + (o-xylene unknowns)

G23. (OH-o-xylene-O_2 adduct) + RO_2 → 0.5 HO_2 + 0.11 HCOCHO + 0.31 CH_3COCHO + 0.17 $CH_3COCOCH_3$ + (o-xylene unknowns)

G24. (OH-o-xylene-O_2 adduct) + RCO_3 → 0.5 HO_2 + 0.11 HCOCHO + 0.31 CH_3COCHO + 0.17 $CH_3COCOCH_3$ + (o-xylene unknowns)

These reactions are included to represent the formation of ring-opened products which are believed to result following the initial formation of the OH-o-xylene-O_2 adducts. Except for the products formed, the kinetics and mechanisms for these reactions are exactly the same as assumed in the model for the ring-opening reactions of the aromatic hydrocarbons discussed above. As for these other aromatic hydrocarbons, the ring-opening mechanism is unknown, and the only available quantitative data concerning ring-opening products are for the α-dicarbonyls. The weighed averages of the reported yields are (Tuazon et al. 1984b, 1986, Bandow and Washida 1985a, and references therein): glyoxal, 0.086 ± 0.012; methyl glyoxal, 0.241 ± 0.018, and biacetyl, 0.129 ± 0.030. These yields are incorporated in the reactions as written above. All the other ring-opened products formed in the o-xylene system are lumped together as "o-xylene unknowns," with the representation of their subsequent reactions in this model being discussed in Section G-8.

5. Reactions of 1,3,5-Trimethylbenzene

G25. $OH + 1,3,5\text{-TMB} \xrightarrow{O_2} 0.02\ PhCH_2OO. + 0.17\ (\text{cresol} + HO_2)$
$+ 0.81\ (OH\text{-}1,3,5\text{-TMB-}O_2\ \text{adduct}) + 0.38$ "lost carbon"

The kinetics of the reaction of OH radicals with 1,3,5-trimethylbenzene (1,3,5-TMB) are not as well studied as for the aromatics discussed above, and Atkinson (1986) makes no recommendation concerning this rate constant. The only published measurements of this rate constant as a function of temperature was carried out by Perry et al. (1977a), and only two data points are available for the lower temperature region of relevance for tropospheric modeling. Thus for this model, we use the room temperature rate constant of Perry et al. (1977a), i.e.,

$$k_{G25} = 6.24 \times 10^{-11}\ \text{cm}^3\ \text{molecule}^{-1}\ \text{sec}^{-1},$$

and neglect the temperature dependence of this reaction, which is not well characterized, but which is probably small.

The reactions as written above are based on the three competing processes which are analogous to those shown above in the discussion of the initial reactions of OH radicals with the other aromatics. In the case of 1,3,5-trimethylbenzene, no data are available concerning the yields of any of the aromatic products, but the kinetic data of Perry et al. (1977a) indicate that the H-atom abstraction route, ultimately yielding 3,5-dimethylbenzaldehyde, occurs 2% of the time. This is consistent with estimates based on the room temperature rate constant for the analogous reactions of the aromatics discussed above, and is thus assumed in this model. As for the xylenes, the yield of phenolic products are estimated based on the cresol yields in the toluene system. As with the other methylbenzenes, the phenolic products are represented by "cresol", and the aromatic aldehydes are represented by benzaldehyde.

G26. (OH-1,3,5-TMB-O_2 adduct) + NO → NO_2 + HO_2 + 0.77 CH_3COCHO
+ (1,3,5-TMB unknowns)

G27. (OH-1,3,5-TMB-O_2 adduct) + HO_2 → -OOH + 0.77 CH_3COCHO
+ (1,3,5-TMB unknowns)

G28. (OH-1,3,5-TMB-O_2 adduct) + RO_2 → 0.5 HO_2 + 0.77 CH_3COCHO
+ (1,3,5-TMB unknowns)

G29. (OH-1,3,5-TMB-O_2 adduct) + RCO_3 → 0.5 HO_2 + 0.77 CH_3COCHO
+ (1,3,5-TMB unknowns)

These reactions are included to represent the formation of ring-opened products which are believed to result following the initial formation of the OH-1,3,5-TMB-O_2 adducts, and except for the products formed they are the same as those used for the ring-opening reactions of the aromatic hydrocarbons discussed above. In the case of 1,3,5-trimethylbenzene, the only α-dicarbonyl product observed (or indeed expected) is methylglyoxal, and the weighed average of the yields reported by Bandow and Washida (1985b) and Tuazon et al. (1986) is 0.62 ± 0.03. This corresponds to a 77% (molar) yield relative to ring opening, which is the closest of any of the other aromatics discussed above to the 100% α-dicarbonyl yield predicted by the "cyclization" ring-opening mechanisms of Atkinson et al. (1980, 1982a) Atkinson and Lloyd (1984), Leone and Seinfeld (1984a) and Leone et al. (1985). The above reactions are based on this yield. No quantitative data are available for the other ring opened products, and these compounds are lumped together as (1,3,5-TMB unknown), with their reactions being discussed in Section G-8.

6. Reactions of Benzaldehyde

Benzaldehyde is formed in the photooxidation of toluene and is also used in the model to represent the reactions of the tolualdehydes and the other aromatic aldehydes formed in the analogous reaction mechanisms of the xylenes and the trimethylbenzenes. These compounds are consumed in the atmosphere by reaction with the OH radical and, to a lesser extent, by photolysis and reaction with NO_3 radicals.

G30. $OH + PhCHO \xrightarrow{O_2} PhCO_3\cdot + H_2O$

This reaction consists of the rate determining abstraction by OH radicals from the labile -CHO group, followed by rapid addition of O_2 to the acyl radical formed. Atkinson and Lloyd (1984) recommend

$$k_{G30} = 1.2 \times 10^{-11} \text{ cm}^3 \text{ molecule}^{-1} \text{ sec}^{-1},$$

independent of temperature, and this is used in this model. Addition of OH radicals to the aromatic ring is ignored, since the rate constant for this process is expected to be less than that for the addition of OH radicals to benzene (i.e., 1.2×10^{-12} cm^3 molecule^{-1} sec^{-1}, or 10% of k_{G30}), since -CHO is an electron withdrawing group.

G31. $PhCHO + h\nu \rightarrow 7$ "lost carbon"

Very little is known concerning the photolysis of benzaldehyde and other aromatic aldehydes under atmospheric conditions. The absorption coefficients for benzaldehyde, taken from a plot given by Majer et al. (1969), are tabulated in Table II-32. Benzaldehyde absorbs to a significant extent in the actinic region, and hence photodecomposition could be important if the quantum yields are sufficiently high. While no

Table II-32. Absorption Cross Sections, σ, (cm^2 $molecule^{-1}$, base e) for Benzaldehyde [derived from Figure 1 of Majer et al. (1969)]

(nm)	$10^{20} \times \sigma$ (cm^2)
299	17.76
304	7.40
306	6.91
309	6.41
313	6.91
314	6.91
318	6.41
325	8.39
332	7.65
338	8.88
342	8.88
346	7.89
349	7.89
354	9.13
355	8.14
364	5.67
368	6.66
369	8.39
370	8.39
372	3.45
374	3.21
376	2.47
377	2.47
380	3.58
382	0.99
386	0.0

data are available concerning these quantum yields under atmospheric conditions, the rate of benzaldehyde consumption observed in toluene + benzaldehyde-NO_x-air irradiations carried out in the SAPRC evacuable chamber are fit by models which assume that the overall quantum yield for benzaldehyde photodecomposition is 0.05. Since the wavelength dependence of this quantum yield is unknown, it is assumed to be independent of wavelength.

The products formed from the photolysis of benzaldehyde are also unknown, except that apparently non-radical products are formed. Model simulations of environmental chamber experiments where benzaldehyde is present in significant amounts are not consistent with the data if benzaldehyde photolysis is assumed to form radicals (Atkinson et al. 1980). Benzaldehyde is known to be an efficient radical inhibitor under atmospheric conditions (Kuntz et al. 1973, Gitchell et al. 1974, Carter et al. 1982b), showing that significant radical production in its photolysis reactions cannot be the case. Formation of benzene + CO is a reasonable non-radical photolysis pathway for benzaldehyde, but yields of benzene observed in toluene + benzaldehyde-NO_x-air environmental chamber experiments were only small fractions of those expected if this were the sole reaction pathway (Atkinson and Lloyd 1984). Because of our lack of knowledge as to the products formed, and because it is not necessary to assume formation of reactive products in benzaldehyde photolysis in order for model calculations to fit the environmental chamber experiments involving benzaldehyde, we assume in this model that only unreactive products are formed from the photolysis of benzaldehyde.

G32. $PhCHO + NO_3 \rightarrow PhCO_3\cdot + HNO_3$

This reaction as written consists of the rate determining H-atom abstraction by NO_3 from the labile -CHO group to form HNO_3 and the PhCO. radical, followed by the rapid addition of O_2 to PhCO. The 298 K rate constant for this reaction, relative to the $NO_2 + NO_3 = N_2O_5$ equilibrium constant, was measured by Atkinson et al. (1984c). Their data, using the $NO_3 + NO_2 = N_2O_5$ equilibrium constants of Kircher et al. (1984) and Tuazon et al. (1984a), yield

$$k_{G32} = 2.0 \times 10^{-15} \text{ cm}^3 \text{ molecule}^{-1} \text{ sec}^{-1} \text{ at 298 K.}$$

This rate constant is remarkably similar to the 298 K rate constant of 2.5 x 10^{-15} cm^3 $molecule^{-1}$ sec^{-1} for NO_3 + acetaldehyde, which suggests that the reaction of NO_3 with benzaldehyde occurs via a similar mechanism. In particular, addition of the NO_3 radical to the aromatic ring is not expected to be significant, since -CHO is an electron withdrawing group [thus addition of NO_3 to the aromatic ring in benzaldehyde should be slower than addition to the ring in benzene, which occurs with a rate constant of $<4 \times 10^{-17}$ cm^3 molecule^{-1} sec^{-1} at 298 K (Atkinson et al. 1984c)].

The temperature dependence of the rate constant for this reaction is not known. Since this reaction has a similar 298 K rate constant as the reaction of NO_3 with acetaldehyde, and is believed to occur via a similar mechanism, we assume that both have the same pre-exponential factor of 3×10^{-13} cm^3 molecule^{-1} sec^{-1} (see Sections C-1 and C-2). Thus we use

$$k_{G32} = 3.0 \times 10^{-13}\ e^{-2970/RT}\ \text{cm}^3\ \text{molecule}^{-1}\ \text{sec}^{-1}$$

in this model.

G33. $PhCO_3\cdot + NO \xrightarrow{O_2} NO_2 + Ph\text{-}OO\cdot + CO_2$

G34. $PhCO_3\cdot + NO_2 \xrightarrow{M} PhC(O)OONO_2$

G35. $PhC(O)OONO_2 \rightarrow PhCO_3\cdot + NO_2$

G36. $PhCO_3\cdot + HO_2 \rightarrow \text{-}OOH + \text{phenol} + CO_2$

G37. $PhCO_3\cdot + RO_2 \rightarrow 0.5\ HO_2 + \text{phenol} + CO_2$

G38. $PhCO_3\cdot + RCO_3 \rightarrow HO_2 + \text{phenol} + CO_2$

The $PhCO_3\cdot$ radical is assumed to react in a manner analogous to the reactions of other acyl peroxy radicals, whose kinetics are discussed in Section B. Reaction (G33) as written consists of the following elementary processes, with the initial reaction with NO being rate determining.

$$PhCO_3\cdot + NO \rightarrow PhCO_2\cdot + NO_2$$

$$PhCO_2\cdot \rightarrow Ph\cdot + CO_2$$

$$Ph\cdot + O_2 \rightarrow Ph\text{-}OO\cdot$$

Reaction (G34) represents the formation of peroxybenzoyl nitrate (PBzN), which is analogous to the formation of PAN and PPN from acetaldehyde and propionaldehyde, respectively, as discussed in Section C. The available data concerning the kinetics of the decomposition of PBzN have been evaluated by Atkinson and Lloyd (1984), and they recommend

$$k_{G35} = 1.6 \times 10^{15}\ e^{-25900/RT}\ \mathrm{sec}^{-1},$$

as used in this model.

As discussed in Section B, the organic products used to represent those from the reactions of peroxy and acyl peroxy radicals with HO_2 and other peroxy and acyl peroxy radicals are those ultimately formed from the reactions of the corresponding alkoxy radicals in the absence of NO_x. In the case of $PhCO_3\cdot$, as indicated by reaction (G33) above and (G44), below, these products are phenol + CO_2. Reactions (G34)-(G38) as written above are based on this representation.

G39. $Ph\text{-}OO\cdot + NO \rightarrow Ph\text{-}O\cdot + NO_2$

G40. $Ph\text{-}OO\cdot + HO_2 \rightarrow \text{-}OOH$ + phenol

G41. $Ph\text{-}OO\cdot + RO_2 \rightarrow 0.5\ HO_2$ + phenol

G42. $Ph\text{-}OO\cdot + RCO_3 \rightarrow 0.5\ HO_2$ + phenol

Phenyl peroxy radicals are assumed to react in a manner exactly analogous to other peroxy radicals in this model. The kinetics of these reactions and the principles used to represent the products of the reactions of these radicals with HO_2 and other peroxy and acyl peroxy radicals are discussed in Section B. As shown below, in the absence of NO_x the corresponding alkoxy radical is assumed to form phenol, so that compound is used to represent these products. As discussed above, the formation of alkyl nitrates in the reactions of aromatic peroxy radicals with NO is assumed to be negligible in this model.

G43. Ph-O. + NO_2 → nitrophenol

The phenoxy radical is unusual compared to other alkoxy radicals in this model in that it is not expected to react with O_2 or undergo decomposition or other unimolecular reactions at significant rates. Thus its most likely fate under atmospheric conditions is reaction with NO_2, provided that sufficient NO_2 is present. Reaction with NO is neglected because phenyl nitrite, like other organic nitrites, is expected to rapidly photolyze back to the PhO. radical + NO under atmospheric conditions, resulting in no net reaction. [See Taylor et al. (1980) for a discussion of the atmospheric lifetime of methyl nitrite. Phenyl nitrite is assumed to be similar.]

The rate constant for the reaction of phenoxy radicals with NO_2 has not been measured, and it is assumed to be the same as that for the analogous reaction of methoxy radicals with NO_2 (reaction C24), which is discussed in Section C-2. Thus we assume

$$k_{G43} = k_{C24} = 1.5 \times 10^{-11} \text{ cm}^3 \text{ molecule}^{-1} \text{ sec}^{-1},$$

independent of temperature.

The reaction of phenoxy radicals with NO_2 is assumed to result in the formation of nitrophenols, based on the data of Niki et al. (1979), where nitrophenols are observed to be the major products formed from Cl_2-NO-benzaldehyde irradiations. The exact mechanism for the formation of nitrophenols in this reaction is uncertain.

G44. Ph-O. + HO_2 → phenol + O_2

G45. Ph-O. + (other species) → phenol

In the absence of NO_x, the phenoxy radical may react with HO_2, with other radicals, and perhaps with other organic compounds which may be present. For simplicity, only the reaction with HO_2 is represented explicitly in this model; all the other potential loss processes for phenoxy radicals are lumped together as reaction (G45). The most probable mode of reaction of phenoxy radicals with HO_2 is transfer of a hydrogen atom as indicated in reaction (G44), above. The rate constant for this reaction is unknown, and we arbitrarily assume that it is the same as that used for the reactions of peroxy and acyl peroxy radicals with HO_2. Thus in this model, we assume

$$k_{G44} = k_{B5} = k_{B6} = 3 \times 10^{-12} \text{ cm}^3 \text{ molecule}^{-1} \text{ sec}^{-1},$$

independent of temperature.

Reaction (G45) represents all other possible loss processes for phenoxy radicals, which might include heterogeneous losses as well as homogeneous reaction. These processes are represented as a pseudo-unimolecular loss of phenoxy radicals, forming phenol, which is arbitrarily given a temperature-independent rate constant of

$$k_{G45} = 10^{-3} \text{ sec}^{-1}.$$

This rate constant is such that reaction (G45) only becomes significant if $[NO_2] < 3$ ppt and $[HO_2] < 10$ ppt. Generally, under polluted atmospheric conditions, either $[NO_2]$ or $[HO_2]$ are sufficiently high that reaction (G45) will be relatively minor.

7. Reactions of Phenols, Cresols, and Nitrophenols

As discussed above, phenol is formed in the photooxidation of benzene, and the phenolic products formed in the photooxidations of the methyl-substituted benzenes are all represented by o-cresol in this model. Nitrophenol is formed from the photooxidation of benzaldehyde and, as indicated below, is also believed to be formed in the reaction of NO_3 radicals with phenol. In addition, nitrophenol is used in this model to represent the reactions of the nitrocresols formed in the analogous reactions of the cresols. While these compounds are expected to be consumed in the atmosphere by reaction with both OH and NO_3 radicals, under most conditions it is the NO_3 radical reaction which is the most important in consuming these species. Thus these NO_3 radical reactions represent an important NO_x sink in the aromatic photooxidation mechanisms.

Atkinson and Lloyd (1984) estimate that the reaction of ozone with cresols is minor under most atmospheric conditions, and we assume that this is also true for phenol and the nitrophenols.

G46. OH + phenol → (OH-phenol intermediates)

G47. (OH-phenol intermed.) + NO → 0.85 (HO_2 + NO_2) + 0.15 nitrophenol + 0.2 glyoxal + 4.7 "lost carbon"

G48. (OH-phenol intermed.) + HO_2 → -OOH + 0.24 glyoxal + 5.52 "lost carbon"

G49. (OH-phenol intermed.) + RO_2 → 0.5 HO_2 + 0.24 glyoxal + 5.52 "lost carbon"

G50. (OH-phenol intermed.) + RCO_3 → 0.5 HO_2 + 0.24 glyoxal + 5.52 "lost carbon"

The only published measurement of the rate constant for the reaction of OH radicals with phenol (G46) is that of Rinke and Zetzsch (1984), who obtained

$$k_{G46} = 2.83 \times 10^{-11} \text{ cm}^3 \text{ molecule}^{-1} \text{ sec}^{-1}$$

at 296 K. This is used in the model. The temperature dependence of this rate constant is assumed to be negligible.

The mechanism for the reactions of OH radicals with phenol is not known, nor are there any phenol-NO_x-air irradiation data suitable to test the possible mechanisms. Since the OH-phenol reaction is a relatively minor process in the photooxidation of benzene, benzene-NO_x-air irradiation data are also unsuitable for this purpose. Thus, our representation in this model of the subsequent reactions of the intermediates formed is derived by analogy with the parameterized model for the reactions of OH radicals with o-cresol (reactions G53-G56), as discussed below. The only change made when applying the o-cresol model to phenol is that methylglyoxal (whose yield is adjusted in order to fit the PAN yields observed in the single o-cresol-NO_x-air experiment) is changed to glyoxal, since phenol has no methyl substituent groups.

G51. NO_3 + Phenol → Ph-O. + HNO_3

The rate constant for this reaction, relative to the $NO_2 + NO_3 = N_2O_5$ equilibrium constant, has been measured by Carter et al. (1981a) and more recently by Atkinson et al. (1984c). While these two determinations are in agreement within the experimental uncertainties, we assume that the more recent measurement, which yields a rate constant ~50% higher than the former, is more accurate, and this is used in the model. Based on our recommended $NO_2 + NO_3 = N_2O_5$ equilibrium constant, the data of Atkinson et al. (1984c) yield

$$k_{G51} = 3.8 \times 10^{-12} \text{ cm}^3 \text{ molecule}^{-1} \text{ sec}^{-1}$$

at 296 K. The temperature dependence of this rate constant is neglected in this model.

As discussed by Atkinson et al. (1984c) and Atkinson and Lloyd (1984), the reactions of NO_3 radicals with phenolic compounds are believed to occur primarily via H-atom abstraction from the -OH substituent group, as indicated above. This is consistent with the observation that the reaction of NO_3 radicals with methoxybenzene is ~4 x 10^4 times slower than the NO_3 radical reaction with phenol. The subsequent reactions of phenoxy radicals, which are also formed in the benzaldehyde system, have been discussed above.

G52. OH + Cresol → (OH-cresol intermediate)

G53. (OH-cresol intermed.) + NO → 0.85 ($HO_2 + NO_2$) + 0.15 nitrophenol + 0.2 CH_3COCHO + 5.5 "lost carbon"

G54. (OH-cresol intermed.) + HO_2 → -OOH+ 0.24 CH_3COCHO + 6.28 "lost carbon"

G55. (OH-cresol intermed.) + RO_2 → 0.5 HO_2 + 0.24 CH_3COCHO + 6.28 "lost carbon"

G56. (OH-cresol intermed.) + RCO_3 → 0.5 HO_2 + 0.24 CH_3COCHO + 6.28 "lost carbon"

As discussed above, o-cresol is used to represent the reactions of all the cresols and other alkyl-substituted phenols formed from the alkylbenzenes. The available kinetic data for the reaction of OH radicals with o-cresol have been reviewed by Atkinson and Lloyd (1984), and they recommend

$$k_{G52} = 4.1 \times 10^{-11} \text{ cm}^3 \text{ molecule}^{-1} \text{ sec}^{-1}$$

at 298 K. This is used in the model. The temperature dependence of this reaction is relatively small in the 299-330 K range (Perry et al. 1977b), and it is neglected in this model.

The data of Perry et al. (1977b), who studied this reaction as a function of temperature, indicate that both OH radical addition and H-atom abstraction occur. These data were evaluated by Atkinson and Lloyd (1984), and they concluded that at 298 K the abstraction route occurs ~7% of the time, and, by comparison with the abstraction rate constants with other aromatics, most of the abstraction occurs at the -OH group (as is the case for the NO_3 radical reaction). Thus under atmospheric conditions, addition to the aromatic ring is the major process.

Essentially nothing is known concerning the reactions of the OH-phenol and OH-cresol adducts, though Atkinson et al. (1980) and Atkinson and Lloyd (1984) give several speculations in this regard. In view of this, and the fact that under most conditions the major reaction route for these compounds is reaction with NO_3, and not OH, radicals, we do not attempt to represent the OH-cresol and OH-phenol mechanisms explicitly. Rather, we use a parameterized model which lumps together the net effects of both the addition and abstraction routes, with the parameters being adjusted to fit the data from the o-cresol-NO_x-air SAPRC evacuable chamber experiment EC-281, the only such experiment in our present data set.

This parameterized model assumes that peroxy-type intermediates are involved, and that (1) in order to fit the results of the cresol-NO_x-air experiment EC-281, it is necessary that some radical inhibition is involved in the OH-cresol reactions, and (2) PAN is observed as a product in that experiment. The unknown product(s) formed from the radical-inhibition processes are represented by nitrophenol, while methylglyoxal is assumed to be the PAN precursor. The yields of these products in reaction (G53) have been adjusted so that the ozone and PAN formation rates predicted in the model simulations agree with the results of EC-281. These assumptions are arbitrary, but they have the advantages that they require the addition of no new reactive species to the model, and the number of reactions required in the model to fit the results of the cresol-NO_x-air experiment are minimized. The fits of the adjusted model calculation to selected data from the o-cresol-NO_x-air experiment are shown in Figure II-17.

Since peroxy-type intermediates are assumed to be involved in the OH-cresol mechanism, the kinetics of reactions (G53-G56) are assumed to be the same as those of the analogous reactions of other peroxy radicals, as discussed in Section B. In addition, the products assumed to be formed in the reactions of the intermediates with HO_2 and other peroxy and acyl peroxy radicals are based on the general principles used for representing the products of these reactions for other peroxy radicals (as also discussed in Section B), together with the assumption that nitrophenol formation does not occur in the absence of NO_x.

G57. NO_3 + cresol → Ph-O. + HNO_3 + "lost carbon"

As indicated above, reaction with NO_3 radicals is the major atmospheric fate for the cresols under most conditions. As is the case with the analogous reaction of phenol, the rate constant for this reaction, relative to the $NO_2 + NO_3 = N_2O_5$ equilibrium constant, has been measured by Carter et al. (1981a) and more recently by Atkinson et al. (1984c), and the two determinations agree within the experimental uncertainties. Using

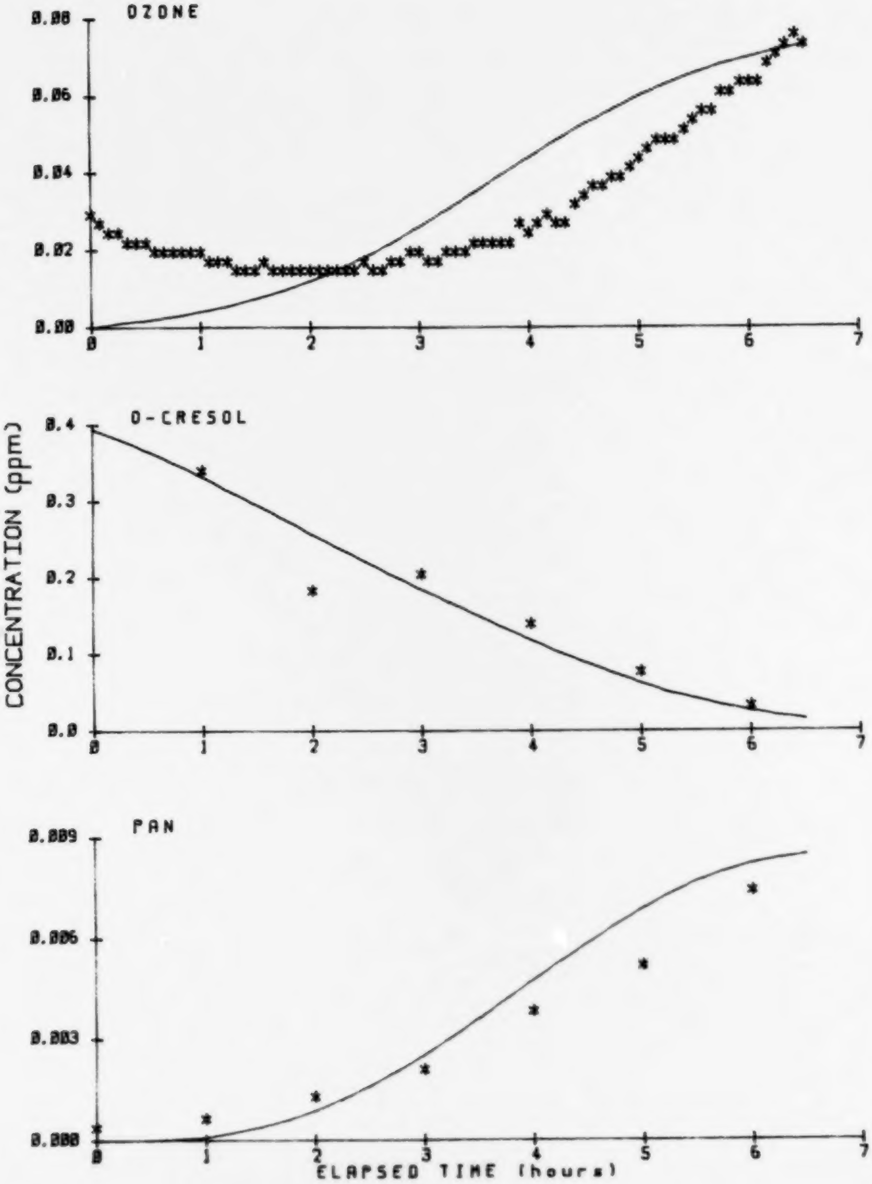

Figure II-17. Plots of observed vs. calculated concentration-time profiles for ozone, o-cresol, and PAN for o-cresol-NO_x-air run EC-281.
* = Experimental data.
----- = Adjusted model calculation.

the more recent and precise value of Atkinson et al. (1984c), and our recommended $NO_2 + NO_3 = N_2O_5$ equilibrium constant, we obtain a rate constant for the reaction of NO_3 radicals with o-cresol of

$$k_{G57} = 2.2 \times 10^{-11} \text{ cm}^3 \text{ molecule}^{-1} \text{ sec}^{-1}$$

at T = 296 K. The temperature dependence of this rate constant is probably small, and is neglected in this model.

As discussed above, the reactions of NO_3 radicals with phenolic compounds is believed to occur primarily via H-atom abstraction from the OH group, giving rise to HNO_3 and a phenoxy radical. The substituted phenoxy radicals formed from the cresols and the other substituted phenols are represented by unsubstituted phenoxy in this model, and the reaction as written above is based on this.

G58. NO_3 + nitrophenol → $Ph(NO_2)$-O. + HNO_3

G59. $Ph(NO_2)$-O. + NO_2 → dinitrophenol

G60. $Ph(NO_2)$-O. + HO_2 → nitrophenol + O_2

G61. $Ph(NO_2)$-O. + (other species) → nitrophenol

Nitrophenols are believed to be the major product formed in the reaction of NO_3 radicals with phenolic compounds under atmospheric conditions, and they are thus formed to a non-negligible extent in the photooxidations of aromatic hydrocarbons. Although there are no data available concerning the atmospheric reaction of nitrophenols, it is probably reasonable to assume that they react in a manner analogous to the reactions of the phenols, which as indicated above are consumed by reaction with OH and NO_3 radicals. However, since nitrophenols are formed primarily under conditions where reaction with NO_3 dominates as the sink for phenols, and their lifetimes relative to loss via this reaction are relatively short, we assume that reaction with NO_3 is the only significant fate for the nitrophenols. Thus only its reaction with NO_3 radicals is included in this model.

The rate constant for the reaction of NO_3 radicals with the nitrophenols is unknown. We tentatively assume that it is similar to that for phenol, i.e., that

$$k_{G58} = k_{G51} = 3.8 \times 10^{-12} \text{ cm}^3 \text{ molecule}^{-1} \text{ sec}^{-1},$$

independent of temperature.

The mechanism for the reaction of NO_3 radicals with the nitrophenols is assumed to be exactly the same as those for for other phenolic compounds, i.e., phenoxy-type radicals are formed. These radicals are assumed to react in exactly the same way and with the same rate constants as the analogous reactions of Ph-O., i.e., reactions (G59-G61) as written above are exactly analogous to reactions (G43-G45), and

$$k_{G59} = k_{G43} = 1.5 \times 10^{-11} \text{ cm}^3 \text{ molecule}^{-1} \text{ sec}^{-1},$$

$$k_{G60} = k_{G44} = 3 \times 10^{-13} \text{ cm}^3 \text{ molecule}^{-1} \text{ sec}^{-1}, \text{ and}$$

$$k_{G61} = k_{G45} = 10^{-3} \text{ sec}^{-1}.$$

The only reasons why $Ph(NO_2)$-O. is not lumped with Ph-O. in this model is to maintain a nitrogen balance and avoid having nitrophenol re-forming itself when it reacts.

It should be pointed out that the reactions of NO_3 radicals with nitrophenols represent a significant nitrogen sink in the aromatic photooxidation mechanism, and thus neglecting these reactions in the model is not a good approximation. As indicated in Section IV, model simulations of most aromatic-NO_x irradiations (except for the 1,3,5-trimethylbenzene runs carried out in the SAPRC ITC) tend to overpredict maximum ozone yields, and if this reaction is neglected this discrepancy becomes greater. For example, Figures II-18 and II-19 show plots of differences between the calculated and observed maximum ozone yields against the hydrocarbon/NO_x ratio for all of the toluene runs used in this program, where the differences shown in Figure II-18 were calculated using the standard model, and those shown in Figure II-19 were calculated with the reaction of NO_3 radicals with nitrophenols being ignored. It can be seen

Absolute Error, $[O_3]^{max}$ (ppm)

```
      I+---------+---------+---------+---------+---------+I
 0.40 +                                                   +
      I                                                   I
      I                                                   I
      I                                                   I
      I                                                   I
      I                                  3                I
 0.24 +                                                   +
      I                           3                       I
      I                                                   I
      I                                                   I
      I                                                   I
      I                                          3        I
 0.08 +                             11   3   1            +
      I                     3       1*      111           I
      I                                       1  2       *I
      I---------------2--------------1--------------------I
      I                                                   I
      I                                                   I
-0.08 +                                                   +
      I                                                   I
      I                                                   I
      I                                                   I
      I                                                   I
      I                                                   I
-0.24 +                                                   +
      I                                                   I
      I                                                   I
      I                                                   I
      I                                                   I
      I                                                   I
-0.40 +                                                   +
      I+---------+---------+---------+---------+---------+I
     0.00      0.31      0.63      0.94      1.26      1.57
```

Log (Initial HC/NOx)

Figure II-18. Plot of calculated-observed maximum ozone concentration in the toluene-NO_x-air irradiations against the log of the initial hydrocarbon/NO_x ratio, where the calculations employed the standard model. Chambers employed: 1 = SAPRC EC; 2 = SAPRC ITC; 3 = UNC chamber.

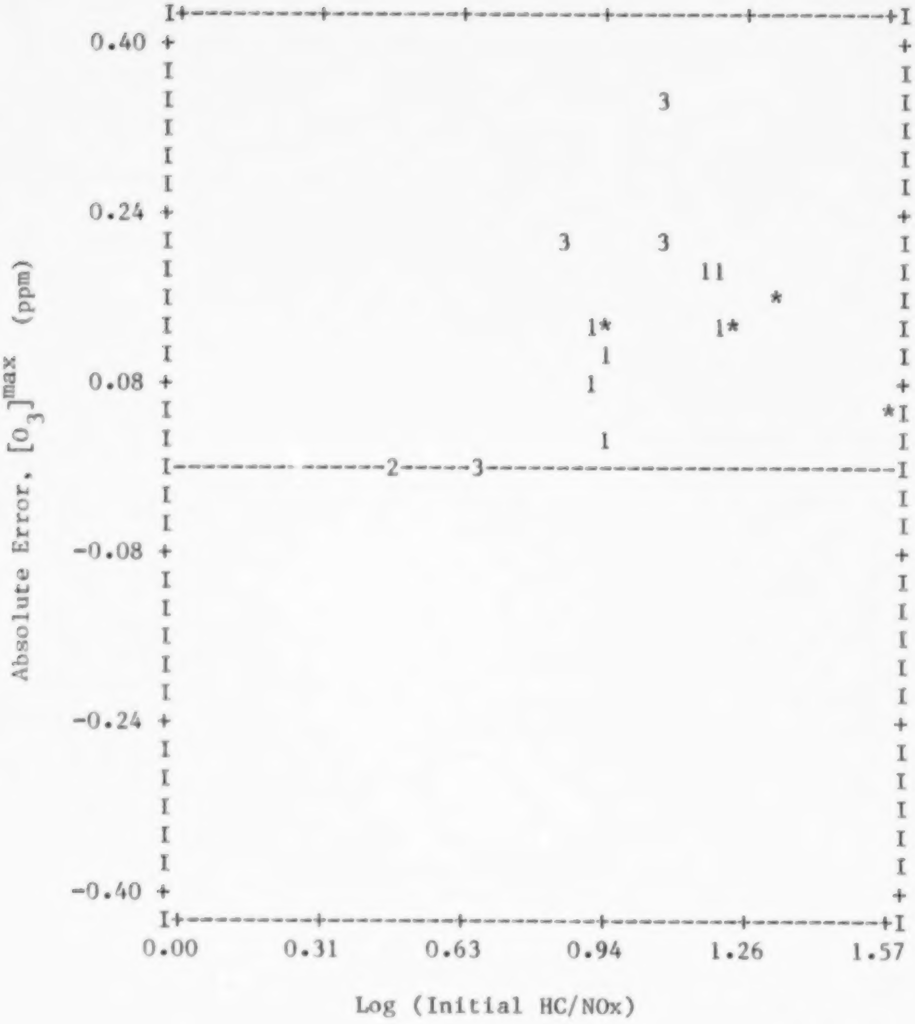

Figure II-19. Plot of calculated-observed maximum ozone concentration in the toluene-NO_x-air irradiations against the log of the initial hydrocarbon/NO_x ratio, where the calculations neglected the reaction between NO_3 radicals and nitrophenols. Chambers employed: 1 = SAPRC EC; 2 = SAPRC ITC; 3 = UNC chamber.

that the discrepancies between the calculated and observed maximum ozone yields are greater when this reaction is neglected.

On the other hand, the analogous reaction of NO_3 radicals with the dinitrocresols are assumed to be negligible. This is because these compounds are probably non-volatile, and thus condense into the aerosol phase or onto the chamber walls before they can undergo further reaction.

8. Reactions of the Unknown Aromatic Ring-Opened Products

The atmospheric photooxidations of benzene and the methylbenzenes are believed to involve ring opening approximately 75% of the time, but the ring opening products which have been quantitatively identified (primarily α-dicarbonyls) account for only 9 to 25% of the carbon which reacts by this route. As discussed in sections G-1 and G-2, the most recent models for the photooxidation reactions of aromatic hydrocarbons are based on the assumption that the ring-opening products other than the α-dicarbonyls consist of 2-butene-1,4-dial and its methyl substituted homologues. However, the results of the qualitative product studies of Shepson et al. (1984) and Dumdei and O'Brien (1984) suggest that a much wider variety of products are formed. This uncertainty concerning the nature and thus the subsequent reactions of the non-α-dicarbonyl ring opening products represents a significant uncertainty in the present aromatic photooxidation mechanisms.

In view of these uncertainties concerning the nature and reactions of these poorly characterized ring opening products, no attempt is made to represent their reactions explicitly in this model. Instead, all of these products from a given aromatic hydrocarbon are lumped together as a single specie [designated "(benzene unknowns)", "(toluene unknowns)", etc.], and their subsequent reactions are treated in a manner designed to represent the net effect of their reactions, without specifying the exact mechanistic details. Since (a) we have no direct knowledge concerning how these species react, and (b) the models based on the assumption that they consist primarily of unsaturated 1,4-dicarbonyls have been shown to give acceptable fits to results of environmental chamber experiments (Atkinson et al. 1980, 1982a, Leone and Seinfeld 1984a, Leone et al. 1985), in our initial model calculations we used the unsaturated 1,4-dicarbonyl mechanism of Atkinson et al. (1980, 1982a) and Leone et al. (1985) as a surrogate for the reactions of all of the non-α-dicarbonyl aromatic ring opening products. Thus in these initial model calculations, the model employed was very similar to previous models, except that, lower α-dicarbonyl yields were assumed for consistency with the recent laboratory data.

However, this initial chemical mechanism significantly underpredicted the observed reactivity in essentially all of the single-component aromatic hydrocarbon-NO_x air chamber experiments. This is shown in Figure II-20, which gives a plot of observed vs. calculated times to attain half the maximum observed change in $[O_3]-[NO]$ for these experiments.

This discrepancy between the initial model calculations and the experimental data can be attributed to the aromatic model not containing enough internal radical sources. The need to assume large internal radical sources in aromatic models has been recognized for some time, and all published aromatic models which have been tested against aromatic-NO_x-air environmental chamber data include such a radical source. In previous models, the photolysis of methylglyoxal and (in the o-xylene system) biacetyl has served as the internal radical source. [Glyoxal is not assumed to form significant amounts of radicals upon photolysis (Calvert and Pitts 1966), and, based on low photolysis rates for acrolein (CH_2=CHCHO) and crotonaldehyde (CH_3CH=CHCHO) (Calvert and Pitts 1966), the photolysis rates of the unsaturated 1,4-dicarbonyls have also been assumed to be slow.] However, as indicated above, the previous toluene or xylene models (which were tested only against results of experiments carried out in the SAPRC EC or the UNC chamber) all assumed much higher α-dicarbonyl yields than is now known to be the case.

Furthermore, it is interesting to note that the reactivity of benzene, which clearly cannot yield methylglyoxal as a product, is also significantly underpredicted, so that methylglyoxal cannot be the only internal radical source in the photooxidation mechanisms of the aromatic hydrocarbons. Glyoxal photolysis cannot provide the needed radicals, since even if the photolysis of glyoxal is assumed to occur to yield radicals with the overall quantum yield measured by Plum et al. (1983), the model still significantly underpredicts the reactivity observed in the benzene-NO_x-air experiments. In addition, for toluene and the xylenes,

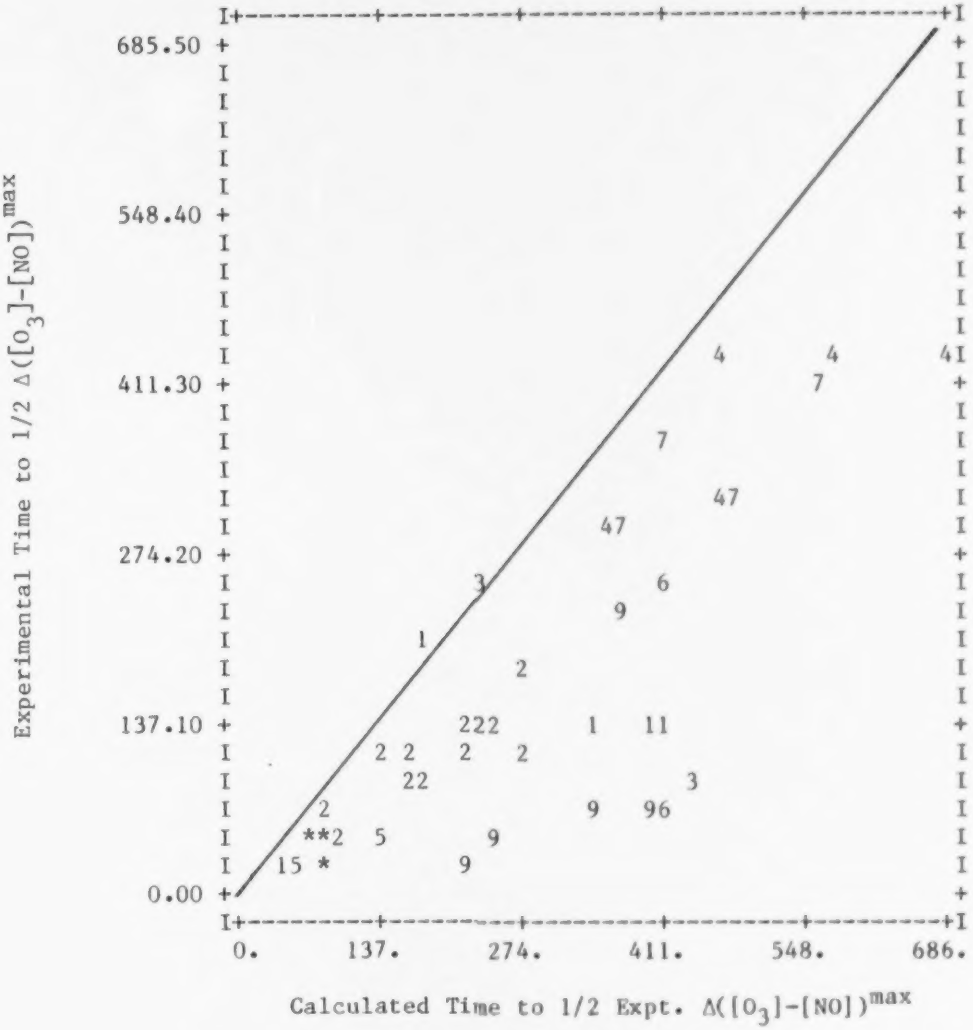

Figure II-20. Plot of predicted vs. experimental times required to achieve one-half the experimentally observed change in ($[O_3]$-[NO]) for the NO_x-air irradiations of the aromatic hydrocarbons, where the calculations assume no photolysis of the unknown aromatic ring-opened products. Symbols employed:

1 = ITC benzene runs
2 = EC toluene runs
3 = ITC toluene runs
4 = UNC toluene runs
5 = EC m-xylene runs
6 = ITC m-xylene runs
7 = UNC o-xylene runs
8 = EC 1,3,5-TMB runs
9 = ITC 1,3,5-TMB runs

even models which used the earlier assumed high α-dicarbonyl yields and which fit the results of experiments carried out in the SAPRC EC and in the UNC outdoor chamber cannot fit the results of the experiments carried out in the SAPRC ITC without having to assume additional radical sources. The photolysis rates for the α-dicarbonyls, relative to that for NO_2, are approximately six times lower in the SAPRC ITC than in the SAPRC EC or the UNC outdoor chamber, because the blacklamps used in the ITC have a much lower relative intensity in the ≥400 nm wavelength region where the α-dicarbonyls absorb most strongly (see Section III for a discussion of the spectral distributions of the light sources used by the environmental chambers). This then means that aromatic hydrocarbon-NO_x-air irradiations carried out in the SAPRC ITC are much more sensitive to radical sources other than from α-dicarbonyl photolysis than the other chambers used to test chemical mechanisms. These results indicate that not only are there additional radical source(s) in the aromatic system, but also that they photolyze in different wavelength region(s) than do the α-dicarbonyls.

Thus, in order to fit the results of the environmental chamber experiments, particularly those carried out using blacklight irradiation, the species used in the model to represent the unknown ring-opening products are assumed to undergo photolysis at rates which were adjusted in order to fit the data. This was also assumed in the recent model of Lurmann et al. (1984, 1986). In addition, to maintain a balance of total carbon and (for the methylbenzenes) of methyl groups, modifications have been made in this model concerning the specific products formed in their reactions with OH radicals. These modifications are discussed below in conjunction with the discussion of the specific reactions employed.

In the following discussion, the index "i" is used to refer to the individual aromatic hydrocarbon, specifically benzene, toluene, m- and o-xylene, and 1,3,5-trimethylbenzene, whose reactions are dealt with in this model. Thus ($aromatic_i$ unknowns) refers to (benzene unknowns), (toluene unknowns), etc., (Aro_i-RCO_3), (Aro_i-R_1O_2), and (Aro_i-R_2O_2) refer to the intermediates formed in the reactions of these species, and (Aro_i-OH-products) and ($aromatic_i$ phot-products) refer to the sets of stable products ultimately formed from the OH radical reactions or the photolysis of these species, and which differ for each aromatic. For each reaction listed below which employs this nomenclature, the model contains a separate reaction for each specific aromatic hydrocarbon.

a. OH Radical Reactions

G62i $(\text{Aromatic}_i \text{ unknowns}) + OH \rightarrow (\text{Aro}_i\text{-RCO}_3) + H_2O$

G63i $(\text{Aro}_i\text{-RCO}_3) + NO \rightarrow (\text{Aro}_i\text{-R}_1O_2) + CO_2 + NO_2$

G64i $(\text{Aro}_i\text{-RCO}_3) + NO_2 \rightarrow (\text{Aro}_i\text{-PAN})$

G65i $(\text{Aro}_i\text{-PAN}) \rightarrow (\text{Aro}_i\text{-RCO}_3) + NO_2$

G66i $(\text{Aro}_i\text{-R}_1O_2) + NO \rightarrow (\text{Aro}_i\text{-R}_2O_2) + NO_2$

G67i $(\text{Aro}_i\text{-R}_2O_2) + NO \rightarrow (\text{Aro}_i\text{-OH-products}) + NO_2$

The reaction sequence written above is based on the assumption that the lumped non-α-dicarbonyl ring-opening products react with OH radicals in a manner directly analogous to the OH radical reaction mechanism used in previous models for 2-butene-1,4-dial and its methyl substituted analogues (see, for example, Atkinson et al. 1982a). The OH + 2-butene-1,4-dial mechanism recommended by Atkinson and Lloyd (1984), and employed in the models of Leone and Seinfeld (1984a) and Leone et al. (1985) is given below, along with an indication of the analogues in the reaction species in the sequence above.

$$\left.\begin{array}{l} \underset{\text{(aromatic unknown)}}{\mathrm{HCOCH{=}CHCHO}} + \mathrm{OH} \rightarrow \mathrm{H_2O} + \mathrm{HCOCH{=}CHCO}\cdot \\[2ex] \mathrm{HCOCH{=}CHCO}\cdot + \mathrm{O_2} \rightarrow \underset{(\mathrm{Aro\text{-}RCO_3})}{\mathrm{HCOCH{=}CHCO{-}O_2}\cdot} \end{array}\right\} \quad \text{(G62)}$$

$$\left.\begin{aligned}
\mathrm{HCOCH{=}CHCO{-}O_2. + NO} &\rightarrow \mathrm{HCOCH{=}CHCO{-}O. + NO_2}\\
\mathrm{HCOCH{=}CHCO{-}O.} &\rightarrow \mathrm{HCOCH{=}CH. + CO_3}\\
\mathrm{HCOCH{=}CH. + O_2} &\rightarrow \mathrm{HCOCH{=}CHOO.}\\
&\quad\ \mathrm{(Aro{-}RO_2)}
\end{aligned}\right] \quad \text{(G63)}$$

$$\begin{aligned}
\mathrm{HCOCH{=}CHCO{-}O_2. + NO_2} &\rightarrow \mathrm{HCOCH{=}CHCO{-}O_2NO_2}\\
&\quad\ \mathrm{(Aro{-}PAN)}
\end{aligned} \qquad \text{(G64)}$$

$$\mathrm{HCOCH{=}CHCO{-}O_2NO_2} \rightarrow \mathrm{HCOCH{=}CHCO{-}O_2. + NO_2} \qquad \text{(G65)}$$

$$\left.\begin{aligned}
\mathrm{HCOCH{=}CHOO. + NO} &\rightarrow \mathrm{HCOCH{=}CHO. + NO_2}\\
\mathrm{HCOCH{=}CHO.} &\rightleftarrows \mathrm{HCOC(.)CHO}\\
\mathrm{HCOC(.)CHO + O_2} &\rightarrow \mathrm{HCOC(OO.)CHO}\\
&\quad\ \mathrm{(Aro{-}R_2O_2)}
\end{aligned}\right] \quad \text{(G66)}$$

$$\left.\begin{aligned}
\mathrm{HCOC(OO.)CHO + NO} &\rightarrow \mathrm{HCOC(O.)CHO + NO_2}\\
\mathrm{HCOC(O.)CHO} &\rightarrow \mathrm{HCOCHO + HCO.} \xrightarrow{O_2} \mathrm{HCOCHO + HO_2 + CO}\\
&\qquad\qquad\qquad\qquad\quad \mathrm{(Aro{-}OH{-}products)}
\end{aligned}\right] \quad \text{(G67)}$$

Atkinson and Lloyd (1984) assume that the OH radical rate constant for H-atom abstraction from -CHO groups in these unsaturated aldehydes is the same per -CHO group, as that for other aldehydes. For 2-butene-1,4-dial and 2-methyl-2-butene-1,4-dial, which have two such groups, they estimate that

$$k_{G62} = 3 \times 10^{-11}\ \mathrm{cm^3\ molecule^{-1}\ sec^{-1}}\ \text{at 298 K.}$$

We use this rate constant for all the the lumped non-α-dicarbonyl aromatic ring-opening products. The temperature dependence for this reaction, which is estimated by Atkinson and Lloyd (1984) to be small and negative, is ignored.

The kinetics of the reactions of NO with the acyl peroxy intermediates (Aro_i-RCO_3) and the peroxy intermediates ($Aro_i-R_1O_2$) and ($Aro_i-R_2O_2$) (e.g., $HCOCH{=}CHCO-O_2\cdot$, $HCOCH{=}CHOO.$, and $HCOC(OO.)CHO$) are assumed to be the same as those for the reactions of NO with other peroxy and acyl peroxy radicals (Section B). In addition, the PAN analogues (Aro_i-PAN) (e.g. $HCOCH{=}CHCO-OONO_2$) are assumed to decompose with the same kinetics as PAN itself, i.e.,

$$k_{G65} = k_{C18} = 2.0 \times 10^{16}\ e^{-26910/RT}\ \mathrm{sec}^{-1}$$

$$= 3.6 \times 10^{-4}\ \mathrm{sec}^{-1} \text{ at } 298 \text{ K.}$$

An alternative route for the reaction of OH radicals with unsaturated 1,4-dicarbonyls is via addition to the double bond, e.g.,

$$\mathrm{HCOCH{=}CHCHO + OH \rightarrow HCOCH(OH)CH(.)CHO \xrightarrow{O_2} HCOCH(OH)CH(OO.)CHO}$$

$$\mathrm{HCOCH(OH)CH(OO.)CHO \xrightarrow{NO} NO_2 + HCOCH(OH)CH(O.)CHO}$$

$$\mathrm{HCOCH(OH)CH(O.)CHO \rightarrow HCOCH(.)OH + HCOCHO \xrightarrow{O_2} 2\ HCOCHO + HO_2}$$

However, this process is neglected in this model for the following reasons: (1) Atkinson and Lloyd (1984) estimated for 2-butene-1,4-dial and its methyl substituted homologues 2-pentene-1-al-4-one and 2-methyl-2-butene-1,4-dial that the addition reaction will occur at only ~15-35% of the rate as the H-atom abstraction reaction, and only for the highly substituted 2-methyl-2-pentene-1-al-4-one is OH radical addition estimated to be faster (by ~33%) than H-atom abstraction; (2) if addition to the double bond is assumed to dominate, the ultimate products formed (as shown above) will be the α-dicarbonyls, with no formation of any PAN analogues such as predicted from the initial H-atom abstraction mechanism. Neglecting the nitrogen sink caused by the PAN analogue in reaction (G64) results in the model predicting maximum ozone yields which are consistently higher than observed in environmental chamber experiments. For example, Figure II-21 show plots of the discrepancy between the observed and calculated maximum ozone yields against the hydrocarbon/NO_x ratio, assuming that the PAN analogue is not a nitrogen sink. (Since this nitrogen sink also represents a radical sink, these calculations were carried out with the product photolysis rate reduced by a factor of two, to better fit the "timing" observed in these experiments. Note, however, that product photolysis is still an important and necessary radical source even when this nitrogen and radical sink is removed.) The results of these calculations plotted in Figure II-21 can be compared with the corresponding plot shown in Figure II-18, which was obtained using the "standard" model in which formation of these PAN analogues in the reactions of the unknown ring-opened products is important. It can be seen that for most experiments the model lacking this nitrogen sink overpredicts the maximum ozone yields to a significantly greater extent than does the standard model.

The ultimate products formed from the reaction of OH radicals with the non-α-dicarbonyl ring-opened species are CO_2 + the species formed in reaction (G67). If 2-butene-1,4-dial is used as the representative compound for these species, these products would then be glyoxal + HCO radical. However, if this is used as the model compound, neither total carbon nor (in the case of the methylbenzenes) methyl groups are conserved. Thus in this model the products formed in reaction (G67) are modified so that both the total number of methyl groups and total carbon are conserved. To conserve methyl groups, part of the glyoxal formed in reaction (G67) is replaced by methylglyoxal, and part of the CO + HO_2 (formed from HCO radicals) are replaced by $CH_3CO_3\cdot$ (formed from $CH_3CO\cdot$ radicals). Since glyoxal has two positions which can be methyl substituted and HCO has one, two thirds of the methyl is asigned to methylglyoxal, and one third is assigned to acetyl radicals. In addition, a sufficient amount of glyoxal is added to the products of this reaction to conserve the number of carbons which were in the aromatic ring.

In the case of benzene, ring opening forms 0.29 glyoxal molecules, and thus the non-α-dicarbonyl product contains 5.42 carbon atoms, and no methyl groups. One of those carbon atoms becomes CO_2 in reaction (G63),

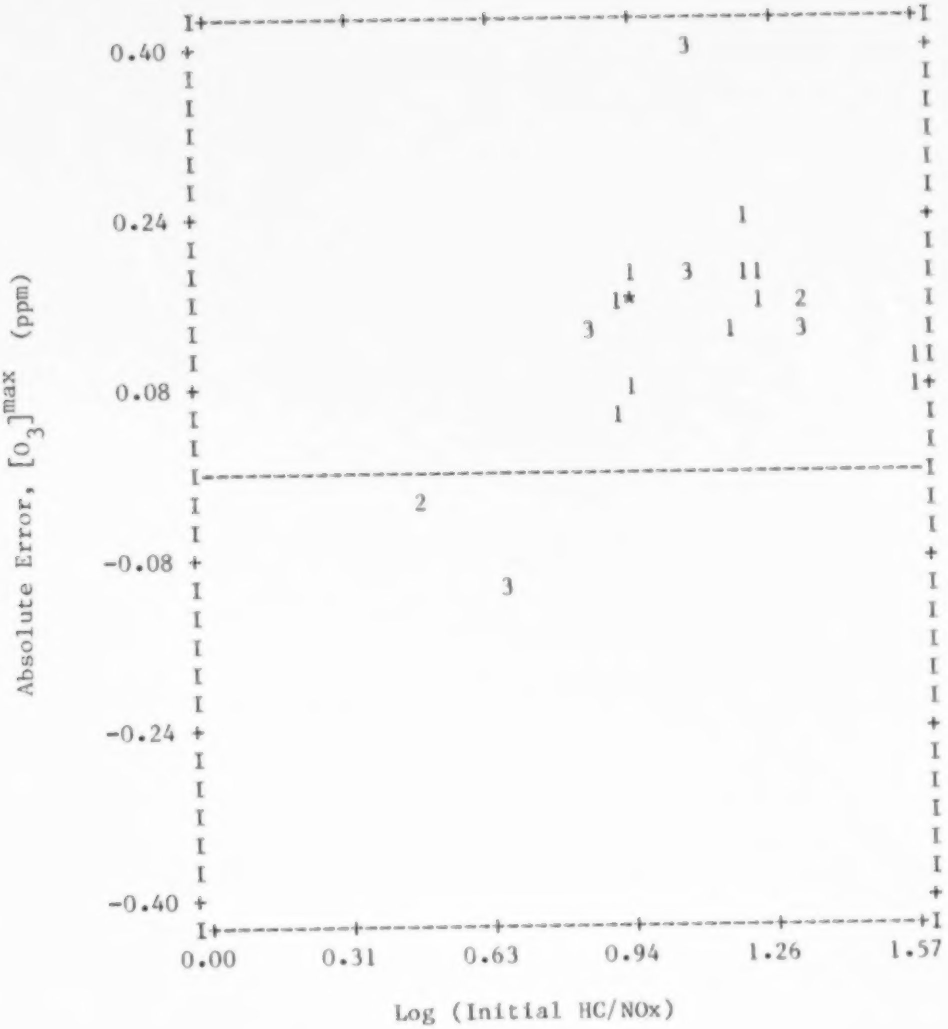

Figure II-21. Plot of calculated-observed maximum ozone concentration in the toluene-NO_x-air irradiations against the log of the initial hydrocarbon/NO_x ratio, where the calculations assumed rapid decomposition of the PAN-analogue formed in the model for the unknown ring-opened products, the product photolysis rates were reduced by a factor of two, compared to the standard model. Chambers employed: 1 = SAPRC EC; 2 = SAPRC ITC; 3 = UNC chamber.

and thus (benzene-OH-products) contains 4.42 carbon atoms. Therefore, to conserve carbon, an additional 0.71 molecules of glyoxal are added to the products of reaction (G67), and thus

$$\text{(Benzene-OH-products)} = 1.71\ HCOCHO + CO + HO_2.$$

In the case of the chemical mechanism for toluene, ring opening forms 0.15 molecules of glyoxal and 0.19 molecules of methylglyoxal, and thus the non-α-dicarbonyl products contain 0.81 methyl groups and 5.32 carbon atoms which were in the aromatic ring. Two thirds of the 0.81 methyl groups appear as 0.54 methylglyoxal, and one third as 0.27 acetyl radicals in the products of reaction (G67). In addition, 0.66 molecules of glyoxal are added to the products to maintain a carbon balance. Hence,

$$\begin{aligned}\text{(Toluene-OH-products)} = {} & 0.54\ CH_3COCHO + 1.12\ HCOCHO + 0.27\ CH_3CO_3\cdot \\ & + 0.73\ (CO + HO_2).\end{aligned}$$

By similar reasoning, the ultimate products formed in the OH reactions of the non-α-dicarbonyl ring-opening products of the xylenes can be derived. These are summarized below:

$$\begin{aligned}\text{(m-Xylene-OH-products)} = {} & 1.07\ CH_3COCHO + 0.41\ HCOCHO + 0.53\ CH_3CO_3\cdot \\ & + 0.47\ (CO + HO_2)\end{aligned}$$

$$\begin{aligned}\text{(o-Xylene-OH-products)} = {} & 0.90\ CH_3COCHO + 0.51\ HCOCHO + 0.45\ CH_3CO_3\cdot \\ & + 0.55\ (CO + HO_2)\end{aligned}$$

In the case of 1,3,5-trimethylbenzene, methylglyoxal cannot be used to represent two-thirds of the methyl groups in the unknown ring-opened products because that quantity is greater than the total α-dicarbonyls in (1,3,5-TMB-products) as determined by the number of aromatic-ring carbons it contains. Thus, for this compound, the maximum methylglyoxal yield allowed by the number of aromatic-ring carbons is used, and a 100% acetyl radical yield is assumed. This accounts for all of the methyl groups and aromatic-ring carbons in the ring-opened products, but unlike the other aromatics, 45%, rather than 33%, of the methyl groups end up in the acetyl radicals. Thus,

$$(1,3,5\text{-TMB-OH-products}) = 1.23\ CH_3COCHO + CH_3CO_3.$$

These product assignments are obviously arbitrary, but in view of our lack of knowledge of the reactions that are actually occurring, they are no less appropriate than any others. It should be noted that because in most experiments the PAN analogue is predicted to be the major product of the reaction of OH radicals with the lumped non-α-dicarbonyl ring-opened products, the model predictions are not particularly sensitive to assumptions concerning the ultimate products formed after the PAN analogue decomposes.

G68i $(Aro_i\text{-}RCO_3) + HO_2 \rightarrow \text{-OOH} + CO_2 + (Aro_i\text{-}RO_2\text{-products})$

G69i $(Aro_i\text{-}RCO_3) + RO_2 \rightarrow 0.5\ HO_2 + CO_2 + (Aro_i\text{-}RO_2\text{-products})$

G70i $(Aro_i\text{-}RCO_3) + RCO_3 \rightarrow 0.5\ HO_2 + CO_2 + (Aro_i\text{-}RO_2\text{-products})$

G71i $(Aro_i\text{-}R_1O_2) + HO_2 \rightarrow \text{-OOH} + (Aro_i\text{-}RO_2\text{-products})$

G72i $(Aro_i\text{-}R_1O_2) + RO_2 \rightarrow 0.5\ HO_2 + (Aro_i\text{-}RO_2\text{-products})$

G73i $(Aro_i\text{-}R_1O_2) + RCO_3 \rightarrow 0.5\ HO_2 + (Aro_i\text{-}RO_2\text{-products})$

G74i $(Aro_i\text{-}R_2O_2) + HO_2 \rightarrow \text{-OOH} + (Aro_i\text{-}RO_2\text{-products})$

G75i $(Aro_i\text{-}R_2O_2) + RO_2 \rightarrow 0.5\ HO_2 + (Aro_i\text{-}RO_2\text{-products})$

G76i $(Aro_i\text{-}R_2O_2) + RCO_3 \rightarrow 0.5\ HO_2 + (Aro_i\text{-}RO_2\text{-products})$

These reactions are included in the model to account for the reactions of HO_2, peroxy, and acyl peroxy radicals with the intermediates formed in the OH + non-α-dicarbonyl ring-opened products. The kinetics of these peroxy and acyl peroxy radical reactions are discussed in Section B.

The representation of the products of these reactions are determined by the principles discussed in Section B, i.e., they are represented by the non-radical products ultimately formed by the reactions of the corresponding alkoxy radicals. Thus, the (Aro_i-RO_2-products) are determined by what is used for (Aro_i-OH-products), except HO_2 is not included, and $CH_3CO_3\cdot$ is replaced by CO_2 + HCHO, the products formed from $CH_3CO_2\cdot$. These are summarized below for the aromatic hydrocarbons in this model:

(Benzene-RO_2-products) = 1.71 HCOCHO + CO

(Toluene-RO_2-products) = 0.54 CH_3COCHO + 1.12 HCOCHO + 0.27 (HCHO + CO_2)
+ 0.73 CO

(m-Xylene-RO_2-products) = 1.07 CH_3COCHO + 0.41 HCOCHO + 0.53 (HCHO + CO_2)
+ 0.47 CO

(o-Xylene-RO_2-products) = 0.90 CH_3COCHO + 0.51 HCOCHO + 0.45 (HCHO + CO_2)
+ 0.55 CO

(1,3,5-TMB-RO_2-products) = 1.23 CH_3COCHO + HCHO + CO_2

b. Photolysis Reactions

G77i. (Aro_i Unknowns) + hν → (Aro_i-phot-products)

These reactions represent the photolysis of the unknown aromatic ring-opened products to form radicals. Although Atkinson and Lloyd (1984) estimated that photodecomposition of the unsaturated 1,4-dicarbonyls, and by analogy the other possible unsaturated carbonyl ring-opening products, should be slow [since acrolein (CH_2=CHCHO) and crotonaldehyde (CH_3CH=CHCHO) are apparently stable under atmospheric conditions (Calvert and Pitts 1966)], it is necessary to assume that these compounds photolyze rapidly in order for the model simulations to even approximately fit the results of the environmental chamber experiments. In particular, if no additional radical source in the aromatics photooxidation mechanism is included in the model, the model significantly underpredicts the overall reactivity observed in the experiments. Exploratory calculations indicated that the best fits to the experimental data are obtained if it is assumed that the additional radical input is due to product photolysis, as opposed to other possibilities such as the reaction of ozone with unsaturated products.

Previous aromatic models (Atkinson et al. 1980, 1982a, Killus and Whitten 1983, Leone and Seinfeld 1984a, Leone et al. 1985) have not had to include any unknown radical sources because those models assumed much higher α-dicarbonyl yields, with the radical initiation from α-dicarbonyl photolysis being sufficient to yield the observed reactivity. We now know that the α-dicarbonyl yields from the aromatic hydrocarbons are much less than assumed in those models, and their photolysis is not sufficient to account for the reactivity observed in aromatic hydrocarbon-NO_x-air environmental chamber experiments. This is particularly true for experiments carried out in the SAPRC ITC, where the spectral distribution of the blacklamp source is such that the photolysis rates of the α-dicarbonyls are much slower than in outdoor chambers or in the SAPRC EC, due to the much lower ITC spectral intensity in the >400 nm α-dicarbonyl absorption region. Even if the high α-dicarbonyl yields assumed in the models of Atkinson et al. (1980, 1982a), Leone and Seinfeld (1984a) and Leone et al. (1985) are used, the model still significantly underpredicts the reactivity observed in experiments carried out in the SAPRC ITC. Aromatic hydrocarbon-NO_x-air experiments carried out in the ITC were not available for use in model testing when these previous chemical mechanisms were developed.

The rate constants for the photolysis of the non-α-dicarbonyl ring-opened products, relative to that for the photolysis of NO_2, were adjusted to fit the results of the benzene-NO_x-air experiments carried out in the SAPRC ITC, and the toluene-NO_x-air, m-xylene-NO_x-air, and 1,3,5-trimethylbenzene-NO_x-air experiments carried out in the SAPRC ITC and in the SAPRC EC. The relative photolysis rates in general depended on both the compound and on the chamber employed, and the approximate "best fit" values obtained are summarized in Table II-33. Because of the greater variability observed when comparing model calculations with results of

Table II-33. Adjusted or Calculated Photolysis Rates for the Lumped Non-α-Dicarbonyl Products Formed from Benzene and Selected Methylbenzenes

Light Source	k_{phot}(arom-unkn)/$k_{phot}(NO_2)$		
	Benzene	Toluene	Di- and Trimethylbenzenes
Adjusted Values			
Blacklights	0.0075	0.05	0.10[a]
SAPRC Solar Simulator	-	0.02	0.05[a]
Calculated Values			
Blacklights	0.0075	0.050	0.100
SAPRC Solar Simulator[b]	0.0038	0.025	0.050
Solar Z=0	0.0051	0.034	0.068
Solar Z=40	0.0048	0.032	0.064
Solar Z=80	0.0035	0.023	0.047

[a] Adjusted to fit m-xylene runs only.

[b] Calculated for the spectral distribution measured around the time of run EC-340. Values will be similar for the other toluene runs and the xylene runs used to derive the adjusted value.

outdoor chamber experiments, these relative photolysis rates were not adjusted to fit the results of the toluene or o-xylene-NO_x-air experiments carried out in the UNC outdoor chamber. However, we found that the results of most of the UNC toluene experiments are satisfactorily fit by the model using the relative photolysis rate adjusted to fit the toluene runs in the SAPRC EC, and the results of most of the UNC o-xylene runs were fit by using the relative photolysis rate which fit the EC m-xylene runs.

The fact that the photolysis rates of the aromatic ring-opening products, relative to the NO_2 photolysis rate, are higher in the SAPRC ITC than in the EC suggests that either (a) this model is invalid, (b) that there is a serious problem with the experimental data or characterization of chamber effects, or (c) that the products involved absorb significantly in the wavelength region where the blacklight light source in the ITC is relatively more intense than the solar simulator light source in the EC.

We assume that (c) is the case. Representative relative spectral distributions of the two light sources, normalized to give the same NO_2 photolysis rate, are plotted together in Figure II-22. (That figure also shows the relative spectral distribution calculated for solar sunlight at a zenith angle of 0^o, for comparison.) It can be seen that the ITC light source is approximately a factor of 2 more intense in the wavelength region centered around 350 nm than is the EC solar simulator light source. If most of the light absorption which results in photodecomposition of the ring-opened products occurs in the 350 nm region or below, then this would account for the apparent difference in photolysis rates of these products in the two chambers.

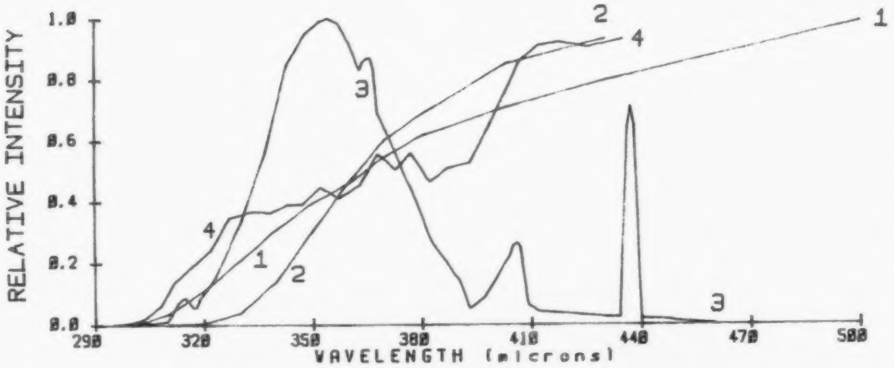

Figure II-22. Representative spectral distributions for various light sources, normalized to give the same NO_2 photolysis rates.

1 = SAPRC solar simulator output, measured around the time of run EC-340.
2 = SAPRC solar simulator output, measured around the time of run EC-900.
3 = SAPRC ITC blacklights output.
4 = Tropospheric solar spectrum for zenith angle of 40^o.

Thus, in this chemical mechanism, we assume that the product of the absorption coefficients and quantum yields for the unknown aromatic are zero above 360 nm, but are constant below 350 nm. The magnitude of [($\lesssim$350 nm absorption coefficient) x (quantum yield)] is determined so that the calculated product photolysis rates in the SAPRC ITC and EC are as close as possible to those which gave the best fits to the experimental data. This assignment is obviously arbitrary, but it yields calculated values which are close to those which yield the best fits to the aromatic-NO_x-air experiments carried out in the SAPRC EC and ITC, without having to use a separate model for each chamber. Use of these values also result in generally acceptable fits of model simulation to the results of the toluene-NO_x-air and o-xylene-NO_x-air experiments carried out in the UNC outdoor chamber. The wavelength dependence of [(absorption coefficient) x (quantum yield)] are summarized in Table II-34 for the lumped non-α-dicarbonyl ring-opening product associated with each of aromatic hydrocarbons (where the products from o- and m- xylene are assumed to have the same photolysis rates), and the calculated values, relative to the NO_2 photolysis rates, for the different chambers and for solar irradiation are given in Table II-33.

Table II-34. [(Absorption Coefficient) x (Quantum Yield)] Assigned for the Lumped Non-α-Dicarbonyl Products formed from Benzene and Selected Methylbenzenes, as a Function of Wavelength

	Absorption coefficient x Quantum yield (cm^2, base e)		
Wavelength Range	Benzene	Toluene	Di- and Trimethylbenzenes
$\lesssim$350 nm	5.93×10^{-21}	3.95×10^{-20}	7.90×10^{-20}
350-360 nm	a	a	a
$\gtrsim$360 nm	0.0	0.0	0.0

[a] Varies linearly from value given for 350 nm to zero at 360 nm.

The products formed in these photodecomposition reactions are obviously unknown, other than that in order to fit the data it must be assumed that radicals are formed. Therefore, these were assigned in a manner similar to that used in assigning the ultimate products of the OH reactions of these lumped ring-opened species, i.e., based on the number of aromatic-ring carbons and methyl groups which are present in these species. In particular, the radical products are represented by HCO. and/or $CH_3CO.$ (i.e., HO_2 + CO and/or $CH_3CO_3.$), and the remainder of the carbon and methyl groups in the photolyzing species are represented by glyoxal and/or methylglyoxal. In terms of assigning methyl groups to glyoxal or acetyl radicals, we found that the best fits to the PAN data are obtained if it assumed that as many of the methyl groups as possible end up as acetyl radicals in the photolysis reaction, so this is assumed in the model. [The PAN yields are much more sensitive to the assumptions concerning the acetyl yield in the photolysis reactions than to their assumed yield in reaction (G67), because for PAN to be formed via reaction (G67), the PAN analogues (Aro_i-PAN) must first undergo decomposition. Under conditions where PAN builds up, (Aro_i-PAN) will also build up, and relatively little of it will decompose.] Based on these assumptions, the following assignments for (Aro_i-phot-products) are derived:

(Benzene-phot-products) = 1.71 HCOCHO + 2 (HO_2 + CO)

(Toluene-phot-products) = 1.66 HCOCHO + 0.81 $CH_3CO_3.$ + 1.19 (HO_2 + CO)

(m-Xylene-phot-products) = 1.48 HCOCHO + 1.68 $CH_3CO_3.$ + 0.32 (HO_2 + CO_2)

(o-Xylene-phot-products) = 1.41 HCOCHO + 1.35 $CH_3CO_3.$ + 0.65 (HO_2 + CO_2)

(1,3,5-TMB-phot-products) = HCOCHO + 0.23 CH_3COCHO + 2 $CH_3CO_3.$

These are obviously arbitrary, but in view of our lack of knowledge about the actual reactions occurring, it is not clear which, if any, alternatives would be better.

c. Other Reactions

G78i (Aro$_i$ unknowns) + O_3 → products

G79i (Aro$_i$ unknowns) + NO_3 → products

Atkinson and Lloyd (1984) gave estimates for the rate constants for the possible reactions of O_3 and NO_3 radicals with unsaturated 1,4-dicarbonyls. If these estimates are representative of the actual non-α-dicarbonyl ring-opening products formed, then these reactions can be neglected. Thus we assume that

$$k_{G78} = k_{G79} = 0$$

for all of the aromatic hydrocarbons.

As discussed above, to fit the results of environmental chamber experiments it is necessary to assume additional radical sources in the aromatic photooxidation mechanism. Because of this, exploratory calculations were carried out in order to determine whether the additional radical initiation could be due to a reaction of ozone with some of the unsaturated ring-opened products, rather than from the photolysis of these products. The results of these calculations did not yield acceptable fits to the results of the chamber experiments, even when k_{G78} was treated as an adjustable parameter. Based on this, we conclude that reaction of ozone with unsaturated aromatic ring-opened products probably does not contribute significantly to the radical input in the photooxidations of the aromatics, and no such reaction is included in this model.

SECTION III

CHAMBER AND LIGHT INTENSITY CHARACTERIZATION

In this section, the derivations of the parameters used to specify light intensity, wall effects and other chamber-dependent effects required to test the model against environmental chamber data are discussed. The specific chambers whose characterization is discussed here are the UNC outdoor chamber, the SAPRC evacuable chamber (EC), the SAPRC indoor Teflon chamber (ITC), and the SAPRC outdoor Teflon chamber (OTC). However, much of this discussion can also be applied to modeling data from other chambers to the extent that they have characteristics in common with these four chambers. The major features of these chambers are summarized below.

The UNC Outdoor Chamber. This chamber consists of a rigid "A"-frame structure which supports sheets of 5-mil thick FEP Teflon film, with an additional sheet of Teflon film to divide the chamber into two equal sides, thus allowing two experiments to be carried out at the same time. Each side of the chamber has a volume of approximately 150,000 liters, which makes it the largest of the four chambers from which data were employed in this program for chemical mechanism testing. Since it is an outdoor chamber, natural sunlight is used as the light source, and there is no provision for covering the chamber. In order to enhance the light intensity in the chamber, a reflective material is located under the Teflon film on the chamber floor. On the night before a typical experiment, each side of the chamber is flushed with unpurified, but relatively clean, rural air. (The chamber is located in a rural area of North Carolina, some distance from the University of North Carolina campus.) For most experiments, except for some "dynamic" runs, the reactants are injected prior to sunrise, and thus the irradiation begins when the sun rises. The characteristics and operating procedures for this chamber are discussed in detail by Jeffries et al. (1982, 1985a-d).

The SAPRC Evacuable Chamber. This 5800-liter indoor chamber consists of a cylindrical aluminum alloy shell whose interior is coated with FEP Teflon and whose ends consist of a Teflon-coated grid structure supporting sixteen 33 cm square quartz windows. This chamber has Teflon-coated aluminum walls and quartz windows, and thus has a different type of surface than the other three chambers whose data are employed in this program, which are all constructed of Teflon film. In addition, it is the only chamber of the four which is evacuable and thermostatted. The light source consists of a 25 KW Xenon arc "solar simulator" which is designed to simulate the deep space solar spectrum in the 300-340 nm region (Beauchene et al. 1973). In order to more accurately simulate sunlight in the lower troposphere, its output is filtered by Pyrex panes to eliminate UV radiation below 290 nm. Pure air for this chamber is provided with an air purification system designed to remove oxides of nitrogen and non-methane organics (Doyle et al. 1977). The chamber is generally evacuated between experiments, and then filled with humidified purified air prior to injection of the reactants. The reactants are mixed by fans contained in the chamber, which are turned off during the irradiations. The irradiation is begun by removing a baffle from in front of the solar simulator, which is allowed to warm up prior to the irradiation to assure a constant light intensity. During the experiments, pure air is used to replace the air removed from the chamber for the purpose of sampling. This facility, and the operating procedures employed, have been described in detail previously (Pitts et al. 1979, Winer et al. 1980).

The SAPRC Indoor Teflon Chamber. This 6400-liter chamber consists of a flexible 2-mil thick FEP Teflon reaction bag fitted inside an aluminum frame of dimensions 8 ft x 8 ft x 4 ft, with one end hinged so the chamber can be collapsed to less than one-fifth its maximum volume. The reaction bag is periodically replaced to avoid buildup of contaminants, and it is also replaced between programs employing different types of experiments. The flexible nature of this reactor means that, unlike the UNC chamber or the SAPRC EC (but like the SAPRC OTC discussed below), experiments can be carried out without dilution due to sample withdrawal. The light source consists of two arrays of blacklights, backed with reflectors, on each side of the chamber. Purified air is supplied by the same air purification system which supplies the SAPRC EC. The reactor is generally flushed, or filled and emptied, with humidified purified air between experiments. After the final fill the reactants are injected and mixed (by fans inside the chamber, which are turned off prior to the irradiation), and the irradiation is initiated by turning on the blacklights. The facility and the procedures employed are described in more detail elsewhere (Carter et al. 1984, 1985).

The SAPRC Outdoor Teflon Chamber. This chamber consists of a flexible ~40,000 to ~60,000-liter pillow-shaped reaction bag constructed of 2-mil thick Teflon film which is held in place on a metal frame by rope netting. The chamber can optionally be divided into two equal halves to allow for simultaneous irradiation of two different reaction mixtures. As with the SAPRC ITC, the reaction bag is replaced periodically (in this case primarily because after one to two months of use it becomes worn and leaks excessively), and its flexible nature means that experiments can be carried out without dilution caused by sample withdrawal. (Leakage of the chamber manifests itself by an excessive rate of reduction of the chamber volume, and not by dilution, because the weight of the netting on the chamber tends to force its contents out.) The chamber can be flattened completely to remove all of its contents at the end of an experiment. Lighting is provided by natural sunlight; but, unlike the UNC outdoor chamber, the chamber is covered by an opaque material between experiments, during the fill and injection procedures, and for "dark" runs. Purified, dry air is provided by an AADCO air purification system, which removes NO_x and non-methane organics. Between experiments, the chamber is filled and flushed with pure dry air, and the reactants are injected while the chamber is covered and thus in the dark. Irradiations are begun, generally around 0900 PST, by removing the chamber cover, and the runs are generally terminated at 1500 PST. In most multi-day runs, particularly those carried out in divided mode, the chamber is covered at 1500 PST and uncovered at 0900 PST the following morning. This is done to avoid differential irradiation of the halves of the divided chamber when the sun is at a very low angle in the early morning or the late evening. The facility and procedures employed for this chamber are discussed in more detail elsewhere (Carter et al. 1984, 1985).

A number of chamber-dependent parameters need to be considered when carrying out computer model simulations of environmental chamber experiments. The specific parameters and effects which we have considered and which are incorporated in our model simulations are the following: (1) light characterization, including both intensity and spectral distribution, and how they vary with time in outdoor experiments; (2) chamber-dependent and heterogeneous radical sources; (3) offgassing of NO_x and other species from the walls; (4) wall loss of ozone and other surface-sensitive species; (5) other heterogeneous reactions; (6) dilution rates; and (7) characterization of temperature and humidity, and (where applicable) how they vary with time. All of these aspects are discussed in this section, together with specific indications of how they are represented in our model calculations.

Although the physical and chemical processes represented by the various chamber-dependent parameters are generally complex, our goal has been to represent them as simply as possible without knowingly omitting any known and non-negligible effects. This procedure was employed because the testing of homogeneous reaction mechanisms for use in ambient air simulations is greatly expedited if the chamber effects model is not overly complex, and has no more adjustable parameters than absolutely necessary. Thus in cases where it does not affect conclusions regarding the overall trends and patterns obtained by comparing the results of calculations to experimental data for the complete data set, parameters which are known to vary from run-to-run are assumed to be constant. Furthermore, some processes are represented by fewer parameters or otherwise simplified compared to their representation in models which are designed to give optimum fits of calculation to results of individual experiments. Because of the large data set now available (see Section IV), such "fine tuning" for individual runs to obtain the closest fits possible is no longer necessary for determining whether or not a particular homogeneous reaction mechanism is consistent with the available data.

III. A. LIGHT CHARACTERIZATION

The appropriate specification of the rates of the photolysis reactions in environmental chamber simulations is clearly very important, since it is these reactions that supply the energy to drive the chemical transformations which the model is attempting to simulate. For both indoor and outdoor chamber simulations, photolysis rate constants were calculated using the following equation,

$$k^{phot}(t) = \sum_{\lambda} J(\lambda,t)\ \sigma(\lambda)\ \phi(\lambda) \qquad \text{(I)}$$

where $k^{phot}(t)$ is a photolysis rate constant at time t, $J(\lambda,t)$ is the intensity, at time t, of the light source in a wavelength region centered at wavelength, λ, and $\sigma(\lambda)$ and $\phi(\lambda)$ are the absorption coefficient for the photolyzing species and the quantum yield for the photolysis reaction over that wavelength region. For each photolysis reaction, the values of the absorption coefficients and quantum yields employed are summarized in various tables given in Section II, as part of the documentation of the homogeneous reaction mechanism. However, the values $J(\lambda,t)$, which are determined by the intensity and spectral distribution of the light source, are chamber dependent and in general vary from experiment to experiment. In this section, the derivation of these values for each of the four chambers, and for the specific experiments carried out in each chamber, are discussed.

1. Indoor Chambers

The characterization of the light intensity and spectral distribution for the SAPRC ITC and EC are similar, and so they are discussed together. In both cases, the light intensity and spectral distribution are assumed to be constant throughout a given experiment; in no indoor experiment modeled in this program was the light intensity deliberately varied as part of the experiment, nor is there any evidence for significant variation of light intensity or spectral characteristics during an experiment for the SAPRC EC or ITC runs modeled here. Thus in modeling these indoor chamber runs, all photolysis rate constants were calculated prior to the beginning of the computer simulation, and were held constant after that. However, since the light intensity and (for the EC) the spectral distribution varied from run-to-run, in general a different set of photolysis rate constants were used for each experiment.

a. Light Intensity

For both chambers, NO_2 actinometry experiments are carried out at periodic intervals, and for each experiment modeled in this program, an NO_2 photolysis rate constant (i.e., a k_1 value) was assigned at the time the results were initially reported. Based on the run-to-run variability of the k_1 measurements, we estimate that these values probably have an uncertainty of approximately 10% for both chambers, with the possible exception of some individual runs which appear anomalous (see discussion of fits of model calculations to the experimental data in Section IV).

In order to determine whether this uncertainty in the light intensity measurements could be a factor to be considered in assessing the quality of fits of model calculations to the experimental data, sensitivity calculations were carried out in which all EC propene-NO_x-air, n-butane-NO_x-air and toluene-NO_x-air runs were simulated with the light intensity increased by 15%. In these sensitivity studies the radical input rates and other chamber-dependent parameters were not changed. Figure III-1 shows plots of the changes in the calculated ozone maximum yields, against the calculated maximum ozone yields, caused by increasing the light intensity by 15%, while Figure III-2 shows similar plots for the parameter which measures the times required to oxidize a given amount of NO, as defined in Section IV-B. It can be seen that for most runs the calculated changes in both these measures of reactivity caused by a 15% change ranges between 5 and 10%. The outlier among the toluene runs on the plot of the ozone change is the toluene run with added benzaldehyde (run EC-339), for which increasing the light intensity caused a 15% change in maximum ozone. Benzaldehyde is unusual in that it is a very efficient radical and NO_x sink when it reacts with OH radicals, and the greater sensitivity of the calculated ozone maximum to light intensity for the run with added benzaldehyde is probably related to this fact, though the exact reason has not been investigated. (Note that the change in the parameter measuring

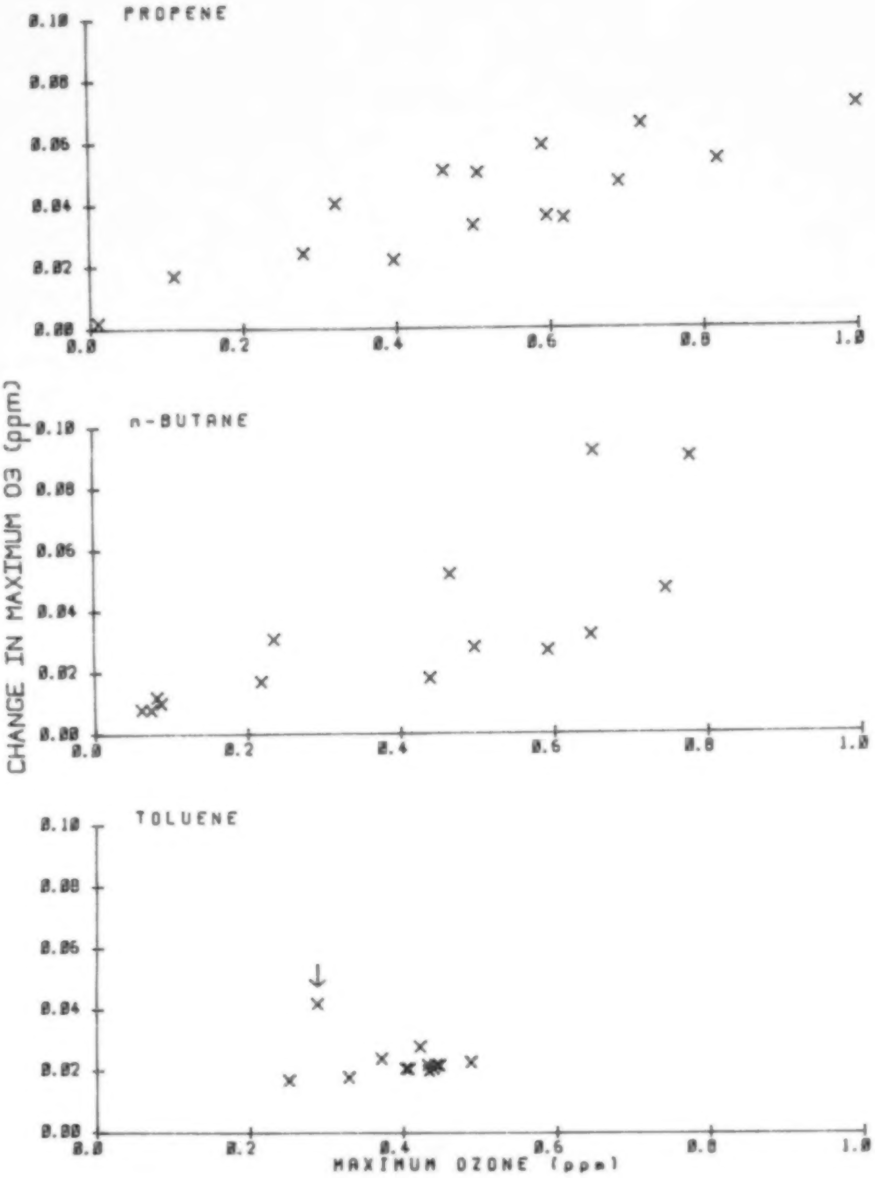

Figure III-1. Plots of changes in calculated maximum ozone yields, caused by increasing the light intensity by 15%, against calculated maximum ozone yields for model simulations of the propene-NO_x-air, n-butane-NO_x-air and the toluene-NO_x-air runs carried out in the SAPRC EC.

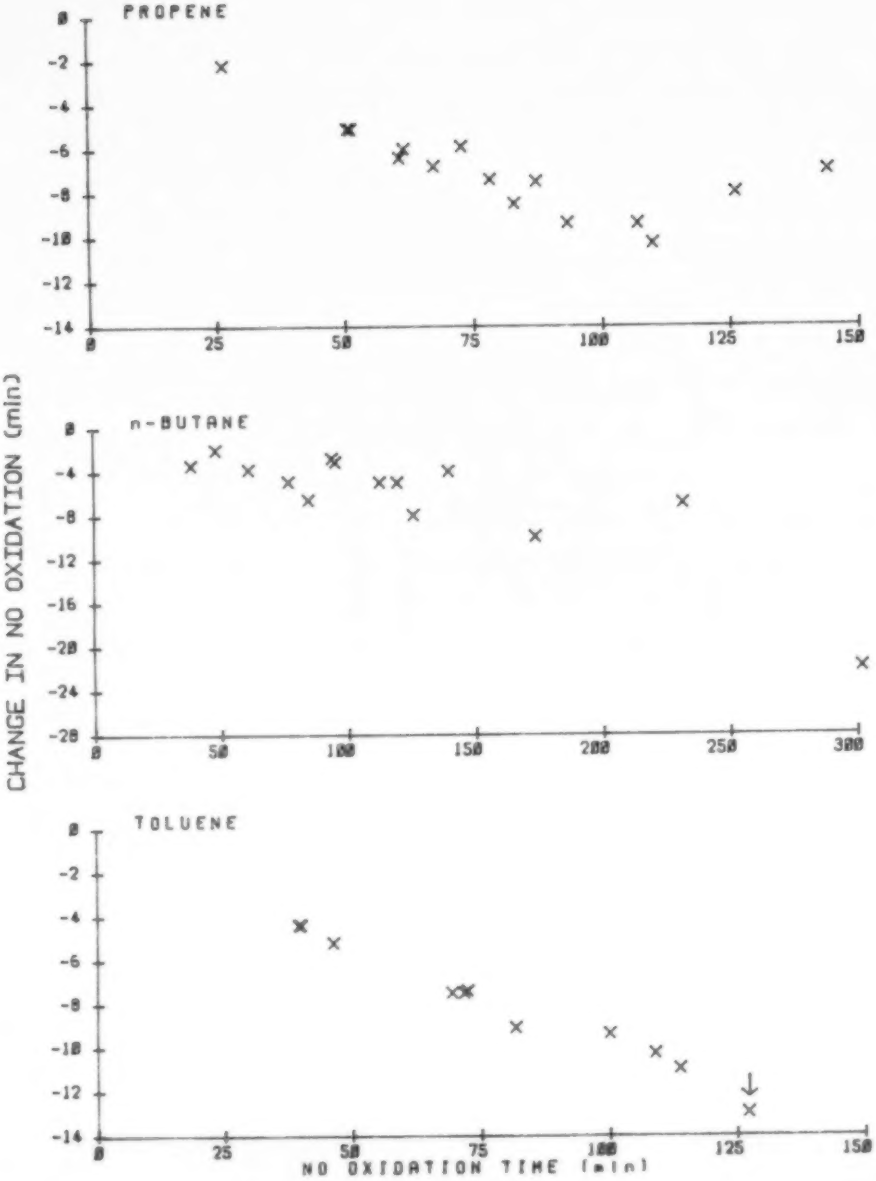

Figure III-2. Plots of changes in calculated times required to achieve one-half the maximum experimental increase in the quantity ($[O_3]-[NO]$), caused by increasing the light intensity by 15%, against the values calculated by the standard model, in model simulations of the propene-NO_x-air, n-butane-NO_x-air and the toluene-NO_x-air runs carried out in the SAPRC EC.

NO oxidation rates is in line with that observed in the other toluene runs -- see arrow on Figure III-2.) However, for most runs the estimated 10% uncertainty in the light intensity corresponds to a less than 10% uncertainty in these calculated measurements of reactivity, and hence this uncertainty does not present a significant problem in the characterization of the data for model testing purposes.

b. Spectral Distribution

The ratios of all the other photolysis rate constants to the k_1 values are determined by the spectral distribution of the light source. For the SAPRC EC runs modeled in this program, the general practice at the time the runs were carried out was to measure the relative spectral distribution during each experiment, and to report these data in the detailed data tabulations. The spectral distributions were measured using a monochromator - photomultiplier system as described by Pitts et al. (1979), which gives relative intensities only. For runs carried out around the same time and with the same lamp, essentially the same spectral distribution is observed, although there is some run-to-run variability of a random nature, which can be attributed to instrumental variability. However, over longer periods of time, systematic changes in the spectral distribution do occur, and thus it is not appropriate to assume the same spectral distribution for all EC runs. In particular, in recent years there has been a steady degradation in the intensity in the near-UV region compared to the visible region, which means that the ratio of the photolysis rates of, for example, formaldehyde or ozone [yielding $O(^1D)$ atoms] to that for NO_2 would decrease.

Thus, based on the above considerations, the spectral distributions of the EC runs modeled in this program were established as follows: all EC runs were assigned to groups based upon the time period in which they were carried out (and upon when the solar simulator lamps were changed), such that the spectral distribution for all runs within each group can be considered identical to within the random run-to-run variability, and an average spectral distribution for each group was calculated. The average spectral distribution for a group was then assumed to apply to all runs within the group. The spectral distribution grouping, and the relative spectral distributions for each group, are given in Table III-1. This table shows how the spectral distribution for the EC has changed over the years.

The spectral distribution for the ITC, which uses blacklamp irradiation, is measured much less frequently. Fortunately, it varies to a much smaller extent than is the case for the EC, since whenever the spectral distribution of the ITC is measured, essentially the same results are obtained. The most detailed spectral distribution measurement for the ITC around the time of most of the experiments to be modeled in this program was carried out on June 30, 1983, and the results are given in Table III-2.

The spectral distributions tabulated in Tables III-1 and III-2 are such that the actual measured distributions are reasonably well approximated by the curves generated by drawing straight line segments connecting each of the tabulated points. This is the method used by the software modules which calculate the photolysis rate constants for indoor chamber runs. More points are given for the ITC spectral distribution in Table III-2 than for the EC spectral distributions in Table III-1 because the blacklight spectrum has more sharp features in the spectral region of importance than has the xenon lamp in the SAPRC solar simulator. For the xenon lamp the sharp features are confined to the longer wavelength region where they are of no importance.

2. Outdoor Chambers

Both the UNC outdoor chamber and the SAPRC OTC use natural sunlight as the light source, and thus the light intensity and spectral distribution will vary with time, depending on the solar zenith angle, the cloud cover, and other meteorological conditions. For these runs, the light intensity and spectral distribution, and thus the photolysis rate constants, are re-calculated for each time step of the integration. The spectral distribution and intensity used in modeling the outdoor chamber runs are derived as discussed in this section.

Table III-1. Summary of Average Relative[a] Spectral Distributions Used in Modeling SAPRC Evacuable Chamber (EC) Experiments

Run Nos.	Wavelength (nm)												
	290	300	310	320	330	340	350	360	370	380	403	430	500
106	0.001	0.039	0.146	0.357	0.572	0.789	1.000	1.119	1.239	1.316	1.425	1.557	1.618
113-116	0.002	0.034	0.128	0.318	0.533	0.758	1.000	1.172	1.338	1.467	1.682	1.921	2.154
120-125	0.000	0.047	0.121	0.292	0.532	0.767	1.000	1.165	1.291	1.406	1.551	1.736	1.788
142-160	0.000	0.018	0.082	0.238	0.464	0.706	1.000	1.214	1.417	1.605	1.892	2.092	2.419
161-172	0.000	0.016	0.077	0.222	0.449	0.705	1.000	1.189	1.451	1.715	2.107	2.334	2.874
177-178	0.001	0.031	0.167	0.379	0.627	0.837	1.000	1.093	1.241	1.371	1.598	1.771	2.134
216-217	0.000	0.023	0.137	0.347	0.608	0.828	1.000	1.089	1.228	1.344	1.534	1.633	1.587
230-233	0.000	0.024	0.131	0.327	0.593	0.810	1.000	1.168	1.316	1.459	1.753	1.939	2.152
237-257	0.001	0.016	0.110	0.289	0.528	0.773	1.000	1.170	1.418	1.634	1.970	2.350	3.147
264-287	0.001	0.018	0.122	0.316	0.565	0.787	1.000	1.117	1.275	1.396	1.502	1.625	1.688
304-309	0.000	0.020	0.125	0.314	0.558	0.798	1.000	1.131	1.309	1.454	1.602	1.756	1.939
314-320	0.001	0.019	0.131	0.369	0.695	0.970	1.000	1.348	1.557	1.691	1.804	1.915	1.861
327-331	0.000	0.003	0.095	0.283	0.517	0.788	1.000	1.142	1.342	1.486	1.691	1.878	2.167
334-340	0.000	0.000	0.093	0.280	0.525	0.783	1.000	1.161	1.382	1.549	1.778	1.998	2.474
343-346	0.000	0.008	0.106	0.284	0.531	0.775	1.000	1.149	1.359	1.530	1.729	1.941	2.277
389-392	0.000	0.004	0.099	0.272	0.529	0.782	1.000	1.173	1.400	1.587	1.817	2.110	2.684
435-465	0.000	0.000	0.083	0.260	0.521	0.773	1.000	1.189	1.366	1.521	1.699	1.898	2.459
596-603	0.000	0.000	0.044	0.208	0.450	0.732	1.000	1.210	1.458	1.734	2.069	2.457	3.187
898-903	0.000	0.000	0.000	0.018	0.122	0.454	1.000	1.520	1.968	2.234	2.766	3.034	3.596

[a] Normalized to give 1.0 at 350 nm.

Table III-2. Relative Spectral Distribution for the Blacklights in the SAPRC 6400-Liter Indoor Teflon Chamber[a]

Wavelength (nm)	Intensity[b]	Wavelength (nm)	Intensity[b]	Wavelength (nm)	Intensity[b]
295.7	0.0	347.8	0.952	405.0	0.258
296.7	0.0019	350.0	0.972	406.0	0.264
298.0	0.0024	351.7	0.990	406.7	0.251
300.7	0.0018	353.7	1.00	408.7	0.0596
302.1	0.0043	356.7	0.982	412.0	0.0387
304.3	0.0058	360.0	0.925	416.7	0.0348
306.3	0.0057	363.3	0.829	423.3	0.0298
310.0	0.0140	364.3	0.859	430.0	0.0227
313.0	0.0728	364.7	0.869	434.3	0.0217
313.7	0.0846	365.5	0.870	436.1	0.641
315.0	0.0879	366.9	0.835	436.7	0.709
315.3	0.0856	368.5	0.685	437.3	0.712
316.7	0.0581	370.0	0.639	438.1	0.651
317.3	0.0564	376.7	0.442	439.7	0.0169
318.7	0.0858	383.3	0.261	443.3	0.0140
323.3	0.1495	390.0	0.1423	450.0	0.0081
330.0	0.331	396.7	0.0885	460.0	0.0
336.7	0.563	393.0	0.0535		
343.3	0.851	404.3	0.223		

[a] As measured on June 30, 1983

[b] Intensity in terms of photons per unit area per unit time, normalized so the maximum intensity = 1.0 units.

The light intensities, $J(\lambda,t,g)$, used in calculating the photolysis rate constants for modeling outdoor chamber experiments are calculated as a function of wavelength (λ), time of day (t), and run group (g) according to the equation:

$$J(\lambda,t,g) = J_0(\lambda,z[t']) \left\{ \frac{f(g)\ UV(t)}{UV_0(z[t'])} \right\} \qquad \text{(II)}$$

where $z[t']$ is the solar zenith angle at time t', which is our best estimate of the true solar time at time t of the experiment, $J_0(\lambda,z[t'])$ is the theoretically-calculated clear-sky light intensity for the wavelength region associated with wavelength λ, UV(t) the experimental UV radiometer reading taken at time t during the experiment, $UV_0(z[t'])$ is the theoretically calculated clear-sky UV radiometer reading for z[t'], and f(g) is a correction factor applied to all UV data for each group of runs. The clear-sky light intensities, J_0, were calculated according to the equation:

$$J_0(\lambda,z[t']) = A(\lambda)\ e^{-B(\lambda)\sqrt{\frac{1 + E(\lambda)}{\cos(z[t'])^2 + E(\lambda)}}} \qquad \text{(III)}$$

where the wavelength-dependent parameters A, B, and E were derived to fit the actinic irradiances tabulated by Peterson (1976) for his "best estimate" surface albedos. These parameters are summarized in Table III-3, which also shows the wavelength intervals used in calculating $J(\lambda)$ and thus the photolysis rates.

It should be noted that the true solar times, t', are not necessarily the same as the times, t, associated with the data points. Theoretically, the difference between t and t' should be constant and depend only on the longitude of the chamber and whether or not standard or daylight savings time is being used. (The UNC chamber always uses daylight savings time, while the SAPRC OTC always uses standard time.) However, it appears that at neither facility are the clocks always accurate; and in practice, the value of (t-t') has to be adjusted in order that the calculated and the theoretical UV [and total solar radiation (TSR)] curved shapes will agree. [In the case of the UNC chamber, the UNC researchers have commented that on occasion they did find the clock on their data acquisition system to be off by as much as 20-30 minutes (Jeffries, private communication), and this is consistent with our findings for runs carried out during certain periods.] Except for a few runs in 1979, when the UNC TSR instrument was known to be malfunctioning, the (t-t') values which fit the UNC UV data also fit the TSR data. Hence the need for this adjustable time offset is unlikely to be due to instrument malfunction. As expected, the time offsets did not vary randomly from run-to-run, but were generally the same for runs carried out around the same time period. For a few runs the light quality was so poor that it was not possible to determine (t-t') using the light intensity data, and those runs were assumed to have the

Table III-3. Parameters[a] Used for Calculating Theoretical Actinic Irradiances for Clear-Sky Conditions and Spectral Response Factors for Eppley UV Radiometers for Given Wavelength Intervals

Wavelength Range (nm)	10^{-17} x A (cm^{-2} min^{-1})	B	E	10^{17} x UV Response (cm^2, base e)
295-300	0.471	5.253	0.046	0.67
300-305	0.498	3.037	0.044	2.13
305-310	0.613	1.981	0.043	3.69
310-315	0.733	1.354	0.035	5.52
315-320	0.754	1.057	0.034	7.64
320-325	0.806	0.896	0.034	9.20
325-330	1.04	0.791	0.032	10.19
330-335	1.03	0.722	0.030	10.83
335-340	0.968	0.671	0.027	11.08
340-345	1.00	0.634	0.025	11.10
345-350	0.975	0.605	0.023	10.89
350-355	1.08	0.578	0.020	10.65
355-360	0.969	0.556	0.018	10.37
360-365	1.05	0.533	0.016	9.52
365-370	1.26	0.513	0.015	8.13
370-375	1.12	0.495	0.013	6.06
375-380	1.22	0.476	0.011	3.33
380-385	0.996	0.458	0.010	1.17
385-390	1.08	0.443	0.009	0.19
390-395	1.10	0.429	0.008	0.0
395-400	1.31	0.414	0.007	
400-405	1.56	0.409	0.007	
405-410	1.73	0.394	0.005	
410-415	1.81	0.384	0.005	
415-420	1.81	0.372	0.004	
420-430	3.5	0.357	0.003	
430-440	3.54	0.339	0.002	
440-450	4.06	0.326	0.002	
450-460	4.60	0.324	0.002	
460-460	4.66	0.312	0.001	
470-480	4.72	0.301	0.001	
480-490	4.64	0.292	0.0	
490-500	4.62	0.285	0.0	
500-510	4.80	0.290	0.0	
510-520	4.69	0.285	0.0	
520-530	4.75	0.282	0.0	
530-540	4.75	0.281	0.0	
540-550	4.66	0.278	0.0	
550-560	4.71	0.280	0.0	
560-570	4.75	0.279	0.0	
570-580	4.85	0.280	0.0	
580-600	9.80	0.273	0.0	

(continued)

Table III-3 (continued) - 2

Wavelength Range (nm)	10^{-17} x A (cm^{-2} min^{-1})	B	E	10^{17} x UV Response (cm^2, base e)
600-620	9.94	0.273	0.0	
620-640	9.83	0.258	0.0	
640-660	10.0	0.251	0.0	
660-680	10.2	0.245	0.0	
680-700	10.0	0.236	0.0	
700-1000[b]	151.	0.236	0.0	

[a] Parameters used in equation (II) to calculate J_0.
[b] Spectral distribution assumed constant for wavelengths beyond 700 nm for the purpose of calculating photolysis rates.
[c] Normalized to yield the theoretically expected UV radiometer value of 65.7 millilangleys at z=0.

same time offset as observed in runs carried out at around the same time.

The experimentally measured UV data are used to take into account local meteorological factors which would affect the light intensity. Although in general one would expect the meteorological factors also to affect the spectral distribution, the present data are not adequate to characterize this effect, so this was not taken into account. For the UNC runs, the UV data rather than the TSR data were used to correct the light intensity because the UV instrument is believed to be more responsive to changes in the wavelength region of most importance in determining most photolysis rate constants. In addition, TSR data are not available for the SAPRC OTC runs modeled in this program, so use of UV data allows a consistent method for deriving light intensities for both chambers. {For some SAPRC OTC experiments, k_1 data are available; but these are not used because (1) The UV data are more precise and taken more frequently; (2) usable k_1 data are not available for some of the OTC runs and all of the UNC runs modeled in this program; and (3) for the runs where good k_1 data are available, the UV measurements taken at the same time are consistent with them [see Carter et al. (1985) for a more complete discussion of these data.]}

The theoretical UV readings, UV_0, are calculated according to the formula

$$UV_0(z[t']) =$$

$$f_U\ [(1-f_{dir}) + f_{dir}\cos(z[t'])]\ \sum_\lambda[J_0(z[t']) * R(\lambda)] \qquad \text{(IV)}$$

where the summation is over all wavelength intervals to which the UV radiometer responds, $R(\lambda)$ are the relative response factors for the instrument, f_U is a scaling factor obtained as described below, and f_{dir} is an empirical parameter representing the fraction of light reaching the detector due to direct, rather than scattered, radiation.

The empirically-derived parameter f_{dir} was adjusted to yield the best fit to the experimental UV curve shapes for runs carried out under clear-, or near clear-sky conditions. Although the value of f_{dir} which gives the best fit to the curve shapes varied somewhat from run to run, most of the data are acceptably fit using

$$f_{dir} = 0.7, \qquad \text{(V)}$$

and this value was used in all the model simulations of outdoor chamber experiments.

The relative response factors, $R(\lambda)$, were taken from the plots given in the calibration data sheet for the UNC UV instrument given to the UNC researchers after its latest calibration by Eppley Laboratories, Inc., and incorporate both the relative spectral response of the photocell and the transmission spectrum of the filter, which were given in separate plots. No such data are available for the SAPRC UV instrument, but since it is the same make and model as the one employed at UNC, we assume that it has the same spectral response. This assumption is supported by the fact that the fits of the calculated to observed curve shapes for the UV data for clear-sky SAPRC OTC runs are of the same quality as the fits for clear-sky UNC runs. The response factors as a function of wavelength are summarized in Table III-3, above.

The response factors summarized in Table III-3 incorporate the scaling factor, f_U, which was derived such that the calculated UV response for a zenith angle of zero is the empirically expected value of 65.7

millilangleys. This value of 65.7 millilangleys is derived from empirical k_1 vs. UV relationships and theoretically calculated k_1 values. Empirical relationships between simultaneous UV and k_1 measurements have been obtained by a number of researchers, with generally consistent results. For example, for a zenith angle of 0, the relationship reported by Zafonte et al. (1977) yields a UV/k_1 ratio of 142 millilangley-min, and the relationship derived from the results of simultaneous UV and k_1 measurements carried out at SAPRC (Carter et al. 1984a) yield a z=0 ratio of 159 millilangley-min. This is within experimental uncertainty of the Zafonte et al. (1977) value, which we use. The z=0 NO_2 photolysis rate calculated using the theoretical actinic irradiances, J_0, derived as described above, and using the NO_2 absorption coefficients and quantum yields given in Table II-1, is 0.46 min^{-1}. This value, when combined with the z=0 UV/k_1 ratio derived by Zafonte et al. (1977), yields the "theoretical" z=0 UV value of 65.7 millilangleys.

For the purpose of comparing the clear-sky light intensities observed in the outdoor chamber experiments with the theoretically expected values, an extrapolated z=0 UV reading is calculated from the UV data obtained from that run by (a) finding a scaling factor, f_U, such that UV readings calculated using equation (IV) agree with the experimental clear-sky UV measurements reported for that run, and then (b) using that adjusted f_U value, and equation (IV), to calculate the UV reading expected for z=0. These z=0 UV readings extrapolated from the data of the various runs, referred to here as the "UV factors" for the runs, are plotted against the day of the year in Figure III-3.

It can be seen that the clear-sky UV data for the SAPRC OTC and the more recent UNC chamber experiments are reasonably consistent with the theoretical UV value of 65.7 millilangleys. However, there is considerable day-to-day variability in overall clear-sky light intensities, and the UNC UV readings for the years prior to 1982 appear to be anomalously low. Figure III-3 also indicates that there is a consistent tendency for the overall light intensity to be higher later in the year, both in California and in North Carolina.

For the purpose of modeling the UNC runs carried out prior to 1982, where the UV data appear to be systematically low, the UV readings are corrected by a factor given by the ratio of the average of the UV factors

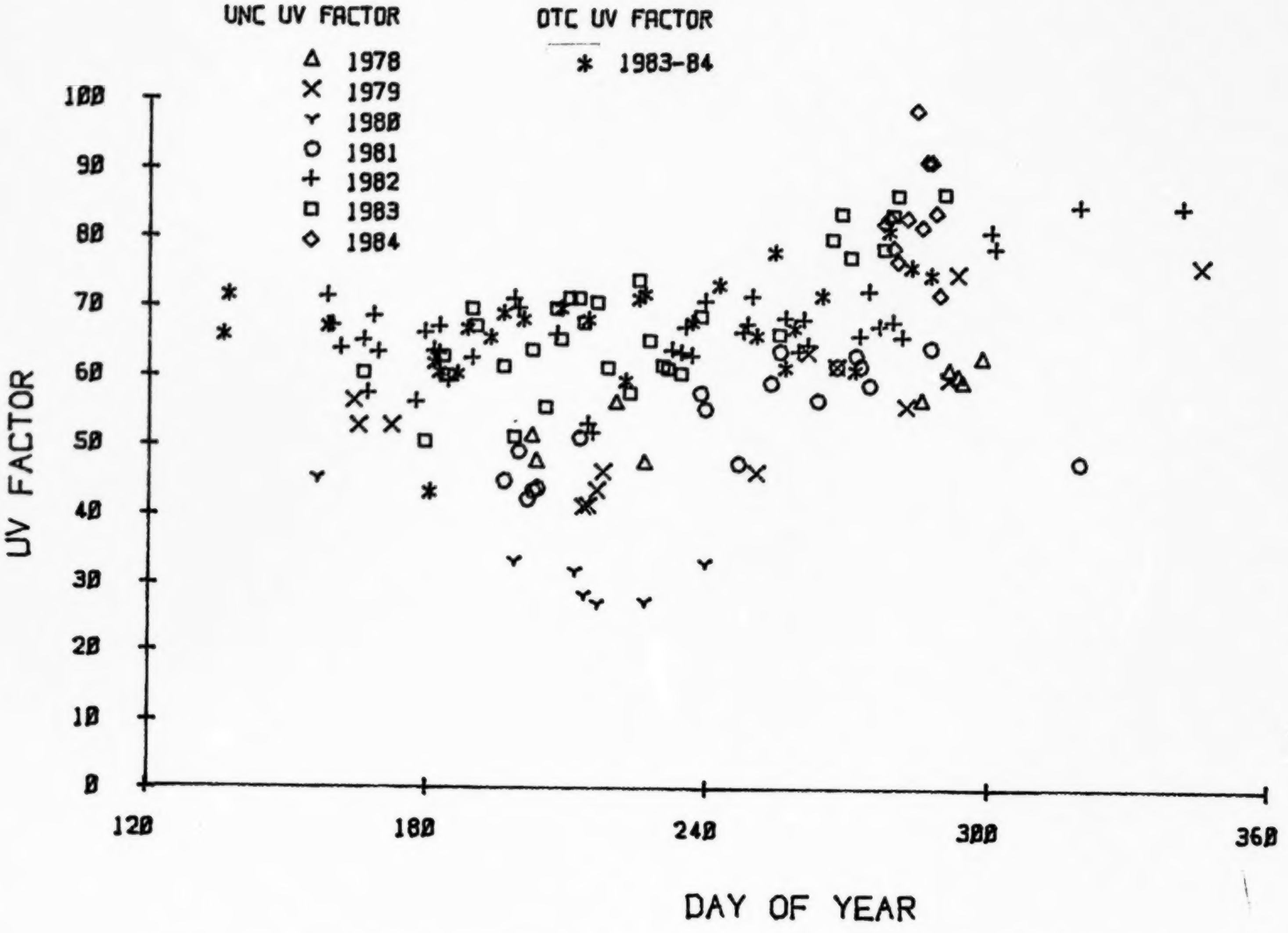

Figure III-3. Plots of extrapolated z=0 UV radiometer readings (in millilangleys) against day of the year for UNC and SAPRC outdoor chamber runs on the present data set.

for the years 1981-1984 (which is essentially the same as the theoretically expected value) to the average of the UV factors for the year the run was carried out. Because the light intensity for the late fall and winter appear to be greater than in the summer months when most experiments were carried out, only the runs carried out during the months of June through September, inclusive, were used in calculating these averages. These averages are summarized in Table III-4, together with the average for the OTC runs and the correction factors applied to the UV data for modeling purposes.

Our finding that the UNC UV readings obtained prior to 1981 need to be corrected are consistent with the preliminary results of a re-evaluation of the UNC chamber light data now being carried out by Jeffries (private communication). Jeffries notes that during those periods, the calibration of the UV instrument was definitely in error, and he is deriving correction factors based on an analysis of the entire UNC light intensity data base during the affected periods. His preliminary results appear to be consistent with the correction factors given in Table III-4, though when his analysis is complete, they will supercede our estimates, since he is using a more complete data base than is available to us.

Table III-4. Averages of Clear-Sky UV Radiometer Readings Extrapolated to Z=0 Derived from Data from UNC and SAPRC OTC Chamber Experiments Carried Out in June through September, and Correction Factors Applied to the UV Data for Modeling Purposes

Chamber	Year(s)	Avg. Z=0 UV (millilangley)	Correction Factor
UNC	1978	50.4 ± 4.1	1.30
	1979	50.3 ± 8.2	1.31
	1980	32.0 ± 6.4	2.06
	1981	52.9 ± 7.7	1.24
	1982	64.6 ± 4.9	1.0
	1983	65.2 ± 7.7	1.0
	1984	a	1.0
OTC	1983-84	66.0 ± 6.7	1.0

[a] None of the 1984 experiments modeled in this program were carried out in June through September.

At both the SAPRC and the UNC outdoor chamber laboratories the UV instrument is located outside the chamber, and thus it does not directly measure the light intensity inside the chamber. In the case of the SAPRC OTC, which consists of a flexible Teflon bag held on a rope netting above a green indoor-outdoor carpet, the major cause for differences in light intensity between the inside and the outside of the chamber is assumed to be the attenuation of the light as it passes through the Teflon walls. The quartz tube used to obtain k_1 measurements during OTC runs is located underneath the reaction bag, and thus light reaching it passes through the chamber walls twice. A plot of observed vs theoretically calculated k_1 readings for these OTC runs (Carter et al. 1985) indicates that the light reaching the k_1 tube under the OTC is attenuated by ~20%. We assume that inside the chamber the light intensity is attenuated by half the amount it is attenuated when it reaches the k_1 tube. Thus in modeling the OTC runs for this program, we used a correction factor, f(g), of 0.9 in equation (II) when calculating the light intensity.

This estimation that a simple 0.9 correction factor takes into account all the differences between the light intensity and spectral distribution inside the OTC and the theoretically calculated values is subject to a number of uncertainties. A more recent re-analysis of SAPRC UV and k_1 data, carried out by comparing observed and calculated k_1 values, indicates that a correction factor of 0.83 might be more appropriate (Carter et al. 1986), though that analysis was carried out after the calculations discussed in this report were completed. In addition, the possibilities that the walls, or reflections from the surfaces and structures around the ITC may be changing the zenith angle dependences of the light intensity, or that attenuation and/or scattering of light as it passes through the walls may cause a change in the spectral distribution are ignored. [See Carter et al. (1985) for a diagram of the structures and surfaces in the vicinity of the OTC. The diagram given for 1983 is appropriate for most of the OTC runs modeled in this program.] These uncertainties are probably the greatest at the higher zenith angles and at the lowest wavelengths, though it should be noted that for most SAPRC OTC runs the chamber is covered before 0900 PST and after 1500 or 1600 PST, so uncertainties associated with light characteristics at high zenith angles probably do not represent significant uncertainties in modeling SAPRC OTC runs. Based on these considerations, we estimate that the light intensity inside the OTC is probably uncertain by ~15%, though this is a subjective estimate. The uncertainty is probably somewhat less at the wavelength region affecting the photolysis of NO_2, and probably somewhat greater at the lower wavelength region which affects the photolysis of aldehydes and the formation of $O(^1D)$ from O_3.

For the UNC chamber, relating the indoor and the outdoor light intensity is further complicated by the fact that their chamber has a reflective floor, which may result in an enhancement of the light intensity inside the chamber. A study in which k_1 measurements were simultaneously made inside and outside the UNC chamber was carried out by Saeger in 1976 (Saeger 1977), which led the UNC researchers and the modelers at SAI to conclude that the light intensity inside the chamber can be enhanced by as much as 20%, with the enhancement depending on the solar zenith angle (Jeffries et al. 1982, Whitten et al. 1983). However, we feel that the data from the k_1 measurements taken inside the chamber and reported by Saeger (1977) are far too scattered to serve as a basis for characterization of the light intensity inside the UNC chamber, and that the UNC chamber must be considered to be uncharacterized in this respect. Since any enhancement of light intensity due to reflections from the chamber floor will be offset at least to some extent by attenuation of light as it passes through the chamber walls and by shadows caused by the supporting structure, we tentatively assume, with the lack of satisfactory data to the contrary, that these factors tend to cancel each other out, and that the light intensity inside the UNC chamber is the same as it is on the outside.

As indicated above, Jeffries (private communication) is carrying out a re-evaluation of the light data associated with the UNC chamber experiments, and this includes an evaluation of the problem of characterizing the light inside the chamber. His preliminary results indicate that the chamber walls may be absorbing more UV light than light at longer wavelengths, and that the reflective floor and other factors introduce zenith angle and wavelength dependences which are not being taken into account in our model. The absorption of UV light by the walls would result in lower rates of photolyses affected by shorter wavelengths, and this is consistent with the fact that the SAI modelers find that reducing the formaldehyde photolysis rate by approximately 35% results in better fits of their model simulations to the results of formaldehyde-NO_x-air runs (Whitten et al. 1985). However, our model simulations of the acetaldehyde-NO_x-air runs do not indicate a need to reduce the photolysis rate of this compound, which is affected by a similar wavelength region -- indeed, the fits to the acetaldehyde consumption rates for those runs would be improved by increasing its photolysis rate (Section IV-D-3). In addition, our simulations of the formaldehyde runs, discussed in Section IV-D-2, do not yield acceptable fits to experimental results either with the standard model or with the 35% reduction in the formaldehyde photolysis rates. Thus it is not clear from modeling alone whether reduction in photolysis rates of species affected by shorter wavelength radiation is appropriate. Until the analysis being carried out by Jeffries is complete, it is unknown which, if any, modifications in the method used to calculate the photolysis rates in the UNC chamber are appropriate, and thus no attempt to correct for these factors was incorporated in the model simulations carried out in this program.

Thus, in modeling UNC chamber runs, the correction factor, f(g), used in equation (II) to calculate the light intensity is just the factor to correct the UV data, derived as discussed above. (For example, f(g) = 1 for runs carried out in 1982-1983, and f(g) = 2.06 for runs carried out in 1980, etc.) Despite problems indicated by the analysis of Jeffries (private communication), the fits of our model calculations to the experimental data, when taken as a whole, do not indicate that the light intensities assumed in our model simulations of the UNC chamber experiments are either consistently too high or consistently too low. However, it is clear that this is a potentially significant area of uncertainty in modeling the experiments carried out in the UNC outdoor chamber.

We estimate that our calculations of NO_2 photolysis rates in UNC experiments are uncertain by approximately 20% (similar to that estimated for the SAPRC OTC), but that our calculation of photolysis rates of species affected by shorter wavelength radiation, such as formaldehyde, or of photolysis rates of all species at large zenith angles, may be significantly more uncertain. (Photolysis at large zenith angles need to be taken into account in modeling UNC chamber experiments, particularly those involving the initial presence of photoreactive species such as aldehydes, because all reactants are injected prior to sunrise, and photolysis starts when the sun rises.) The light intensity is also more uncertain in runs carried out in years, such as 1980, where large corrections to the UV data are indicated. Further analysis of light characteristics of the UNC chamber, such as that now being carried out by Jeffries, may significantly reduce these uncertainties.

In order to assess the effect of uncertainties in total light intensity on model predictions for the UNC chamber experiments, sensitivity calculations were carried out in which the light intensity was increased by 20% in simulations of all of the UNC propene-NO_x-air, n-butane-NO_x-air, and toluene-NO_x-air runs used in this study. The sensitivity of the model predictions to this increase in light intensity is shown in Figure III-4, which gives plots of the change in the calculated ozone maxima against the calculated ozone maxima, and in Figure III-5, which gives corresponding plots for the calculated parameter measuring the rate of NO oxidation, defined as described in Section IV-B. It can be seen that in general, the sensitivities of these calculated reactivity measurements to changes in light intensity are variable, but in most cases the percentage change is less than the percentage change in the light intensity.

It should be pointed out that if there is a systematic error in our representation of the light intensity in the UNC chamber runs in the model calculations, this should show up as a systematic discrepancy between the fits of the model to the UNC experiments, compared to results of simulations of similar experiments carried out in a chamber where the light intensity and spectral distribution is better characterized. A good test for this arises from comparing the results of the simulations of the propene runs, since (a) despite some uncertainties in the ozone-propene mechanism, the major features of the propene-NO_x-air mechanism are reasonably well characterized, (b) we have data for a large number of propene runs carried out in both the UNC chamber and the SAPRC EC, and (c) in terms of light intensity and spectral distribution, the SAPRC EC is probably the best characterized of the four chambers whose data are employed in this study. The results of the model simulations for these runs are given in more detail in Section IV-D-7, but an indication of the performance of the model in the simulations of these runs is given in

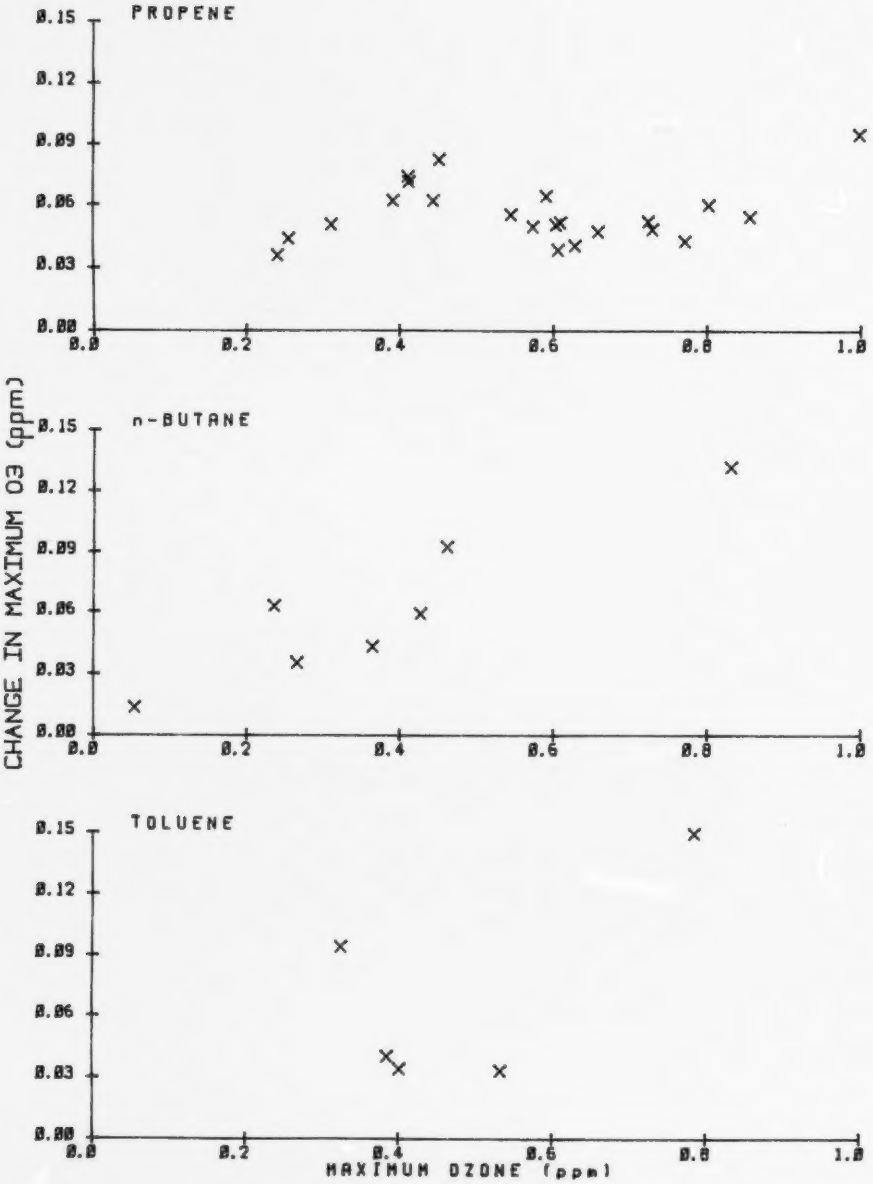

Figure III-4. Plots of changes in calculated maximum ozone yields, caused by increasing the light intensity by 15%, against calculated maximum ozone yields for model simulations of the propene-NO_x-air, n-butane-NO_x-air and the toluene-NO_x-air runs carried out in the UNC outdoor chamber.

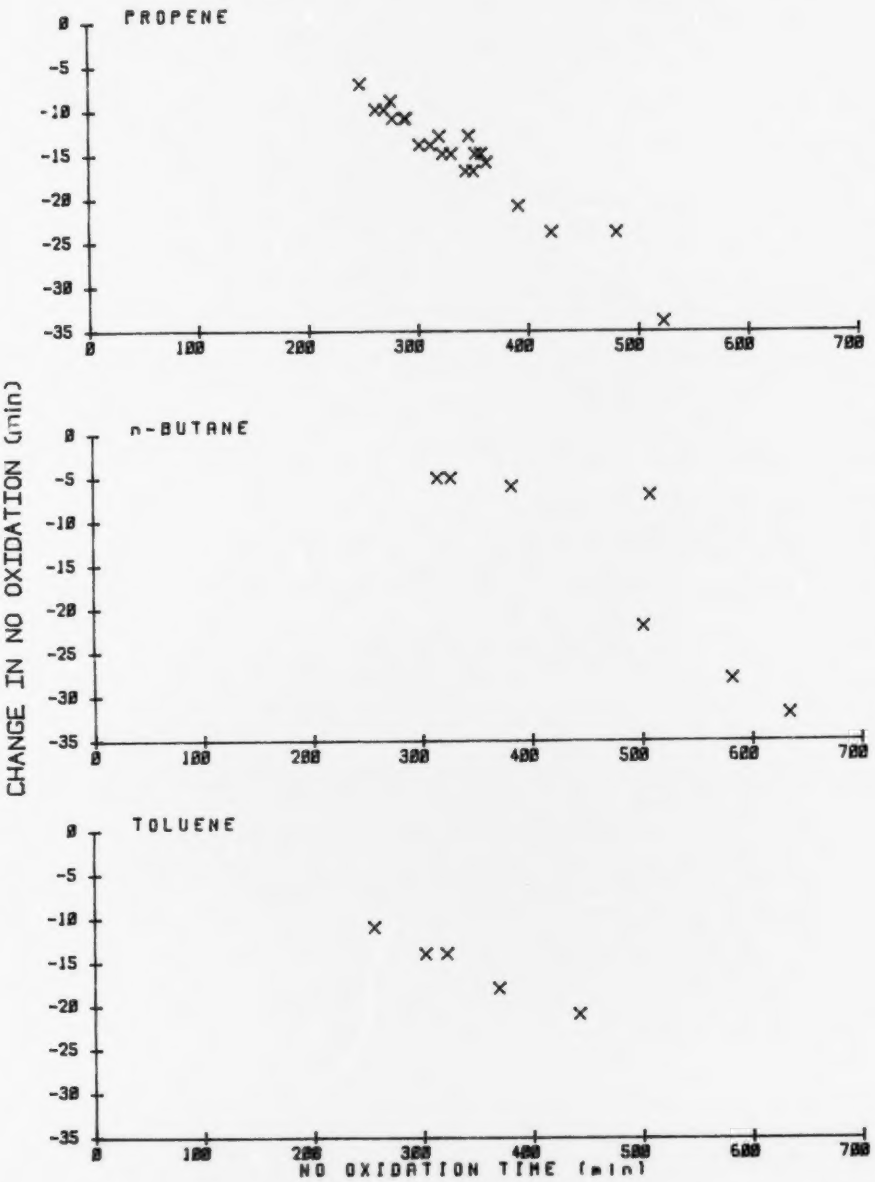

Figure III-5. Plots of changes in calculated times required to achieve one-half the maximum experimental increase in the quantity ($[O_3]-[NO]$), caused by increasing the light intensity by 15%, against the values calculated by the standard model, in model simulations of the propene-NO_x-air, n-butane-NO_x-air and the toluene-NO_x-air runs carried out in the UNC outdoor chamber.

Figure III-6, which shows bar graphs of the discrepancies between the observed and predicted ozone maxima for the propene runs carried out in those two chambers.

Figure III-6 shows that in terms of maximum ozone yields, the fits of the model to the experiment tends to be somewhat more variable in the model simulations of the UNC chamber than in the SAPRC EC, with the discrepancies in the simulations of the UNC propene runs appearing to be more random than systematic. Although the figure suggests that for the UNC experiments there might be some dependence of the distribution on the year the run was carried out, note that for both 1978 and 1983 there is a very wide distribution of discrepancies. (The figure also shows that the model tends to systematically overpredict the ozone yields observed in the EC propene experiments, but since the light intensity and spectral distribution in the SAPRC EC is considered to be reasonably well characterized, this probably reflects problems in the chemical mechanism or in the characterization of other chamber effects.) Although this high variability in the model fits to the UNC experiments may be due to variability in other chamber effects, such as initial HONO levels or the chamber radical source (discussed in Section III-B), the uncertainty in the light intensity may be playing an important role; and if so, then these simulations suggest that the uncertainties in the light intensity may be of a more random, rather than systematic, nature.

For runs with less-than-clear-sky conditions, the ratio $UV(t)/UV_0(z[t'])$ in equation (II) will in general have frequent and large discontinuities (being caused, for example, by passing clouds) and, if in the model calculation this ratio is updated by the software at every time step, the computation time would become excessive due to the necessity for the solver to take very small time steps when discontinuities occur. Thus, the calculations were not carried out in that manner. Instead, each run with less-than-clear-sky conditions was subjectively divided into 2-5 time intervals such that the amount the light intensity is suppressed relative to clear-sky conditions can be assumed to be approximately constant in each time interval. Then, for each interval, the ratio of the area under the experimental UV vs. time curve to that calculated for clear-sky conditions is taken to be the light suppression factor for the entire interval. Thus, discontinuities in the light intensity occur only

```
-----------------------------------------------------
 Calculated -
 Observed [O3]   SAPRC EC              UNC Chamber
 Maximum (ppb)
-----------------------------------------------------

      < -0.33    :                     :
 -0.33 - -0.27   :                     :
 -0.27 - -0.21   :                     :93
 -0.21 - -0.15   :                     :9
 -0.15 - -0.09   :                     :99233
 -0.09 - -0.03   :X                    :88023
 -0.03 -  0.03  -:XXX                 -:844
  0.03 -  0.09   :XXXXXXXXX            :844
  0.09 -  0.15   :XX                   :88
  0.15 -  0.21   :                     :3
  0.21 -  0.27   :X                    :
  0.27 -  0.33   :                     :
       >  0.33   :                     :
-----------------------------------------------------
```

Figure III-6. Summary of distributions of discrepancies in the maximum ozone yields observed in the model simulations of the propene-NO_x-air runs carried out in the SAPRC EC and the UNC outdoor chamber. Symbols for UNC runs coded by year: 8 = 1978, 9 = 1979, 0 = 1980, 2 = 1982, 3 = 1983, 4 = 1984.

a few times in the model calculation, resulting in a significant savings in computation time. Tests in which model calculations with frequent and sharply varying light intensities are compared with those which use average light intensity factors over larger intervals have shown that the errors introduced by employing this approximation are not significant.

In order to serve as a check that the model calculation program is receiving the appropriate input characterizing the changes in light intensity for a particular outdoor chamber run, the program calculates the expected observed UV readings using the same J values as it uses to calculate the photolysis rate constants (i.e., according to equation (IV), only using $J(\lambda,t,g)$ from equation (II) rather than $J_0(z[t'])$.) These calculated UV values should fit closely with the observed UV values if the program receives the correct input (except for the 1978-1981 UNC runs, where the experimental UV data is considered to be off by a constant factor). A comparison of observed vs calculated UV readings for a less-than-clear-sky day is shown in Figure III-7.

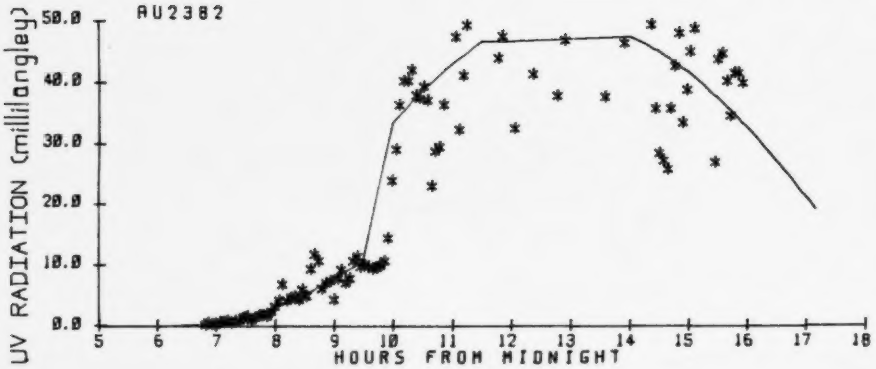

Figure III-7. Observed (*) and calculated (----) UV radiometer readings for a representative UNC outdoor chamber run with variable light quality.

III. B. CHAMBER RADICAL SOURCES

It has been recognized for several years that overall rates of initiation in environmental chambers are higher than can be accounted for by known homogeneous processes, and for certain types of experiments model calculations can only be made to be consistent with the experimental data if the model incorporates some type of radical input process whose physical meaning is unknown or speculative. Some of this excess radical initiation can be accounted for by assuming the initial presence of nitrous acid (HONO), since, as discussed in Section II-A, it undergoes rapid photolysis to form OH radicals. This HONO could either be injected as a contaminant with the NO_x or formed heterogeneously prior to the irradiation. Indeed, HONO has been shown to be formed in the dark from NO_2 at non-negligible rates in environmental chambers (Sakamaki et al. 1983, Pitts et al. 1984), and this process is included as part of our chamber effects model, as discussed below. However, any initially present nitrous acid is rapidly consumed, and in experiments, such as alkane-NO_x-air or radical tracer-NO_x-air irradiations, which do not have sufficient radical initiators formed in the homogeneous photooxidation process, a continuous radical source is required in the model for the calculation to fit the data. The rate of HONO formation from NO_2 in the dark, as determined by Sakamaki et al. (1983) and Pitts et al. (1984), while non-negligible, is not enough to supply these needed radicals.

The need for this additional, continuous radical input has been treated differently by different modeling groups. For example, the SAI and UNC groups, particularly when modeling UNC chamber data, have assumed continuous offgassing of formaldehyde (a radical initiator) to account for this effect, and attribute this to contamination from previous reaction mixtures. In our previous modeling work (Carter et al. 1979a, Atkinson et al. 1980), we represented it in the models as a constant OH radical flux with an unspecified source, and found empirically that the magnitude of the flux which best fit the data was correlated with the NO_x levels and not the hydrocarbons present or, except in unusual cases, with the types of experiments carried out previously. Subsequent experiments carried out at SAPRC, in which OH radical levels were measured in NO_x-air irradiations carried out in several chambers, tended to confirm that the radical source, at least in the SAPRC evacuable chamber, was NO_x dependent and was a heterogeneous process and not a contamination effect (Carter et al. 1981b, 1982b, Pitts et al. 1983). However, in the same study it was found that the magnitude of the radical source in chambers constructed of Teflon film (such as the SAPRC ITC and OTC and the UNC chamber), while non-negligible, was significantly less, and more variable, than in the SAPRC EC, and its NO_x dependence could not be unambiguously established. Thus the role of contamination in contributing to the radical source in Teflon chambers cannot be entirely ruled out.

In this section, the manner in which we treat continuous chamber radical sources and our assumptions regarding the presence of initial nitrous acid is discussed. Based on our previous studies of chamber radical sources, the most appropriate treatment appears to be different for the SAPRC evacuable chamber than for the Teflon bag chambers at SAPRC, so these two types of chambers are discussed separately. Since the UNC chamber walls consist of the same type of material as the SAPRC Teflon chambers, it is discussed in conjunction with our discussion of those chambers. As discussed below, the results of this study indicate that grouping the UNC chamber with the SAPRC Teflon chambers is probably appropriate.

1. The SAPRC Evacuable Chamber

a. Continuous Radical Source

Chamber-dependent radical sources in the SAPRC EC have been extensively studied by us previously (Carter et al. 1982b, Pitts et al. 1983), and thus this chamber was already highly characterized in this regard. Briefly, the radical source in the evacuable chamber was found to be linearly dependent on light intensity, to increase with increasing NO_2 concentration but be independent of the NO concentration, to increase with increasing temperature and relative humidity, to be independent of total pressure, and to be heterogeneous in nature rather than a contamination effect (since cleaning the chamber by "pumping and baking" caused it to increase rather than decrease). With respect to this program, the main parameter of interest concerns its dependence on the NO_2 concentration, since for most runs humidity and temperature were not widely varied, and all runs were carried out at at atmospheric pressure with the chamber in a well-conditioned state. At ~50% relative humidity, the humidity of most of the EC experiments modeled in this program, the radical input rate can be predicted, to within approximately 30%, from the NO_2 concentration, the light intensity as measured by k_1, and the NO_2 photolysis rate, by the following expression (Pitts et al. 1983).

$$\underset{(\text{ppm min}^{-1})}{\text{Radical flux}} = \underset{(\text{min}^{-1})}{k_1} \times (3.9 \times 10^{-4} + 1.37 \times 10^{-3} \times \underset{(\text{ppm})}{[NO_2]}) \qquad \text{(VI)}$$

However, part of the dependence of the radical source on the NO_2 concentration indicated in equation (VI) can be attributed to the heterogeneous hydrolysis of NO_2 to form HONO, since the rapid photolysis of HONO to form OH radicals and NO means that the formation of HONO is essentially equivalent to the formation of an equal amount of OH radicals. NO_2 in environmental chambers is known to form HONO in the dark (Sakamaki et al. 1983, Pitts et al. 1984), and this process has been studied in the SAPRC evacuable chamber by Pitts et al. (1984). They observed that both the consumption of NO_2 and the formation of HONO is first order in NO_2, that the NO_2 consumption and HONO formation rates increase, though not necessarily linearly, with humidity, and that the yield of HONO from NO_2 depended on the chamber employed, and was approximately 0.5. Other than relatively low yields of NO, no other products of this process were detected by Sakamaki et al. (1983) or Pitts et al. (1984), and it is assumed that the remaining nitrogen is absorbed to the wall. At 50% RH and 300 K, the conditions of most of the EC experiments modeled in the present study, the pseudo-first-order rate constant for NO_2 consumption was found to be 2.8×10^{-4} min^{-1} in the EC. Thus, in model simulations experiments carried out in the SAPRC EC, this process is represented in the model as

$$NO_2 \xrightarrow{H_2O} 0.5\ \text{HONO} + 0.5\ (\text{wall } NO_x) \qquad k = 2.8 \times 10^{-4}\ \text{min}^{-1}.$$

This "dark" HONO formation process is not sufficient to account for all of the radical flux observed in the evacuable chamber irradiations.

In particular, since the experiments from whose results equation (VI) was derived were carried out with a light intensity corresponding to a k_1 of approximately 0.49 min^{-1}, this reaction contributes only ~20%, or $0.5 \times (2.8 \times 10^{-4}/0.49) = 2.9 \times 10^{-4}$, to the 1.37×10^{-3} NO_2-dependent parameter in equation (VI) above. Thus, if we take out the contribution of the "dark" HONO formation to the radical source (since it is represented in the model by the reaction given above) the radical input rate from unknown sources in the EC is given by:

$$\underset{(\text{ppm-min}^{-1})}{\text{Corrected radical flux}} = \underset{(\text{min}^{-1})}{k_1} \times (3.9 \times 10^{-4} + 1.08 \times 10^{-3} \times \underset{(\text{ppm})}{[NO_2]}) \qquad \text{(VII)}$$

This process is represented in the model by the following two "reactions":

$$h\nu \longrightarrow OH \qquad \text{rate} = k_1 \times 3.9 \times 10^{-4} \text{ ppm min}^{-1}$$

$$NO_2 + h\nu \xrightarrow{H_2O} 0.5\ HONO + 0.5\ (\text{wall } NO_x) \qquad k = k_1 \times 2.16 \times 10^{-3} \text{ min}^{-1}$$

where k_1, the NO_2 photolysis rate, is in units of min^{-1}. The most appropriate way to represent the NO_2-dependent portion of the radical source is not known (except that it should be first order in NO_2), and we assume that the overall process is the same as the dark NO_2 hydrolysis, only that its rate is enhanced by the presence of light.

As indicated by the model simulation results summarized in Section IV, use of the above representation of the chamber radical source in the chamber effects model for the EC yield generally fair fits of calculation to experiment, and do not indicate that these estimated radical input rates are consistently high or low. However, for butane-NO_x-air, other alkane-NO_x-air, and radical tracer-NO_x air runs, which are highly sensitive to this parameter, significantly better fits can be attained if the overall radical input rates are adjusted from run-to-run in order to optimize the fits. For example, for the n-butane runs carried out in the SAPRC EC, Figure III-8 shows the distributions of the relative discrepancies [i.e., (observed-calculated)/observed] in the "timing" parameter

```
--------------------------------------------------------------------
(Calculated-
 Observed) /          No Adjustment of          Adjusted Radical
 Calculated          Radical Input Rates          Input Rates
 Times
--------------------------------------------------------------------

       < -0.55         :X                          :
 -0.55 - -0.45         :                           :X
 -0.45 - -0.35         :XXXXX                      :X
 -0.35 - -0.25         :X                          :
 -0.25 - -0.15         :                           :X
 -0.15 - -0.05         :X                          :XXXXXXX
 -0.05 -  0.05        -:                          -:XX
  0.05 -  0.15         :X                          :XX
  0.15 -  0.25         :                           :
  0.25 -  0.35         :X                          :
  0.35 -  0.45         :                           :
  0.45 -  0.55         :XX                         :
       >  0.55         :X                          :
--------------------------------------------------------------------
```

Figure III-8. Distributions in the relative discrepancies in the times required to change the quantity ($[O_3]-[NO]$) by an amount equal to half the experimentally observed change for the n-butane runs carried out in the SAPRC EC, calculated with and without run-to-run adjustment of the chamber radical source.

obtained when using equation (VII) to calculate the radical input rates, and when these input rates were adjusted from run-to-run within the limits of 0.5 to 2 times the values predicted by equation (VII). This timing parameter is, as discussed in Section IV, defined as the time required for the quantity ($[O_3]-[NO]$) to change by an amount equal to half of its maximum change observed experimentally. It can be seen that a significantly better distribution is obtained when the radical source is adjusted. The discrepancies still observed in Figure III-8 for the adjusted model can be attributed in part to the fact that (a) the adjustment was carried out in order to obtain a subjectively acceptable fit to ozone, without "fine-tuning" to obtain the optimum fits to the "timing" parameter shown in Figure III-8; and in part to the fact that (b) three runs, EC-306 through EC-308, appeared to have anomalously low radical input rates, with run EC-308 being carried out at 289 K rather than the usual 303 K, and the results of these experiments could not be fit by using the lower-limit value of 0.5 times that calculated using Equation (VII).

With the exception of the apparently anomalous runs EC-306 and EC-307, and the low temperature run EC-308, the adjustment factors which gave the best fits were generally within a factor of two, and appeared to vary essentially randomly. In particular, no correlation or other relationship between the radical input rate adjustment factor and the initial NO_x, the initial hydrocarbon, and the initial hydrocarbon/NO_x ratio were observed, nor (except for the apparently anomalous runs EC-306 through EC-308, where consistently low adjustment factors were required) was any other systematic pattern in the variability of this adjustment factor observed. Because of this we consider it unlikely that this variability indicates any consistent problem with the chemical mechanism used for n-butane, or that necessarily better fits could be obtained, without run-to-run adjustment, if a more complex, multi-parametered representation of the radical source was used in the model.

It should be pointed out that no run-to-run adjustment of the radical source was incorporated in the standard model calculations whose results are summarized in the figures and tables in Section IV. Most of the other runs modeled in this program were not nearly as sensitive to chamber radical sources as the n-butane runs discussed above, and adjusting the radical source within a factor of two yielded a significantly smaller effect than that indicated on Figure III-8 for the n-butane runs. Thus for those runs this apparent variability in chamber-dependent radical input rates does not represent a dominant factor in assessing the performance of the model as a whole. However, for the alkane-NO_x runs, which are highly sensitive to assumptions concerning chamber radical sources, this source of variability needs to be taken into account when assessing overall model performance.

b. Initial Nitrous Acid

In conjunction with the study of the continuous radical source in the SAPRC EC discussed above (Carter et al. 1982b, Pitts et al. 1983), experimental measurements were made of HONO levels in the EC prior to a number of radical tracer-NO_x-air irradiations. In addition, initial HONO levels were estimated for a number of these experiments from fitting the observed OH radical concentration-time profiles by model calculations. These data indicate that the concentrations of HONO initially present are influenced primarily by the amount of NO_2 present. For runs carried out at ~300 K and 50% RH (the conditions of most of the EC runs to be modeled in this program), the ratio of initial HONO to initial NO_2 ranged from ~4% to ~14%, with an average value of 7 ± 3%. Thus in our model calculations simulating experiments in the SAPRC evacuable chamber, we assume that HONO is initially present at concentrations given by multiplying the initial NO_2 concentration by 0.07. In this study, the initial HONO levels were not adjusted from run-to-run in our model simulations.

Although the initial HONO levels can be important in affecting results of tracer-NO_x-air irradiations, because of the relatively high continuous radical input rates characteristic of the SAPRC EC most experiments are not very sensitive to assumptions concerning initial HONO. Previous modeling studies which indicated that initial HONO levels were an important parameter generally did not include continuous radical input in the model. In most cases the runs found to be very sensitive to the assumed initial HONO were those, such as propene-NO_x-air irradiations, where the chemistry is such that rates of homogeneous radical initiation increase with time during the run. If no continuous radical source is assumed in the model simulation, the use of initial HONO can compensate for this deficiency by "getting the run started" and forming the radical initiators which then supply the necessary radicals for the run to proceed. For runs such as n-butane-NO_x-air irradiations, where the chemistry is characterized primarily by internal radical sinks, the assumed initial HONO levels have relatively little effect on the results of the model simulations.

2. Teflon Film Chambers

a. Continuous Radical Sources in The SAPRC Teflon Chambers

The SAPRC ITC and OTC and the UNC outdoor chamber are all similar in that their walls are constructed of FEP Teflon film, though the UNC chamber uses a thicker, and much more "aged," film than do the SAPRC chambers. As indicated above, we have previously carried out a number of experiments measuring the radical input rates in the SAPRC ITC and OTC (Carter et al. 1982b, Pitts et al. 1983), and such characterization experiments also have been routinely carried out in subsequent and ongoing chamber programs at SAPRC (Carter et al. 1984a,b). The results of these experiments indicate that radical input rates in the large Teflon bag chambers at SAPRC are generally lower than those observed in the SAPRC EC, but that they tend to be much more scattered. The data do not indicate any significant dependence on NO_x of the radical input rates, at least for the NO_x concentration range generally employed in environmental chambers. Thus, if any dependence of the ITC chamber radical source on NO_x does exist, its effects are less than the scatter of the available experimental data. [Some NO_2 dependence is expected due to the "dark" formation of HONO from NO_2. However, as discussed below in Subsection d, in Teflon film chambers this process is relatively minor compared to the light-dependent radical sources, and is thus not taken into account in analyzing the results of Carter et al. (1982b) and Pitts et al. (1983).] Thus for the Teflon bag chambers, the light-dependent radical input rate is represented simply by the "reaction"

$$h\nu \rightarrow OH \qquad\qquad k = k_1 \times k_{RS}$$

whose rate constant is proportional to the light intensity (as measured by the NO_2 photolysis rate), with k_{RS} being the proportionality factor.

Distribution plots of the proportionality factor for the radical input rates observed in reported tracer-NO_x-air runs carried out at SAPRC (Pitts et al. 1983) are shown in Figure III-9. It can be seen that this factor varies from less than approximately 0.1 ppb up to 1 ppb or more for both chambers. The 50,000-liter OTC exhibits the most scatter, with the

```
N   8-                        O T C
o
.   6-    X X
          X X
R   4-    X X           X
u         X X   X       X
n   2-    X X   X X     X     X
s         X X X X X X   X X X X         X     X X           X
    0--+-+-+-+-+-+-+-+-+-+-+-+-+-+-+-+-+-+-+-+-+-+-+-+-+-+-+-+-+
      0.0     0.2     0.4     0.6     0.8     1.0     1.2     1.4
```

```
   12-                          I T C
N                   X
o  10-              X
.                   X
    8-              X
R             X   X X   X
u   6-        X   X X   X
n             X   X X   X X
s   4-        X X X X   X X   X X         X
          X   X X X X   X X X X X X       X
    2-    X X X X X X X X X X X X X X     X X
        X X X X X X X X X X X X X X X   X X X
    0--+-+-+-+-+-+-+-+-+-+-+-+-+-+-+-+-+-+-+-+-+-+-+-+-+-+-+-+-+
      0.0     0.2     0.4     0.6     0.8     1.0     1.2     1.4
```

Radical input rate / k_1 (ppb)

Figure III-9. Distribution plot of radical input rates normalized by light intensity for SAPRC indoor Teflon chamber (ITC) and outdoor Teflon chamber (OTC) runs reported by Pitts et al. (1983) and by Carter et al. (1984, 1985).

largest number of runs with both very low or very high radical input rates. However, it should be noted that when environmental chamber experiments are being carried out at SAPRC and radical input rates corresponding to k_{RS} values of approximately 0.8 ppb or greater are observed, the reactor is considered to be unduly contaminated and it is either replaced or re-conditioned. Hence for modeling purposes, values greater than 0.8 ppb should probably not be considered to be acceptable. If these values are rejected, then the median value of k_{RS} is ~0.3 ppb for the ITC and ~0.2 ppb for the OTC. However, since there are more data for the ITC and in view of the scatter of the data, it is unclear whether there is a significant difference between these two chambers.

In our model simulations of all SAPRC ITC and OTC runs, a value of k_{RS} = 0.3 ppb has been used, without any run-to-run adjustment. However, it should be noted that for the alkane-NO_x-air runs, which as indicated above are highly sensitive to this parameter, much of the observed variability in the fits of the model simulations to the data (see Section IV) can be attributed to the apparent variability of the chamber radical source. For most other experiments, however, this variability is of much less importance in assesing the overall performance of the model.

b. OH Radical Flux in the UNC Chamber

Since results of radical tracer-NO_x-air irradiations for the purpose of characterizing radical input rates are not available for the UNC outdoor chamber, we make the assumption the radical source in the UNC chamber can be represented in an analogous manner to that assumed for the SAPRC Teflon bag chambers, and that the radical input rates are similar. This seems a reasonable assumption in view of the fact that they have similar walls, and in view of the fact that the radical input rates in the approximately 50,000-liter OTC are not significantly different than those in the 6,400-liter ITC. Thus in the model simulations of the experiments carried out in the UNC chamber, a continuous radical input flux corresponding to k_{RS} = 0.3 ppb is assumed.

The results of the model simulations of the UNC n-butane-NO_x-air irradiations, summarized in Section IV, indicate that this assumption is reasonable. In particular, in three of those seven runs the reactivity was overpredicted, and in four the reactivity was underpredicted. Furthermore, reasonably good fits for all of these n-butane-NO_x-air irradiations could be obtained by adjusting the radical source by a factor of $\lesssim 2$. The apparent variability in the radical source for the UNC chamber, as indicated by the results of modeling these n-butane runs, thus appears to be comparable to the SAPRC EC. As with the simulations of the runs carried out in the other chambers, the standard model simulations of the UNC chamber runs summarized in Section IV were carried out without any run-to-run adjustment of this parameter, and this should be taken into account when evaluating the quality of the fits obtained, particularly for the alkane-NO_x-air runs which are very sensitive to this parameter.

c. Formaldehyde Offgassing in the UNC Chamber

As indicated above, in previous modeling studies of the UNC chamber, formaldehyde offgassing was assumed in the model simulations rather than the light-dependent OH radical flux we use in our calculations. This assumption is supported by the fact that formaldehyde is known to be absorbed on the walls of that chamber under high humidity conditions (Jeffries, private communication), suggesting that it may later be released, and that it is possible to fit model calculations to the experimental data without having to include a hypothetical OH radical flux in the model. However it can be argued that the assumption of formaldehyde offgassing is equally hypothetical, since we are aware of no direct evidence for significant formaldehyde offgassing in the UNC chamber or in any of the SAPRC chambers.

In order to examine whether better fits to the UNC chamber data can be obtained by assuming formaldehyde offgassing rather than the light-dependent OH flux discussed above, model simulations of all of the UNC NO_x-air runs in the present modeling set were carried out based on this assumption. Although Jeffries (private communication) uses a 2-parameter model to characterize formaldehyde offgassing (one parameter being the amount of formaldehyde assumed to be on the walls, the other being the rate at which it goes into the gas phase), we use a 1-parameter model because (1) a chamber characterization model with more adjustable parameters is less useful for model testing than one which has fewer such parameters but gives comparable fits to the data, and (2) we could satisfactorily fit the data using a 1-parameter model for the OH flux, so if the formaldehyde offgassing model is to be considered as a practical alternative, it should also work with one parameter. Thus, we represented formaldehyde offgassing by the following process:

$$h\nu \rightarrow HCHO \qquad k = k_1 \times k_{HCHO}$$

where k_{HCHO} = 1×10^{-3} ppm, obtained by adjusting k_{HCHO} to provide the chamber radical input rates required to fit the data of the n-butane-NO_x-air runs. (The n-butane runs were used for this purpose because they are among the most sensitive to the chamber radical source. In addition, because of the hydrocarbon present, the n-butane runs are not as affected by the additional NO to NO_2 conversion caused by the offgassed formaldehyde as are the NO_x-air runs.)

The results of the simulations of the UNC NO_x-air runs indicate that in general more consistent fits to the data are obtained using the OH flux model rather than the HCHO offgassing model. This is shown in Figure III-10, which gives, for both sets of model calculations, the distributions of the discrepancies between the observed and predicted changes in NO and NO_2 concentrations occurring during the UNC NO_x-air runs. Although the fits are clearly variable, the distribution of the discrepancies for the formaldehyde offgassing model appears to have a bias towards overpredicting the change in NO and, to a lesser extent, underpredicting the change in NO_2, while the discrepancies for the OH flux model appear to be of a more random nature. This tendency of the HCHO offgassing model to overpredict NO consumption can be attributed to the conversion of NO to NO_2 caused by the reactions of offgassed formaldehyde.

A typical example of the differences between simulating the UNC NO_x-air runs with the formaldehyde offgassing model as opposed to the OH flux model is shown in Figure III-11, where NO, NO_2 and formaldehyde profiles for run AU2082R, calculated using the formaldehyde offgassing model, are compared with the experimental data and with results of the calculation using our standard OH-flux model. There are no formaldehyde data for that run or any other UNC NO_x-air runs in our present data set, though as indicated below such data are available for a pure air irradiation carried out at UNC. However, the results of the model simulations of the changes in the NO and the NO_2 concentrations observed in these NO_x-air runs indicate that representing the chamber radical source by a light-dependent OH flux is preferable to using the formaldehyde offgassing model.

Another type of experiment for which model calculations are sensitive to formaldehyde offgassing rates are pure air irradiations. As indicated in Section IV, model simulations of three such experiments were carried out. For these experiments, much better fits to the ozone yields were obtained if the model used formaldehyde offgassing rather than the OH flux model for the chamber radical source. This is shown in Figure IV-12 for the UNC run OC0684R, and the results for the other two runs were very similar. However, note that the formaldehyde levels are significantly

```
----------------------------------------------------------------------
(Calc.-Expt.)                 NO                          NO2
Change/Initial     ----------------------     ----------------------
     NOx           OH Flux      HCHO Flux     OH Flux      HCHO Flux
                    Model         Model        Model         Model
----------------------------------------------------------------------

           <  -0.22   :            :X            :             :
   -0.22   -  -0.18   :            :             :             :
   -0.18   -  -0.14   :            :X            :             :
   -0.14   -  -0.10   :X           :XXX          :             :
   -0.10   -  -0.06   :X           :XXXX         :XX           :
   -0.06   -  -0.02   :X           :XXXXX        :XXX          :
   -0.02   -   0.02  -:XX         -:            -:XX          -:
    0.02   -   0.06   :XXXX        :             :X            :XXX
    0.06   -   0.10   :XXXXX       :             :XXXX         :XX
    0.10   -   0.14   :            :             :XX           :XXXX
    0.14   -   0.18   :            :             :             :XXX
    0.18   -   0.22   :            :             :             :X
           >   0.22   :            :             :             :X
----------------------------------------------------------------------
```

Figure III-10. Distributions of the discrepancies in the change in the NO and NO_2 concentrations in the model simulations of the UNC NO_x-air irradiations, calculated using the standard, OH flux model and calculated assuming formaldehyde offgassing instead of the OH flux.

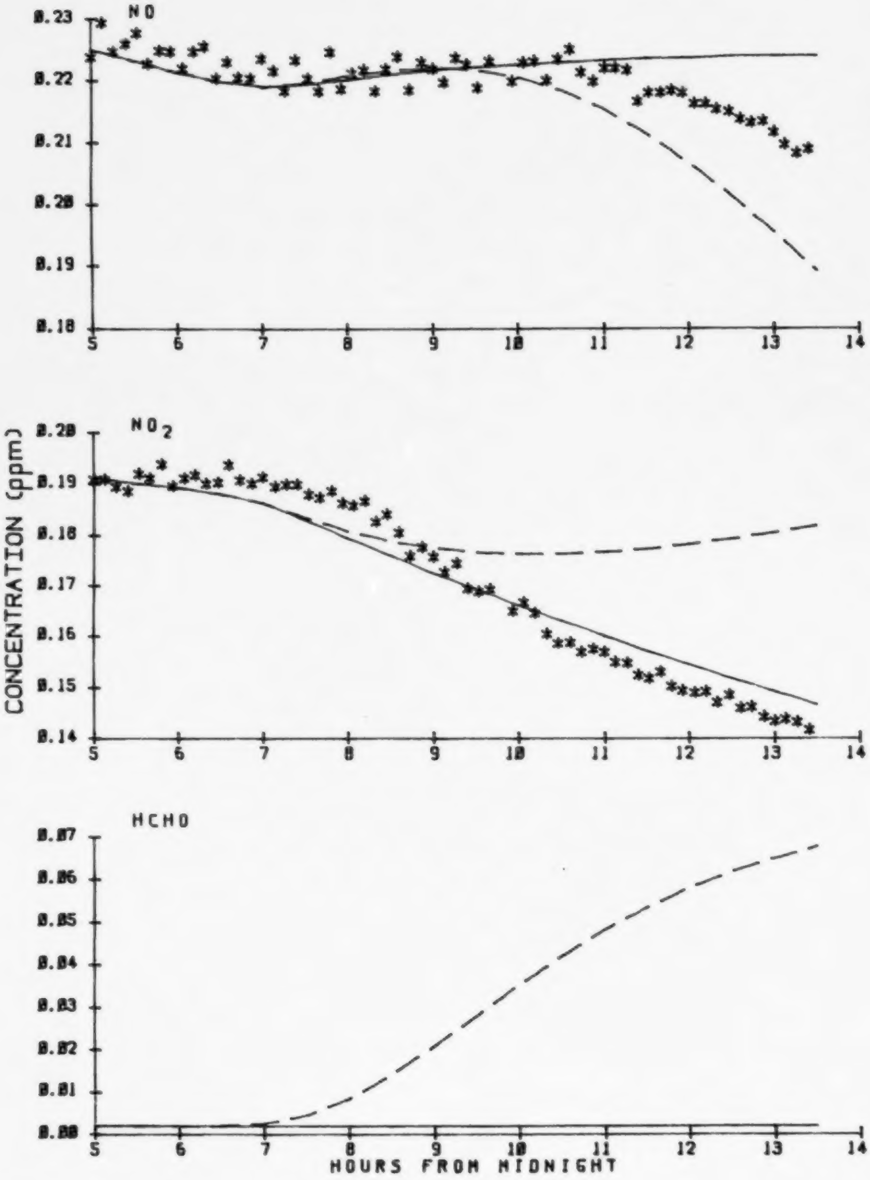

Figure III-11. Plots of experimental data and results of model calculations for selected species measured in UNC outdoor chamber run AU2082R.
* = Experimental data.
----- = Standard model calculation.
-- -- = Model calculation with no OH flux and with formaldehyde offgassing at a rate of k_1 x 1 ppb.

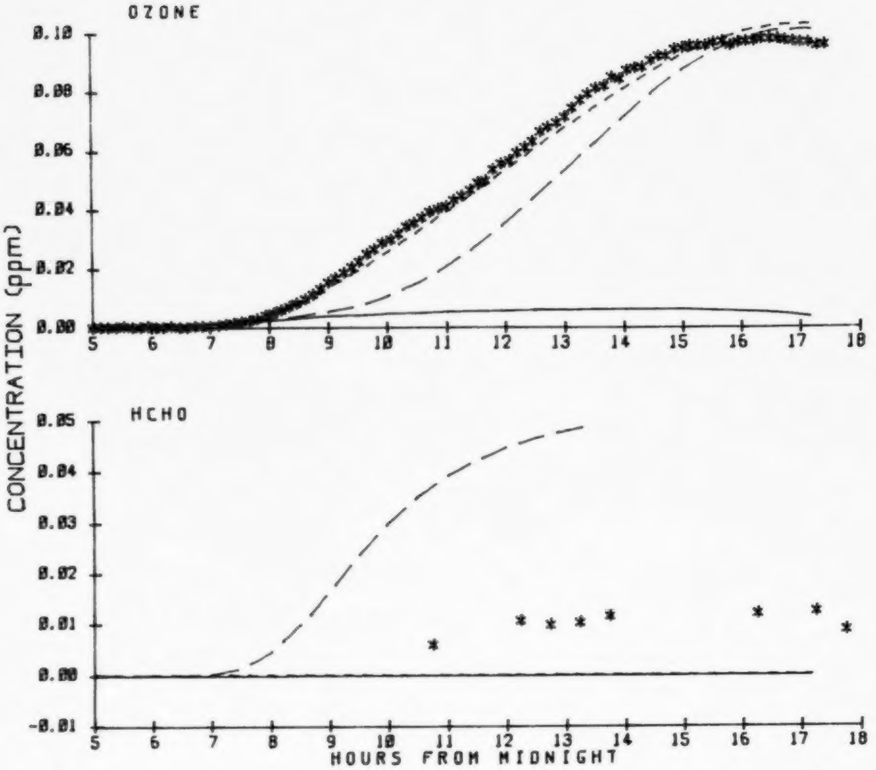

Figure III-12. Experimental and calculated concentration-time profiles of ozone and formaldehyde for the UNC pure irradiation experiment OC0684R.

* = Experimental data.

-------- = Standard model calculation: OH flux radical source model and no background or contaminant organics.

--- --- = Model calculation using HCHO offgassing as the radical source, with no other contaminant organics.

-- -- -- = Model calculation using the OH flux radical source and background or contaminant reactivity of 500 min^{-1}.

overpredicted by the model simulation using formaldehyde offgassing as the radical source. Calculations carried out using the 2-parameter formaldehyde offgassing model employed by Jeffries (private communication), with the "wall formaldehyde concentration" adjusted to give the radical input rates required to fit the n-butane runs also overpredict formaldehyde levels observed in this experiment. Thus if these formaldehyde measurements are accurate, they constitute evidence against formaldehyde offgassing being the major chamber-dependent radical source in the UNC chamber.

[It should be pointed out that the formaldehyde data obtained during the OC0684 run discussed above was not obtained using the technique normally employed at UNC. Indeed, the formaldehyde monitoring techniques normally used when carrying out the chamber experiments at both UNC and SAPRC chamber experiments are not sufficiently sensitive or precise to reliably monitor formaldehyde at the levels observed or calculated for the OC0684 experiment. However, for this and other runs carried out in October of 1984, formaldehyde was also monitored by Unisearch Associates, Inc., using a tuneable diode laser absorption spectrometer, and this technique appears to be sufficiently sensitive to monitor formaldehyde at these levels. Although the UNC researchers (Jeffries and Sexton, private communication) consider the Unisearch formaldehyde data for these experiments to be questionable because Unisearch did not heat their sample line (which might result in wall losses at lower temperatures or higher humidities), and because the Unisearch technique tended to give lower yields of formaldehyde compared to the values obtained using their standard technique, we found that our model predictions of formaldehyde yields in the ethene and propene runs carried out during this period were more consistent with the Unisearch formaldehyde data than with the formaldehyde yields obtained using the standard UNC technique (see Section IV). Since our model gives excellent predictions of formaldehyde yields in ethene runs carried out in the SAPRC EC, and its predictions of formaldehyde yields in SAPRC propene runs are not inconsistent with the data (if the experimental uncertainties involved are taken into account), and since the major chemical processes involving formaldehyde formation from propene and ethene appear to be reasonably well understood, this leads us to believe that the Unisearch formaldehyde data are probably valid. UNC and

Unisearch formaldehyde data, and their consistency with our model predictions, are discussed further in Section IV-B-5-f.]

The fact that our standard, OH flux, model does not correctly predict the ozone yields observed in the pure air irradiations is not surprising, since this model did not include any representation for background or contaminant organics. If an additional "reaction"

$$OH \rightarrow HO_2$$

is included in the model to represent the effects of peroxy radicals formed by the reactions of OH radicals with background or contaminant organics, then the ozone yields observed in all three of the UNC pure air irradiations modeled are well fit by using a "rate constant" of 500 min^{-1} for this "reaction." This is shown in Figure III-12 for run OC0684R, and the results are similar for the other two runs modeled. This level of excess OH to HO_2 conversion corresponds to contamination by, for example, only ~7 ppb of propene or ~50 ppb of n-butane (taking into account their OH radical rate constants and the number of peroxy radicals involved in their photooxidations), a not unreasonable level of contamination. Thus, it is not necessary to assume that the chamber radical source is due entirely to formaldehyde offgassing to account for the observed formation of ozone in the pure air irradiations carried out at UNC.

It should also be noted that, in terms of testing photochemical mechanisms, the question of whether formaldehyde offgassing is the chamber radical source, or even of the presence of background or reactive organics at the levels indicated by the modeling of the pure air irradiations, is usually a very minor consideration. This is because, as indicated above, the main difference between representing the chamber-dependent radical source by formaldehyde offgassing, as opposed to the OH flux model, is the extra NO to NO_2 conversions caused by the emitted formaldehyde. In most runs where reactive organics are deliberately included in the reaction mixture (obviously by far the major type of runs used for model testing) the amount of NO to NO_2 conversion caused by the reactions of the organic(s) injected into the chamber is much greater than that caused by the relatively small amounts of formaldehyde or of other reactive organics which may be initially present or emitted from the walls.

d. Dark Formation of HONO from NO_2

As with the SAPRC EC, part of the continuous radical input in the Teflon film chambers can be attributed to the dark formation of HONO from NO_2. This process was not studied directly in the SAPRC ITC, OTC, or in the UNC chamber, but Pitts et al. (1984) did study HONO formation from NO_2 in a 4300-liter Teflon chamber made of the same material as used in the OTC and the ITC, and a similar material as used in the UNC chamber. Pitts et al. (1984) observed that, as was the case with the SAPRC EC, the rate of NO_2 consumption and of HONO formation was first order in NO_2, but that the HONO yield ranged from 10-20% of the NO_2 consumed, as opposed to 50% for the EC. The pseudo-first-order rate constant for NO_2 consumption in that 4300-liter chamber was observed to be 1.6×10^{-4} min^{-1} at 50% RH and 296-298 K. This NO_2 consumption rate is lower than observed in the EC, despite the smaller volume of this 4300-liter chamber.

For the purpose of representing this process in the model in the simulations of the SAPRC Teflon chamber experiments, we assume that the rate of this reaction is approximately proportional to the surface/volume ratio of the chamber (approximated by the cube root of the volume) and that a 20% HONO yield from NO_2 occurs. This process is thus represented as

$$NO_2 \xrightarrow{H_2O} 0.2\ HONO + 0.8\ (wall\ NO_x)$$

with

$$\begin{aligned} k &= 1.4 \times 10^{-4}\ min^{-1} \text{ for the SAPRC ITC,} \\ &= 0.9 \times 10^{-4}\ min^{-1} \text{ for the SAPRC OTC,} \\ &= 0.5 \times 10^{-4}\ min^{-1} \text{ for the UNC chamber.} \end{aligned}$$

Although this reaction is included in the model, it represents only a minor contribution to the radical input rate. For example, for an ITC experiment with an NO_2 photolysis rate constant k_1 of 0.3 min^{-1} (a typical value) and an average NO_2 concentration of 0.5 ppm (a relatively high value), the HONO input rate from this process is calculated to be 0.014 ppb min^{-1}. This dark HONO formation rate can be compared to the continuous radical input rate of 0.09 ppb min^{-1} calculated with k_{RS} = 0.3 ppb. For most ITC and all OTC and UNC experiments the relative contribution of the dark formation of HONO via this process would be even less. For that reason, this process does not need to be taken into account in deriving the most appropriate value of k_{RS} to use in the model.

e. Initial HONO in Teflon Chambers

Since the heterogeneous hydrolysis of NO_2 to form nitrous acid is slower in Teflon chambers than in the SAPRC EC (Pitts et al. 1984), it is reasonable to assume that the initial HONO levels will also be lower in these chambers than in the SAPRC EC. Thus the levels of initial HONO appropriate for the EC (~0.07 $[NO_2]_0$) can be considered to be upper limits to the initial HONO levels for experiments carried out in chambers constructed of Teflon film. In view of this, and since we find that fits of calculations to experimental data carried out in these chambers are not significantly improved if initial HONO is assumed to be present (in most cases they are insensitive, and in others the fits are made worse), we assume no HONO is initially present when modeling these experiments. However, if the data indicate that the overall rates of reaction in the first ~30-60 min. of the experiment are significantly faster than predicted by the model, adjusting the initial HONO level up to ~5% of the initial NO_2 may be appropriate. However, this was not done for any runs modeled in this program.

III. C. NO_x OFFGASSING

In all four chambers used for model testing in this program, there is evidence that some provision for NO_x offgassing must be included in the chamber characterization model. The most direct evidence in this regard is the fact that PAN is formed when acetaldehyde is irradiated in the absence of initially present NO_x, since such PAN formation is clearly impossible if no source of NO_x were present. In addition, it is necessary to assume NO_x offgassing in the chamber model in order to account for the observed formation of O_3 in aldehyde-air irradiations and to fit NO_2 profiles in NO_x-air irradiations carried out with low initial NO_2 concentrations. Figures III-13 and III-14, show the observed and predicted ozone and PAN profiles for an acetaldehyde-air run carried out in the UNC chamber and in the SAPRC EC, respectively. Figure III-15, shows the observed and predicted NO and NO_2 rofiles for a representative UNC NO_x-air irradiation with low initial NO_x, where the calculations represent various assumptions regarding NO_x offgassing and initial NO_x (see below for further discussion regarding these assumptions). Clearly, for these runs the assumptions regarding NO_x offgassing are an important factor affecting the quality of fits of model calculations to the experimental data.

While the major impact of NO_x offgassing is on the predictions for experiments where NO_x was not injected by the experimenters, the assumptions regarding this effect can also impact model simulations of the organic-NO_x-air experiments, although one would expect that its importance would decrease as the amount of initially present NO_x increases. In order to check this, we carried out sensitivity calculations on the propene-NO_x-air and the n-butane-NO_x-air experiments in which the assumed NO_x offgassing rates were varied. The results of these calculations indicated that when the initial NO_x is relatively low assumptions regarding NO_x offgassing can have a moderate effect on ozone, PAN, and, for some experiments, NO_2, but are not a major factor in modeling experiments when NO_x is $\gtrsim$0.1-0.2 ppm. As examples of the effects of NO_x offgassing for two of the more sensitive of these runs, Figure III-16 shows plots of the observed and calculated ozone, NO_2, and PAN for a propene-NO_x-air run carried out in the EC containing ~0.1 ppm initial NO_x, while Figure III-17 shows similar

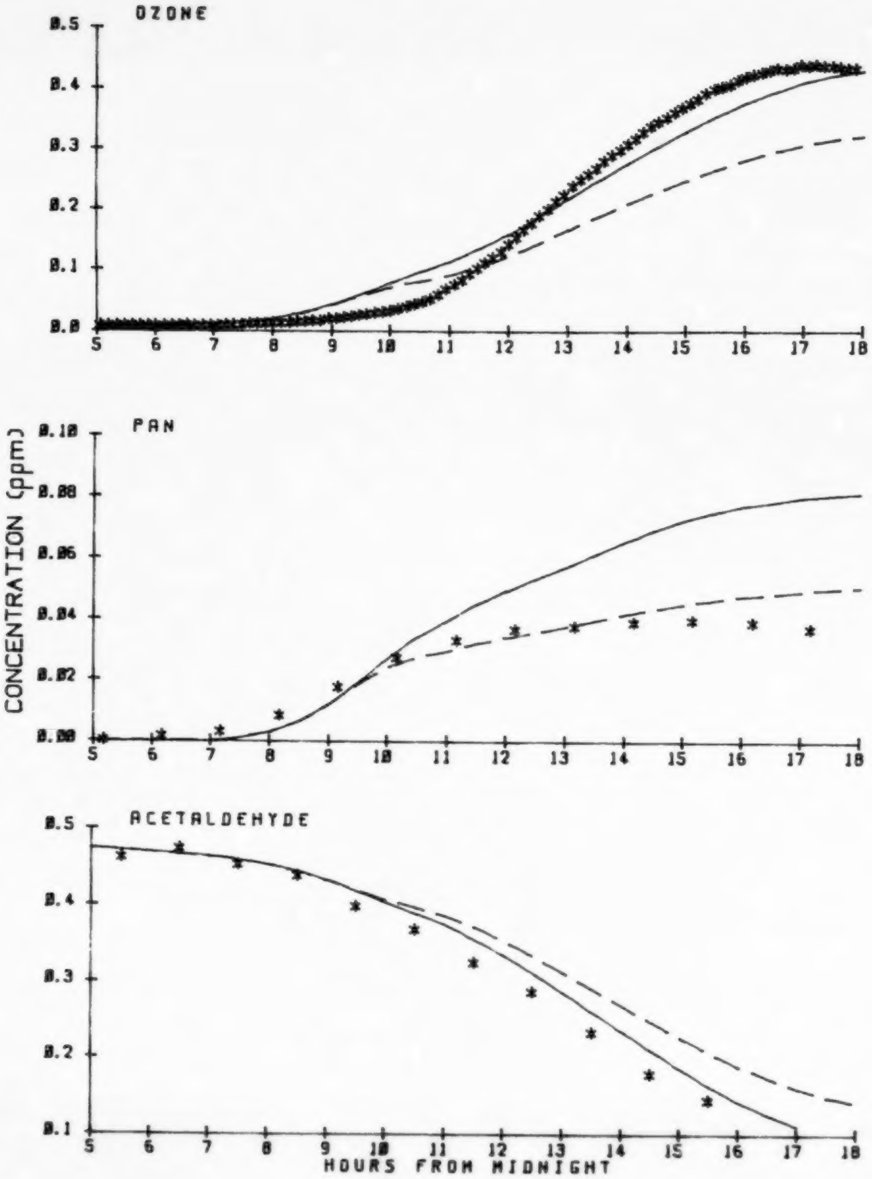

Figure III-13. Plots of experimental data and results of model calculations for selected species measured in UNC acetaldehyde-air run AU0483B.

* = Experimental data.

----- = Calculation assuming k_{EN} = 0.4 ppb.

-- -- = Calculation assuming k_{EN} = 0.2 ppb.

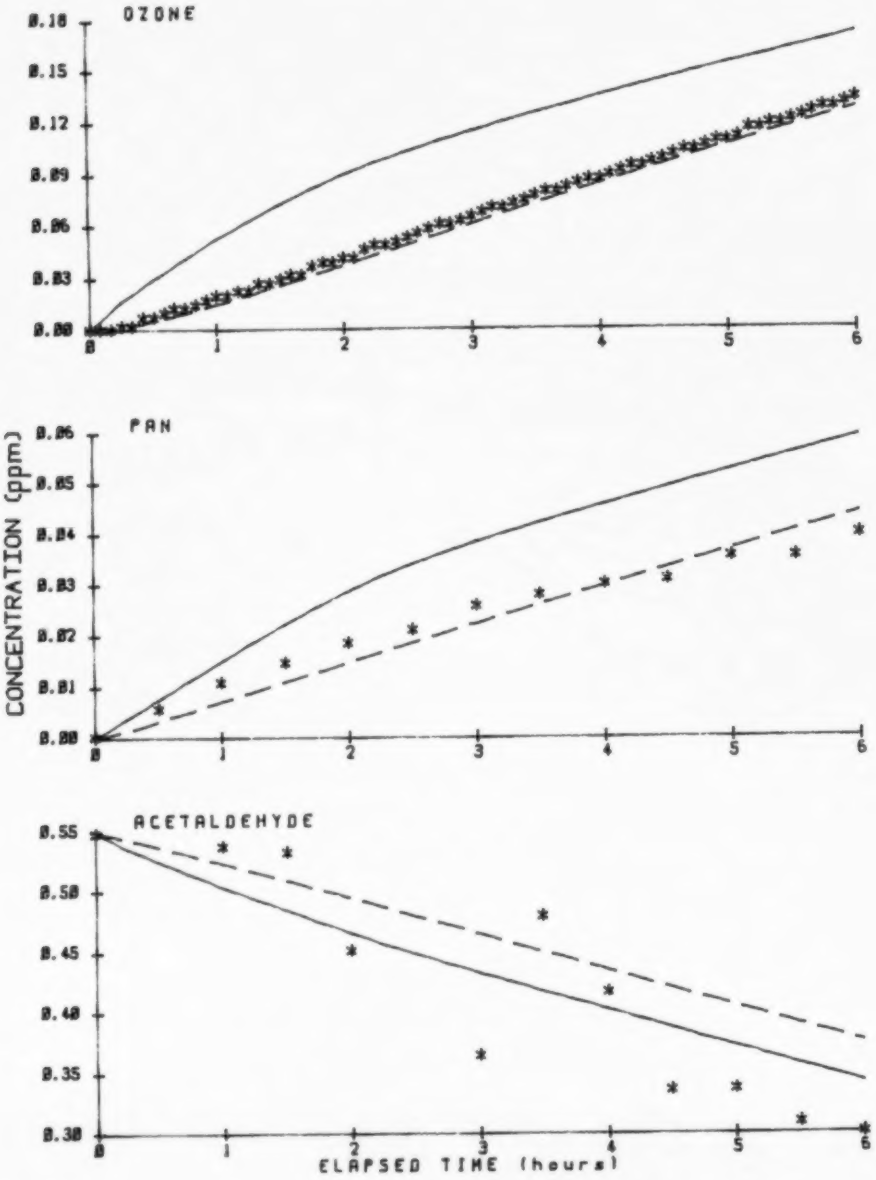

Figure III-14. Plots of experimental data and results of model calculations for selected species measured in SAPRC acetaldehyde-air run EC-253.

* = Experimental data.

----- = Calculation assuming k_{EN} = 0.3 ppb and initial [NO] = [NO_2] = 10 ppb.

-- -- = Calculation assuming k_{EN} = 0.5 ppb and initial [NO] and [NO_2] = 0.

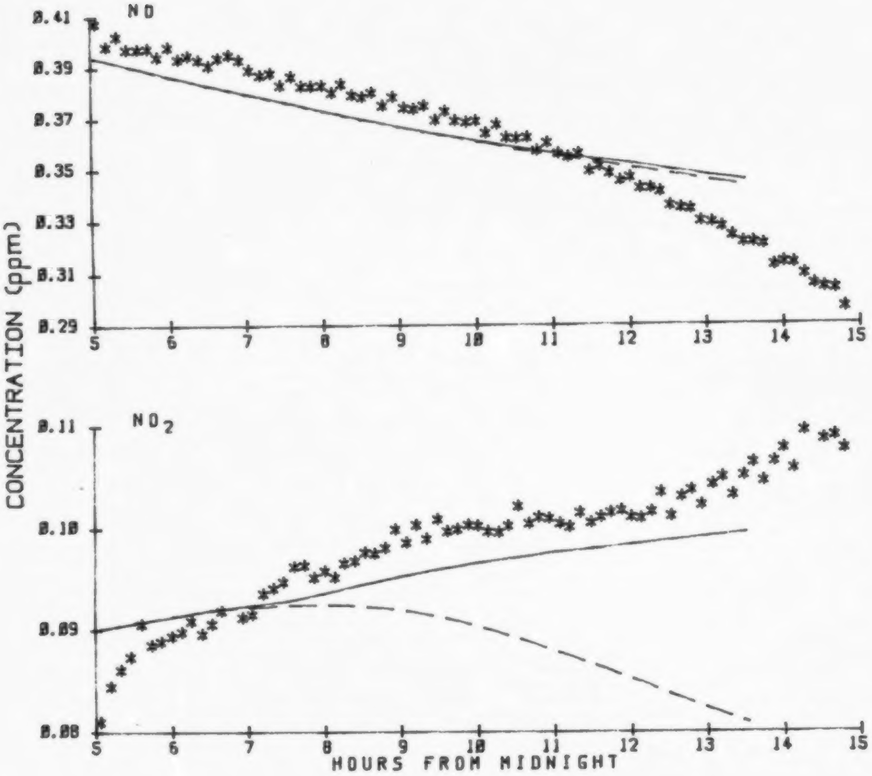

Figure III-15. Plots of experimental data and results of model calculations for selected species measured in UNC NO_x-air run JL2483B.

* = Experimental data.

----- = Calculation assuming k_{EN} = 0.4 ppb.

-- -- = Calculation assuming k_{EN} = 0.2 ppb.

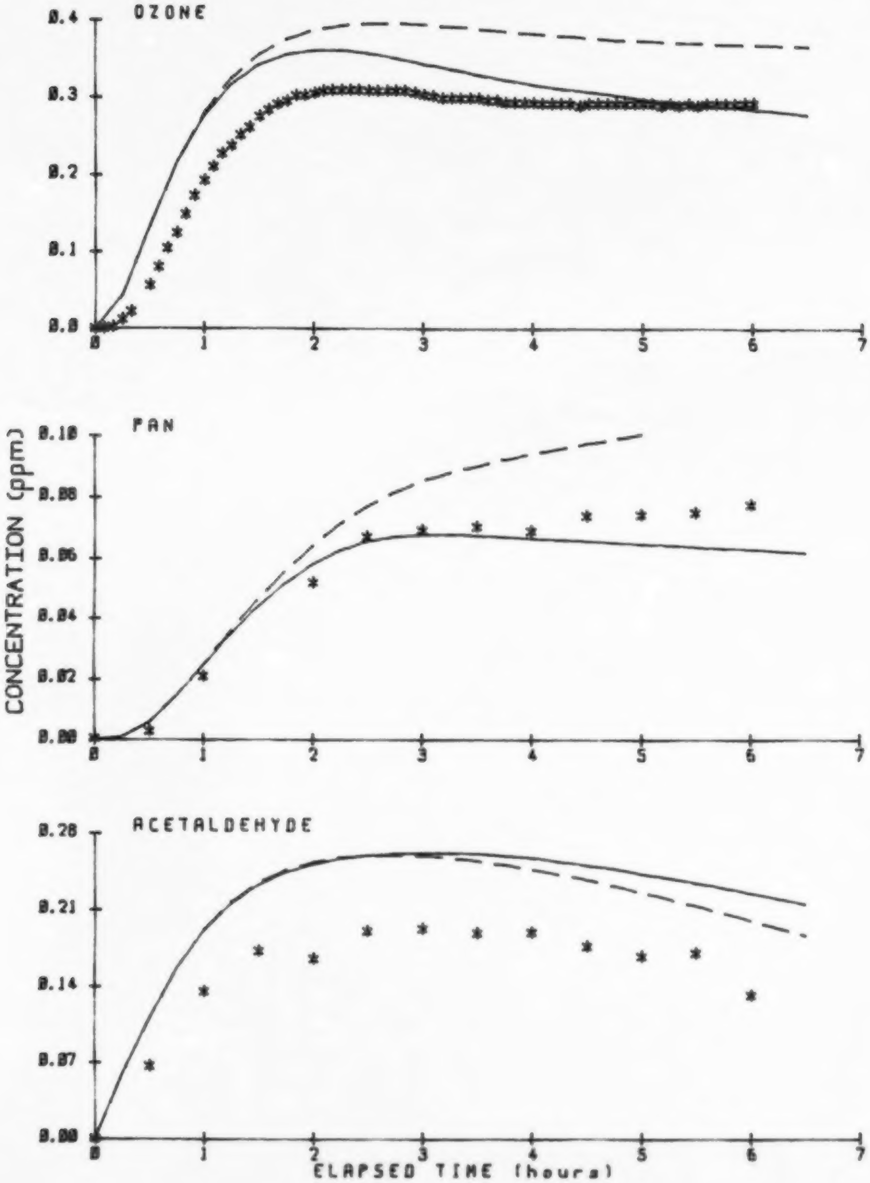

Figure III-16. Plots of experimental data and results of model calculations for selected species measured in SAPRC evacuable chamber propene-NO_x-air run EC-277.
* = Experimental data.
-- -- = Calculation assuming k_{EN} = 0.5 ppb.
----- = Calculation assuming k_{EN} = 0.

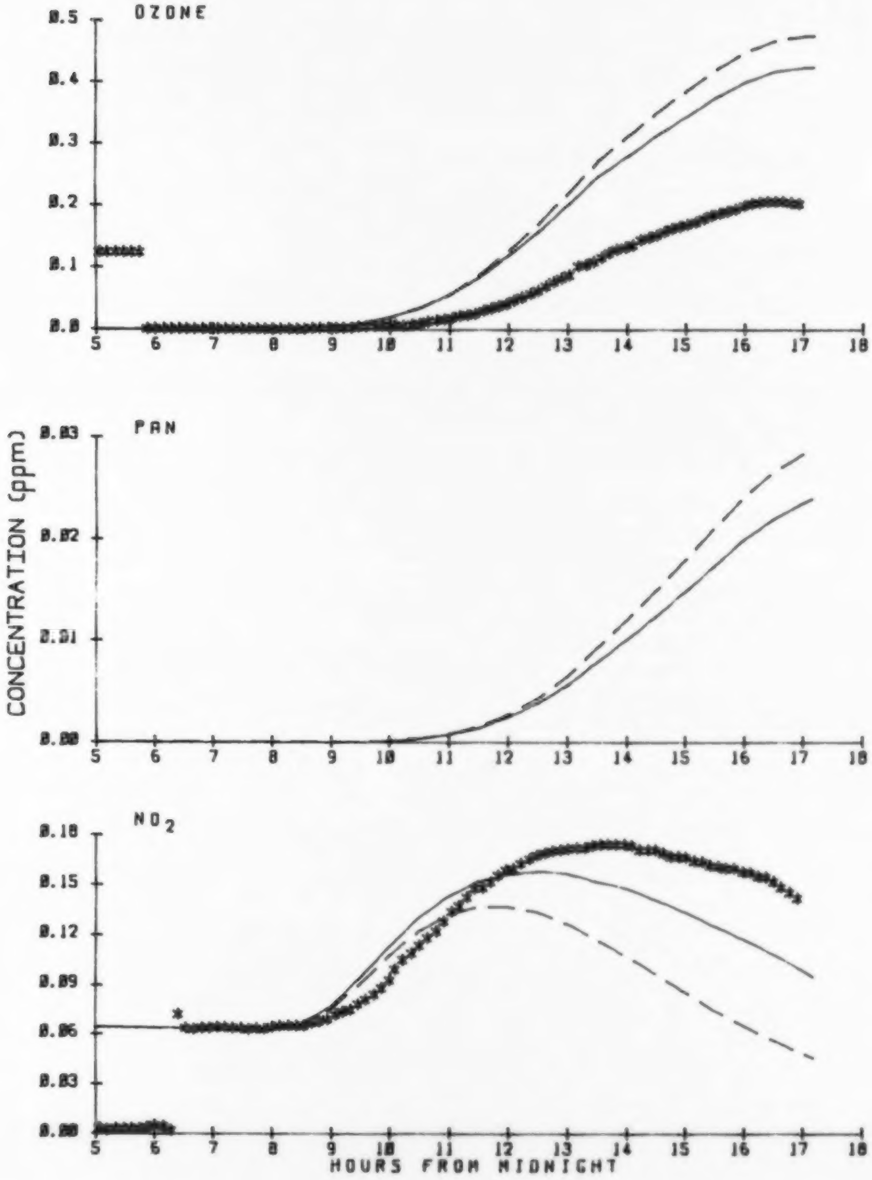

Figure III-17. Plots of experimental data and results of model calculations for selected species measured in UNC n-butane-NO_x-air chamber run OC1879B.

* = Experimental data.

----- = Calculation assuming k_{EN} = 0.3 ppb.

-- -- = Calculation assuming k_{EN} = 0.

plots for an n-butane run containing ~0.2 ppm initial NO_x carried out in the UNC chamber. (Note that for the UNC n-butane-NO_x-air run, increasing the NO_x offgassing rate has the effect of decreasing the rates of ozone and PAN formation, in contrast to the results for the aldehyde-air irradiations and other runs. This is because in this run, rates of ozone and PAN formation are determined by radical levels and not by the availablity of NO_x. NO_x offgassing results in a higher average NO_2 concentration, which results in a slightly lower OH radical concentration because of increased consumption of OH radicals due to its reaction with NO_2.) Most other propene and n-butane-NO_x-air runs modeled in this study are less sensitive to NO_x offgassing than the two shown in Figures III-16 and III-17. In particular, NO_x offgassing does not appear to have a large effect in causing continued ozone formation following the consumption of NO_x in high reactivity runs such as UNC run OC2078B, as shown in Figure III-18.

Jeffries (private communication) represents NO_x offgassing in the UNC outdoor chamber by a two-parameter model, one parameter being the amount of NO_x assumed to be absorbed on the wall, and the other being a light-dependent first-order rate constant for the "wall NO_x" to be converted into gas-phase NO_2. The rationalization for this representation is that there is expected to be only a finite amount of NO_x on the walls at the beginning of an experiment, and that the rate of its emission from the walls will decrease with time as it becomes depleated. However, this does not take into account the possibility that absorpion of NO_x onto the walls may also be occurring during these irradiations when it is present in higher levels, or that nitric acid or other N-containing species formed on these irradiations (e.g., N_2O_5, discussed below) may become absorbed on the walls and contribute to the effective levels of "wall NO_x". Thus under some conditions, the amount of absorbed NO_x may increase, rather than decrease, with time. Indeed, the fact that NO_x offgassing occurs at all tends to imply that some form of NO_x absorption must also be occurring. Thus it is not clear whether representation used by Jeffries is necessarily any more accurate than assuming the effective amount of NO_x absorbed on the walls is constant. We are aware of no experimental data which indicate that one type of representation of NO_x offgassing is necessarily more realistic than another. In view of this, and the fact

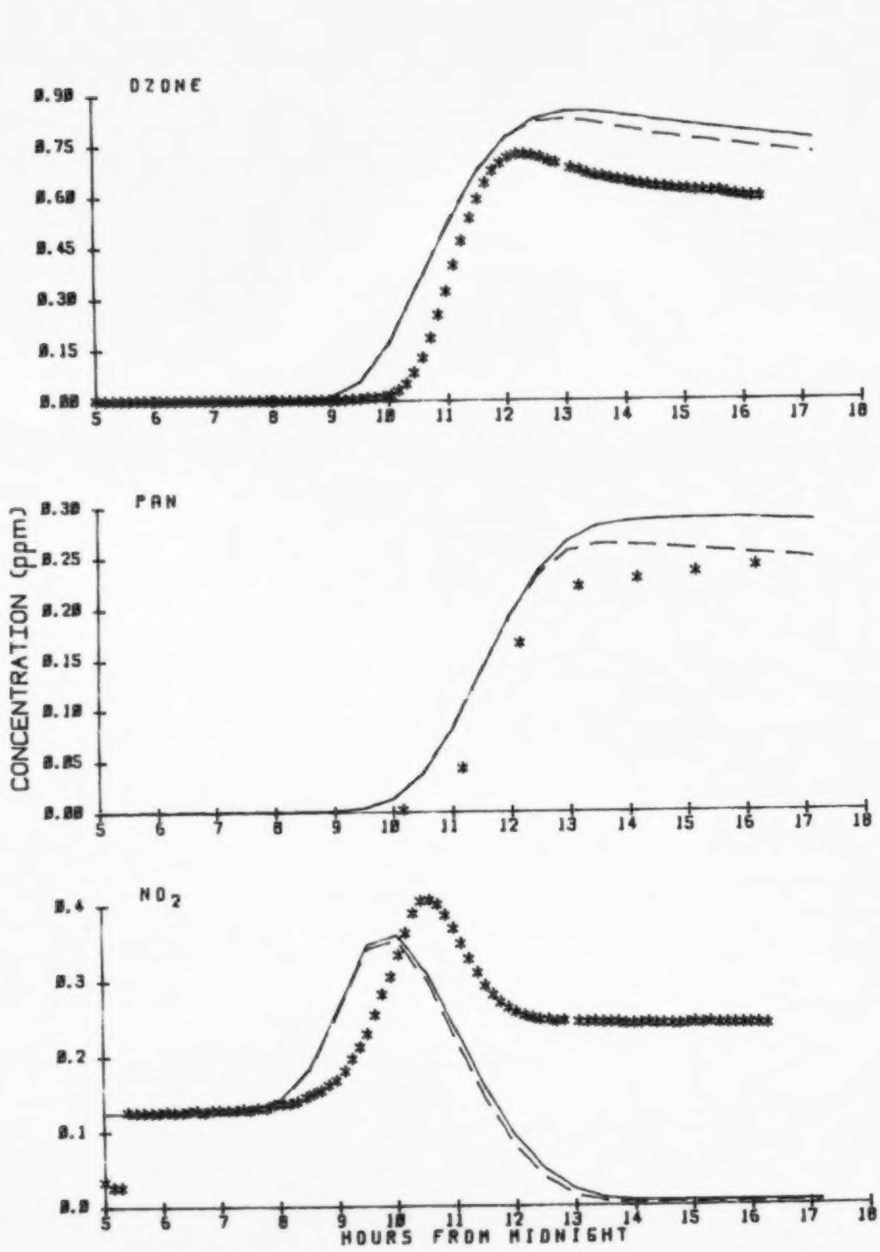

Figure III-18. Plots of experimental data and results of model calculations for selected species measured in UNC outdoor chamber run OC2078B.

* = Experimental data.

—— = Calculation assuming k_{EN} = 0.3 ppb.

-- -- = Calculation assuming k_{EN} = 0.

that for the purposes of this program it is useful to minimize the number of adjustable chamber-dependent parameters, NO_x offgassing is represented in this model by the simple one-step process

$$h\nu \rightarrow NO_2 - (\text{wall } NO_x) \qquad k = k_1 \times k_{EN}$$

where k_{EN}, the ratio of the NO_x offgassing rate to the NO_2 photolysis rate, is the only parameter representing this effect, and is assumed to be constant for each chamber. We recognize that the representation is obviously a gross over-simplification of reality, and that it is likely that NO_x offgassing varies not only with time, but from run-to-run, but we find that generally satisfactory results can be obtained without having to use a more complex representation, or having to adjust k_{EN} from run-to-run.

Our "best fit" values of the NO_x offgassing parameter, k_{EN}, for each of the four chambers employed in this program are as follows:

Chamber	k_{EN} (ppb)
SAPRC EC	0.5
SAPRC ITC	0.15
SAPRC OTC	0.10
UNC Outdoor	0.3

The derivation of these values for the specific chambers is discussed below.

1. The SAPRC Evacuable Chamber

The NO_2 offgassing rate in this chamber was adjusted to fit the O_3 and the PAN yields in acetaldehyde-air run EC-253, since that is the most sensitive run in our data set to this effect. The value of k_{EN} which best fit the data depended on whether the measured initial NO and NO_2 concentrations, which amount to approximately 20 ppb total, are assumed to reflect the true initial values or are due to instrumental interferences. (NO_x was not added in this run, so any initially present NO_x could arise only as an impurity in the output of the SAPRC air purification system, or as offgassing from the chamber walls in the dark prior to the beginning of the irradiation.) If it is assumed that the 20 ppb NO_x readings are real, the final O_3 and PAN values are fit by assuming that k_{EN} = 0.33 ppb, while if it is assumed that no NO_x is initially present, the data are fit by assuming k_{EN} = 0.5 ppb. Plots of observed ozone and PAN against results of calculations based on these two assumptions are shown in Figure III-14. It can be seen that while both calculations predict the observed final ozone and PAN values, the concentration-time profiles are much better fit if it is assumed that the instrumental readings at these low levels reflect only interferences, and that very little or no NO_x is initially present. (Similar results are obtained when carrying out analogous model calculations on acetaldehyde-air runs carried out in the SAPRC ITC and OTC, so run EC-253 is not unique in this regard.) Thus in modeling the evacuable chamber experiments for this program, we assume k_{EN} = 0.5 ppb, which fits the data if NO_x is assumed not to be initially present.

2. The SAPRC Indoor Teflon Chamber

The value of the NO_x offgassing parameter, k_{EN}, appropriate for the SAPRC ITC was obtained in exactly the same way as discussed above, except in this case data from two acetaldehyde-air runs, ITC-627 and ITC-636, were used. As when modeling run EC-253 discussed above, much better fits were obtained if it was assumed that NO_x was not initially present than if it was assumed that the low initial NO and NO_2 readings were meaningful. The ozone and PAN concentration-time profiles for both runs were satisfactorily fit by using k_{EN} = 0.15 ppb, so this value is used in our chamber model for the ITC.

3. The SAPRC Outdoor Teflon Chamber

The appropriate value for the NO_x offgassing parameter for the SAPRC OTC was obtained in an analogous manner as discussed above. In this case, the results of two runs were used: OTC-200, and OTC-206, though both runs were carried out when the chamber was in divided mode, so actually four experiments were modeled. The data for those four experiments, taken as a set, were best fit by k_{EN} = 0.1 ppb, though, as indicated in Section IV, the quality of the fits were not quite as good as obtained in the corresponding runs in the other two SAPRC chambers. This may be due to the greater difficulty in completely characterizing conditions of outdoor chamber experiments, compared to runs using indoor chambers.

4. The UNC Outdoor Chamber

The NO_x offgassing parameter k_{EN} for the UNC outdoor chamber was obtained in the same general manner as discussed above for the SAPRC chambers, although results of NO_x-air irradiations with low NO_2 levels, which are also sensitive to this parameter, were also considered. The specific experiments employed were the four 1983 acetaldehyde-air runs in our present UNC data set, and, to a lesser extent, four NO_x-air irradiations with low NO_2 levels carried out in 1982 and 1983.

In general the quality of fits to the results of the UNC acetaldehyde-air irradiations was not nearly as good as obtained when modeling the corresponding SAPRC runs, with the ozone being significantly underpredicted if k_{EN} is adjusted to fit the PAN yields, and PAN being overpredicted if it is adjusted to fit ozone. In addition, unlike the SAPRC runs, the PAN concentration-time profiles were fit slightly better if it is assumed that NO_x was initially present at the levels indicated by the NO-NO_x monitor. Although there is some variation, in general the PAN yields in the acetaldehyde-air experiments are fit by assuming k_{EN} = ~0.2 ppb, while the ozone yields in the acetaldehyde experiments are best fit by k_{EN} = ~0.4 ppb. The NO_2 profiles in three of the four NO_x-air runs with low NO_2 are better fit by assuming that k_{EN} = 0.4 ppb or higher. Plots of ozone and PAN data from a representative acetaldehyde-air run are shown in Figure III-13 above, and plots of NO and NO_2 data from a representative NO_x-air run with low initial NO_2 are shown in Figure III-15, together with results of model calculations using k_{EN} = 0.2 and 0.4 ppb.

These results indicate that in order to adequately fit the data for all of the UNC chamber runs which are highly sensitive to NO_x offgassing effects, we have to investigate more complex representations of NO_x offgassing and other chamber-specific effects in the UNC chamber. This will almost certainly involve additional adjustable parameters, and possibly also involve treating one or more of these parameters as adjustable from run-to-run. However, in view of the fact that most experiments used for model testing are very much less sensitive to this effect than are the acetaldehyde-air irradiations and the NO_x-air irradiations with low initial NO_2, we do not consider such a course of investigation to be essential to the overall objectives of this program. Thus for modeling purposes, we use an intermediate value of k_{EN} of 0.3 ppb, but recognize that if a UNC run is found to be highly sensitive to this parameter, it cannot be considered to be well enough characterized in our present model for this chamber to be useful for testing kinetic mechanisms. However, in view of the types of experiments which were used for model testing, this is probably not a significant limitation.

III. D. OTHER HETEROGENEOUS PROCESSES

Several other heterogeneous processes need to be considered in models simulating environmental chamber experiments. The most important of these which are incorporated into the model are the heterogeneous hydrolysis of N_2O_5 and the wall loss of ozone. In addition, the model also includes provisions to represent the wall losses of nitric acid and (for the SAPRC EC) of H_2O_2, though these latter two processes significantly affect only predicted levels of HNO_3 or H_2O_2, which are not used for model testing since experimental measurements for these species are not available for any of the experiments modeled. The representation of these processes in the model, and the derivation of their rate constants used in the model simulations of the experiments carried out in the specific chambers, are discussed in this section.

1. N_2O_5 Hydrolysis

The hydrolysis of N_2O_5 to nitric acid can be an important NO_x sink and, in experiments where ozone formation is limited by the availablity of NO_x, assumptions concerning its rate constant can affect the predicted maximum ozone yields. This reaction was studied by Tuazon et al. (1983) in the SAPRC EC and in a 3800-liter Teflon chamber. Although it is clear that this reaction is highly surface dependent, it may also occur in the gas phase. Tuazon et al. (1983) observed the formation of gas-phase HNO_3 from N_2O_5 in yields ranging from 0.5 to 1.7, and suggested that the formation of gas-phase HNO_3 may represent a gas phase reaction (since HNO_3 formed on the walls might be expected to remain on the walls), and that the portion that reacts without forming gas-phase HNO_3 is due to the reaction on the walls. This suggestion was supported by the fact that the rates of conversion of N_2O_5 to gas-phase HNO_3 were first order in both N_2O_5 and gas-phase water concentration, and that the rate constant for this process were the same, to within experimental uncertainty, for both of the chambers employed in the study of Tuazon et al. (1983). However, in more recent experiments carried out in these chambers, different rates of formation of gas-phase HNO_3 were observed (Atkinson et al. 1986b), suggesting that the conjecture of Tuazon et al. (1983) that the formation of gas-phase HNO_3 can be identified with a homogeneous reaction may not be correct. On the other hand, the rate constant derived by Tuazon et al. (1983) from the gas-phase HNO_3 measurements are within the range of "effective" $N_2O_5 + H_2O$ rate constants derived by Atkinson et al. (1986a) for ambient air. For this reason, in this model we assume that the rate constant derived by Tuazon et al. (1983) for the conversion of N_2O_5 to gas-phase HNO_3 is appropriate for atmospheric simulations, and an N_2O_5 + H_2O reaction is included as part of the "homogeneous" inorganic reaction mechanism which is discussed in Section II-A.

However, the data of Tuazon et al. (1983) indicate that a chamber- and water-dependent loss of N_2O_5 to the walls of the chamber is also occurring. This is indicated by the facts that (a) in both chambers the observed HNO_3 yields were less than the stoichiometrically expected value, that (b) the total N_2O_5 loss rates differed in the two chambers, and that (c) plots of the N_2O_5 loss rates against gas-phase water concentration yielded non-zero intercepts (Tuazon et al. 1983). Thus the chamber effects model must include a provision for this additional, obviously heterogeneous, process. This process is represented in the chamber-dependent model by the following two "reactions",

$$N_2O_5 \xrightarrow{H_2O} 2\ (\text{wall } NO_x) \qquad k_a$$

$$N_2O_5 + H_2O \longrightarrow 2\ (\text{wall } NO_x) \qquad k_b$$

where k_a is determined by the intercept, and k_b is determined by the slope of such plots, which were different for the two chambers employed.

For the SAPRC EC, the data of Tuazon et al. (1983) yield $k_a = 4.65 \times 10^{-3}$ min^{-1} and $k_b = 7.2 \times 10^{-7}$ ppm^{-1} min^{-1}, which we use in the model for that chamber. For the 3800-liter Teflon-film chamber, the data of Tuazon et al. (1983) yield $k_a = 2.8 \times 10^{-3}$ min^{-1} and $k_b = 6 \times 10^{-8}$ ppm^{-1} min^{-1}, and these are used to obtain estimates for the Teflon-film chambers of interest in this study. In lack of other data, we assume that the rate constants for these heterogeneous reactions are approximately proportional to the surface/volume ratio, which is approximated by the cube root of the volume of the chamber. Thus the values of k_a and k_b used in modeling experiments carried out in the Teflon-film chambers of interest in this report are as indicated below:

Chamber	k_a (min^{-1})	k_b (ppm^{-1} min^{-1})
SAPRC ITC	2.5×10^{-3}	5×10^{-8}
SAPRC OTC	1.6×10^{-3}	3×10^{-8}
UNC outdoor	0.9×10^{-4}	2×10^{-8}

2. Wall Loss of Ozone

Ozone is known to undergo a dark wall loss process, and it is necessary to represent this process in the model when simulating environmental chamber experiments. Fortunately, this is straightforward to measure, and ozone wall loss data are available for all four chambers whose data are employed in this study. Although ozone decay rates tend to be somewhat variable, the decay rates in these four chambers are sufficiently low that the model predictions are not strongly affected by these variations, and use of a single decay rate in model simulations of all experiments carried out in a given chamber is considered to be appropriate.

For the SAPRC EC, Pitts et al. (1979) reported ozone dark decay rates of 1.6×10^{-3}, 0.7×10^{-3}, and 1.0×10^{-3} min^{-1}, which yields an average value of 1.1×10^{-3} min^{-1}. This is used in the model, since most of the EC data used for model testing were obtained from that report. Ozone dark decay experiments carried out subsequently in that chamber give results which are consistent with this value.

For the SAPRC ITC and the SAPRC OTC, ozone dark decay experiments were carried out around the same time as the experiments used for model testing. The ozone decay rates obtained are summarized in Table III-5. The average ozone decay rates for the ITC and the OTC are $(1.3 \pm 0.7) \times 10^{-4}$ and $(1.7 \pm 0.7) \times 10^{-4}$ min^{-1}, respectively, which are used in the model for these two chambers. Note that they are within experimental error with each other, and they are approximately seven times less than that for the SAPRC EC.

For the UNC outdoor chamber, the ozone dark decay rate (corrected for dilution) observed at night on August 5-6, 1979 was 1.7×10^{-4} min^{-1}, and was 1.17×10^{-4} min^{-1} on the night of April 15-16, 1981. These yield an

Table III-5. Results of Ozone Dark Decay Experiments Carried Out in the SAPRC ITC and the SAPRC OTC

Chamber	Run No.	10^4 x Ozone Decay Rate (min^{-1})[a]
ITC	624	2.0
ITC	641	0.6
ITC	697	1.8
ITC	803	0.7[b]
OTC	147	1.6
OTC	158	1.8
OTC	176	0.8
OTC	183	2.5

[a] Data from Carter et al. (1985) except as noted.
[b] Data from Carter et al. (1984).

average value of 1.4×10^{-4} min^{-1}, which is used in the model. This is essentially the same as the ozone decay rates assumed for the SAPRC ITC and OTC, which is not surprising considering the similar nature of the walls of these chambers. However, it is surprising that there appears to be no apparent dependence of chamber volume on the ozone decay rates observed in these Teflon-film chambers.

3. Wall Loss of Nitric Acid

Gas phase nitric acid tends to be absorbed on chamber walls and on other surfaces. Although the assumptions regarding this process will not affect model predictions for species other than gas-phase HNO_3 (or the amount of NO_x adsorbed on the wall), the model includes a reaction representing this effect so it can be used to obtain estimates for those species. This is represented in the model by

$$HNO_3 \rightarrow (\text{wall } NO_x)$$

with a rate constant that depends on the chamber. Plum et al. (unpublished SAPRC results) observed that nitric acid decays in the SAPRC EC with a rate constant of 0.01 min^{-1} at 50% RH, which we use in the model for that chamber.

No data are available concerning the HNO_3 decay rate in the other chambers of interest in this study. For the ITC, we estimate it to be a factor of 2 times lower than observed in the EC because the H_2O-independent portion of the N_2O_5 hydrolysis is approximately a factor of 2 slower in the ITC than in the EC. For the other two Teflon-film chambers, we assume that this HNO_3 decay rate is proportional to the surface/volume ratio, as assumed for the other heterogeneous processes. Thus the estimated HNO_3 wall decay rates for those chambers are as follows:

Chamber	HNO_3 decay rate (min^{-1})
SAPRC ITC	0.005
SAPRC OTC	0.003
UNC outdoor	0.002

4. Wall Loss of H_2O_2

Although H_2O_2 was not monitored in any of the experiments used for model testing in this study, several determinations of the H_2O_2 decay rate were carried out in the SAPRC EC, with H_2O_2 being monitored by in situ longpath Fourier transform infrared spectroscopy (Pitts et al. 1979). H_2O_2 was observed to decay in the dark with a first order rate constant of 1.5×10^{-3} min^{-1} in the SAPRC EC. This is included in the model for the evacuable chamber, even though this is of totally negligible importance in affecting the results of simulations of other species. H_2O_2 decay is ignored in the models for the other three chambers; based on the other heterogeneous reactions, it is almost certainly slower in those chambers than in the SAPRC EC.

5. Offgassed or Background Reactive Organics

Model simulations of the UNC pure air irradiations discussed above in Section III-B-2-c and summarized in Section IV, and of the NO consumption rates observed in the NO_x-air irradiations of SAPRC chamber experiments discussed by Carter et al. (1982b) and Pitts et al. (1983) indicate that a small amount of contamination by reactive organics is present in all of the four chambers used in this program. However, as indicated in Section III-B-2-c, the concentrations of reactive organics which correspond to the level of contamination by reactive organics indicated by the model simulations of the pure air irradiations are minor compared to the amount and reactivity of organics injected in most experiments used for model testing. Likewise, the amounts of excess NO oxidation observed in the SAPRC NO_x-air irradiations (Carter et al. 1982b, Pitts et al. 1983) also correspond to very low amounts of reactive organics compared to those present in most organic-NO_x-air irradiations. Thus the effects of the presence of background or contaminant reactive organics is neglected in our model simulations, unless indicated otherwise.

Background air and NO_x-air irradiations are expected to be the most sensitive to the presence of background or contaminant organics, since these are the only organics present in these runs. The relatively large sensitivity of the model simulations of the background air irradiations to this have been discussed above in Section III-B-2-c in conjunction with the discussion of formaldehyde offgassing and radical sources in the UNC chamber. In order to determine the sensitivity of the simulations of the NO_x-air irradiations to assumptions regarding this effect, model simulations of all of the UNC NO_x-air irradiations used in this study were carried out using the $OH \rightarrow HO_2$ "reaction" to represent peroxy radical input caused by contaminant or background organic reactions, with the rate constant adjusted to fit the results of the pure air irradiations (as discussed in Section III-B-2-c). The distributions in the discrepancies in the model predictions of the changes in the NO and the NO_2 concentrations observed in those calculations are compared with those from the standard model, which neglects this effect, in Figure III-19 (both models include the defaults for the other chamber effects discussed in this section). It can be seen that including provision for organic contamination in the NO_x-air irradiations shifts the centers of the distributions of the discrepancies somewhat closer to zero, and thus slightly improves the fits of the model simulations to the results of these runs. However, it is clear from this figure, and from examining concentration-time plots of NO and NO_2 for the individual runs (not shown), that the results of the model simulations of the NO_x-air runs are much less sensitive to this than are the background air irradiations. The extreme sensitivity of the background air irradiations to background organics can be attributed to the fact that the major radical sink in NO_x-air irradiations arises from the reaction of OH radicals with NO_2, and thus the lower NO_2 levels in the background air irradiations result in higher radical levels, and thus higher reaction rates for the contaminant and background organics. Since the background or contaminant organics at these levels are expected to be even less important in the organic-NO_x-air irradiations than in the NO_x-air irradiations, neglecting them in the model simulations of the organic-NO_x-air runs is appropriate.

```
-----------------------------------------------------------------------
(Calc. - Expt.)                  NO                        NO2
Change / Initial     ------------------------    ------------------------
      NOx            Standard     OH -> HO2      Standard     OH -> HO2
                     Model         Model         Model         Model
-----------------------------------------------------------------------

        <  -0.22     :            :              :            :
  -0.22 -  -0.18     :            :              :            :
  -0.18 -  -0.14     :            :X             :            :
  -0.14 -  -0.10     :X           :              :            :
  -0.10 -  -0.06     :X           :X             :XX          :
  -0.06 -  -0.02     :X           :X             :XXX         :XXX
  -0.02 -   0.02    -:XX         -:XXX          -:XX         -:XX
   0.02 -   0.06     :XXXX        :XXXXXX        :X           :XX
   0.06 -   0.10     :XXXXX       :XX            :XXXX        :XXXXX
   0.10 -   0.14     :            :              :XX          :XX
   0.14 -   0.18     :            :              :            :
   0.18 -   0.22     :            :              :            :
        >   0.22     :            :              :            :
-----------------------------------------------------------------------
```

Figure III-19. Distributions of the relative discrepancies in the change in the NO and NO_2 concentrations in the model simulations of the UNC NO_x-air irradiations, calculated using the standard model and calculated assuming background organics convert OH radicals to HO_2 with an effective rate constant of 500 min^{-1}.

III. E. OTHER CHAMBER- AND RUN-DEPENDENT PARAMETERS

1. Dilution

In both the SAPRC evacuable chamber and the UNC outdoor chamber some dilution of the reactants in the chamber occurs during the course of an experiment, and provision for this must be included in the model. In the case of the SAPRC EC, which has rigid walls and a fixed volume, the contents of the chamber are diluted by pure air which is added to the chamber to compensate for the air which is removed from the chamber due to sample withdrawal, so the pressure remains constant during the course of an experiment. Thus for this chamber, the dilution rate during an experiment is the same as the total of the sampling rates of all of the instruments and analyses employed. The sampling rates of the instruments which make the greatest contribution are measured periodically, and are generally reported on the data sheets for the EC runs (Pitts et al. 1979). Although there is some small run-to-run variation, for almost all EC experiments the total sampling rates correspond to a dilution rate of 3 x 10^{-4} min^{-1}. This is used in the model simulations of all EC runs.

For the UNC chamber, where each half is approximately 25 times larger than the SAPRC EC, sampling is a relatively minor factor affecting dilution, and the main cause of dilution is believed to be leakage and exchange with outside air. Thus the dilution rate in that chamber is expected to be influenced by factors such as changes of temperature and the intensity of the winds, which means that in general it is more variable than for the SAPRC EC. These factors, and results of experiments in which the dilution rate was measured by monitoring levels of inert tracers in the UNC chamber, are discussed by Jeffries et al. (1982). They state that the dilution can vary over a range of (1-3) x 10^{-4} min^{-1}, and dilution rates obtained by tracer data in experiments carried out in July-September, 1980, and summarized by Jeffries et al. (1982) average approximately 2 x 10^{-4} min^{-1} for both sides, in the middle of this range. Thus, except for "dynamic dilution" experiments, where the contents of the chamber were deliberately diluted at higher rates, a dilution rate of 2 x 10^{-4} min^{-1} was used in our model calculations. Although this might be uncertain by as much as a factor of 2, dilution is not so high in the UNC chamber that it represents a major uncertainty in affecting the model predictions, and the dilution rates were not adjusted or optimized for any of the experiments modeled in this study.

For the "dynamic dilution" experiments, the dilution rates recommended by the UNC researchers, and given in the "documentation" section of their chamber data sets, were employed without adjustment or modification in the model calculations. The results of the simulations indicated that the values they recommended are appropriate.

Both the SAPRC ITC and the SAPRC OTC have flexible walls and are constructed in such a way that they can collapse when air is withdrawn from them, and thus sample withdrawal results in a reduction of the volume of the chamber and not dilution. Also, unlike the UNC chamber, changes in temperature do not necessarily cause exchange with the outside air, because the volume of the chamber can change accordingly. Although some exchange of air may be occurring in these chambers due to small leaks, dilution caused by this is expected to be minor, and probably can be neglected in the model. The Teflon bag reactors employed in these chambers are tested for leaks after they are constructed, and although, because of its exposure to the elements, the OTC can develop leaks over a period of time, these leaks are manifested primarily by the bag collapsing at an excessive rate, and not by dilution of its contents. Thus, dilution is assumed to be negligible in the model simulations of the experiments carried out in these chambers.

2. Temperature

Temperature can have a significant effect on a number of the rate constants in the chemical mechanism, and thus it is an important input parameter in the model simulations. Chamber temperature data exist for all experiments considered suitable for modeling. In particular, since the temperature in outdoor chambers can vary significantly with time and from day-to-day, outdoor chamber runs which did not have temperature data, or whose temperature data are questionable, were not used for model testing purposes. For outdoor runs which were modeled, plots of the measured temperature values against time were approximated by a series of straight lines, and parameters defining these lines which were included in the input data to the model calculation program. During the model simulation calculation, the temperature, and thus the temperature-dependent rate constants, were updated at every time step of the calculation.

For the indoor chamber runs the temperature can be assumed to be constant, and for most runs except for a few evacuable chamber runs where non-standard temperatures were used, it is well approximated by assuming T = 303 K. This was assumed for all indoor chamber runs unless the data indicated this was inappropriate. For evacuable chamber runs with non-standard temperature, the average of the temperature readings made during the experiment was used.

3. Humidity

The concentration of water in the gas phase affects the rate of N_2O_5 hydrolysis and the rate of formation of OH radicals from $O(^1D)$ atoms formed in ozone photolysis, and it thus needs to be specified in the model simulations. Most of the indoor chamber runs were carried out at a temperature of around 303 K and at 50% RH, which corresponds to a water concentration of $\sim 2 \times 10^4$ ppm. This was used as the default water concentration for the indoor chamber runs for which the humidity was not reported. For many indoor chamber runs, humidity measurements were made at the time the chamber was filled, and for those runs the water concentrations calculated from those measurements were employed.

For most of the outdoor chamber runs, dew point data are available from which the water concentration can be calculated. For runs which have such data, the dew point readings are converted into water concentrations, plots of these water concentrations against time were approximated by a series of straight lines, and parameters defining these lines were included in the input data to the model calculation program as for the temperature data. As noted by Jeffries et al. (1982), the water concentrations tended to increase somewhat with time for the UNC runs, due to evaporation of liquid water adsorbed on the walls. For the SAPRC OTC runs, which employed unhumidified purified air, water condensation generally did not occur (unless it had rained outside during the previous night and some water leaked in), and the water concentrations tended to be more constant. For some OTC runs, only a few reliable dew point measurements are available, and for those runs the water concentration was assumed to be constant.

Several UNC and OTC runs had no reliable dew point or humidity data, and for those runs the default water concentrations were employed. For the UNC runs, which used ambient air, a default water concentration of 2 x 10^4 ppm, corresponding to 50% RH at 300 K, was employed. For OTC runs, which as noted above used unhumidified pure air, the average water concentration in runs where it was measured was ~5 x 10^3 ppm, and this was used as the default for the runs for which such data were not available.

It should be pointed out that the lack of water data did not constitute a reason to reject chamber runs for use for model testing. The initial sets of model simulations of many of the runs employed in this program were carried out using the default water concentrations for all runs; and when the actual dew point or humidity measurements were subsequently incorporated into the input data, the changes in the results of the simulations were relatively small, especially compared to the effects of varying the light intensity or the chamber radical source within their uncertainties.